GENETIC ANALYSES OF XLF AND KU AND THEIR FUNCTIONAL IMPACTS ON DNA-DOUBLE STRAND BREAK REPAIR IN HUMAN CELLS

BY

AHMED MOHAMED AHMED AL EMAM

A thesis submitted to The University of Birmingham (UB) for the degree of

Doctor of Philosophy

College of Medicine and Dentistry

School of Clinical and Experimental Medicine

The University of Birmingham

October 2011

Abstract

XRCC4-like factor (XLF) is the most recently discovered core member of the nonhomologous end joining (NHEJ) machinery. XLF enhances ligation of DNA ends by DNA ligase IV (*LIG4*) and functionally interacts with KU70. Previous results showed that some polymorphic changes in *LIG4* impact on the efficiency of double strand breaks (DSBs) repair. A random Caucasian population sample was screened for *XLF* polymorphic mutations with similar functional impact. This analysis identified two novel noncoding single nucleotide polymorphisms (SNPs). To address the regulation of XLF and KU70, the acetylation status of both proteins were analysed. It has been found that XLF undergoes acetylation both *in vitro* and *in vivo* and the acetylation sites were mapped *in vitro* by mass spectrometry. Preliminary analysis has indicated that XLF deacetylation might be histone-deacetylase (HDAC3) dependent. For KU70, it has been found that lysine residues K317, K331 and K338 are critical for NHEJ. Cells overexpressing aceto-mimicking or aceto-blocking mutants of these residues are radiosensitive and defective in DSBs repair (DSBR). This indicates that the dynamic regulation of the acetylation/deacetylation status of these residues is critical for DSBR in response to ionizing radiation. These findings establish the importance of non-histone repair protein acetylation in the regulation of NHEJ and define new possible therapeutic targets for cancer treatment.

Acknowledgement

I am extremely grateful to my supervisor Dr. Boris Kysela. In truth, he gave me a real opportunity to explore the world of science by joining his laboratory. Dr. Kysela has been a source of practical counsel and support throughout. He provided me with invaluable guidance and inspiration. I am indebted to him for his time and patience. Without his guidance, I would never have got to the end. Also, I would like to thank Professor Eamonn Maher, my second supervisor for his guidance and academic support throughout my project.

I would like to show my deep thanks to Dr. Chris Bruce who generously helped me and provided endless support especially during my early days in the laboratory. Many thanks to my fellow student, Dr. Darren Arbon, for his help during the long hours of laboratory work. Special thanks to Dr Sarah Blair-Reid who gave me a great deal of encouragement especially during my last year of laboratory work and for reviewing my thesis. Also, I'm really grateful to Diana Walsh whose results contributed to Chapter four of this thesis. In fact, Sarah, Diana and Darren made our team a wonderful and challenging one. Many thanks also to all the members of Medical and Molecular Genetics at the University of Birmingham for their friendship, advice and for providing a wonderful working environment.

I am very thankful and appreciative to all my friends especially, Dr. Ahmed Nabil who was my trigger to do research while he was doing his at the University of Nottingham. Most of all, I would like to extend my endless thanks and appreciation to my parents and my family; Hala, Mena and Moaz for all their help, inspiration and support. Last but not least, many thanks to the Egyptian government and Mansoura University for funding this project.

Table Of Contents

List of Figures……..... xi

List of Tables……..xii

List of Abbreviations…….xiv

CHAPTER ONE: INTRODUCTION.....1

1.1 DNA Damage 2

1.2 Sources and Types of DNA Damage.....2

1.3 The Family of DNA Repair Pathways.....4

1.3.1 The Repair of Damaged Bases 4

1.3.1.1 Direct Reversal Repair of the Damage (DRR).....4

1.3.1.2 Excision Repair 6

1.3.2 Strand Break Repair.....15

1.3.2.1 Single Stand Break Repair (SSBR).....15

1.3.2.2 Double Strand Break Repair (DSBR) 15

1.4 Repair Pathway Selection.....32

1.5 Cernnunos/XRCC4-Like Factor (XLF).....34

1.5.1 The Structure of XLF 35

1.5.2 The Functions of XLF 38

1.6 KU Complex.....39

1.6.1 The Structure of KU Proteins 39

1.6.2 The Cellular Localisation of KU Proteins 42

1.6.3 The Biological Functions of KU Proteins 43

1.6.3.1 The Role of KU Proteins in DSBR 43

1.6.3.2 The Role of KU Proteins in Telomere Maintenance 44

1.6.3.3 The Role of KU Proteins in Apoptosis 44

1.6.3.4 The Role of KU Proteins in Transcription 45

1.6.3.5 The Enzymatic Activities of KU Proteins 45

1.7 General Objectives: 46

CHAPTER TWO: MATERIALS AND METHODS 47

2.1 DNA-Related Techniques 48

2.1.1 Polymerase Chain Reaction (PCR) 48

2.1.2 Agarose Gel Electrophoresis 48

2.1.3 DNA Gel Purification 50

2.1.4 Purification of PCR Products (Exo-SAP) 50

2.1.5 Cloning PCR Products into pGEM-T-Easy Vector 51

2.1.5.1 Preparation of Luria-Bertani (LB) Broth 51

2.1.5.2 Preparation of Luria-Bertani (LB) Agar Plates 51

2.1.5.3 Ligation Reaction 51

2.1.5.4 Bacterial Transformation by Heat Shock 53

2.1.5.5 Plasmid DNA Extraction....53
2.1.6 DNA Sequencing Reaction....54
2.1.7 Ethanol Precipitation of DNA....54
2.1.8 Sequencing Analysis....55
2.1.9 Creating Wild Type Constructs....56
2.1.9.1 First-Strand cDNA Synthesis....56
2.1.9.2 Proofreading PCR of *KU70* and *KU80* wild type cDNA....56
2.1.10 Restriction Digestion....59
2.1.11 Cloning of the Wild Type Constructs into pFlag-CMV-4 Vector....59
2.1.12 Site-Directed Mutagenesis (SDM)....61
2.1.13 Cloning the Wild Type and Mutant Constructs into pET-28a....64
2.1.13.1 Subcloning of the Wild Type and Mutant Constructs into pET-28a....64
2.1.14 Generation of Recombinant Bacmid....66
2.1.14.1 Isolation of Recombinant Bacmid DNA....68
2.2 Tissue Culture Techniques....69
2.2.1 Preparation of Cell Culture Media....69
2.2.2 Revival of Cells from Liquid Nitrogen....69
2.2.3 Subculturing Cells....70
2.2.4 Cell Counting....70
2.2.5 Cell Reseeding....71
2.2.6 Cell Cryopreservation and Storage in Liquid Nitrogen....71

2.2.7 Creating Stable Cell Lines 71
2.2.7.1 Transfection of MRC5VA Cell Line 71
2.2.8 Irradiation of Cells 73
2.2.9 Clonogenic Survival Assays 73
2.2.10 Immunofluorescence Analysis 74
2.2.10.1 Cells Fixing 74
2.2.10.2 Immunostaining 75
2.2.10.3 Mounting and Visualization 75
2.2.11 γH2AX Quantification 76
2.3 Protein Related Methods 77
2.3.1 Protein Extraction 77
2.3.2 Quantification of Protein 77
2.3.3 Sodium Dodecyl Sulphate Polyacrylamide Gel Electrophoresis (SDS-PAGE). 78
2.3.4 Gel Loading and Electrophoresis 78
2.3.5 Transfer of Proteins from Gel to Polyvinylidene Fluoride Membrane (PVDF). 78
2.3.6 Western Blotting 79
2.3.7 Visualisation Using Luminescence and Autoradiography 80
2.3.8 *In Vitro* Protein Purification from E. coli 80
2.3.8.1 Induction of Recombinant Proteins 81
2.3.8.2 Extraction and Purification of GST-XLF Recombinant Protein 81

2.3.8.3 Extraction and Purification of His-KU70 and His-KU80 Recombinant Proteins… 82

2.3.8.4 Coomassie Staining and Drying of SDS-PAGE Gels 84

2.3.8.5 Mass Spectrometry 84

2.3.8.6 SDS-PAGE Gel Drying 84

2.3.9 *In vitro* Acetylation of XLF and XRCC4 84

CHAPTER THREE: *XLF* SINGLE NUCLEOTIDE POLYMORPHISM (SNP) ANALYSIS 86

3.1 Introduction 87

3.2 Aims 90

3.3 Results 91

3.3.1 SNP Analysis of *XLF* 91

3.3.2 Restriction Fragment Length Polymorphism (RFLP) Analysis of *XLF* 98

3.3.3 *XLF* Exonic Deletion 100

3.3.4 Double Line Sequence of the 7th Coding Exon of *XLF* 102

3.4 Discussion 104

CHAPTER FOUR: CHARACTERIZATION OF XLF ACETYLATION STATUS (XLF ACETYLOME) 108

4.1 Introduction 109

4.2 Acetylation Switches 110

4.3 Acetylation and NHEJ Repair Pathway 113

4.4 Aims 115

4.5 Results 116

4.5.1 Cloning, Overexpression and Purification of GST-XLF in E. coli 116

4.5.2 Analysis of XLF Acetylation Sites 119

4.5.2.1 Bioinformatics-based Prediction of XLF Acetylation Sites 119

4.5.2.2 Mapping *in vitro* Acetylation Sites of XLF and XRCC4 120

4.5.3 *In vivo* Acetylation Study 123

4.6 Discussion 126

CHAPTER FIVE: *IN VIVO* ANALYSIS OF THE IMPACT OF ACETYLATION/DEACETYLATION OF KU70 LYSINE RESIDUES K317, K331 AND K338 ON THE REPAIR OF IR-INDUCED DSBS 130

5.1 Introduction 131

5.2 Aims 134

5.3 Results 135

5.3.1 Making pFlag-*KU70*/wt and pFlag-*KU80*/wt Constructs 135

5.3.2 Creating pFlag-KU70 Mutants by SDM 135

5.3.3 Establishing Stable Cell Lines Overexpressing pFlag-KU70/wt, pFlag-KU80/wt and pFlag-KU70 Mutants 139

5.3.4 Establishing His-tag Overexpression Systems for *KU70*/wt, *KU80*/wt and *KU70* Mutants. 141

5.3.5 *In Vivo* Analysis of the Impact of Overexpression of KU70 Mutants on DDR in Response to IR 145

5.3.5.1 Clonogenic Survival Assay 145

5.3.5.2 Expression and Cellular Localization of the pFlag-KU70 Mutants 146

5.3.5.3 γH2AX DNA Repair Foci Assay 150

5.3.5.4 γH2AX Pan-nuclear Staining 152

5.4 Discussion 157

CHAPTER SIX: SUMMARY AND RECOMMENDATIONS 164

CHAPTER SEVEN: APPENDICES 168

CHAPTER EIGHT: REFERENCES 181

List of Figures

Figure 1.1: Direct reversal repair 5

Figure 1.2: Representation of BER and its subpathways 8

Figure 1.3: Diagrammatic representation of NER 11

Figure 1.4: Diagrammatic representation of MMR 14

Figure 1.5: Diagrammatic representation of the steps of ATM activation 18

Figure 1.6: Diagrammatic representation of DDR 23

Figure 1.7: Diagrammatic representation of HR and C-NHEJ repair pathways 31

Figure 1.8: XLF crystal structure 37

Figure 1.9: KU70/KU80 heterodimer superimposed on broken DNA duplex 41

Figure 2.1: pGEM-T-Easy plasmid map 52

Figure 2.2: pFLAG-CMV-4 plasmid map 60

Figure 2.3: pET-28a plasmid map 65

Figure 2.4: pFast-Bac-HTb plasmid map 67

Figure 2.5: pGEX-2TK-p plasmid map 83

Figure 3.1: Diagrammatic representation of the structure of *XLF* 93

Figure 3.2: PCR optimization and PCR products of the seven coding exons of *XLF* 94

Figure 3.3: Chromatograms of the observed genotypes of the 2nd and 3rd introns of *XLF* 95

Figure 3.4: Chromatograms of the observed genotypes of the novel noncoding SNPs of *XLF* 96

Figure 3.5: Potential coding SNP of the 2nd coding exon of *XLF* and RFLP 99

Figure 3.6: *XLF* potential exonic deletion 101

Figure 3.7: Double line sequence of the 7th coding exon of *XLF* 103

Figure 4.1: Lysine side chain modifications 112

Figure 4.2: pGEX-2TKp-*XLF* double digestion and colony PCR.....117

Figure 4.3: GST-XLF purification in E. coli.....118

Figure 4.4: Strategy for studying protein acetylation.....121

.....124

Figure 4.5: Expression status of pFlag-XLF, pFlag-XRCC4 and pFlag-HDAC3 cell lines..124

Figure 4.6: Pan-Ac-K antibody Western blot.....125

Figure 5.1: pFlag-*KU70*/wt and pFlag-*KU80*/wt constructs.....136

Figure 5.2: pFlag-*KU70* mutant constructs.....137

Figure 5.3: Sequence chromatograms of pFlag-*KU70*/wt and pFlag-*KU70* mutant constructs...

.....138

Figure 5.4: Overexpression of pFlag-KU70/wt, pFlag-KU80/wt and pFLag-KU70 mutants140

Figure 5.5: pET-28a double digestion and colony PCR.....142

Figure 5.6: Trial purification of his-KU70/wt and his-KU80/wt in E. coli.....143

Figure 5.7: pFast-bac-HTb double digestion and PCR of Bacmids.....144

Figure 5.8: Clonogenic survival of pFlag-KU70 aceto-blocking mutant cell lines in response to IR.....147

Figure 5.9: Clonogenic survival of pFlag-KU70 aceto-mimicking mutant cell lines in response to IR.....148

Figure 5.10: Expression and cellular localization of the pFlag-KU70 mutants.....149

Figure 5.11: γH2AX foci of the pFlag-KU70 aceto-blocking mutant cell lines.....153

Figure 5.12: γH2AX foci of the pFlag-KU70 aceto-mimicking mutant cell lines.....154

Figure 5.13: γH2AX residual foci of the pFlag-KU70 mutant cell lines 24 hours post-irradiation.....155

Figure 5.14: Pan-nuclear γH2AX staining of the pFlag-KU70 mutant cell lines.....156

List of Tables

Table 2.1: *XLF* primers sequences 49

Table 2.2: Plasmid primers for sequencing 55

Table 2.3: *KU70* and *KU80* cloning and sequencing primers 58

Table 2.4: *KU70* SDM primers 63

Table 2.5: List of the antibodies used 80

Table 3.1: Percentages of the observed *XLF* SNP genotypes in the studied population sample 97

Table 4.1: Acetylation prediction software packages 119

Table 4.2: Prediction of XLF acetylated lysine residues 119

Table 4.3: *In vitro* acetylation sites of XLF by mass spectrometry 122

Table 4.4: *In vitro* acetylation sites of XRCC4 by mass spectrometry 122

Table 5.1: Statistical analysis of the surviving fractions at 6Gy and 8Gy 179

Table 5.2: Statistical analysis of the γH2AX residual foci at 5Gy 180

List of Abbreviations

APS – Ammonium PerSulphate

AP – Apurinic/Apyrimidinic (abasic) site

APE1 – Apurinic/Apyrimidimic Endonuclease 1

ATM – Ataxia Telangiectasia Mutated

ATP – Adenosine TriPhosphate

ATR – Ataxia Telangiectasia mutated and RAD-3 Related

BAX – BCL-2-Associated X Protein

B-NHEJ – Backup Non-Homologous End Joining

BER – Base Excision Repair

BRCA1 – Breast and Ovarian Cancer Associated Protein 1

BRCT – Breast and Ovarian Cancer Associated Protein Carboxyl Terminus Domain

BSA – Bovine Serum Albumin

CBP – CREB-binding protein

CK2 – Casein Kinase

CPDs – Cyclobutane Pyrimidine Dimers

CS – Cockayne Syndrome

DAPI – 4', 6-DiAmidino-2-PhenylIndole

DDR – DNA Damage Response

DMEM – Dulbecco's Modified Eagles Medium

DNA-PK – DNA Dependent Protein Kinase

DNA-PKcs – DNA Dependent Protein Kinase Catalytic Subunit

dRP – Deoxy-Ribose Phosphate

DRR – Direct Reversal Repair

DSBs – Double Strand Breaks

DTT – DiThioThreitol

DUB – Deubiquitinase

EDTA – EthyleneDiamineTetraAcetic Acid

FBS – Foetal Bovine Serum

FEN-1 – Flap Endonuclease 1

FHA – Fork Head Associated

53PB1 – p53 Binding Protein 1

GG-NER – Global Genome Nucleotide Excision Repair

HAT – Histone Acetyl Transferase

HDAC – Histone Deacetylase

HP1β – Heterochromatin Protein 1 beta

HR – Homologous Recombination

H3K9me3 – Histone 3 trimethylated lysine 9

IDLs – Insertion Deletions Loops

IPTG – IsoPropyl ThioGalactoside

IR – Ionising Radiation

LP-BER – Long Patch-Base Excision Repair

MDC1 – Mediator of the DNA damage Checkpoint 1

MGMT – O^6-MethylGuanine-DNA MethylTransferase

MMR – Mismatch Repair

MMS – Methyl Methane Sulfonate

MRE11 – Meiotic Recombination 11

MRN – MRE11/RAD50/NBS1

NBS1 – Nijmegen Breakage Syndrome 1

NER – Nucleotide Excision Repair

NHEJ – Non-Homologous End Joining

Pan-Ac-K Ab – Pan-Acetyl-Lysine Antibody

PARP1 – Poly ADP-Ribosyltransferase 1

PBS – Phosphate Buffered Saline

PCAF – P300/CBP-Associated Factor

PCNA – Proliferating Cell Nuclear Antigen

PCR – Polymerase Chain Reaction

PIKK – Phosphatidyl Inositol-3-Kinase related Kinases

PMSF – PhenylMethylSulfonylFluoride

PNKP – PolyNucleotide Kinase Phosphatase

POL β – DNA Polymerase beta

POL δ – DNA Polymerase delta

POL ε – DNA Polymerase epsilon

6-4PPs – Pyrimidine-(6-4)-Pyrimidone photoproducts

PTM – Post Translational Modification

PVDF – PolyVinyliDene Fluoride

RFC – Replication Factor C

RNF8 – Ring Finger Protein 8

RNF168 – Ring Finger Protein 168

ROS – Reactive Oxygen Species

RPA – Replication Protein A

SDS – Sodium Dodecyl Sulfate

SDS-PAGE – Sodium Dodecyl Sulfate PolyAcrylamide Gel Electrophoresis

SMC – Structural Maintenance of Chromosomes

SP-BER – Short Patch-Base Excision Repair

SSA – Single Strand Annealing

SSBs – Single Strand Breaks

ssDNA – Single Stranded DNA

SUMO – Small Ubiquitin-Related Modifier

TC-NER – Transcription-Coupled Nucleotide Excision Repair

TDP1 – Tyrosyl-DNA Phosphodiesterase 1

TEMED – Tetra-Methyl Ethylene Diamine

TFIIH – Transcription Factor IIH complex

3' UTR – Three Prime Untranslated Region

TIP60 – Tat Interactive Protein

TOP1 – Topoisomerase I

UV – Ultra Violet

UV-DDB – UV-Damaged-DNA-Binding protein

XLF – XRCC4-Like Factor

XP – Xeroderma Pigmentosum

γH2AX – Phosphorylated H2AX

CHAPTER ONE: INTRODUCTION

1.1 DNA Damage

Cells cannot withstand damage to their DNA as this results in compromising the integrity and the accessibility of the fundamental information in the genome. DNA lesions may impair transcription and replication resulting in cell cycle arrest, mutations and even cell death. Moreover they have been recently linked to several inherited diseases, carcinogenesis, genetic disorders and aging (Barnes and Lindahl, 2004; Evans et al., 2004; Martin et al., 1996). As unrepaired or inappropriately repaired DNA lesions have serious consequences leading to genomic instability and cellular dysfunctions, cells have developed a network of complementary DNA-repair mechanisms involving more than 130 known human genes. Studying the basic mechanisms for DNA repair has revealed an unexpected complexity with overlapping specificity within the same pathway as well as extensive functional interactions between proteins involved in repair pathways (Altieri et al., 2008; Krokan et al., 2004; Wood et al., 2001).

1.2 Sources and Types of DNA Damage

A plethora of chemical and physical agents can induce DNA damage. Moreover, DNA damage might occur due to the intrinsic instability of chemical bonds in DNA. In mammals, many thousands of apurinic/apyrimidinic (AP) sites are generated per cell each day due to loss of purine or pyrmindine bases. Purines are lost more easily than pyrimidines with the highest number of AP sites occurring in the brain, heart and colon (Nakamura and Swenberg, 1999).

Sunlight, ionizing radiation (IR), ultraviolet radiation (UV), chemical compounds and genotoxic drugs are examples of exogenous sources of DNA damage. In addition, endogenous

sources include replication errors, programmed DSBs in lymphocyte development, and DNA-damaging agents. Reactive oxygen species (ROS) and reactive nitrogen species such as nitric oxide represent the major category of endogenous DNA-damaging agents. They are produced as by-products of normal metabolism or in response to environmental stresses (Altieri et al., 2008; Cadet et al., 2003; Klaunig et al., 2010).

IR and UV are the major exogenous sources of DNA damage. IR can generate highly ROS resulting in the generation of a broad spectrum of cellular DNA lesions. UV induces photoproducts, mainly cyclobutane pyrimidine dimers (CPDs) and pyrimidine-(6-4)-pyrimidone photoproducts (6-4PPs). CPDs are more cytotoxic and mutagenic than 6-4PPs (Huang et al., 2004; Pfeifer et al., 2005; Ravanat et al., 2001).

Briefly, the types of DNA damage can be categorized into base damage (modified or mismatched), crosslinks (intrastrand or interstrand crosslinks) and strand breaks (single strand breaks (SSBs) or DSBs). However, DNA damage can be highly diverse and may comprise random combinations of strand breaks, base damage and sugar damage to generate a highly complex spectrum of compound lesions. These complex lesions challenge not only the cellular repair machineries, but also anyone who attempts their systematic classification. Hence, it is necessary to review all the available repair mechanisms every now and then. In the next pages the different repair pathways and damage signalling will be briefly discussed, and XLF and KU complex will be discussed in detail in the context of DNA DSBR, as this may help understanding the possible complex interactions between the repair pathways and the coordination among pre-repair, repair and post-repair events.

1.3 The Family of DNA Repair Pathways

1.3.1 The Repair of Damaged Bases

1.3.1.1 Direct Reversal Repair of the Damage (DRR)

DRR is accomplished without the need to break the DNA sugar phosphate backbone. Alkylation of DNA can occur at various sites, however alkylation at the O^6 position of guanine (O^6-meG) has the highest potential in terms of mutagenesis. The mammalian O^6-methylguanine-DNA methyltransferase (MGMT) directly removes methyl groups at the O^6 position of guanine, instantaneously reversing the DNA base damage in one step (Figure 1.1). Shuttling the alkyl group from the alkylated base to MGMT irreversibly inactivates it and targets it for ubiquitination and proteolysis, hence MGMT is called the suicide enzyme (Pegg, 2000; Sekiguchi et al., 1996). Another example of DRR, UV-induced pyrimidine dimers are reversed by photolyase enzyme (Sancar, 2003). Furthermore, alkylated DNA repair proteins (AlkBH2 and AlkBH3, human homologues of E. coli AlkB) revert both DNA and RNA alkylation damage (Aas et al., 2003; Duncan et al., 2002).

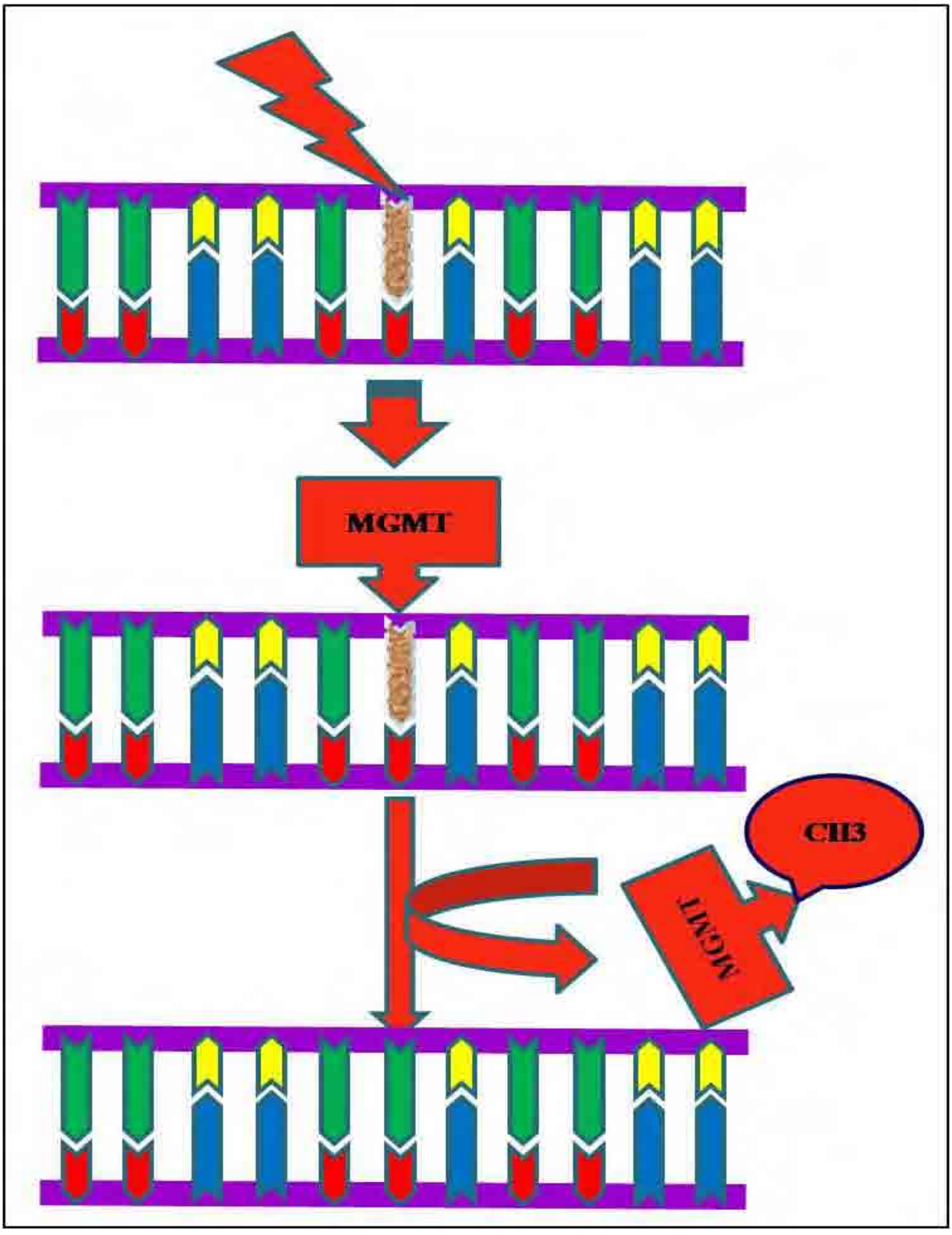

Figure 1.1: **Direct reversal repair**
MGMT removes the methyl group from the damaged base, brownish in colour, reversing the damage and restoring the original base (Kreklau et al., 2001).

1.3.1.2 Excision Repair

1.3.1.2.1 Base Excision Repair (BER)

BER lies among the most active DNA repair pathways that deal with the specific recognition and excision of a damaged DNA base. BER fixes the majority of damage generated by the attack of ROS except for DSBs (Dizdaroglu, 2005; Evans et al., 2004; Hazra et al., 2007; Hitomi et al., 2007; Wilson and Bohr, 2007). BER consists of five basic steps catalyzed by different enzymes (Figure 1.2). First of all, DNA N-glycosylase removes the damaged base. Secondly, the resulting AP sites are processed by an AP endonuclease or an AP lyase leaving SSBs, which might need extra-processing to generate unblocked 5' and 3' ends. Then, the gaps are filled in by a DNA polymerase, either with a single-nucleotide (short patch repair (SP-BER)) or with a longer patch (long patch repair (LP-BER)). The choice of the BER sub-pathway appears to be dependent on the nature of the damage. At the end, a DNA ligase seals the break (Fortini and Dogliotti, 2007; Izumi et al., 2003; Sung and Demple, 2006).

The recognition and excision of damaged bases are carried out by either monofunctional or bifunctional DNA N-glycosylases. They cleave the N-glycosidic bond between the damaged base and the sugar phosphate backbone of the DNA. This cleavage generates an AP site in the DNA (Denver et al., 2003; Huffman et al., 2005; Krokan et al., 1997; Vernole et al., 2003).

The apurinic/apyrimidimic endonuclease (APE1) enzyme has AP endonuclease and 3'phosphodiesterase activities to generate unblocked 3' and 5' ends. It cleaves the DNA backbone immediately 5' to the AP site, resulting in a 3' hydroxyl group and a transient 5' abasic deoxyribose phosphate (dRP). Then DNA polymerase (POL β) removes the dRP via its AP lyase activity and adds one nucleotide to the 3' end of the nick. Finally, the strand break is

sealed by X-ray cross-complementing protein 1 XRCC1/DNA ligase III (LIG3). This is SP-BER, which represents approximately 80-90% of all BER (Demple and Sung, 2005; Kelley and Parsons, 2001; Tell et al., 2005; Wilson, 2003).

The LP-BER deals with modified bases resistant to the AP lyase activity of POL β. Unlike SP-BER, LP-BER depends on proliferating cell nuclear antigen (PCNA). Replication factor C (RFC) helps loading of PCNA to act as a sliding clamp on DNA in LP-BER as it does during replication. DNA polymerase delta or epsilon (POL δ or ε), instead of POL β, adds several nucleotides (approximately 2-10 nucleotides) to fill the gap, concomitantly raising the dRP as part of a flap. The resulting oligonucleotide flap is excised by flap endonuclease (FEN1), which is recruited by PCNA, prior to sealing of the nick by DNA ligase I (LIG1) (Frosina et al., 1996; Matsumoto et al., 1994).

In cases where base damage generates a 3' blocking end that APE1 cannot deal with, polynucleotide kinase/phosphatase (PNKP) can process such ends. PNKP demonstrates dual 3' phosphatase and 5' kinase activities, yet has high affinity to IR-induced 3' phosphate ends (Karimi-Busheri et al., 1999). In fact, without APE1, mammalian Nei-like (NEIL) glycosylases and PNKP generate polymerase compatible 3' OH termini essential for BER repair to proceed. NEIL-PNKP-dependent repair may represent an alternative APE1-independent repair pathway (Das et al., 2006; Hazra et al., 2007).

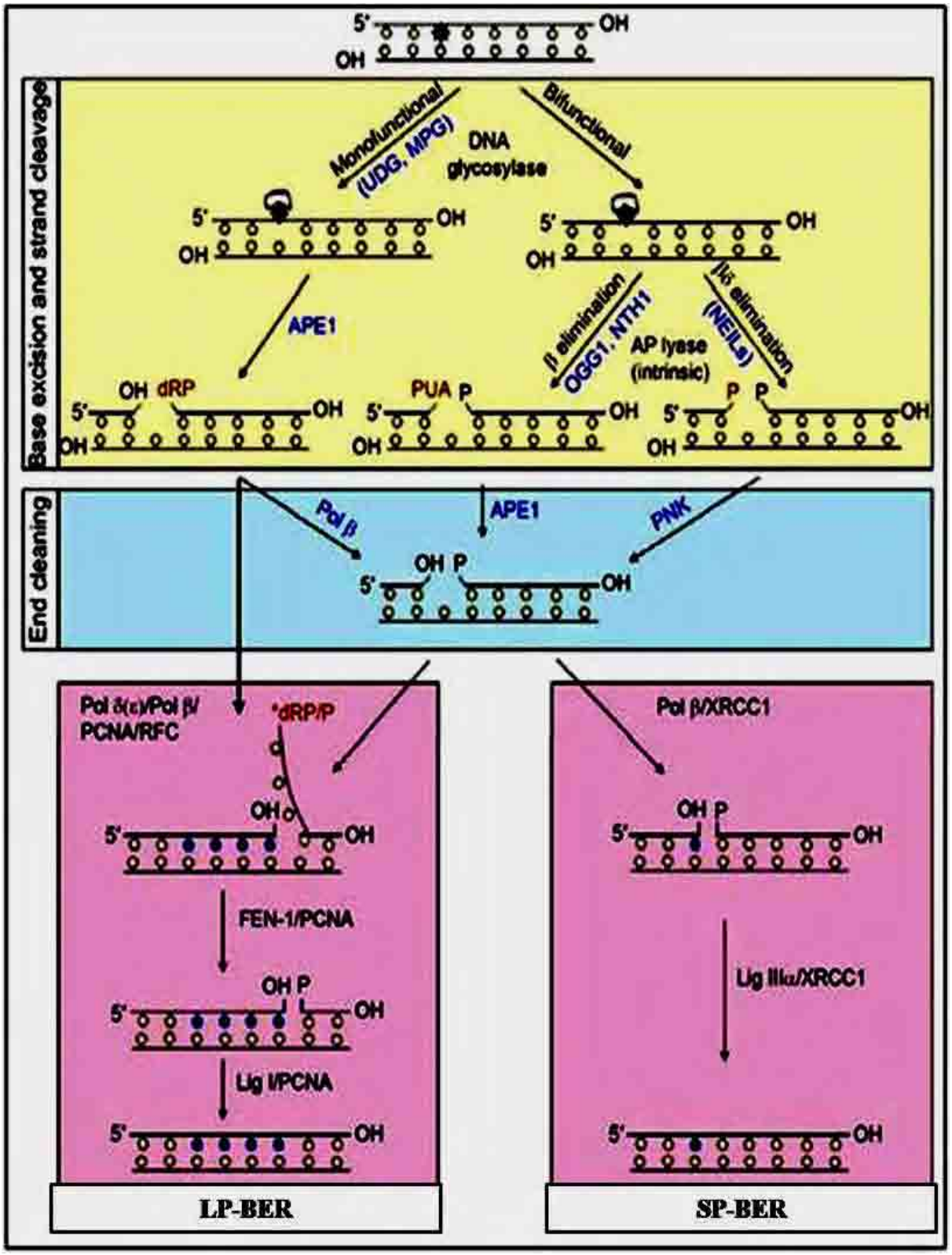

Figure 1.2: Representation of BER and its subpathways
First the damaged base is excised by glycosylases then the strand backbone is cleaved by either APE1 or bifunctional glycosylases depending on the type of damage. Secondly, end cleaning is carried out by APE1, polymerase lyase activity or PNKP, again depending on the structure of the cleaved end. Then either short patch or long patch repair follows (Hegde et al., 2008).

1.3.1.2.2 Nucleotide Excision Repair (NER)

NER has evolved in living organisms to recognize damaged regions by their abnormal helix distorting structure, as BER is not sufficient to handle all types of damage. Thus, it functions as a backup system. It can correct a wide diversity of structurally unrelated DNA lesions, especially UV-induced CPDs and 6-4PPs, benzopyrene-induced bulky chemical adducts and, chemotherapeutics-induced crosslinks (Batty and Wood, 2000; D'Errico et al., 2007). Most NER genes start with the letters XP or CS simply because they were first identified in genetic studies of xeroderma pigmentosum (XP) or Cockayne Syndrome (CS) respectively.

NER involves the actions of 20 to 30 proteins in successive steps: DNA-damage recognition, lesion demarcation and local opening of the DNA duplex around the lesion by assembly of a multiprotein complex at the damaged site, double incision of the damaged strand and removal of the damage-containing oligonucleotide between the two breaks. The resulting gap is filled by polymerization, then the nick is ligated (Figure 1.3). NER can be divided into two subpathways: global genome (GG-NER) and transcription-coupled (TC-NER). GG-NER corrects damage in transcriptionally silent areas of the genome, whereas TC-NER repairs lesions in the areas of active transcription. Both share the same repair mechanism, with a difference in the DNA-damage recognition step (de Boer and Hoeijmakers, 2000; Hanawalt, 2002; Hoeijmakers, 2001; Park and Choi, 2006).

In GG-NER, XPC heterodimerizes with human RAD23B (HR23B). XPC/RAD23B complex in conjunction with UV-damaged-DNA-binding protein (UV-DDB), also known as XPE, a component of an E3 ubiquitin ligase detects CPDs, bends DNA and recruits the rest of GG-NER factors to the site of damage (Bunick et al., 2006; Kim et al., 2005a; Kusumoto et al.,

2001; Sugasawa et al., 2005). The transcription factor IIH (TFIIH), together with XPA and replication protein A (RPA), builds up an open complex demarcating the lesion. XPB and XPD subunits of TFIIH unwind a stretch of 20 to 30 nucleotides of DNA helix around the damaged site via their helicase activity, forming a preincision structure (Dip et al., 2004; Gervais et al., 2004; Riedl et al., 2003). TFIIH complex recruits both XPA and XPG. XPA and RPA facilitate DNA unwinding and protect the single undamaged strand from nuclease attack as well (Bochkareva et al., 2001; Daughdrill et al., 2003; Lee et al., 2003). XPG and excision repair cross complement protein 1 ERCC1/XPF endonucleases cut the damaged strand in the preincision structure (Bunick and Chazin, 2005). XPG cuts a few nucleotides away from the 3' end of the open complex. It always cuts before, and independent of, ERCC1/XPF. Afterwards, ERCC1/XPF cuts at 15 to 24 nucleotides away from the 5' side of the open complex. Subsequently, POL δ or ε with the aid of RFC and PCNA, efficiently synthesizes the new strand, concomitantly displacing the damage-containing oligonucleotide and NER components. Finally, LIG1 seals the break (Araujo et al., 2001; Dunand-Sauthier et al., 2005).

The more poorly understood TC-NER employs all GG-NER proteins except XPE, XPC, and HR23B, implying that damage recognition in transcribed strands occurs via a different mechanism. The stalling of RNA polymerase II (POL II) presumably acts as a damage recognition signal. At the same time, it has to depart from the lesion allowing access for the repair enzymes to fix the lesion. CSA and CSB dependent ubiquitination of POL II might signal its degradation (Lee et al., 2002). TC-NER's next steps are principally the same as GC-NER. Additionally, XPB and XPD helicase subunits of TFIIH and XPG might play special roles in the resumption of transcription, beyond their roles in GG-NER (Coin et al., 2008).

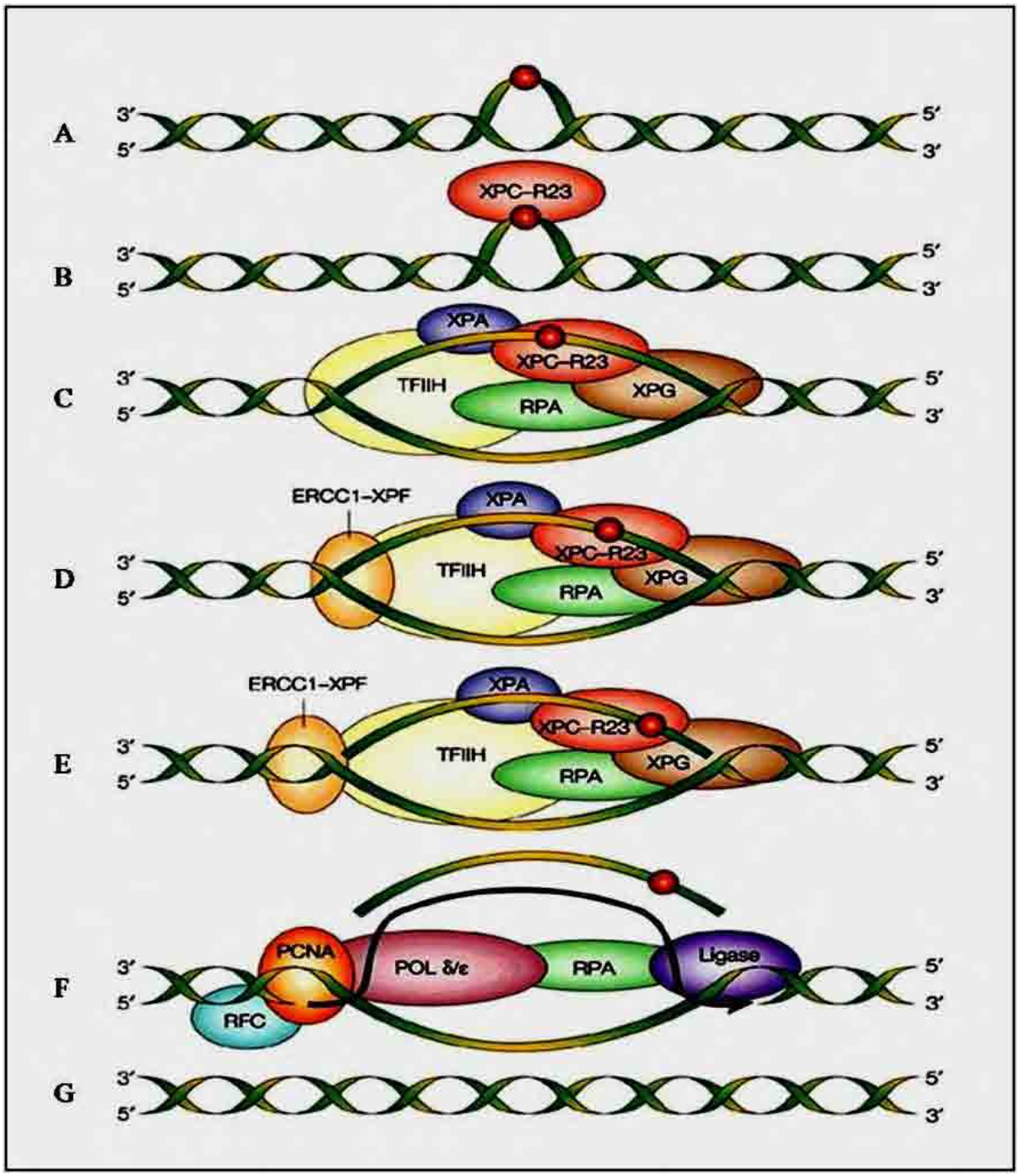

Figure 1.3: **Diagrammatic representation of NER**
(A) NER corrects base damage that causes alterations in the chemistry and structure of the DNA duplex. (B) XPC/HHRAD23 recognizes the damage. (C) TFIIH complex unwinds the DNA duplex in the immediate vicinity of the base damage generating a bubble in the DNA. (D) The subsequent binding of ERCC1/XPF heterodimeric complex completes the assembly of the NER multiprotein complex. (E) XPG endonuclease cuts the damaged strand 3' to the site of base damage, whereas ERCC1/XPF endonuclease cuts the damaged strand 5' to the site of base damage. (F) The excised fragment is removed from the genome and concomitantly the repair synthesis that requires DNA polymerases delta or epsilon, as well as the accessory replication proteins PCNA, RPA and RFC fill the gap. Finally, LIG1 seals the nick. (G) The native DNA chemistry and configuration is restored (Friedberg, 2001).

1.3.1.2.3 Mismatch Repair (MMR)

MMR functions as a spell-checker, fixing replication errors that evade the proofreading activity of DNA polymerase. It maintains the fidelity of both mitotic and meiotic recombination events and supports the first step of checkpoint responses (Jiricny, 2006; Kunkel and Erie, 2005; Young et al., 2003). It has been found that defective MMR increases microsatellite instability (MSI) (Aaltonen et al., 2007). MMR proteins participate in DNA damage surveillance. Briefly, MMR proteins bind to damaged DNA and recruit several checkpoint proteins such as ataxia telangiectasia mutated (ATM), ataxia telangiectasia-related (ATR) and the checkpoint kinases CHK1 and CHK2. These kinases, in turn, activate p53 and p53-related proteins (Jascur and Boland, 2006; Jun et al., 2006).

1.3.1.2.3.1 Mammalian MMR

Noticeably, MMR is also considered one of the most flexible repair pathways, however it is not well understood because of its increased complexity and the numerous homologous proteins involved. Unlike in E. coli, the strand signals that trigger eukaryotic MMR have not yet been characterized. However, it has been observed that strand discontinuities, as gaps between Okazaki fragments associated with replication, may direct the repair (Jascur and Boland, 2006; Modrich, 2006).

MMR (Figure 1.4) is initiated by recognition of the mismatch or insertion deletion loops (IDLs) by either MSH2-MSH6 heterodimer (known as MutSα) or MSH2-MSH3 heterodimer (known as MutSβ). MutSα recognizes the mismatched bases and single-base IDLs, whereas larger IDLs are usually recognized by MutSβ with partial redundancy in substrate specificity (Genschel et al., 1998). Then, MutSα or β undergoes a conformational shift and translocates

along the DNA away from the mismatch in an ATP dependent manner, until additional MMR proteins are encountered (Blackwell et al., 1998; Gradia et al., 1999). Higher order protein complexes are formed, including those containing MLH1-PMS2 heterodimer (MutLα), MLH1- PMS1 (MutLβ) or MLH1-MLH3 (MutLγ) and replication factors (Genschel et al., 1998; Gradia et al., 1999; McCulloch et al., 2003).

For the mismatch excision, MutS, together with MutL, guides a specific exonuclease in a PNCA dependent manner. In fact, a 200 bp oligonucleotide or longer (1000bp) DNA tract residing either 3' or 5' of the mismatch is excised including the mismatch itself. Exo1 (5'→ 3' exonuclease) and DNA polymerase or meiotic recombination 11 (MRE11) (3'→ 5' exonuclease) are thought to carry out this guided excision (Constantin et al., 2005; Dzantiev et al., 2004; Kadyrov et al., 2006; Lee and Wilson, 1999; Vo et al., 2005). RPA stimulates the excision, stabilizes the gap against the endonuclease attack and promotes DNA repair synthesis. The initiation of DNA excision might require the interaction of high mobility group box 1 protein (HMGB1) with MutSα (Yuan et al., 2004). POL δ or ε, FEN1, PCNA, and RFC are known to catalyze DNA resynthesis. Finally, the nicks are sealed by LIG1 (Genschel and Modrich, 2003; Zhang et al., 2005).

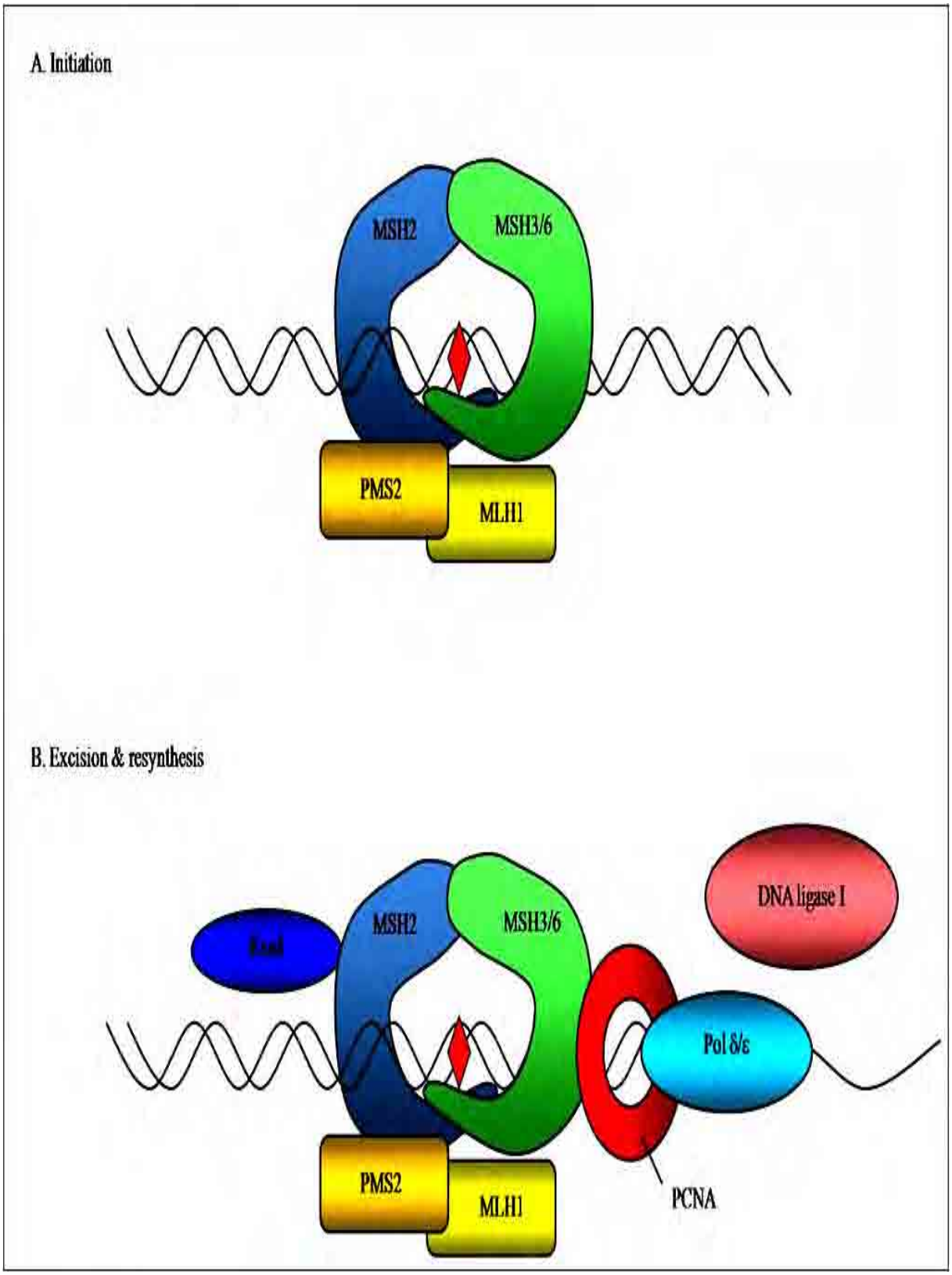

Figure 1.4: Diagrammatic representation of MMR
(A) MMR is initiated by recognition of the DNA damage by the MutSα or β complex and recruitment of the MutLα complex. (B) Excision of the damaged strand and resynthesis are carried out by Exo1, PCNA, DNA polymerase δ or ε and LIG1 (Helleman et al., 2006).

1.3.2 Strand Break Repair

1.3.2.1 Single Stand Break Repair (SSBR)

IR and oxidizing compounds can induce SSBs. Also SSBs arise as by-products of DNA metabolism. Being both mutagenic and cytotoxic as they interfere with DNA replication, SSBs need to be repaired. Their repair can be performed through the BER pathway simply because they are also intermediates of this repair process. Poly ADP-ribosyltransferase 1 (PARP1), an enzyme that catalyzes the poly ADP-ribosylation of several protein substrates, has been implicated in SSBs detection (Chalmers, 2004; Schreiber et al., 2006). PARP1 interacts with XRCC1, which in turn recruits other proteins to the site of the break (Okano et al., 2003). Moreover, XRCC1 interacts with PNKP, stimulating its kinase and phosphatase activities to process any blocking ends. Furthermore, it has been found that XRCC1, PNKP and tyrosyl-DNA phosphodiesterase 1 (TDP1) complex process topoisomerase I (TOP1)-induced transient SSBs for religation. Although, this TOP1-induced cleavage is intended to relax supercoiled DNA ahead of transcription or replication machinery, their accumulation may lead to the formation of DSBs (Pommier et al., 2003).

1.3.2.2 Double Strand Break Repair (DSBR)

DNA DSBs are considered the most lethal threat to cell survival and can initiate genomic rearrangements that eventually result in either carcinogenesis or apoptosis (Hoeijmakers, 2001). Interestingly, despite the potential dangers of DSBs, mammals have developed clever ways to harness the intentional generation of DSBs to arm their immune system and diversify their genes in meiosis (Maizels, 2005; Whitby, 2005). To combat the risk of the potentially harmful genomic rearrangements that could result from both purposeful and non-purposeful DSBs, mammals have developed intricate DNA repair pathways. DSBs can be repaired by the

NHEJ that rejoins broken DNA ends quickly in all cell cycle phases, yet this is error prone. During S and G2 phases of the cell cycle, homologous recombination (HR) ideally dominates, exploiting the already available sister chromatids for accurate repair (Arnaudeau et al., 2001; Mills et al., 2004; Sonoda et al., 2006). These highly toxic DSBs require complex signalling and processing to be perfectly repaired.

1.3.2.2.1 DNA Damage Signalling

DNA damage response (DDR) to numerous insults is a highly integrated network evolved to deal with any kind of genomic instability. In response to DNA damage, the cells activate cell cycle checkpoints and cease cell division granting time for damaged cells to orchestrate their repair pathways to faithfully recover their genomic stability. In fact, DDR involves a growing number of proteins. These proteins crosstalk via their posttranslational modifications (PTMs) including phosphorylation, ubiquitylation, sumoylation, acetylation and methylation, to relay damage signals and execute appropriate repair (Hakem, 2008; Harrison and Haber, 2006). When cells fail to repair DSBs, DDR initiates the activities of kinases such as ATM and ATR, thus leading to senescence or apoptosis (Mallette et al., 2007; Zhivotovsky and Kroemer, 2004). Failure to detect, signal or repair DSBs can result in damaged cells escaping the cell cycle checkpoints and surviving. These damaged cells could undergo uncontrolled proliferation, passing harmful mutations or chromosomal aberrations to their offspring. Such genomic instability is considered as a trigger for the development of various human syndromes, immunodeficiency, ageing and cancer (Hakem, 2008; Jackson and Bartek, 2009).

1.3.2.2.1.1 Acetylation and DSB Signalling

The highly compacted chromatin structure has to relax so the damage signal can be transduced to initiate the repair machinery. Although the early changes in chromatin structure at DSBs are not fully understood, the elimination of the heterochromatin protein 1 (HP1β) exposing the pre-existing trimethylated lysine 9 of histone 3 (H3K9me3) mark might be the trigger of the distal signalling and repair cascades. Interestingly, it has been found that casein kinase (CK2) becomes active and phosphorylates HP1β in response to DSBs. This CK-induced phosphorylation releases HP1β, uncovering the H3K9me3 mark (Sun et al., 2009). In parallel with the initial release of HP1β, MRE11/RAD50/NBS1 (MRN) complex has been found to interact with ATM and recruit it to DSBs (Lee and Paull, 2005; Stewart et al., 2003). Moreover, it has been shown that MRN recruits tat interactive protein 60 (TIP60), a histone acetyltransferase (HAT) that has a critical role in DNA damage repair and has been implicated in the regulation of ATM and DNA-dependent protein kinase (DNA-PK) (Jiang et al., 2006b). Surprisingly, the binding of the TIP60 chromodomain to H3K9me3 allosterically stimulates its HAT activity. Subsequently, TIP60 acetylates ATM (Sun et al., 2005). This acetylation induces autophosphorylation of ATM which in turn phosphorylates H2AX, a histone H2A variant, on its S139 (Figure 1.5). These events are followed by hyperacetylation of histones H3 and H4 resulting in relaxation of chromatin, initiating repair (Sun et al., 2009).

Interestingly, TIP60 has also been found to acetylate phosphorylated H2AX (γH2AX). Moreover, it associates with the E2 ubiquitin conjugating enzyme (UBC13) to ubiquitylate the acetylated γH2AX. This acetylation-dependant ubiquitylation of γH2AX has been assumed to facilitate γH2AX dephosphorylation and/or turnover and to be a prerequisite for eviction of γH2AX (Ikura et al., 2007; Keogh et al., 2006).

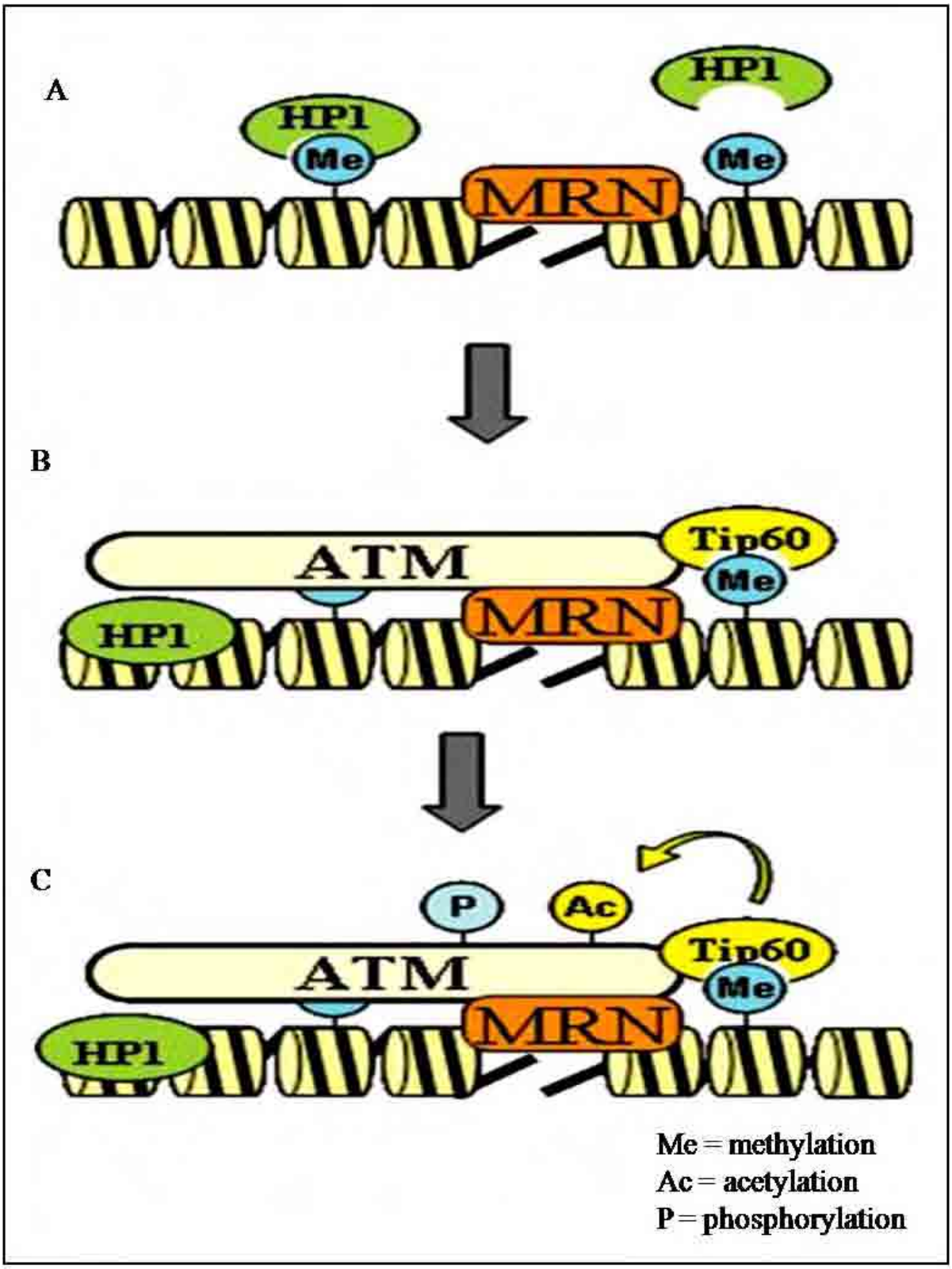

Figure 1.5: Diagrammatic representation of the steps of ATM activation
(A) MRN is recruited to DSB. In parallel, phosphorylation of HP1 proteins results in its release from the histone mark H3K9me3. (B) MRN sitting on DSBs recruits inactive TIP60/ATM complex facilitating the interaction between TIP60 chromodomain and H3K9me3. (C) Binding of TIP60 to MRN stimulates its HAT activity which in turn acetylates ATM. Acetylation of ATM by TIP60 activates ATM's kinase activity (Sun et al., 2010).

1.3.2.2.1.2 Phosphorylation and DSB Signalling

Three members of the phosphatidylinositol-3-kinase related kinases (PIKK) family are indispensable for the response to DSBs. These kinases are ATM, ATR and DNA-PK. ATM and DNA-PK mainly signal DSBs while ATR is mainly involved in the response to SSBs and stalled replication forks (Bartek and Lukas, 2007; Jazayeri et al., 2006; Shiloh, 2003). In fact, ATM and ATR phosphorylate more than 900 sites in over 700 proteins in response to DNA damage (Matsuoka et al., 2007). Although, ATM, DNA-PK and ATR functions are all essential, it has been shown that DNA-PK can compensate for defective ATM to a certain extent (Bohgaki et al., 2010; Bredemeyer et al., 2008; Callen et al., 2009).

The inactive ATM polymers that do exist in absence of stress dissociate into active monomers upon DSB-induced ATM autophosphorylation of serine 1981(S1981), S367 and S1893 (Bakkenist and Kastan, 2003; Lavin, 2008). It is noteworthy that, in unstressed cells, the serine/threonine phosphatase PP2A associates with ATM, whereas they dissociate in response to DSBs (Goodarzi et al., 2004). Moreover, WIP1 dephosphorylates S367 and S1981 (Shreeram et al., 2006), while PP5 has been shown to stimulate ATM in response to stress (Ali et al., 2004). This indicates that the three phosphatases PP2A, PP5 and WIP1 regulate ATM activation.

Most importantly, in response to DSBs, activated ATM, DNA-PK or ATR rapidly phosphorylates H2AX (Rogakou et al., 1998). Also, activated ATM recruits the mediator of DNA damage checkpoint protein 1 (MDC1) as shown in Figure 1.6 (Lavin, 2008). Moreover, H2AX tyrosine residue 142 (Y142) is constitutively phosphorylated and its subsequent dephosphorylation in response to DNA damage may enhance MDC1 and ATM recruitment to

extend H2AX phosphorylation (Xiao et al., 2009). The recruitment of MDC1 to γH2AX is mediated by its tandem BRCA1 C-terminal (BRCT) domains. This promotes further recruitment of active ATM and MRN to spread and maintain H2AX phosphorylation around the DSBs. In fact, this acts as a positive feedback loop, expanding γH2AX up to 2 megabases around the break and allowing access for other signaling and repair proteins including E3 ubiquitin ligases: the ring finger proteins (RNF8 and RNF168), breast cancer associated 1 (BRCA1) and p53 binding protein 1 (53PB1) (Goldberg et al., 2003; Lukas et al., 2004; Stewart et al., 2003; Stucki et al., 2005).

Interestingly, the eviction of γH2AX at DNA damage sites is required for appropriate repair. In mammals , dephosphorylation of H2AX is regulated by phosphatases PP2A (Chowdhury et al., 2005; Chowdhury et al., 2008; Nakada et al., 2008) and PP4 (Chowdhury et al., 2005; Chowdhury et al., 2008). In fact, the absence of their catalytic subunits PP2Ac and PP4c results in defective repair (indicated by persistence of γH2AX foci) and prolonged checkpoint arrest (indicated by prolonged MDC1 retention) respectively.

1.3.2.2.1.3 Ubiquitylation and DSB Signalling

It has recently been shown that ubiquitylation plays a major role in the signalling of DSBs (Bartek and Hodny, 2010; Galanty et al., 2009; Morris et al., 2009; Morris et al., 2006). Whereas K63 polyubiquitylation plays important roles in relaying signals during immune, cell cycle and DNA damage responses (Bennett and Harper, 2008; Haglund and Dikic, 2005; Hayden and Ghosh, 2008; Panier and Durocher, 2009; Polanowska et al., 2006), K48 polyubiquitylation targets its substrates for proteolysis (Hershko and Ciechanover, 1998).

In response to DSBs, RNF8 is recruited via its N-terminal fork head associated (FHA) domain to the conserved threonine/glutamine/X/phenylalanine (T-Q-X-F) clusters of MDC1, after their ATM-mediated phosphorylation (Kolas et al., 2007; Mailand et al., 2007; Matsuoka et al., 2007). Subsequently, RNF8, which possesses a C-terminal ring finger domain, acts in conjunction with UBC13 to ubiquitylate K63 residue of H2A and H2AX at the sites of the DNA lesion (Figure 1.6) (Brooks et al., 2008). Subsequently, the ubiquitylated H2A (uH2A) recruits RNF168 through its ubiquitin interacting motif 2 (UIM2) (Doil et al., 2009; Pinato et al., 2009; Stewart et al., 2009).

RNF168 and UBC13 polyubiquitylate K63 residue of H2A, and this polyubiquitylation has been proposed to modulate chromatin structure, facilitating the recruitment of 53BP1 to the sites of DSBs. H2A-K63 polyubiquitylation recruits receptor-associated protein 80 (RAP80) via its tandem UIMs (Feng et al., 2009; Shao et al., 2009; Wang and Elledge, 2007; Wang et al., 2009; Wu et al., 2009). Then, RAP80 interacts with ubiquitylated histones facilitating the recruitment of the BRCA1-A complex to the sites of DSBs (Figure 1.6). The BRCA1-A complex contains BRCA1, BARD1, ABRAXAS/FAM175A, BRCC3/BRCC36, BRE/BRCC45 and MERIT40/NBA1, in addition to RAP80 itself (Wang and Elledge, 2007). BRCA1 has recently been found to ubiquitylate the phosphorylated C-terminal binding protein (CTBP) interacting protein (CTIP), and CTIP ubiquitination is critical for its chromatin association and DNA damage response. This indicates that BRCA1 may participate in G2/M checkpoint control (Yu et al., 2006). Similarly, BRCA1 ubiquitylates FANCD2, a fanconi anaemia protein which also plays a role in HR during the S phase of the cell cycle through interaction with RAD51 (Taniguchi et al., 2002).

1.3.2.2.1.4 Sumoylation and DSBs Signalling

SUMO (small ubiquitin-related modifier) modification is considered as one of the most important PTMs. Recent studies have underscored the intimate relationship of sumoylation with ubiquitylation during DSB signalling (Galanty et al., 2009; Morris et al., 2009), in addition to its importance in DNA repair and replication (Bergink and Jentsch, 2009; Arakawa et al., 2006; Frampton et al., 2006; Hoege et al., 2002; Leach and Michael, 2005). In fact, the SUMO E3 ligases, protein inhibitor of activated STAT (signal transducer and activator of transcription) PIAS1 and PIAS4 have been found to recruit RNF8 and RNF168 to DSBs and mediate their sumoylation, in addition to RAP80 as well. Moreover, they enhance RNF8 and RNF168 ubiquitin liagse activities (Morris, 2010; Yan et al., 2007b). Interestingly, it has recently been shown that 53BP1 and BRCA1 undergo SUMO1 modifications (Figure 1.6) in response to DSBs and that sumoylation of BRCA1 is critical for its E3 ubiquitin ligase activity (Morris et al., 2009; Galanty et al., 2009).

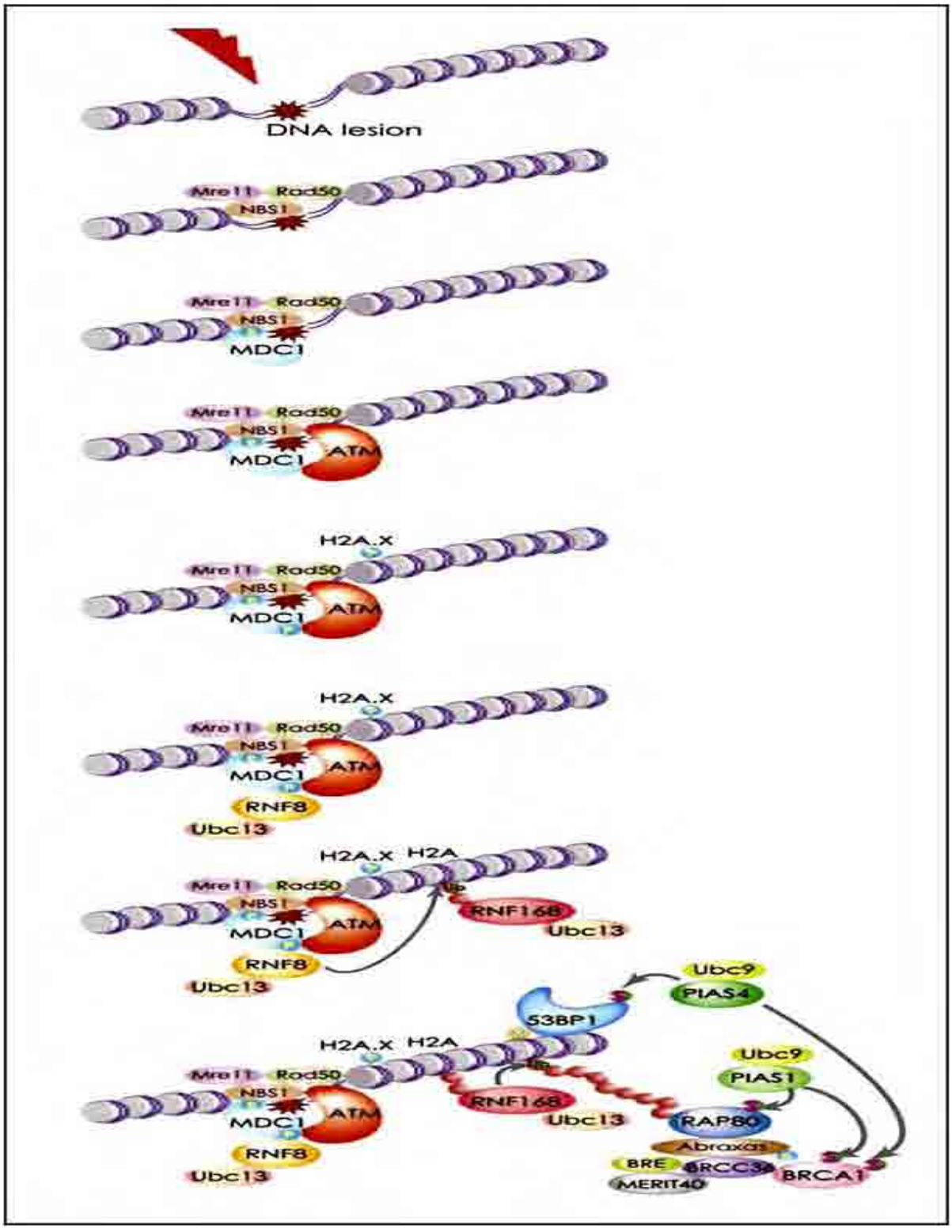

Figure 1.6: Diagrammatic representation of DDR
MRN detects DSBs and activated ATM phosphorylates multiple substrates including H2AX and MDC1. MDC1 binds to γH2AX. MDC1 recruits RNF8 to DSB sites. Then, RNF8 associates with UBC13 and ubiquitylates H2A. Subsequently, RNF168 is recruited to uH2A and, in conjunction with UBC13, further polyubiquitylates uH2A resulting in modification of the chromatin structure. Then, BRCA1A complex is recruited to the polyubiquitylated H2A. Also, 53BP1 is recruited to di-methylated lysine 20 of histone H4 (H4K20me2) (Bohgaki et al., 2010).

1.3.2.2.2 Single Strand Annealing (SSA)

SSA is a non-conservative HR process that repairs DSBs between two repeat sequences. Unlike HR, SSA does not require homologous sister chromatids, yet it uniquely uses identical repeat sequences on single DNA duplex as a repair template. Briefly, DNA around the break is trimmed by 5' exonuclease activity generating 3' ssDNA overhangs. These 3' ssDNA tails are coated with the RPA-RAD52 complex, which helps aligning and annealing of the two complementary repeat sequences. After annealing is complete, leftover non-homologous flaps of the 3' overhangs are cut away by RAD1-RAD10 endonucleases (Lyndaker and Alani, 2009; Mimitou and Symington, 2009). New DNA synthesis fills in any gaps and ligation restores the DNA duplex as two continuous strands. SSA might result in loss of DNA sequence between the repeats. Hence it is considered the most mutagenic and the least desirable option for the cells, as it deletes genetic material. In fact, it is suppressed by both KU80 and RAD51 allowing the more conservative NHEJ and HR to dominate (Mansour et al., 2008).

1.3.2.2.3 Translesional DNA Synthesis (TLS)

TLS is a mechanism of replicative bypass of base damage that employs accurate (error free) or mutagenic (error prone) TLS polymerases, relieving arrested DNA replication (Lehmann, 2006). E. coli have three specialized DNA polymerases (POL II, POL IV, and POL V), whereas, to date, 10 mammalian polymerases have been identified (REV1 and DNA polymerases ζ, η, κ, ι, λ, μ, β, θ and ν). Most of these polymerases bypass the damage, and fall off after inserting a few nucleotides and then allow an accurate replicative polymerase to continue. In fact, PCNA ubiquitination appears to act as a switch regulating the access of polymerases to the lesions (Galkin et al., 2005; Plosky and Woodgate, 2004).

1.3.2.2.4 Homologous Recombination (HR)

HR of DNA DSBs is generally accurate because it elegantly copies the undamaged sister chromatid. So, it is largely restricted to late S/G2 phases, whereas NHEJ can repair DSBs throughout the cell cycle (Helleday et al., 2007; Wyman and Kanaar, 2006). The MRN complex is the sensor of this repair pathway (Figure 1.7A). The binding of its subunit NBS1 to γH2AX recruits it to DSBs (Hopfner et al., 2001; Riballo et al., 2004; Tauchi et al., 2002). Then, its subunit MRE11 endonuclease-mediated resection at the DSB ends generates 3' ssDNA tails (D'Amours and Jackson, 2002; Stracker et al., 2004). Moreover, its subunit RAD50 nucleotide binding motifs are required for its DNA end-tethering activity (Moreno-Herrero et al., 2005). The 3' ssDNA tails are coated with RPA. Then, RAD52 subsequently targets RAD51 to the RPA-coated 3' ssDNA tails exchanging RPA for RAD51 to form the RAD51 nucleoprotein filament (Benson et al., 1998; New et al., 1998; Shinohara and Ogawa, 1998).

RAD51 is the central player in almost all homology-directed repair events and directs the 3' ssDNA tail of the nucleoprotein filament to search out, invade and pair with undamaged homologous sequences, forming heteroduplex DNA. RAD51 is assisted by a number of protein factors that include BRCA2, RAD52, RAD54, RAD54B and probably also the RAD51 paralogues RAD51B, RAD51C, RAD51D, XRCC2 and XRCC3 (Shin et al., 2004; Valerie and Povirk, 2003; Wyman and Kanaar, 2006). BRCA2, for example, is involved in the control of RAD51 recombinase activity and its loading onto ssDNA (Galkin et al., 2005; Shin et al., 2004).

The process of strand invasion and formation of heteroduplex DNA leads to the displacement of a DNA strand in the sister chromatid forming a so-called D-loop. After D-loop formation, the annealed 3' end is then extended by polymerization beyond the original break site to restore the missing sequence information at the break point. On the other side of the D-loop, an X structure called a Holliday junction is formed at the border between hetero- and homoduplex. This process may generate flaps or gaps depending on the degree to which the 3' end was extended during repair synthesis. Flaps can be trimmed by endonucleases, such as the XPF/ERCC1 complex, whereas the remaining gaps are filled and sealed by PCNA-dependent POL δ or **ε** and LIG1. In fact, several proteins can bind Holliday junctions and modulate the ability of these junctions to slide in either direction. For example, RAD54, WRN and BLM may facilitate Holliday junction migration (Constantinou et al., 2000; Karow et al., 2000). To complete the repair after recombination, the DNA strands have to be uncrossed or cut by structure-specific nucleases called Holliday-junction resolvases. In eukaryotes, in addition to the resolvase GEN1, which will symmetrically cleave the DNA at the Holliday junction, two RAD51 paralogues, XRCC3 and RAD51C, appear to be associated with resolvase activity (Liu et al., 2004). Alternatively, the crossed strands can be separated by the combined activity of BLM helicase and topoisomerase III (Raynard et al., 2006). Finally, LIG1 seals the breaks.

1.3.2.2.5 Non-Homologous End Joining (NHEJ)

NHEJ is considered the simplest mechanism to repair a DSB, yet is error prone. It can be classified into classical-NHEJ (C-NHEJ) and backup-NHEJ (B-NHEJ).

1.3.2.2.5.1 Classical NHEJ (C-NHEJ)

C-NHEJ proceeds through the following stages: sensing the DSBs, DNA end-processing and DNA end ligation (Figure 1.7B).

1.3.2.2.5.1.1 Sensing the DSBs

The KU70/80 heterodimer, the sensor, forms a ring that can bind to DNA ends. Then the DNA-KU complex recruits and activates the DNA-PK catalytic subunit (DNA-PKcs) (Weterings et al., 2003). Moreover, DNA-PKcs binding causes KU complex to move one helical turn inward from the end, thereby facilitating the access of end processing and other NHEJ proteins. The inward translocation of KU also allows DNA-PKcs to interact with the extreme termini of the DNA (Yoo and Dynan, 1999). The two DNA-PKcs molecules interact across the DSB forming a synaptic complex. This interaction stimulates the kinase activity of DNA-PKcs. DNA-KU-PKcs complex also helps tether the ends together protecting them from nuclease attack (DeFazio et al., 2002). Although DNA-PK phosphorylates KU70, KU80, XRCC4, XLF, Artemis and LIG4 *in vitro* in addition to its own autophosphorylation, these phosphorylation events do not seem to be required for NHEJ (Douglas et al., 2005b; Goodarzi et al., 2006; Wang et al., 2004; Yu et al., 2008; Yu et al., 2003). Its own autophosphorylation results in kinase inhibition and its dissociation from DNA-KU, suggesting that autophosphorylation of DNA-PKcs may regulate the disassembly of the DNA-PK complex (Chan and Lees-Miller, 1996; Merkle et al., 2002). However, it should also be noted that the *in vivo* effects of its own autophosphorylation may be highly complex, because phosphorylation at regions of the molecule enhance HR, whereas phosphorylation at different sites can either positively or negatively affect DNA end-processing (Cui et al., 2005; Meek et

al., 2009). It is noteworthy that during NHEJ, the MRN may facilitate tethering of the broken ends for further processing (D'Amours and Jackson, 2002; Stracker et al., 2004).

1.3.2.2.5.1.2 DNA End Processing

DSBs vary according to the chemical composition of their ends. For example, IR produces non-ligatable DNA ends, as the IR-induced ROS cause base and sugar damage besides the DNA strand breaks. These non-ligatable DNA ends are not proper substrates for ligation and require editing. They can be processed by PNKP, which interacts with XRCC4, generating 3' OH and 5' phosphate ends suitable for ligation. Other incompatible DNA ends can be specifically processed by Artemis endonuclease (Ma et al., 2005). Artemis is recruited to the broken ends through the interaction with DNA-PKcs, which is required for its activity. WRN exonuclease might be involved in the processing of damaged DNA ends. Moreover, terminal deoxynucleotidyl transferase (TDT) and POL μ and λ have been implicated in end-processing. Whereas TDT can add untemplated nucleotides to DNA ends, POL μ and λ can fill in 5' single-stranded extensions (Ma et al., 2004; Nick McElhinny et al., 2005). Furthermore, MRN, ATM and γH2AX are required for efficient joining of difficult breaks (Riballo et al., 2004). KU is considered the principal factor in orchestrating all these activities, as it interacts with Artemis (through DNA-PKcs), POL μ, POL λ and the XRCC4/LIG4 complex (Ma et al., 2004). The reversible interaction of the processing factors with the core components does not require a strict order, providing great flexibility in the combination of different ends that can be rejoined (Ma et al., 2004; Wyman and Kanaar, 2006).

1.3.2.2.5.1.3 Ligation of DNA Ends

The final ligation is performed by XRCC4/LIG4. XRCC4 acts as a cofactor required for the proper targeting and stabilization of LIG4 to broken DNA ends. Moreover, it stimulates its adenylation and ligase activity (Mari et al., 2006). Recently, XLF has been identified as an interaction partner of the XRCC4/LIG4 which enhances the final ligation step of NHEJ (Ahnesorg et al., 2006; Buck et al., 2006). XLF will be discussed in detail in Section 1.5.

1.3.2.2.5.2 Backup NHEJ (B-NHEJ)

B-NHEJ has come to the forefront of DSBR and to the centre of carcinogenesis as well. It has been described under different names: alternative NHEJ (A-NHEJ, or alt-NHEJ), microhomology-mediated end-joining (MMEJ), KU-independent end-joining, LIG4-independent NHEJ and backup NHEJ (Corneo et al., 2007; Han and Yu, 2008; Iliakis, 2009; Liang et al., 2008; Ma et al., 2003). In fact, efficient DNA end joining in C-NHEJ-deficient monkey cells provided evidence for an alternative end-joining pathway (Roth et al., 1985). Moreover, in the late 1990s, studies carried out with cells deficient in *DNA-PKcs* (DiBiase et al., 2000), *KU* (Wang et al., 2001a), *LIG4* and other factors of C-NHEJ or wild type cells treated with DNA-PKcs kinase inhibitors (Wang et al., 2001b) have shown that all these cells were repairing practically all DSBs, but at a slower rate. In addition, studies in the severe combined immunodeficiency (SCID) mouse model have demonstrated similar results (Nevaldine et al., 1997). The slow repair noticed in C-NHEJ-deficient cells could not be attributed to HR, as chicken B-cells (DT40) harbouring both HR and C-NHEJ mutants were still able to repair with the same slow kinetics (Wang et al., 2001a). So it has been concluded that higher eukaryotes possess an alternative backup end joining process which dominates in the absence of C-NHEJ yet with slower kinetics. This B-NHEJ is error-prone, as it increases

chromosomal aberrations (Virsik-Kopp et al., 2003) and the risk of carcinogenesis after exposure to IR (Couedel et al., 2004). Moreover, *XRCC4* and *LIG4*-deficient mice showed that B-NHEJ possess near wild type class switch recombination (CSR) and variable, diversity and joining (VDJ) recombination, but again associated with chromosome abnormalities confirming the error prone nature of B-NHEJ (Soulas-Sprauel et al., 2007; Yan et al., 2007a).

1.3.2.2.5.2.1 B-NHEJ Machinery

It has been proposed that B-NHEJ operates according to NHEJ principles. It has been found that PARP1 detects the damage and hence acts as the sensor of B-NHEJ for damage detection. However, the higher affinity of KU for DNA ends makes C-NHEJ dominate and places B-NHEJ as a backup (Wang et al., 2007). In line with this is the finding that isogenic human cell strains lacking *KU* (but not other NHEJ components) are remarkably proficient in B-NHEJ (Fattah et al., 2010). Interestingly, the MRN complex has recently been implicated in B-NHEJ, indicating that MRE11 end processing is a step in this backup pathway (Davis and Chen, 2010; Deriano et al., 2009; Rahal et al., 2010; Rass et al., 2009; Xie et al., 2009). LIG3 has been shown to be the functional ligase in this pathway (Wang et al., 2001b; Windhofer et al., 2007). Moreover, the PARP1/XRCC1/LIG3 (PLX) complex has been shown to be involved in the repair of SSBs and base damage (McKinnon and Caldecott, 2007). Furthermore, as KU helps aligning the DNA ends prior to ligation in C-NHEJ (Feldmann et al., 2000), histone H1 might do the same in B-NHEJ. Moreover, H1 dramatically enhances the activity of LIG3 greater than that of LIG4 (Rosidi et al., 2008).

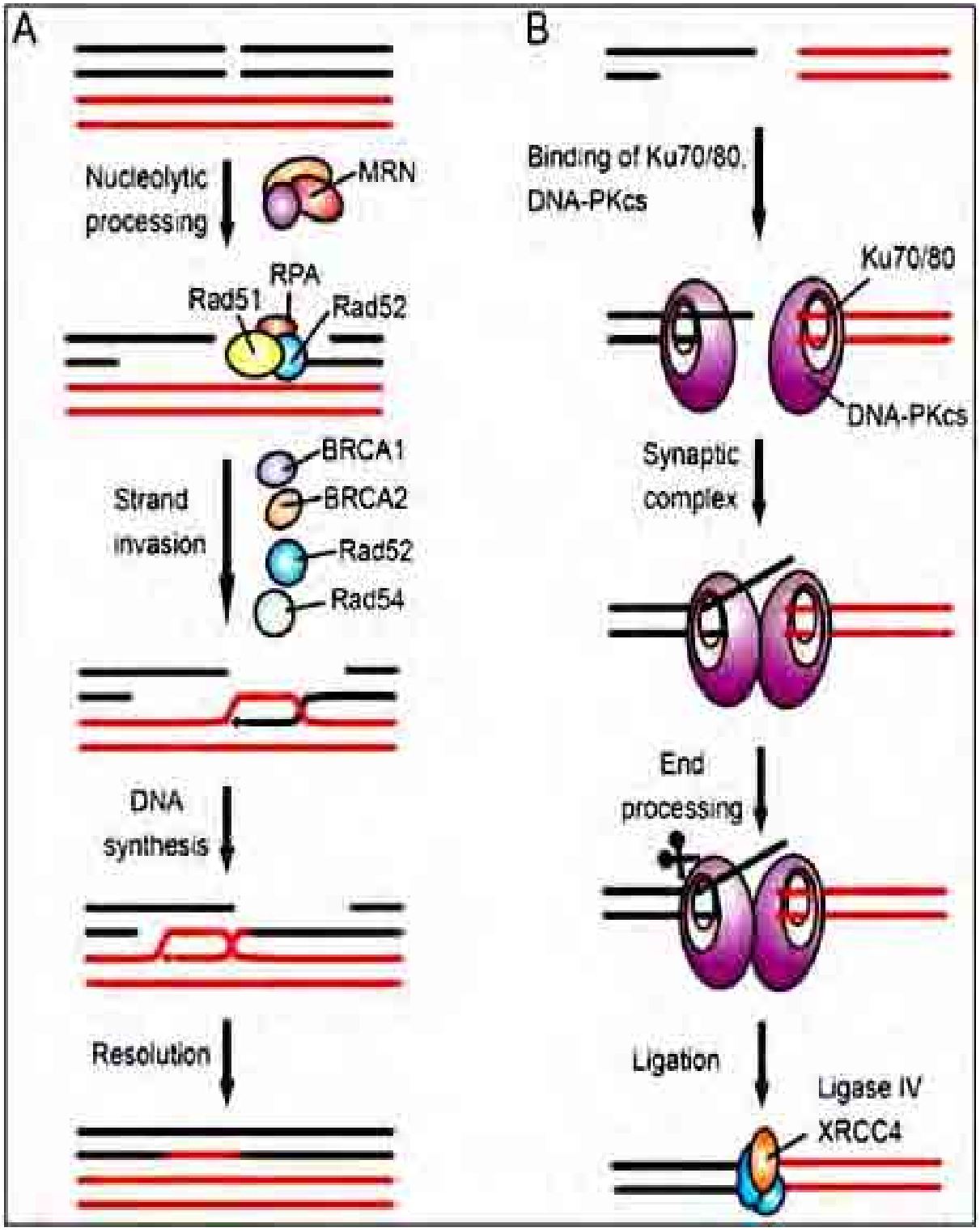

Figure 1.7: Diagrammatic representation of HR and C-NHEJ repair pathways
(A) HR utilizes a homologous sister chromatid to accurately repair the DSB. MRN senses and processes DNA ends, creating single-strand overhangs. RAD51, RAD52 and RPA associate with these overhangs, followed by the formation of a joint molecule by the damaged and the undamaged strands. Template guided DNA synthesis and resolution of the two strands then complete the repair of DSBs. (B) C-NHEJ directly joins DSBs by the formation of a synaptic complex, consisting of two DNA ends, two KU70/KU80 and two DNA-PKcs molecules. Non-compatible DNA ends are processed to form ligatable termini, followed by repair of the break by XRCC4/LIG4 complex (Weterings and Chen, 2008).

1.4 Repair Pathway Selection

Competition between the pathways was the most popular model for how a cell chooses to repair DNA-DSBs by C-NHEJ, B-NHEJ or HR. However, maintenance of genomic integrity requires the interplay of multiple repair pathways. It is noteworthy that the predominant NHEJ pathways act primarily in all cell cycle phases, whereas HR is restricted to the late S and G2 phases based on the availability of sister chromatids, which is the key determinant for selectivity between the two pathways. Based on the biphasic kinetics of repair (Han and Yu, 2008; Iliakis et al., 1991; Kim et al., 2005b; Mao et al., 2008; Metzger and Iliakis, 1991), a partial explanation for how cells choose to repair their breaks is that repair is divided into distinct phases: C-NHEJ represents the rapid phase which starts first, but if it fails, B-NHEJ or HR representing the slower repair phase then follows. In 2011, Jessica Neal and Katheryn Meek proposed that both KU and MRN localize to DSBs perhaps facilitated by an interaction between KU70 and MRE11 (Goedecke et al., 1999), then subsequent activation of ATM and its downstream targets would promote NHEJ by stabilizing the NHEJ synapse. If rapid C-NHEJ fails, MRN would be positioned to promote the slower pathways - either HR or B-NHEJ. Moreover Neal and Meek have proposed an attractive model on how DNA-PK phosphorylation sites can regulate pathway choice: when DNA-PK activation occurs on a single un-synapsed complex (as would occur at a collapsed replication fork) J, K and T phosphorylations would occur, disengaging NHEJ. However, when DNA-PK synapses with another DNA-PK complex, ABCDE and PQR phosphorylations implement the downstream NHEJ factors promoting rapid and appropriate end joining (Neal and Meek, 2011).

Interestingly, the PLX complex, which plays a central role in SSB repair, is also implicated in the repair of DSBs. However, the much higher affinity of KU for DNA ends, which far

exceeds PARP1's, will limit the contribution of B-NHEJ to instances in which the C-NHEJ is compromised (Caldecott, 2001). Moreover, biochemical studies revealed that DNA-PK is a substrate of PARP1. Thus, PARP1 may play a role in controlling DSB repair as it suppresses DNA-PK allowing HR to take the upper hand (Hochegger et al., 2006).

It is important to mention that the common fanconi anaemia (FA) signalling pathway coordinates several aspects of DDR, including end processing, recruitment of HR and TLS repair and cell cycle checkpoint activation to rescue arrested replication (Kennedy and D'Andrea, 2005). For instance, FA nuclear complex FANCD2 might antagonize KU70 activity by processing DNA ends, thereby diverting DSBR away from abortive NHEJ and toward HR (Pace et al., 2010). The phosphorylation of CTIP regulates its end processing activity and thus regulates the choice between HR and NHEJ (Huertas and Jackson, 2009). Interestingly, CTIP has recently been identified as an interacting partner of SIRT6. Moreover, SIRT6 deacetylates CTIP, facilitating its DSBs ends processing and favouring HR (Sun et al., 2010).

Interestingly, DNA-PK can bind and be activated by SSBs (Plumb et al., 1999). In addition, DNA-PK-dependent phosphorylation of XRCC1 has been demonstrated to affect XRCC1 function in living cells, indicating an interplay between BER and DNA-PK (Levy et al., 2006). Furthermore, Professor George Iliakis and colleagues have shown that DNA-PK facilitates repair of non-DSB oxidatively-induced clustered DNA lesions in human cells (Peddi et al., 2010). Taken together, the above mentioned evidences, albeit still with many gaps, highlight that not only DSB repair pathways, but also all the different repair pathways are interconnected in an integrated network.

1.5 Cernnunos/XRCC4-Like Factor (XLF)

XLF is a newly identified core factor of NHEJ, and loss of its function causes a new syndrome of human severe combined immunodeficiency (SCID), characterized by profound T_B lymphocytopenia associated with microcephaly, growth retardation and radiosensitivity (Ahnesorg et al., 2006; Buck et al., 2006).

In fact, the story of *XLF* started in 2003 when Dr. Penny Jeggo's laboratory reported the first patient with novel SCID (Dai et al., 2003). Although the fibroblasts of this patient displayed NHEJ defects, there were no detectable abnormalities in the known genes involved in NHEJ, strongly indicating that an additional core NHEJ factor was missing. In 2006, two research groups independently identified the candidate gene for this human disease. The first group, in France, used functional complementation and isolated the gene mutated in five patients who displayed SCID phenotype with increased radiosensitivity, and named it Cernunnos (an enigmatic Celtic god of the hunt, the underworld, fertility, and possibly more). The clinical phenotype of *XLF*-deficient patients shares several characteristics with *NBS* and *LIG4* deficiency. Although *XLF* deficiency does not lead to impaired cell cycle checkpoints, as observed in NBS condition, it leads to a NHEJ defect, as observed in *LIG4* deficiency (Buck et al., 2006). The second group, in Steve Jackson's laboratory, identified a novel XRCC4-like factor (XLF) by yeast two-hybrid screening and found that this gene was inactivated in the patient reported by Dr. Penny Jeggo's laboratory (Ahnesorg et al., 2006). Then, it was found that Cernunnos and XLF were identical. Although Cernunnos and *XLF* are the most commonly used names for this gene, it has been officially registered in the Gene Bank as nonhomologous end-joining factor 1 (*NHEJ1*).

1.5.1 The Structure of XLF

Human *XLF* consists of eight exons, the first of which is non-coding. It is located on chromosome 2q35 and it has been found ubiquitously expressed in a wide range of tissues (Ahnesorg et al., 2006; Buck et al., 2006). *XLF* has been found to be evolutionarily conserved among eukaryotes (Ahnesorg et al., 2006; Callebaut et al., 2006; Hentges et al., 2006).

XLF protein is composed of 299 amino acids with a molecular weight of 33kDa (Ahnesorg et al., 2006; Buck et al., 2006). Its primary amino acid sequence does not display any known functional domains or motifs, except a nuclear localization signal. In fact, despite the low sequence homology between both XRCC4 and XLF proteins, computational analysis of the tertiary structures of these two proteins has shown that they are significantly similar in terms of structure (Ahnesorg et al., 2006; Callebaut et al., 2006). The crystal structure of XLF, as shown in Figure 1.8, consists of an N-terminal globular head domain followed by a coiled-coil region and C-terminal helices. Its N-terminal head has been found to be structurally similar to that of XRCC4. Moreover, the coiled-coil region provides a tight interaction between two monomers of XLF. Remarkably, its C-terminus adopted a compact folded structure. Whereas the extended C-terminus of XRCC4 possesses the LIG4-binding domain, the folded C-terminus of XLF wraps back towards its N-terminal head. Structural and biochemical analyses demonstrated that XLF forms homodimers, however it does not heterodimerize with XRCC4 under physiological conditions, in spite of their structural similarities (Andres et al., 2007; Hentges et al., 2006; Li et al., 2008).

In fact, the XLF extreme C-terminus 75 amino acids were found to be essential for the DNA binding and the activation of XRCC4/LIG4. The three amino acids, leucine174 (L174),

arginine178 (R178) and leucine179 (L179), residing in the XLF evolutionarily conserved hinge region, were found to be critical for the LIG4 activity, as their substitutions by site-directed mutagenesis abolished the stimulation of the LIG4 activity, whereas mutating them did not affect the association with XRCC4 or DNA (Andres et al., 2007). Moreover, the missense mutations R57G and C123R found in *XLF* defective patients (Buck et al., 2006) were structurally mapped on the surface of the N-terminal globular domain. Interestingly, although the R57G mutant protein has the typical nuclear localization signal (NLS) at its C-terminus, it was retained in the cytoplasm (Lu et al., 2007).

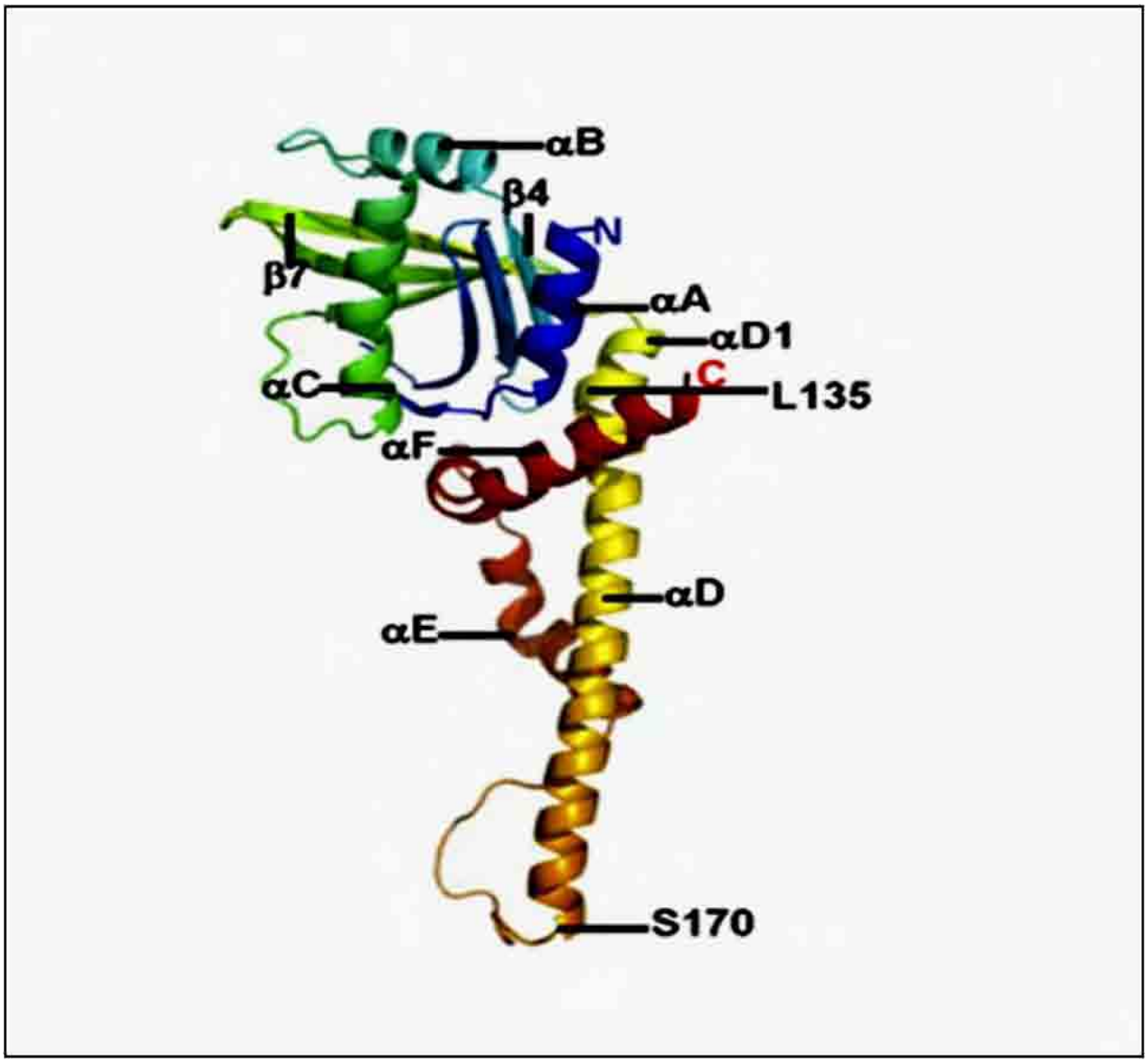

Figure 1.8: XLF crystal structure
XLF consists of an N-terminal globular head that starts at the navy-blue α-helix and C-terminal α-helices that ends at the red α-helix (Li et al., 2008).

1.5.2 The Functions of XLF

It has been found that XLF plays a major role in NHEJ, enhancing XRCC4/LIG4 activity (Hentges et al., 2006). Although XRCC4/LIG4 has been shown to rejoin compatible DNA ends efficiently, and mismatched or incompatible DNA ends to a lesser extent (Gu et al., 2007a), XLF enhanced the ligation of mismatched and noncohesive DNA ends at the physiological concentrations of Mg^{+2} (Gu et al., 2007b; Tsai et al., 2007).

In vitro studies have demonstrated that XLF binds DNA in a DNA-length-dependent manner. XLF binds to 83bp oligonucleotides or longer, however it fails to form a stable complex with 60bp oligonucleotides (Hentges et al., 2006; Lu et al., 2007). Interestingly, although XLF and KU proteins do not associate with each other in the absence of DNA, they do form a stable complex with shorter DNA. This indicates that XLF interacts with KU in a DNA-dependent manner similar to thevKU-DNA-PKcs interaction (Yano et al., 2008).

Also a recent *in vivo* study has shown that XLF responds to DSB induction quickly and starts to accumulate at the damaged site within a few seconds. Although this rapid accumulation was KU-dependent, it was not XRCC4-dependent, providing strong evidence that XLF plays an important role in the first step of NHEJ, sensing DSBs, in addition to enhancing the final ligation step (Yano and Chen, 2008). In fact this study has shaken the traditional assumption that the NHEJ factors are sequentially assembled on DSBs in a step-by-step manner from KU to XRCC4/LIG4. Moreover, it highlights that the assembly of the NHEJ machinery is flexible and the order of recruitment might depend on the nature of DNA-DSBs (Mari et al., 2006; Yano and Chen, 2008).

1.6 KU Complex

KU is a heterodimeric DNA binding protein complex. It consists of two subunits of about 70kDa and 80kDa, known as KU70 and KU80 respectively. This complex was originally identified two decades ago as a major target of autoantibodies from Japanese patients with scleroderma-polymyositis overlap syndrome. It has also been found in subsets of patients suffering from a number of different autoimmune diseases including systemic lupus erythematosus and scleroderma (Mimori et al., 1981).

1.6.1 The Structure of KU Proteins

The molecular structures of both KU70 and KU80 have been elucidated using atomic force microscopy as well as crystallography. Although their sequence-based structural alignment is only 14% identical, KU70 and KU80 are structurally similar (Cary et al., 1997; Walker et al., 2001). Each subunit is composed of an N-terminal α/β domain, a central β-barrel domain and an α-helical C-terminal domain. Both the C-terminal and α/β domain bind to proteins that form the DNA repair complex (Nick McElhinny et al., 2000; Wu and Lieber, 1996). The β-barrel domain binds non-specifically to the sugar-phosphate backbone of DNA. The amino acids from positions 396 to 404 bury themselves into the minor groove of the DNA double helix. The C-terminal helical domain of each KU subunit has important interactions (Myung et al., 1997): they dimerize with the β-barrel domain of the other subunit, KU80 C-terminus associates with a 460kDa DNA-PKcs, possibly controlling its activity, and KU70 C-terminus could have a role in DNA binding during the NHEJ reaction in addition to its role in apoptosis (Cohen et al., 2004a; Koike et al., 1999b; Rivera-Calzada et al., 2007).

KU heterodimers form pseudo-symmetrical basket-like shapes with a preformed ring extending from a broad base. During DNA repair, the two ends of DSBs are threaded through the ring in the KU heterodimer which is formed by intermolecular bridging between specific domains of each subunit (Figure 1.9). The KU heterodimer regulates the action of DNA-PKcs and the other NHEJ core members. The KU heterodimer together with the DNA-PKcs constitute DNA-PK (Cary et al., 1997).

Heterodimerization of KU70 and KU80 is indispensible for the stabilization of each subunit as well as the regulatory function of KU (including activation of DNA-PK) (Jin and Weaver, 1997). Accordingly, failure of KU heterodimerization results in significant decrease in the level of the remaining KU subunit (Errami et al., 1996; Gu et al., 1997; Singleton et al., 1997). Although the absence of the KU80 resulted in the loss of the KU70 (Singleton et al., 1997; Taccioli et al., 1994), it has been found that failure of heterodimerization resulted in intracellular accumulation of both KU70 and KU80 (Tuteja and Tuteja, 2000). Moreover, these two subunits have been found to possess unique functions, independent of each other, as monomers of each subunit have been observed to accumulate in certain cell types. However, the mechanisms involved in their *in vivo* hetero-/homo-dimerization, their functional consequences and/or degradation still need further exploration (Ochem et al., 1997).

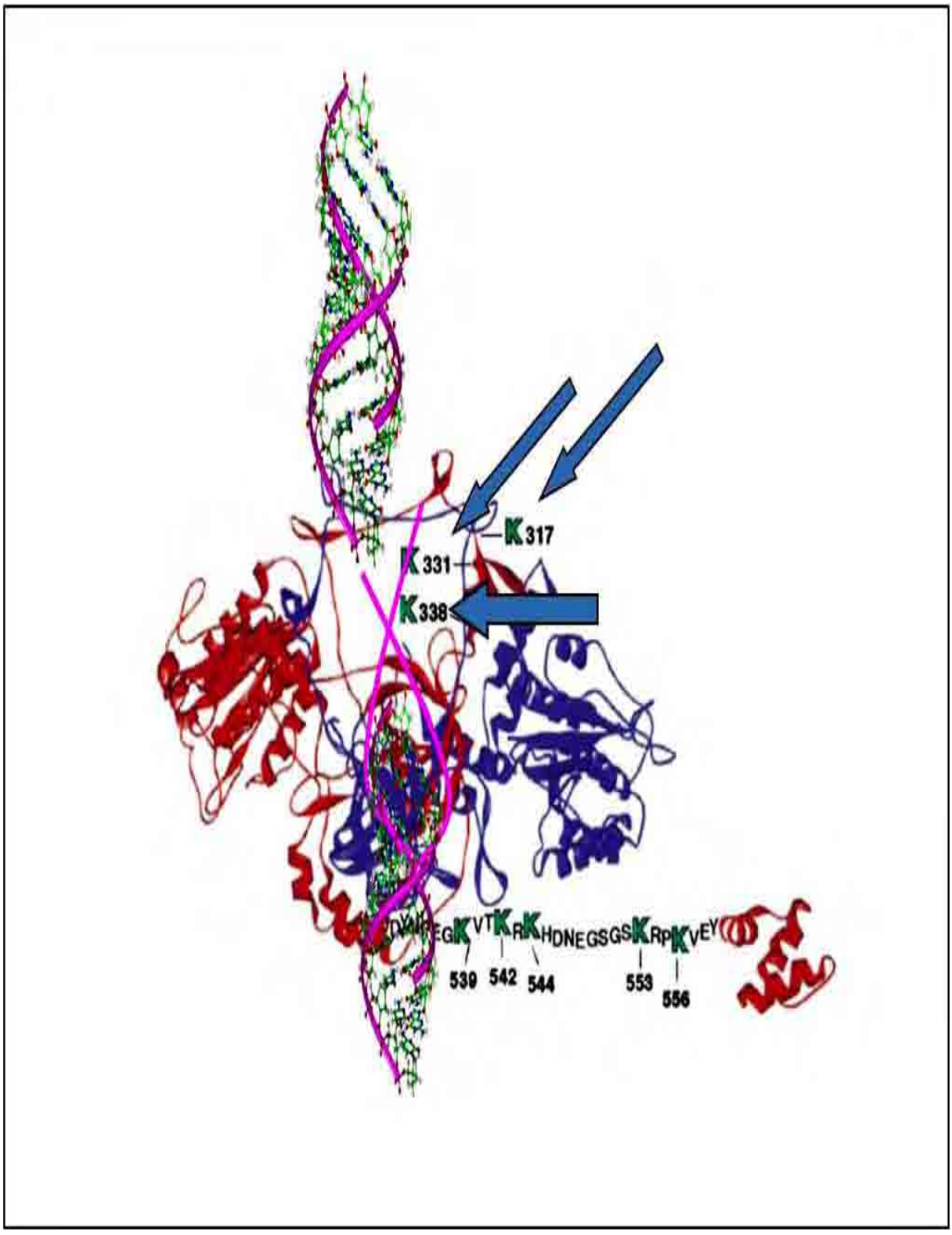

Figure 1.9: KU70/KU80 heterodimer superimposed on broken DNA duplex
KU70 and KU80 subunits are shown in red and blue respectively. Lysine residues in the DNA-binding domain of KU70, which are targeted for acetylation in vivo, are indicated by the blue arrows. The lysine residues of the KU70 C-terminus are superimposed on a ribbon diagram of KU70 based on a crystal structure (Walker et al., 2001).

1.6.2 The Cellular Localisation of KU Proteins

KU proteins are predominantly localized to the nucleus, especially to its transcriptionally active regions. They are components of the nuclear matrix and diffusely distributed in the nucleoplasm (Higashiura et al., 1992; Koike et al., 1999a; Yaneva and Jhiang, 1991; Yu et al., 1998). The NLS of the two subunits are different. Hence, different NLS receptors could be involved in the regulation of KU70 and KU80 nuclear transport (Koike et al., 1999a; Koike et al., 1999b). KU80 NLS belongs to the single-basic type (Taccioli et al., 1994), while KU70 NLS belongs to bipartite-basic type (Koike et al., 1999b). So, nuclear translocation of the two subunits, either NLS-dependent or heterodimerization-dependent, might result in distinct biological functions that may be mediated by the individual subunits either separately or cooperatively.

Interestingly, KU proteins have also been observed in the cytoplasm of several types of cultured human and monkey cells (Bakalkin et al., 1998). Moreover, it has been suggested that the KU heterodimer (but not DNA-PKcs) is present in the cytoplasm but not in the nucleus during mitosis, then dissociates and that the return of KU70 to the nucleus may precede that of KU80 as cells enter the G1 phase of the cell cycle. This indicates that KU70 and KU80 are not always associated and that their nuclear import may occur independently (Koike et al., 1999a; Koike et al., 1999b). Furthermore, KU proteins have been found in the cell membrane of a number of cell types. Although they lack plasma membrane localization signal, they do contain a hydrophobic region, which may facilitate their cell surface expression (Dalziel et al., 1992; Prabhakar et al., 1990). In fact, it has been shown that KU80 protein mobilized from the cytoplasm to the cell surface in multiple myeloma cells could function as a cell adhesion molecule (Teoh et al., 1998).

1.6.3 The Biological Functions of KU Proteins

The KU complex has many functions. It acts as the primary sensor of DNA-DSBs. Moreover, KU, as a complex or as separate subunits, has been implicated in other cellular processes including telomere maintenance, apoptosis, tumour suppression, G2/M checkpoint regulation and transcriptional regulation. Interestingly, they have also displayed more than one enzymatic activity.

1.6.3.1 The Role of KU Proteins in DSBR

KU is absolutely essential for the maintenance of genomic stability. Although both KU proteins and DNA-PKcs bind independently to the DNA ends, the greater part of this function is performed by the KU heterodimer rather than DNA-PKcs itself (Hammarsten and Chu, 1998). In fact, KU heterodimer increases the affinity of DNA-PKcs for DNA ends by several fold, enhancing repair (West et al., 1998). Structural studies suggested that during DNA repair, KU heterodimer brings the broken DNA ends close together, facilitating repair via XRCC4/LIG4. Following successful repair, the release of DNA-PK from the repaired DNA is hypothesized to require proteolysis of the holoenzyme complex. Proteolysis might presumably occur at the exposed bridge-region (Walker et al., 2001; Postow et al., 2008). VDJ recombination, CSR, DNA replication, and HR are physiological processes that involve KU-dependent DSBR (Smith and Jackson, 1999). A recent study showed that mice with mutated KU80 display reduced HR events. Moreover, these mice also exhibit developmental delays (Reliene et al., 2004).

1.6.3.2 The Role of KU Proteins in Telomere Maintenance

The KU complex protects exposed DNA ends from nucleolytic attack and nucleotide loss, especially at the telomeres, as well as at sites of DSBs. KU proteins bind to telomeric sequences (Bianchi and de Lange, 1999; Hsu et al., 1999) and facilitate telomerase mediated synthesis of a complimentary strand of DNA that prevents DNA end-to-end fusion (Bailey et al., 1999; Samper et al., 2000). In fact, the KU heterodimer physically associates with human telomere reverse transcriptase, which is essential for the addition of telomeric repeat sequences (Chai et al., 2002).

1.6.3.3 The Role of KU Proteins in Apoptosis

It has been shown that cytoplasmic KU70 binds to the pro-apoptotic protein BAX and inhibits BAX-mediated apoptosis (Sawada et al., 2003b). This is mediated by the KU70 C-terminus, as mimicking acetylation of K539 and K542 residues blocks the inhibition of BCL-2-associated X protein (BAX) by KU70. Moreover, it has been suggested that, upon apoptotic stimuli, CREB-binding protein (CBP) and P300/CBP-associated factor (PCAF) HATs acetylate KU70, releasing BAX towards the mitochondria, leading to initiation of apoptosis (Cohen et al., 2004a). Interestingly, it has been found that, following apoptotic stimuli, KU70 itself (via its intrinsic deubiquitinase (DUB) activity) deubiquitylates BAX protecting it from proteolysis, and the free cytosolic un-ubiquitylated BAX localizes to the mitochondria initiating apoptosis (Amsel et al., 2008). So, KU70 might possess both pro-apoptotic and anti-apoptotic functions.

1.6.3.4 The Role of KU Proteins in Transcription

It has been claimed that KU proteins could function as transcription factors, as they bind in a sequence-specific manner to promoter elements; for example, KU80 binds to the promoters and regulates the genes of the heat shock proteins (HSP) and glucose-regulated peptide (GRP78 and GRP94) (Giffin et al., 1996; Li et al., 1995; Liu and Lee, 1991). In addition, it has been shown that KU proteins could regulate transcription in a sequence-independent manner, as they associate with RNA POL II elongation sites. Moreover mutant KU80 inhibits transcriptional re-initiation but it has no effect on DNA repair (Mo and Dynan, 2002; Woodard et al., 2001). This indicates that their roles in transcription and repair are separate.

1.6.3.5 The Enzymatic Activities of KU Proteins

It has been observed *in vitro*, that the individual subunits (KU70 and KU80), as well as the heterodimerized complex, possess an ATPase activity. Moreover, the KU70 subunit displays a DNA helicase activity, although its structure does not seem to have domains that contain helicase activity (Ochem et al., 1997). Recent findings have demonstrated that KU70 is associated with the proapoptotic protein BAX and possesses intrinsic DUB activity (Amsel et al., 2008). Also, it has been discovered that KU70 possesses 5'deoxyribose-5-phosphate/abasic lyase (5'dRP/AP lyase) activity that is required for efficient removal of abasic sites at or near the ends of DSBs (Roberts et al., 2010).

1.7 General Objectives:

The work undertaken in this thesis will be discussed in three results chapters. Chapter Three covers SNP analysis of the seven coding exons of *XLF* in a random Caucasian population sample by PCR and sequencing. XLF purification is discussed in Chapter Four. In addition, Chapter Four will describe the characterization of the acetylation status of XLF including mapping XLF *in vitro* acetylation sites by mass spectrometry, XLF acetylation prediction analysis and *in vivo* acetylation study. At the end, Chapter Five includes designing aceto-blocking and aceto-mimicking mutant constructs of *KU70* lysine residues K317, K331 and K338, and creating stable cell lines overexpressing these mutants. Moreover, Chapter Five details the characterization of the effect of mimicking acetylation and deacetylation of KU70 lysine residues K317, K331 and K338 on cell survival and DSBR.

CHAPTER TWO: MATERIALS AND METHODS

2.1 DNA-Related Techniques

2.1.1 Polymerase Chain Reaction (PCR)

Standard PCR was carried out to amplify the seven coding exons of *XLF* from genomic DNA, 94 samples (50% males and 50% females) collected by the West Midlands Regional Genetics Unit, using the designed *XLF* primers (Table 2.1). After several optimization trials, the chosen PCR mixture consisted of 1x PCR buffer (20mM Tris-HCl pH 8.0 and 50mM KCl), 1.5mM $MgCl_2$, 1mM dNTP mixture, 10pM of each primer, 50-100ng of genomic DNA and 1U of *Taq* DNA polymerase (Invitrogen) in a 50µl reaction volume. The PCR reaction was carried out using the following cycling conditions: 95°C for 5 minutes, then 40 cycles of denaturation at 95°C for 30 seconds, annealing at 55°C for 30 seconds and extension at 72°C for 30 seconds.

2.1.2 Agarose Gel Electrophoresis

Agarose gel electrophoresis was used after every PCR to check for the presence and expected size of product. 1% agarose gel was prepared by boiling a mixture of 1.5g of agarose powder in 150ml of 1x Tris borate EDTA (TBE). After cooling to 60°C, 7µl of ethidium bromide was added to a final concentration of 0.4µg/ml in order that the PCR product could be visualised under UV light. Then, the agarose was poured into a gel casting tray with a comb to solidify. After 20 minutes, the comb was removed and the tray containing the agarose gel was placed in a running tank and covered by 1x TBE. 20µl of 1Kb DNA ladder was added to the first well so that the size of the product could be easily estimated. 10µl of each PCR product mixed with 2µl DNA loading dye was loaded into the neighbouring wells lane by lane from the 96 well-plate to keep the order. The gel was then electrophoresed at 180V for 30 minutes and photographed using a UV transilluminator at 260nm wavelength and a camera.

	Forward Primer Sequence	Reverse Primer Sequence
XLF 1st exon	F: 5'ATCAGTGCCCAGGCCCAGAA3'	
XLF 1st intron	F.1: 5'ATGCTCTCTGGGCCTCTA3' F.2: 5'CAGGCTTTGAGGATGGCCAT3' F.3: 5'CATCGATCCCTGAGCGTTTGA3'	
XLF 2nd exon	F: 5'GATACAGACTGGTTTGGGTG3'	R:5'CAACCCGATTCAACCTTC3'
XLF 3rd exon	F: 5'GGGCTTTCCTTTGCTGTT3'	R: 5'AAGACACTCAGTACTCTGCTCC3'
XLF 4th exon	F1: 5'AATGGGTTACTTGCCTATGA3' F2. Nested: 5'CTGGTACCTAATACTGAATTGG3'	R1 : 5'GGTGGCGTGCGTCTACAATC3' R2. Nested: 5'TCTAATGCAAATGAGTCTCCC3'
XLF 5th exon	F : 5'CAGATGCTGCCACCAAAC3' F2: 5'GCACCTTCCTCCTCTTTC3'	R: 5'ACAAGCCACCTAACACCC3'
XLF 6th exon	F: 5'GGTTCTGCATGTGGGGTAT3'	R: 5'CACTTGAAATGTGGCTACTGC3'
XLF 7th exon	F: 5'CCCTGGCCTTTATCAGAAT3'	R: 5'TGAGGCAGTGCCAATGAA3'
XLF 8th exon	F1: 5'CCTAACCAGGAGCCATGAGA3' F2. Nested: 5'GAGCCATGAGAGGAAGAAAGT3'	R1: 5'TTCTTGCTGACTTGCCCTAT3' R2. Nested: 5'CTGGCTTCCACTTGAACA3'

Table 2.1: *XLF* primers sequences
The primers were designed guided by the wild type sequence of *XLF* published in the ensembl genome browser database and according to the general guidelines. The primers were ordered from Invitrogen. The annealing temperature was 55°C for all the listed primers.

2.1.3 DNA Gel Purification

DNA was purified using Wizard QIAquick PCR Purification Columns (Qiagen). The DNA fragment was excised from the agarose gel with a clean scalpel. The gel slices were placed in a clean 1.5ml microcentrifuge tube and weighed. Three volumes of Buffer QG were added to one volume of gel, for example if the gel slice weighed 100mg, 300µl of Buffer QG was added to the tube. Samples were then incubated at 60°C for 10 minutes. To help the gel dissolve, samples were vortexed every 2-3 minutes during the incubation. After the gel slices were completely dissolved, one gel volume of isopropanol was added to each sample and mixed thoroughly (if agarose gel slice was 100mg, 100µl of isopropanol was added to the sample). To bind the DNA, samples were added to a QIAquick centrifuge column, and centrifuged for 1 minute at maximum speed (13,000rpm). The flowthrough was discarded and the QIAquick column was placed back in the same collection tube. To remove all traces of agarose, another 0.5ml of Buffer QG was added to each sample and the QIAquick column was centrifuged for 1 minute at maximum speed. To wash the DNA, 0.75ml of Buffer PE was added to each QIAquick column and centrifuged for 1 minute. The flowthrough was discarded and the samples were centrifuged for an additional 1 minute. The Qiaquick columns were replaced into a clean 1.5ml clean microcentrifuge tube. To elute the DNA, 30µl of elution buffer was added to the centre of each tube, centrifuged for 1 minute at maximum speed. The eluted DNA was stored at - 20°C.

2.1.4 Purification of PCR Products (Exo-SAP)

PCR products were cleaned up by an enzymatic treatment. The Exo-SAP reagent (New England Biolabs) consists of Exonuclease I and Shrimp alkaline phosphatase, to digest excess

PCR primers and to degrade excess nucleotides carried over from the PCR. The PCR products were diluted 5 times and 3µl of the Exo-SAP reagent were added to 10µl of the diluted PCR products. The reactions were incubated at 37°C for 15 minutes followed by 80°C for 15 minutes. This purified DNA was then used in a DNA sequencing reaction.

2.1.5 Cloning PCR Products into pGEM-T-Easy Vector

2.1.5.1 Preparation of Luria-Bertani (LB) Broth

Luria-Bertani (LB) broth was produced by autoclaving distilled water containing 2g of LB broth powder (40% casein peptone, 20% yeast extract and 40% NaCl) per 100ml. Once cooled, the LB broth was stored at 4°C and the antibiotic ampicillin was added to a final concentration of 100µg/ml.

2.1.5.2 Preparation of Luria-Bertani (LB) Agar Plates

The LB plate mix was produced by autoclaving distilled water containing 2g of LB powder (40% casein peptone, 20% yeast extract and 40% NaCl) and 1.5g of select agar per100ml. The agar was allowed to cool before the addition of ampicillin to a final concentration of 100µg/ml. Plates were poured, allowed to set and stored at 4°C.

2.1.5.3 Ligation Reaction

Briefly, the ligation reaction was performed using 2µl of linearized pGEM-T-Easy vector (for vector map see Figure 2.1), 3µl of PCR products, 1U of T4 DNA ligase (Promega), 2µl of ligase buffer and the final volume was made up to 10µl with distilled H_2O. The mixture was incubated at room temperature for 1 hour.

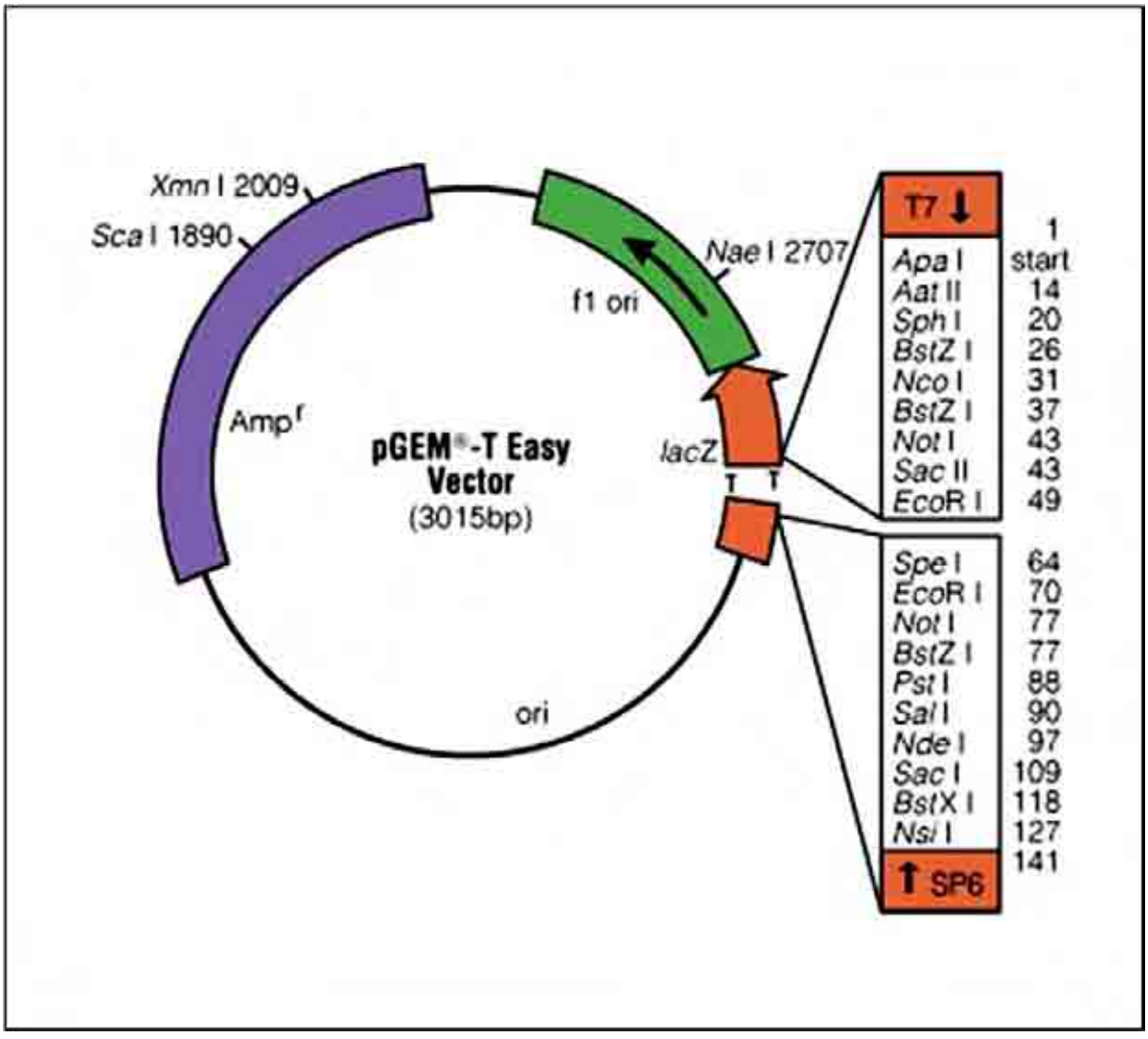

Figure 2.1: pGEM-T-Easy plasmid map
pGEM-T-Easy is a plasmid used to clone A-tailed PCR fragments. The plasmid is supplied in linear form and becomes circularized upon insertion and ligation of PCR products. The multiple cloning sites (MCS) contains many restriction sites including the double EcoRI site which can be used in a single digest to excise any inserted DNA out of the plasmid.

2.1.5.4 Bacterial Transformation by Heat Shock

Transformation reactions were performed using 50µl aliquots of DH5α (Invitrogen) competent E. coli, which were left to thaw out on ice. For each transformation reaction, 20µl of bacteria were mixed with 2µl of the ligation reaction. Then, the reactions were incubated on ice for 30 minutes to stabilize the bacteria. The E. coli was subjected to a heat shock at 42°C for 45 seconds followed by immediate cooling on ice for 2 minutes. Room temperature super optimal broth with catabolite repression (SOC) medium (250µl) was then added before incubation at 37°C with shaking at 220rpm for 1 hour. The transformed bacteria was spread onto 2 LB agar plates supplemented with 100µg/ml of the antibiotic ampicillin together with 100µl of 100mM IPTG (isopropyl-beta-D-thiogalactopyranoside) and 20µl of X-gal (5-bromo-4-chloro-3-idolyl-alpha-D-galactopyrinoside), to allow screening for the presence of inserts. The plates were incubated at 37°C for 18 hours. White colonies were selected from the plates. Every single selected colony was allowed to grow up into 5ml of LB broth and incubated in a shaking incubator at 37°C overnight.

2.1.5.5 Plasmid DNA Extraction

Plasmid DNA was extracted using a plasmid miniprep kit (Qiagen). Minipreps were prepared according to manufacturer's instructions. Briefly, after culturing a single colony in 5ml LB broth, containing the appropriate selective antibiotic, for 20 hours at 37°C in a shaking incubator at 220rpm, the bacterial cells were harvested by centrifugation at 13,000rpm for 2 minutes. The supernatant was discarded and the bacterial pellet was completely resuspended by addition of 250µl of buffer P1 (50 Tris-HCl, PH 8.0; 10mM EDTA; 100µg/ml RNase A) and vortexing. Then, 250µl of lysis buffer P2 (200mM NaOH; 1% SDS (W/V) was added and mixed gently by inversion. Bacterial genomic DNA, proteins, cell debris and lysis buffer SDS

were precipitated by addition of 350µl of neutralization buffer P3 (3.0M Potassium Acetate, pH 5.5). The mixture was mixed by inversion and centrifuged at 13,000rpm for 10 minutes. The supernatant was collected and added to a QIAquick centrifuge column before centrifugation at 13,000rpm for 1 minute. The column was washed by the addition of 750µl of buffer PE and centrifuged at 13,000rpm for 1 minute. The plasmid DNA was then eluted with 30µl of elution buffer and centrifugation at 13,000rpm. The plasmid preparation was then visualized by agarose gel electrophoresis.

2.1.6 DNA Sequencing Reaction

Direct sequencing of the PCR products and plasmid DNA was performed using the ABI Prism Big Dye Terminator DNA Sequencing kit version 3.1. (Applied Biosystem). The primers listed in Table 2.1 were used for sequencing *XLF*, whereas those listed in Table 2.2 were used for sequencing all the plasmids used throughout this thesis. The sequencing reaction consisted of 1µl PCR product or plasmid DNA, 4µl of Big-Dye buffer (25mM Tris-HCl pH8.7, 4mM MgCl2), 2µl of Big-Dye, 1µl of forward or reverse primer and 12µl distilled water. The sequencing reaction was carried out using the following conditions: 95°C for 2 minutes, then 35 cycles of denaturation at 95°C for 30 seconds, annealing at 50°C for 30 seconds and extension at 60°C for 4 minutes.

2.1.7 Ethanol Precipitation of DNA

After the sequencing reaction, the DNA was precipitated by adding 60µl of 100% ethanol and 3µl of 3M sodium acetate (NaAc) pH 5.2, vortexing and incubation at room temperature for 5 minutes. Samples were then centrifuged at 13,000rpm for 30 minutes. Supernatant liquid was discarded and 60µl of 70% ethanol was added, samples were then vortexed and centrifuged at

13,000rpm for 30 minutes. The supernatant liquid was removed and washing with 60µl of 70% ethanol was repeated. To dry pellets, samples were kept at 95°C for 5 minutes.

2.1.8 Sequencing Analysis

Ten microlitres of Hi-Di formamide (Applied Bioystems) was added to each sequencing reaction using the multi-channel pipette. The reactions were denatured at 95°C for 3-5 minutes and then rapidly cooled on ice. The reactions were sequenced on the ABI-3730 DNA capillary sequencer (Applied Bioystems). The results were analysed and printed out using the ABI sequencing analysis v5.2 software. Bioedit alignment software was used to analyse sequence changes in comparison to the wild type sequence published in the ensembl database.

	Forward Primer	Reverse Primer
M13/pUC	5'CCCAGTCACGACGTTGTAAAACG3'	5'AGCGGATAACAATTTCACACAGG3'
N-CMV	5'AATGTCGTAATAACCCCGCCCCGTTGACGC3'	3'TATTAGGACAAGGCTGGTGGGCAC5'
T7 Promoter	5'TAATACGACTCACTATAGGG3'	5'GCTAGTTATTGCTCAGCGG3'
pGEX	5'CCGGGAGCTGCATGTGTCAGAGG3'	5'GGGCTGGCAAGCCACGTTTGGTG3'

Table 2.2: Plasmid primers for sequencing
Listed primers were used for sequencing all the plasmids used throughout this thesis. M13/pUC forward and reverse primers were used for sequencing pGEM-T-easy vector and pFastBac-TH-b, whereas N-CMV-30 as a forward and N-CMV-24 as a reverse were used for sequencing pFLAG-CMV4 vector. T7 promoter primers and pGEX primers were used for sequencing pET-28a and pGEX-2TK-p plasmids respectively.

2.1.9 Creating Wild Type Constructs

2.1.9.1 First-Strand cDNA Synthesis

First-strand cDNA was synthesized using Thermoscript Reverse Transcriptase (Invitrogen). Samples were set up in duplicate; one sample was used to synthesize cDNA whilst the other was used as a control. No thermoscript enzyme was added to the control, therefore any products observed from this sample might be due to contaminating genomic DNA. Briefly, 2µl of 50µM oligo$(dt)_{20}$, 5µg of total RNA (2µl) and 2µl of 10mM dNTP mix were added to a nuclease free microcentrifuge tube and made up to 13µl with ultra-pure/RNase free sterile distilled water. The mixture was then heated to 65°C for 5 minutes and then placed on ice for at least 1 minute. Following this, 4µl of 5x first-strand buffer, 1µl of 0.1M DTT, 1µl of ultra-pure/RNase free sterile distilled water and 1µl of thermoscript RT (15U/µl) were added to the microcentrifuge tube. For control reactions, a further 1µl of ultra-pure/RNase free sterile distilled water was added. The tubes were incubated at 50°C for 60 minutes. Then the reaction was inactivated by incubation at 85°C for 15 minutes. In order to verify cDNA synthesis, PCR was carried out by the housekeeping gene glyceraldehyde-3-phosphate dehydrogenase (GAPDH) forward and reverse primers and the PCR products were electrophoresed.

2.1.9.2 Proofreading PCR of *KU70* and *KU80* wild type cDNA

Primers listed in Table 2.3 were designed with end-incorporated restriction sites (NotI and BamHI restriction sites for *KU70* and BamHI and HindIII restriction sites for *KU80*) to subclone *KU70* and *KU80* wild type cDNAs in frame into pFlag-CMV-4 vector. Simply, the proofreading PCR was set up by adding 2µl of first-strand cDNA,

1µl of each 50µM *KU70* or *KU80* wild type forward and reverse primers (1µM final concentration), 0.5µl of failsafe PCR enzyme mix (1.25U) (Epicentre) and 21.5µl sterile distilled water into a PCR tube then 25µl of failsafe PCR 2X premix were added to a final reaction volume of 50µl. The PCR reaction was carried out using the same conditions as described in Section 2.1, but the extension time was 1 minute/1kb of expected product. The PCR products were electrophoresed. The bands corresponding to *KU70* and *KU80* (2kb and 2.2kb respectively) were cut out of the gel with a clean scalpel and gel purified. Then the gel purified products were cloned into pGEM-T-Easy, transformed into E. coli, and minipreped. The minipreps were sequenced to verify the wild type sequence. Then glycerol stocks were made from the wild type clones.

	Forward Primer	Reverse Primer
KU70/wt	F.(NotI): 5'GCAG-GCGGCCGC-T-ATGTCAGGGTGGGAGTCATA3'	R.(BamHI): 3'GCAG-GGATCC-TCAGTCCTGGAAGTGCAAGG5'
	F.(BamHI): 5'GCAG-GGATCC-ATGTCAGGGTGGGAGTCATA3'	R.(XhoI): 3'GCAG-CTCGAG-TCAGTCCTGGAAGTGCTTGG5'
	Internal F1: 5'ATGCACCTGAAGAAACCTGG3' Internal F2: 5'CCGCAGGAACATCCCTCCTTAT3'	Internal R1: 3'CCTGTGGCACCAAAGCCAC5' Internal R2: 3'GGATATGTCAAAGCCCCCAGGT5'
KU80/wt	F.(HindIII): 5'GCAG-AAGCTT-ATGGTGCGGTCGGGGAATAA3'	R.(BamHI): 3'GCAG-GGATCC-CTATATCATGTCCAATAAAT5'
	F.(BamHI): 5'GCAG-GGATCC-ATGGTGCGGTCGGGGAATAA3'	R.(HindIII): 3'GCAG-AAGCTT-CTATATCATGTCCAATAAAT5'
	Internal F1: 5'CCTTTCGCTTAGGTGGCCATG3' Internal F2: 5'GATGATGAGGCAGCTGCAGTTGC3' Internal F3: 5'CATGAAGATGGACCTACAGC3'	Internal R1: 3'CTGAGCAGTCACTTGATCCT5' Internal R2: 3'CCTTTAGAACTTGATTTCCCATG5' Internal R3: 3'CGAAAGGGGCCATCTCCTCTGTC5'

Table 2.3: *KU70* and *KU80* cloning and sequencing primers
The forward primer with NotI and the reverse with BamHI were used for cloning *KU70*/wt into pFlag-CMV-4, whereas and the forward primer with BamHI and the reverse with XhoI were used for cloning *KU70*/wt into pET-28a. The forward primer with HindIII and the reverse with BamHI were used for cloning *KU80*/wt into pFlag-CMV-4, whereas the forward primer with BamHI and the reverse with HindIII were used for cloning *KU80*/wt into pET-28a. The internal primers were used for sequencing the full length of *KU70* and *KU80* bidirectionally. For the wild type sequence of *KU70* and *KU80* see Appendices 2 and 3.

2.1.10 Restriction Digestion

The KU70 cDNA was double digested with NotI and BamHI restriction endonucleases, whereas HindIII and BamHI were used for double digestion of KU80 cDNA, to create sticky ends. All the restriction endonuclease enzymes were ordered from New England Biolabs. All the restriction digests were performed in a total volume of 30µl: 3µl 10x buffer, 3µl 10x bovine serum albumin (BSA), 1µl of each restriction enzyme, 10µl of PCR product or of plasmid DNA and 12µl distilled H_2O. Buffer 2 was used for all the enzyme combinations in this thesis, but buffer 3 was used for NotI and BamHI double digestion, to achieve optimal enzyme activity. All the restriction digests were incubated at 37°C for 4 hours. The digested products were electrophoresed and the bands were gel purified (Section 2.1.5).

2.1.11 Cloning of the Wild Type Constructs into pFlag-CMV-4 Vector

The gel purified wild type *KU70* and *KU80* wild type were ligated into gel purified pFlag-CMV-4 (Figure 2.2), double digested with the same enzymes to get the insert in frame. E. coli was transformed with the ligated products. Individual colonies were selected and grown in 5ml LB broth overnight and minipreps were double digested with the same enzymes to check for the presence of the inserts. Plasmid DNA was stored at -20°C for transfecting MRC5VA cells. Glycerol stocks were made from the clones that contained the wild type inserts.

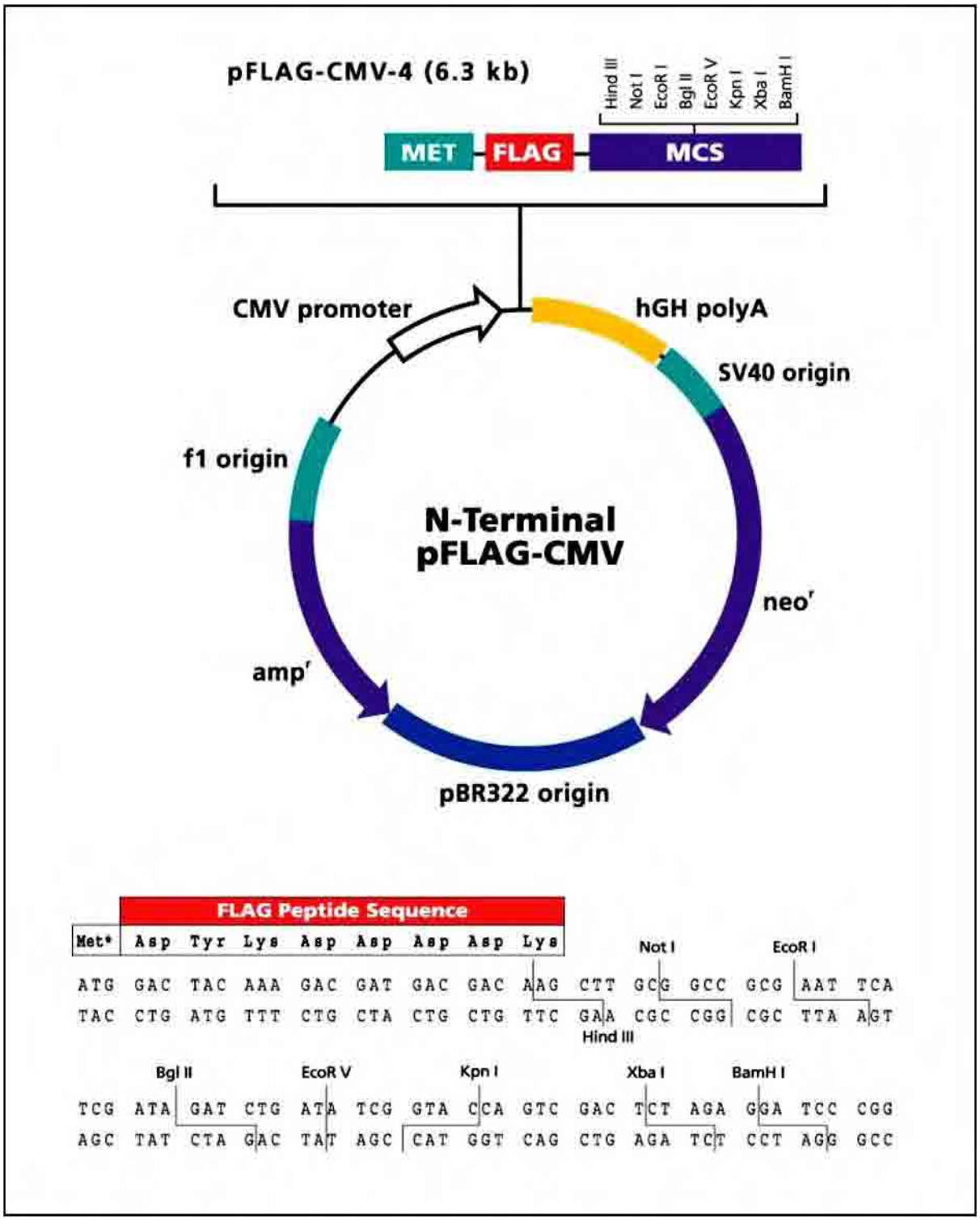

Figure 2.2: pFLAG-CMV-4 plasmid map
pFlag-CMV-4 is a mammalian expression vector which adds the Flag peptide sequence (DYKDDDDK, red filled box) at the amino terminus of the cloned gene. *KU70* wild and mutants were cloned into pFlag-CMV-4 by using NotI and BamHI restriction enzymes, whereas *KU80* wild was cloned into the same vector by using HindIII and BamHI restriction enzymes. pFlag-CMV-4 contains both the ampicillin resistance gene and geneticin (G418) resistance gene for selection in both bacteria and mammalian cells respectively.

2.1.12 Site-Directed Mutagenesis (SDM)

To change each of the *KU70* lysine residues K317, K331 and K338 to arginine and glutamine, two complementary primers containing the desired mutation in the middle of the primer (Table 2.4) were designed. Then the QuickChange II XL Site-Directed Mutagenesis Kit (Stratagene) was used as described below in a rapid three-step procedure.

2.1.12.1.1 Mutant Strand Synthesis

The reaction mixture consisted of 5µl of 10x PfuUltra buffer, 125ng of each primer, 10nmoles of dNTPs, 2ng of template DNA and 1µl of proofreading DNA polymerase (2.5U/µl) in a total volume made up to 50µl with water. PCR reaction was carried out using the following cycling conditions: 95°C for 5 minutes, then 18 cycles of denaturation at 95°C for 50 seconds, annealing at 60°C for 30 seconds and extension at 68°C for 1 minute/1kb of expected product. The PCR products were electrophoresed.

2.1.12.1.2 Dpn I Digestion

One microlitre of the Dpn I restriction enzyme (10U/µl) was directly added to each amplification reaction and each reaction mixture was gently and thoroughly mixed by pipetting the solution up and down several times. Then, the reaction mixtures were centrifuged at 13,00rpm for 1 minute and the reactions immediately incubated at 37°C for 1 hour to digest the parental (non-mutated) supercoiled dsDNA.

2.1.12.1.3 Transformation of XL10-Gold Ultracompetent Cells

The XL10-Gold ultracompetent cells were transformed with 2µl of the Dpn I-treated DNA. Two microlitres of beta mercapto-ethanol (β-ME) were added to the 10µl of cells. Minipreps of the selected clones were sequenced to verify that the insert of interest contained the desired mutation. Finally, the inserts containing the desired mutation were religated into fresh gel purified pFlag-CMV-4 plasmid to take away any misincorporated bases in the vector backbone that could have been introduced during the SDM PCR. Then, the ligation products were retransformed, minipreped and double digested again with the above mentioned enzymes to check for the presence of the insert. Glycerol stocks were made and stored at -80°C. Plasmid DNA was stored at -20°C for transfecting MRC5VA.

	Forward Primer	Reverse Primer
KU70-K317R	5’CTGCCTAGCGATACCAGGAGGTCTCAGATC3’	3’GATCTGAGACCTCCTGGTATCGCTAGGCAG5’
KU70-K317Q	5’CTGCCTAGCGATACCCAGAGGTCTCAGATC3’	3’GATCTGAGACCTCTGGGTATCGCTAGGCAG5’
KU70-K331R	5’CGTCAGATTATACTGGAGAGAGAGGAAACAGAAGAGC3’	3’GCTCTTCTGTTTCCTCTCTCTCCAGTATAATCTGACG5’
KU70-K331Q	5’CGTCAGATTATACTGGAGCAAGAGGAAACAGAAGAGC3’	3’GCTCTTCTGTTTCCTCTTGCTCCAGTATAATCTGACG5’
KU70-K338R	5’GAAACAGAAGAGCTAAGACGGTTTGATGATCCAGG 3’	3’CCTGGATCATCAAACCGTCTTAGCTCTTCTGTTTC5’
KU70-K338Q	5’GAAACAGAAGAGCTACAACGGTTTGATGATCCAGG 3’	3’CCTGGATCATCAAACCGTTGTAGCTCTTCTGTTTC5’

Table 2.4: *KU70* SDM primers
Listed are the primers that were designed and used for replacing the *KU70* wild type lysine (K) residues *KU70-K317*, *KU70-K331* and *KU70-K338* with arginine (R) and glutamine (Q) by site-directed mutagenesis PCR. Replacing the wild type lysine with arginine mimics deacetylation, whereas replacing the wild type lysine with glutamine mimics acetylation. The triple codons of arginine and glutamine are highlighted in purple and red respectively. The triple codons of the *KU70* wild type lysine residues *KU70-K317R*, *KU70-K331R* and *KU70-K338R* are highlighted in green in Appendix 3.

2.1.13 Cloning the Wild Type and Mutant Constructs into pET-28a

Using another set of primers designed with end-incorporated restriction sites (BamHI and XhoI restriction sites for *KU70*/wt and *KU70*/mutants and HindIII and BamHI restriction sites for *KU80*) (Table 2.3), proofreading PCRs were performed to amplify *KU70*/wt, *KU80*/wt and *KU70*/mutants from pFlag-*KU70*/wt, pFlag-*KU80*/wt (Section 2.1.11) and pFlag-*KU70*/mutant plasmids (Section 2.1.12) as templates. The PCR products were electrophoresed, gel purified, ligated into pGEM-T-Easy, transformed into E. coli and minipreped. Then, the minipreps were sequenced to verify the sequence. The PCR products were electrophoresed. The bands corresponding to *KU70*/wt, *KU80*/wt and *KU70*/mutants were gel purified. Then the gel purified products were cloned into pGEM-T-Easy, transformed into E. coli, and plasmid minipreps made. The minipreps were sequenced. Then glycerol stocks were made from the clones containing the desired sequence. The plasmid DNA with the desired sequence was double digested with the aforementioned enzymes. The digested products were gel purified.

2.1.13.1 Subcloning of the Wild Type and Mutant Constructs into pET-28a

The gel purified products in the previous section were ligated into pET-28a expression vector (for vector map see Figure 2.3) which was double digested with the same restriction enzymes to create sticky ends and allow in frame insertion with the amino-terminal poly-histidine tag. The ligated products were transformed into competent E. coli. Selected colonies were minipreped and the pET-28a plasmids DNA were double digested with the same enzymes to check for the presence of the desired inserts. Then, glycerol stocks were made from the clones containing the desired inserts. The plasmid DNA was stored at -20°C.

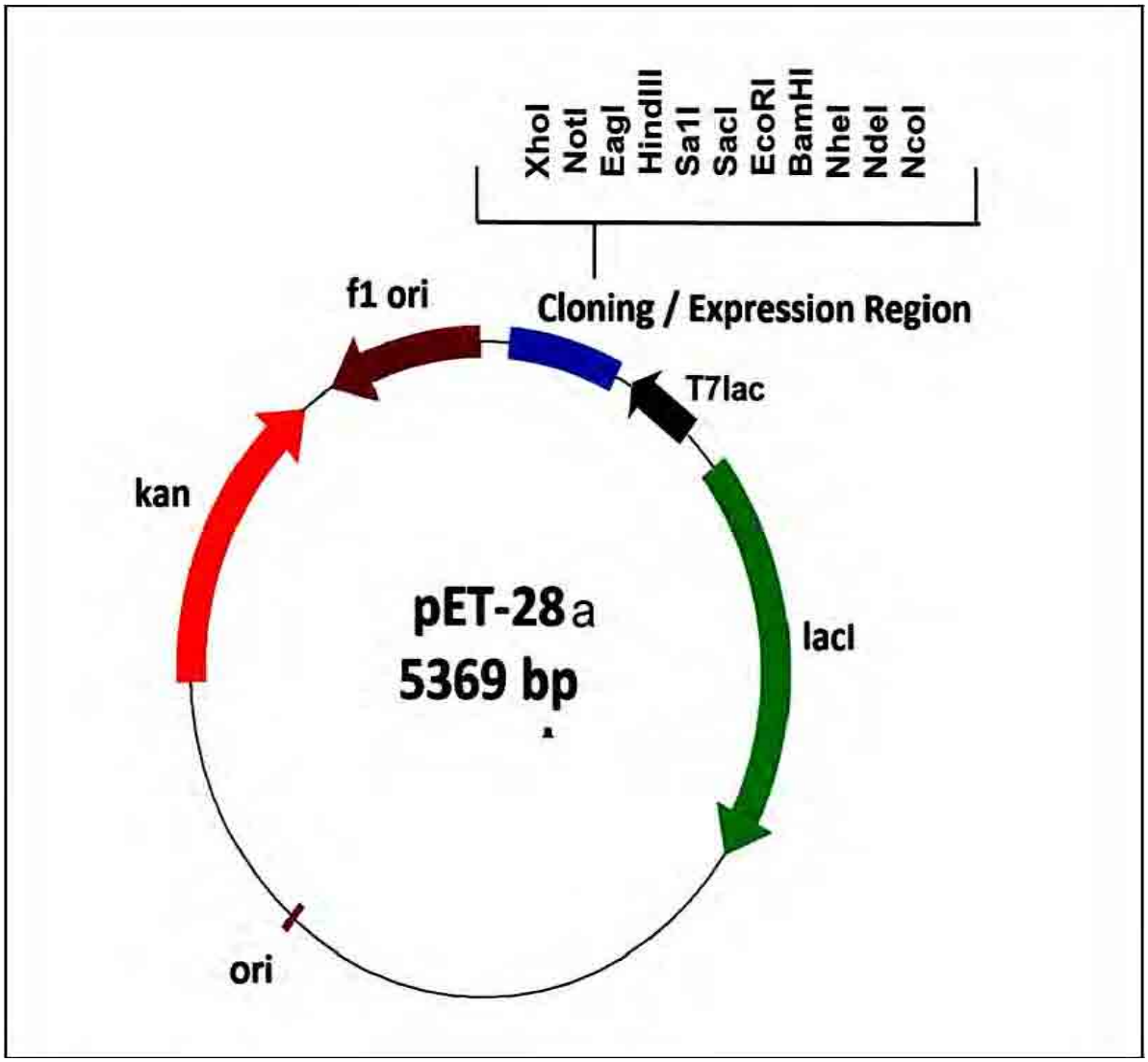

Figure 2.3: pET-28a plasmid map
pET-28a is a protein expression plasmid. *KU70* wild and mutants were cloned into it by using BamHI and XhoI restriction enzymes, whereas *KU80* wild was cloned into the same vector by using BamHI and HindIII restriction enzymes. The pET-28a vector carries an N-terminal his-tag/thrombin/T7-promoter, in addition to an optional C-terminal his-tag sequence. Note, a stop codon has been added to the end of each insert, so that the C-terminal his-tag was not expressed.

2.1.14 Generation of Recombinant Bacmid

The *KU70*/wt, *KU80*/wt and *KU70*/mutant constructs that were previously cloned into the pET-28a vector were double digested out of the pET-28a vector using BamHI and XhoI, gel purified and ligated in frame into pFast-Bac-HTb (Invitrogen), for vector map see (Figure 2.4). The ligated products were transformed into E. coli, minipreped and the inserts were checked by double digestion of the pFast-Bac-HTb using the same enzymes and electrophoresis. The pFast-Bac-HTb plasmids were used as donor plasmids for trasposition of the aforementioned constructs into bacmid DNA. The pFast-Bac-HTb plasmid DNA was transformed into DH10Bac cells (Invitrogen). DH10Bac frozen competent cells were thawed out on ice and 20µl aliquot of the cells dispensed into a 1.5ml microcentrifuge tube pre-chilled on ice. To this, 1µl of diluted (1:10) recombinant pFast-Bac-HTb donor plasmid DNA was added and gently mixed. This mixture was incubated on ice for 30 minutes, followed by heat shock at 42ºC for 45 seconds. The tubes were chilled on ice for 2 minutes and 980µl aliquot of SOC medium was added into each tube. The resulting bacterial suspension was incubated at 37°C for 3 hours, diluted and spread on LB agar plates (containing 50µg/ml kanamycin, 7µg/ml gentamicin, 10µg/ml tetracycline, 100µg/ml Bluo-gal and 40µg/ml IPTG). The plates were incubated for 48 hours at 37°C. The recombinant bacmid colonies were selected by antibiotics and blue white screening. Selected colonies were inoculated into 5ml LB medium supplemented with the same antibiotic and incubated at 37°C for 24 hours with shaking at 250rpm. 1.5ml of cultured cells was transferred into a clean microcentrifuge tube and pelleted by centrifugation.

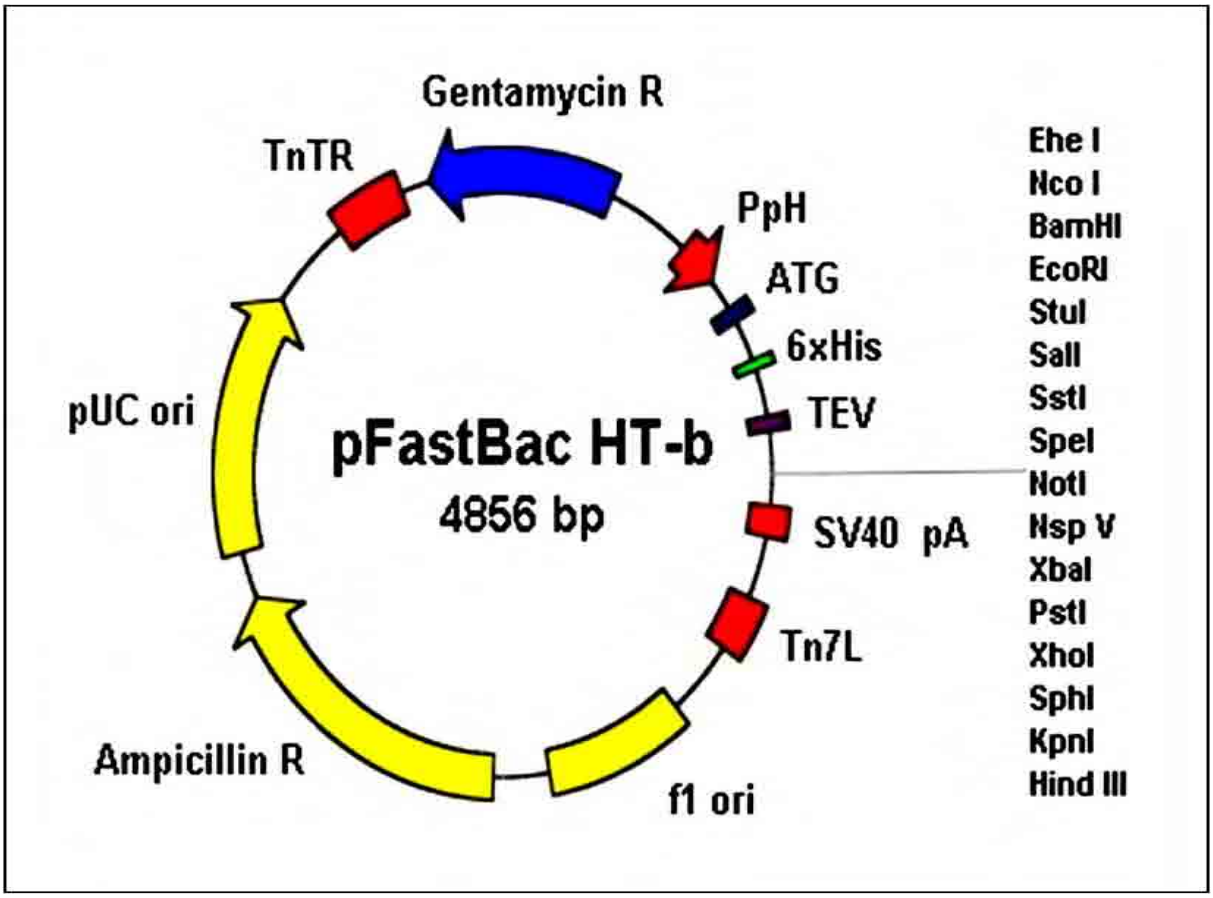

Figure 2.4: pFast-Bac-HTb plasmid map
pFast-Bac-HTb is a mammalian protein expression plasmid. *KU70*/wt, *KU70*/mutants and *KU80* wild were cloned into it by using BamHI and XhoI restriction enzymes. The pFast-Bac-HTb has a strong polyhedrin (P_H) promoter for high-level protein expression, an N-terminal 6xHis-tag for purification of recombinant fusion proteins using metal-chelating resin and a TEV protease cleavage site for removal of the 6xHis-tag following protein purification. Note, a stop codon has been added to the end of each insert.

2.1.14.1 Isolation of Recombinant Bacmid DNA

The pellets prepared in the previous step were resuspended in 200µl of solution I (15mM Tris-HCl pH 8.0, 10mM EDTA, 100µg/ml Rnase A) by vortexing. To this, 200µl of solution II (0.2N NaOH, 1% SDS) was added with gentle mixing. Each tube was incubated at room temperature for 5 minutes followed by slow addition of 150µl of potassium acetate (3M, pH 5.5). The mixture was placed on ice for 5 to 10 minutes. The tubes were then centrifuged for 5 minutes at 14,000 rpm and the resulting supernatant was transferred to another tube containing equal volumes of phenol and chloroform. Then, the tubes were gently inverted a few times to mix and placed on ice for 5 to 10 minutes, followed by centrifugation for 15 minutes at 13,000rpm. After centrifugation the supernatant was removed and the DNA pellet was washed with 0.5ml of 70% ethanol. The DNA was then pelleted again by centrifugation for 5 minutes at 13,000rpm. The resulting pellet was air-dried at room temperature for 5-10 minutes. The DNA was dissolved in 50µl Tris EDTA (TE) (pH 8.0). The bacmid DNA solutions were stored at -20°C. As the verification of the insertion of DNA of interest is difficult using classical restriction digestion, PCR was performed using M13 forward and M13 reverse primers. The PCR products were electrophoresed to check the size of the expected products.

2.2 Tissue Culture Techniques

All solutions and equipment used in cell maintenance were either obtained sterile or autoclaved, where appropriate, prior to use. All cell culture work was undertaken in sterile conditions in a class 2 tissue culture hood (Holten LaminAir). Cells were maintained in a humidified chamber (37°C, 5% CO2, 95% O2; MCO-15AC, Sanyo) in 75cm^2 cell culture flasks (Corning) containing 10ml of complete cell culture media (as described below).

2.2.1 Preparation of Cell Culture Media

Complete cell culture medium was prepared by using Dulbecco's modified Eagle's Medium (DMEM), 1000mg/L glucose, supplemented with 10% (v/v) foetal bovine serum (FBS), 2mM L-glutamine, 5% non-essential amino acids, 5% sodium pyruvate and 100units/ml penicillin. All media and solutions used for cell culture were ordered from PAA Laboratories, prewarmed to 37°C prior to use in a clean water bath.

2.2.2 Revival of Cells from Liquid Nitrogen

Cryovials of MRC5VA, embryonic human lung fibroblast cells which have been immortalised by SV40 transformation as a control, pFlag-XLF, pFlag-XRCC4 and pFlag-HDAC3 overexpressing cell lines (laboratory stocks provided by Dr Darren Arbon)**,** were removed from liquid nitrogen and placed immediately in a 37°C water bath for ~1 minute. The entire 1ml of cells in freezing media was slowly dripped into a flask already containing 10ml of complete DMEM for MRC5VA and complete DMEM supplemented with G418, 600µg/mL, for pFlag-XLF, pFlag-XRCC4 and pFlag-HDAC3 overexpressing cell lines. Cells were placed in a 37°C incubator to seed.

2.2.3 Subculturing Cells

Cells were seeded at ~2x10^5cells/flask and routinely passaged on day 3. Upon reaching confluence, adherent cells were passaged by aspirating media from the flask using a sterile pipette, washing with 10ml of prewarmed phosphate buffered saline (PBS; 2.7mM KCl, 137mM NaCl, 10mM phosphate buffer, pH 7.4, Sigma). PBS was then aspirated and replaced with 3ml of 1x trypsin-EDTA (0.25%:0.02%), prewarmed at 37°C (PAA Laboratories). Flasks were then placed in a humidified chamber until the cells detached from the bottom (~3 minutes), sometimes requiring gentle agitation. Following detachment, 7ml of supplemented DMEM was added and the cell suspension gently mixed using a sterile pipette in order to inactivate trypsin. The suspension was subsequently transferred into a 15ml centrifuge tube (Falcon) and centrifuged at 1500rpm for 5 minutes at 20°C. The supernatant was then carefully aspirated without disturbing the pellet. The cell pellet was then either reseeded or frozen.

2.2.4 Cell Counting

After trypsinisation, the 10ml of complete DMEM was gently pipetted up and down several times to ensure that cells were in suspension. 20µl of cell suspension was added to the chamber of the haemocytometer beneath the cover slip. Cells were counted within the marked counting grid of the haemocytometer, the average of 2 squares was calculated and the figure multiplied by 10^4 to give the number of cells per ml.

2.2.5 Cell Reseeding

Trypsinised cell pellets were resuspended in 5ml of supplemented DMEM and a 500µl aliquot transferred to a 75cm^2 cell culture flask containing 10ml of supplemented DMEM. The flask was then gently agitated to ensure an even distribution of the cells, and then placed in a humidified chamber and allowed to grow to confluence (~ 3 days)

2.2.6 Cell Cryopreservation and Storage in Liquid Nitrogen

Cells were firstly removed from the adherent flask surface as described above and collected by centrifugation for 5 minutes at 1500rpm and resuspended in 2ml FBS containing 10% (v/v) dimethylsulphoxide (DMSO) as a cryoprotectant. The cell suspension was then separated between 2 cryovials (Nunc) and placed in a cryogenic freezing vessel, Mr. Frosty (Nalgene). The container was then stored for 24 hours at -80°C, after which the cryovials were removed and placed into liquid nitrogen for long-term storage.

2.2.7 Creating Stable Cell Lines

2.2.7.1 Transfection of MRC5VA Cell Line

MRC5VA cell line was transfected with the pFlag-*KU70*/wt, pFlag-*KU80*/wt and pFlag-*KU70*/mutants (pFlag-*KU70-K317R*, pFlag-*KU70-K331R*, pFlag-*KU70-K338R*, pFlag-*KU70-K317Q*, pFlag-*KU70-K331Q* and pFlag-*KU70-K338Q*) using three transfection reagents: FuGENE 6, FuGENE HD and Lipofectamine 2000 as described in the following sections.

2.2.7.1.1 Transfection of MRC5VA Cell Line Using FuGENE 6 and FuGENE HD

FuGENE 6 and FuGENE HD transfection reagents (Roche) are multi-compound lipid based transfection reagents that complex with DNA and transport it into the cell during transfection. They provide very high transfection efficiency and demonstrate low toxicity in many cell types. On the day of transfection cells were 60-70% confluent. For each transfection, 6µl of FuGENE reagent was added directly to 194µl of serum free media and mixed gently to avoid the contact of undiluted FuGENE reagent with the plastic surface of the centrifuge tube. Then, 2µg of the plasmid was added to the above mixture and mixed gently (the ratio of FuGENE: DNA was always 3:1). The mixture was incubated for 30 minutes at room temperature, meanwhile the media on the 6-well plate was changed and cells were incubated at 37°C for 15 minutes. The 200µl of FuGENE-DNA mixture was added to each well drop wise. The wells were swirled to ensure even dispersal of the transfection mixture. The cells were then incubated at 37°C for 24-48 hours. After 48 hours, the media was aspirated and replaced with G418-supplemented complete DMEM allowing the selection of stably transfected cells. After 24 hours the cells were trypsinised and reseeded into 10ml tissue culture treated petri-dishes. The dishes remained in a humidified chamber, with frequent media changes, for 2-3 weeks to allow stably transfected colonies to grow. Once colonies had begun to grow and contained ~150 cells, they were scraped from the bottom of the well with a sterile 200µl pipette tip and transferred to a separate well into a 6-well plate containing G418-supplemented complete DMEM. Two aliquots of each picked colony were frozen down before harvesting for protein extraction and assessing for expression by Western blot. The plates were placed in a humidified chamber and allowed to grow to 90% confluence before being transferred to a 75cm^2 cell culture flask. The flasks were kept in G418-supplemented complete DMEM to maintain a stably transfected population.

2.2.7.1.2 Transfection of MRC5VA Cell Line Using Lipofectamine 2000

The transfection was carried out by adding 2µl of plasmid DNA to a 1.5ml microcentrifuge tube containing 50µl serum free media and at the same time 10µl of Lipofectamine 2000 (Invitrogen) was added to a different microcentrifuge tube containing 50µl serum free media. Both tubes were left at room temperature for 5 minutes. The two microcentrifuge tubes were then mixed and left at room temperature for 20 minutes. This mixture then was added to each well of a 6-well plate (Corning) containing 80% confluent MRC5VA cells in 2ml complete DMEM and placed in a humidified chamber. Then the same steps, as in (Section 2.3.7.1.1), were followed to obtain a stably transfected population in a 75cm^2 cell culture flask maintained in G418-supplemented complete DMEM.

2.2.8 Irradiation of Cells

MRC5VA as a control cell line, pFlag-XLF, pFlag-XRCC4 and pFlag-HDAC3 overexpressing cell lines were grown, each cell line in 3 separate 75cm^2 cell culture flasks until 90% confluence. Two flasks of each cell line were irradiated with 20Gy of IR (Caesium ^{137} source) and the third left as a non-irradiated control. After irradiation, the non-irradiated flask and one irradiated flask were incubated at 37°C in the humidified chamber for 1 hour and the other irradiated flask for 2 hours. Then, the cells were pelleted and stored at -80°C for protein extraction.

2.2.9 Clonogenic Survival Assays

MRC5VA, pFlag-Ku70/wt, pFlag-Ku80/wt and Empty-pFlag expressing cell lines, as control cell lines, and stable cell lines overexpressing pFlag-KU70/mutants (pFlag-KU70-K317R,

pFlag-KU70-K331R, pFlag-KU70-K338R, pFlag-KU70-K317Q, pFlag-KU70-K331Q and pFlag-KU70-K338Q) were grown in 75cm^2 cell culture flasks until 70% confluence, trypsinised and counted using a haemocytometer and serially diluted into 10ml universals. Cells were irradiated with 2, 4, 6 and 8Gy of IR (Caesium ^{137} source), with one sample left un-irradiated. Cells were seeded out at 50, 100, 500, 1000, 5000 and 10000 cells per well into a 6-well plate for 0, 2, 4 and 6Gy exposures. For 8Gy exposures 500, 1000, 5000, 10000, 50000 and 100000 cells were seeded out. The 6-well plates were incubated in a humidified chamber and left for ~2 weeks until colonies of ~50 cells were visible. The media was aspirated and a few drops of crystal violet (0.4% crystal violet, 50% methanol) were added to each well. This was agitated for a few seconds and washed off with distilled water. Colonies that contained between 50 and 100 cells were counted in the wells. The experiment was repeated in triplicate and the data statistically analysed using the students' two-tailed t-test.

2.2.10 Immunofluorescence Analysis

2.2.10.1 Cells Fixing

For γH2AX staining, MRC5VA, pFlag-KU70/wt, pFlag-KU80/wt and Empty-pFlag expressing cell lines (as control cell lines) and stable cell lines overexpressing pFlag-KU70/mutants (pFlag-KU70-K317R, pFlag-KU70-K331R, pFlag-KU70-K338R, pFlag-KU70-K317Q, pFlag-KU70-K331Q and pFlag-KU70-K338Q) were grown in 6-well dishes containing a 22mm x 22mm glass coverslip (VWR), sterilized under UV light for 30 minutes. At the point of fixation, the media was aspirated and the coverslips were washed with PBS. To each coverslip 1ml of immunofluorescence lysis buffer was added (10mM PIPES pH 6.8, 300mM sucrose, 20mM NaCl, 3mM MgCl2, 0.5% Triton X-100) and incubated on ice for 7 minutes. The slides were washed in PBS and 1ml of 4% paraformaldehyde (diluted in PBS)

was added and left on ice for 10 minutes. The paraformaldehyde was aspirated. Then, the fixed cells were washed 3 times with PBS. For the purpose of pFlag immunoflourescence staining, cell permeabilization buffer (20mM Hepes PH 7.4, 50mM NaCl, 3mM MgCl2, 300mM Sucrose, 0.5% Triton X-100) was used to permeabilize the cells for 5 minutes at 4^{o}C after paraformaldehyde fixation.

2.2.10.2 Immunostaining

In order to block non-specific proteins, 10% FBS was added to the slides and incubated on a rocking platform for 1 hour at room temperature. FBS was removed and the slides washed with PBS. Subsequently, 100µl PBS supplemented with 2% FBS and primary antibody (Table 2.5) was added and incubated at 37^{o}C for 1 hour on a rocking platform. The coverslips were washed 3 times, 5 minutes each, with PBS. Then, 100µl PBS supplemented with 2% FBS and a fluorescently tagged secondary antibody (Table 2.5) was added and incubated at 37^{o}C for 1 hour in the dark on a rocking platform. The coverslips were again washed 3 times, 5 minutes each, with PBS in the dark.

2.2.10.3 Mounting and Visualization

The coverslips were mounted with Vectashield (Vector Laboratories) mounting media, containing 4', 6-diamidino-2-phenylindole (DAPI), onto microscope slides (VWR). The coverslips were sealed with clear nail varnish and kept at 4^{o}C overnight before analysis. Slides were analysed with a Carl Zeiss microscope using a 100x objective and Smart Capture2 software.

2.2.11 γH2AX Quantification

The four control cell lines and the six stable cell lines overexpressing pFlag-KU70/mutants were grown on coverslips in 6-well dishes (Section 2.2.10.1). Cells were irradiated with 5Gy of IR and placed in a humidified chamber. At 30 minutes and 24 hours post-irradiation the cells were fixed. Cells were incubated with anti-γH2AX primary antibody and then followed by the secondary fluorescent antibody. After mounting and visualization, a minimum of 100 nuclei per time point per sample were examined and γH2AX foci per nuclei were counted using Photoshop Software (Adobe). The experiment was repeated twice and the data was statistically analysed using Students' two-tailed t-test.

2.3 Protein Related Methods

2.3.1 Protein Extraction

When cells had reached 90% confluence they were trypsinised and reseeded as explained in Section 2.2.3 and 2.2.5. The excess cell suspension was then centrifuged at 1500rpm for 5 minutes at 20°C, the media aspirated and the cells were resuspended in 5ml PBS and again centrifuged. The supernatant was then removed and the pellet was resuspended in twice the volume of the cell pellet in RIPA buffer (50mM Tris-HCl pH7.5, 1mM EDTA, 150mM NaCl, 0.1% SDS, 0.5% deoxycholic acid, 1% Igepal CA-360 (Sigma) with 10% protease inhibitor (Roche) and placed on ice for 20 minutes. The suspension was then centrifuged at 13000rpm for 5 minutes at 4°C. The supernatant was then carefully aspirated and placed into a fresh 1.5ml microcentrifuge tube. For testing the Pan-Acetyl-Lysine Antibody (Pan-Ac-K Ab), each of the frozen pellets (Section 2.2.8) were washed in PBS and resuspended in 500µl of lysis buffer (50mM Tris pH7.4, 150mM NaCl, 0.5mM EDTA, 1% Triton, protease inhibitors tablets (Roche) and phosphatase inhibitors cocktail tablets (Roche). The samples were placed on a blood rotor for 30 minutes at 4^{o}C and centrifuged at 13,000rpm for 10 minutes at 4^{o}C.

2.3.2 Quantification of Protein

The protein concentration was then determined by the Bradford method (Bradford, 1976). 1ml of 0.5x Bradford Reagent (Sigma) was placed into a 1ml disposable cuvette, to which 5µl of sample was added. Absorbance was read at 595nm using a Genova spectrophotometer against a standard curve (5-30µg BSA).

2.3.3 Sodium Dodecyl Sulphate Polyacrylamide Gel Electrophoresis (SDS-PAGE)

SDS-PAGE gels for immunoblotting consist of two parts: a resolving gel segment and an overlaying stacking gel segment. The resolving gels were made with 9% polyacrylamide (30% acrylamide Protogel, National Diagnostics), 375mM Tris (pH8.8) and 0.1% SDS and polymerized with 10% ammonium persulphate (APS) and tetramethylethylenediamine (TEMED) (Sigma)The resolving gel was poured and covered with isopropanol whilst the gel set. The isopropanol was then removed and replaced with a stacking gel. The stacking gels were made with 3% polyacrylamide, 50mM Tris (pH 6.8) and 0.1% SDS and polymerized with 10% APS and TEMED. Combs were immediately inserted into the stacker gel and allowed to set. Once set the gels were placed into an electrophoresis tank (Biorad Mini) partly filled with running buffer (25mM Tris, 192mM Glycine, 0.1% SDS) and the teeth removed.

2.3.4 Gel Loading and Electrophoresis

An aliquot of 15µg of each protein sample was then diluted with 5x loading buffer (65mM Tris-HCl, pH 8.0, 10% (v/v) Glycerol, 2.3% (w/v) SDS, 0.01 Bromophenol blue, 1% DTT), denatured at 100°C for 5 minutes and then placed immediately on ice. The samples, including a protein standard (Sigma), were loaded into the wells of the gel and run at 20mA per gel for 45 minutes approximately. Once the loading dye was near the bottom of the gel, the gel was transferred.

2.3.5 Transfer of Proteins from Gel to Polyvinylidene Fluoride Membrane (PVDF)

Proteins were routinely transferred onto PVDF transfer membrane, 0.2µm pore size Immobilon transfer membrane (Millipore). The membrane was briefly immersed into

methanol to activate, then equilibrated in 1x chilled transfer buffer. The membrane and the gel were sandwiched between two sponges and filter paper and placed into a transfer cassette which was placed into the transfer tank. This was filled to the top with CAPS buffer (10mM CAPS (Sigma), 10% methanol) and run at 215mA for 90 minutes. The membrane was subsequently blocked using 5ml of 5% non-fat milk in PBS + 0.1% Tween overnight at 4°C with agitation in order to reduce non-specific immunoglobulin binding.

2.3.6 Western Blotting

The PVDF membrane was placed into a 50ml centrifuge tube (Falcon), with the protein bound side of the membrane facing inwards, contaning 5ml of 5% non-fat milk in PBS + 0.1% Tween and the primary antibody diluted at 1/1000. The centrifuge tube was placed on a tube roller and incubated at room temperature for 1 hour. Then, the membrane was removed from the centrifuge tube and placed face up into a container containing PBS + 0.1% Tween and placed on a rotating tray for 5 minutes. This was repeated twice with fresh PBS + 0.1% Tween. The membrane was placed again inside another 50ml centrifuge tube containing 5ml of 5% non-fat milk protein in PBS + 0.1% Tween and the secondary antibody diluted at 1/1000 and placed on a tube roller and incubated at room temperature for 1 hour. The membrane was removed from the centrifuge tube and washed three times, 5 minutes each, in PBS + 0.1% Tween. All the antibodies used are listed in Table 2.5.

Primary Antibody	Species	Application	Secondary Antibody
Anti-pFLAG (Sigma)	Mouse	Western blot	Rabbit anti-Mouse-HRP (Dako)
		Immunofluorescence	AlexaFluor 594 (Invitrogen)
Anti-Pan-Ac-K (Abcam)	Rabbit	Western blot	Goat anti-Rabbit-HRP (Dako)
Anti-H2AX (Upstate)	Mouse	Immunofluorescence	AlexaFluor 594

Table 2.5: List of the antibodies used
All the primary and secondary antibodies were used at 1:1000 dilutions. AlexaFluor 594 was raised in goat.

2.3.7 Visualisation Using Luminescence and Autoradiography

Bound antibody was detected with an enhanced chemiluminescence detection kit (Amersham). The membrane was overlaid with ECL plus substrate (1ml of solution A mixed with 20µl of solution B) for 1 minute. The excess ECL plus was removed and the membrane was wrapped in Saran wrap and placed within a light protected autoradiography cassette. The membrane was used to expose X-ray sensitive film (Kodak) for 30 seconds to 10 minutes depending on the strength of the signal.

2.3.8 *In Vitro* Protein Purification from E. coli

pGEX 2TK-p-*XLF* (a generous gift from Professor Steve Jackson's laboratory : for sequence see Appendix 1 and for vector map see Figure 2.5) and his-KU70 and his-KU80 (Section 2.1.13.1) plasmid DNA was transformed into competent E. coli capable of protein expression (BL21 (DE3)pLysS; Promega), and plated out onto LB agar containing 100µg/ml ampicillin (for GST-XLF) or 25µg/ml kanamycin(for his-KU70 and his-KU80) and left at 37°C

overnight. Overnight cultures were obtained from individual colonies. The screening for the presence of the inserted gene was performed by colony PCR with the primers listed in Table 2.2. Positive colonies were used to generate recombinant proteins and to make glycerol stocks.

2.3.8.1 Induction of Recombinant Proteins

An overnight culture was transferred into 50mL of LB broth and incubated at 37°C in an orbital shaker until the OD600 reached 0.6-1.0. In the case of GST-XLF expression was typically induced by the addition of 0.5mM IPTG, whereas his-KU70 and his-KU80 expression were induced by the addition of 1mM IPTG. The induction of GST-XLF was allowed to continue overnight at room temperature, whereas the induction of his-KU70 and his-KU80 were allowed to continue for 4 hours at 37^{o}C. The bacterial culture was pelleted by centrifugation at 4,000rpm for 20 minutes and the pellet was placed at -80°C.

2.3.8.2 Extraction and Purification of GST-XLF Recombinant Protein

The pellet was thawed out on ice and lysed with the addition of GST-tag lysis buffer (PBS buffer containing 2mM dithiothreitol (DTT) (Sigma) and 0.2mM phenyl methyl sulphonyl fluoride (PMSF) (Sigma) at pH 7.5. The bacteria were further lysed by sonication: four pulses, 20 seconds each, whilst on ice to prevent protein degradation. After sonication, Triton X-100 was added to the supernatant to a final concentration of 1% (v/v), followed by end-over-end rotation at 4^{o}C for 30 minutes. The lysate was centrifuged at 15,000 rpm at 4^{o}C for 30 minutes and the soluble fraction (supernatant) was mixed with Glutathione Sepharose 4B beads (GE Healthcare), pre-equilibrated in PBS, by end-over-end rotation for 30 minutes, to allow the GST-tagged protein to bind to the beads. The flow-through containing the unbound

proteins was discarded and the column was washed with 10x column volumes of PBS. Proteins were then eluted in GST-tag elution buffer (50mM Tris-HCl, pH 8.0, 10mM glutathione) in 500µl fractions, each fraction was then analysed by SDS-PAGE and the fraction containing the protein of interest was stored at -80^{o}C.

2.3.8.3 Extraction and Purification of His-KU70 and His-KU80 Recombinant Proteins

The same steps as described in the previous section were followed using the his-tag lysis buffer (50mM Tris/HCl pH 7.5, 300mM NaCl, 1% Triton, 0.06% ß-ME, 1mM benzamidine and 0.2mM PMSF) and TALON metal affinity resin (Clontech) pre-equilibrated in his-tag lysis buffer. The wash and elution buffers were the same as the lysis but with 5mM imidazole in the wash and 300mM imidazole in the elution buffer.

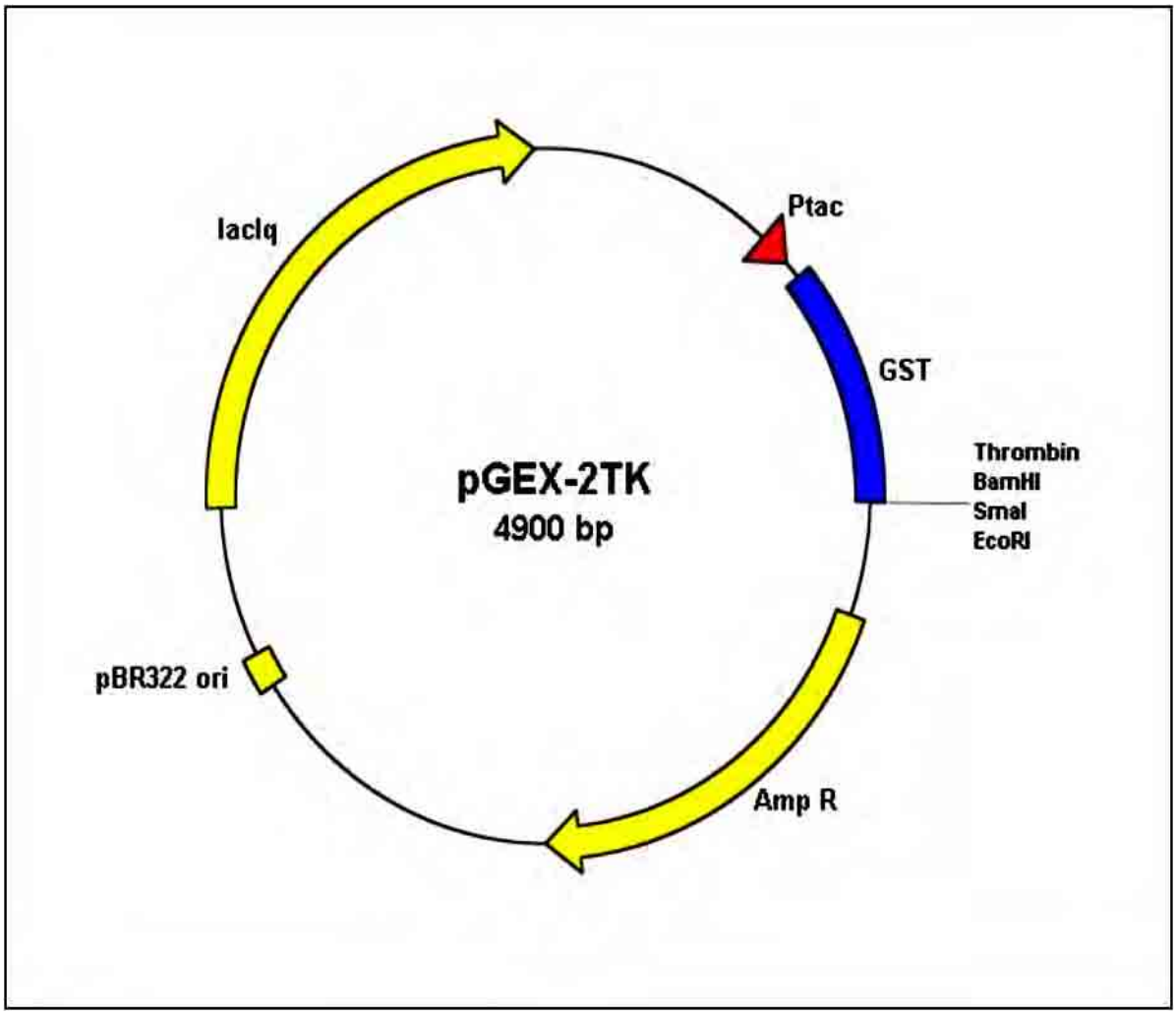

Figure 2.5: pGEX-2TK-p plasmid map
Plasmid pGEX-2TK-p was derived from pGEX-2TK plasmid (Amersham) by insertion of the sequence AATTCTAGACTCCATGGGTCGACTGAGCTCAAGCT at the EcoRI site. The *XLF* was cloned into pGEX-2TK-p in-between EcoRI and XhoI, see Appendix 1.

2.3.8.4 Coomassie Staining and Drying of SDS-PAGE Gels

SDS-PAGE gels were stained using PageBlue (Fermentas). Simply, the gel was placed in 20ml distilled water and heated to boiling point. The water was removed and replaced with fresh water. This was repeated twice more. Finally, the gel was boiled in 20ml PageBlue reagent. The gel was left on a rocker for approximately 1 hour until banding had become clear. Then, the gel was destained with several washes of distilled water. The bands were cut out of the gel and sent for mass spectroscopy.

2.3.8.5 Mass Spectrometry

Mass spectrometry analysis was carried out by the Functional Genomics Unit, University of Birmingham, and the results were returned in Microsoft Excel format.

2.3.8.6 SDS-PAGE Gel Drying

In order to dry the gel, it was sandwiched between filter paper and Saran wrap and vacuum dried at 80^{o}C for 60 minutes on a Gel Master Gel Dryer Vacuum System (Welch).

2.3.9 *In vitro* Acetylation of XLF and XRCC4

The HATs tested included PCAF, P300, CBP and GCN5 (Enzo Life Sciences). Protein samples of XLF, XRCC4 and H1X (as a positive control for acetylation) were provided by Dr. Darren Arbon. The proteins were also tested for the basal levels of acetylation, which may present before the *in vitro* acetylation reaction. A master mix of 2x reaction buffer was made up of 100mM Hepes, pH8 (Sigma), 20% glycerol (Sigma), 2mM DTT, 2mM 4-(2-aminoethyl) benzenesulfonyl fluoride hydrochloride (AEBSF) (Sigma), 10mM sodium

butyrate (Sigma) and nuclease free water. Sixteen reactions were set up in total; each reaction contained 1µg of protein, 1µg of a particular histone acetyl transferase (HAT), 1µl of acetyl coenzyme A, 15µl of 2x reaction buffer and 12µl of nuclease free water in order to create a 30µl reaction. The reactions were set up in duplicate; half of the reactions contained C^{14}-acetyl coenzyme A, while the other half contained non-radioactive acetyl coenzyme A. The reactions were incubated at 30°C for 1 hour. The samples were then run on a 4-20% gradient Mini-Protean precast gel (BioRad) at 150V for 1 hour. The gels were stained overnight with Page Blue (Fermentas). Bands that corresponded to XLF and XRCC4 were excised from the non-radioactive gel and sent for analysis by mass spectrometry in order to determine specific levels of acetylation and to map the particular sites of acetylation. The radioactive gels were dried then placed face down onto a storage phosphor screen (Molecular Dynamics) and left to expose for 1 week. The results were visualised using a STORM Phosphoimager (Molecular Dynamics).

CHAPTER THREE: *XLF* SINGLE NUCLEOTIDE POLYMORPHISM (SNP) ANALYSIS

3.1 Introduction

IR induces various types of DNA damage, including both SSBs and DSBs. Since DSBs are arguably the most detrimental form of DNA damage, they are repaired efficiently in eukaryotes by two major pathways: HR and NHEJ, as mentioned in Section 1.3.2.2.5 and 1.3.2.2.6. HR is an error free repair of high fidelity, whereas NHEJ is an error prone repair of low fidelity. HR predominantly operates in the S and G2 phases of the cell cycle, whereas NHEJ is active throughout all the phases of the cell cycle, particularly the G0/G1 phases. NHEJ deficiencies can lead to increased genomic instability and cause increased carcinogenesis. However, their precise roles in these processes are not well understood (Pfeiffer et al., 2004; Shrivastav et al., 2008; Zhu et al., 2002).

The DNA-repair capacity (DRC) varies considerably among individuals and reduced DRC is strongly associated with increased risk of carcinogenesis. Polymorphisms represent the most subtle and common variations in a DNA sequence that may lead to altering the activity of the encoded gene (Dybdahl et al., 1999; Stern et al., 2009; Vogel et al., 2002; Winsey et al., 2000). They can be very helpful diagnostic markers of an individual's sensitivity to carcinogens and anticancer drugs. Because DNA repair enzymes are correctives for DNA damage induced by carcinogens and anticancer drugs, it is very likely that SNPs in DNA repair genes may play an important role in the development of cancer, the clinical phenotype and the outcome of drug treatment (Divine et al., 2001; Ratnasinghe et al., 2001; Stern et al., 2001; Sturgis et al., 1999; Wu et al., 2008). It is noteworthy that it has also been established that SNPs of DNA repair genes are not only associated with or increase the risk of certain types of cancer, however they could also affect the patient response to anticancer agents (Abraham et al., 2006; Efferth and Volm, 2005; Madhusudan and Middleton, 2005).

Interestingly, one comprehensive study used a multiple gene analysis to evaluate the association of multiple genetic polymorphisms in DNA repair and cell cycle genes with bladder cancer risk. This study has shown that the risk of bladder cancer increased in individuals with a higher number of polymorphisms in DNA repair and cell cycle genes (Wu et al., 2006). This highlights the importance of including multiple genetic polymorphisms in the risk assessment of cancer and other complex diseases.

To highlight the importance of polymorphisms of DNA repair genes more, a few examples will be enumerated. Different SNPs of *XRCC1* have been reported to be associated with the risk of different types of cancers including renal, prostatic, gastric, lung, head and neck cancers (Hirata et al., 2007). In addition, the risk of development of childhood acute lymphoblastic leukaemia varies depending on different alleles and haplotypes of *XRCC1*. One allele and haplotype of *XRCC1* was protective, whereas the other allele and haplotype of the same gene increased the risk for this malignancy (Pakakasama et al., 2007). Furthermore, SNPs of *ATM*, *LIG1*, *LIG3*, *MLH1* and *MSH6* were found to be associated with tobacco-induced lung cancer (Landi et al., 2006).

Certain SNPs of *BRCA2* were found to be associated with an increased risk of breast cancer (Healey et al., 2000), whereas SNPs of *BRCA1* may affect ovarian cancer risk (Dunning et al., 1997; Durocher et al., 1996; Janezic et al., 1999; Smith et al., 2001). Moreover, SNPs of DSBR genes such as *XRCC2*, *XRCC4*, *XRCC6* and *LIG4* were found to be associated with increased risk of breast cancer (Fu et al., 2003; Han et al., 2004; Kuschel et al., 2002; Rafii et al., 2002) .

Despite the limited availability of sensitive assays to evaluate the effect of polymorphisms on protein function, one interesting study has shown that two linked polymorphisms in *LIG4* N-terminus (A3V + T9I) mildly but reproducibly reduced adenylation and ligation activity (2-3 folds). More importantly, when these two linked polymorphisms were coupled with *LIG4* (R278H) mutation, there was an additive impact that likely reduced the protein activity to a level below that required for normal development. It is to be noted that the R278H mutant protein allowed 5-10% residual adenylation activity, yet no residual activity was detectable in the R278H + A3V + T9I mutant protein. These findings correlated with the severity of the patient's clinical features (Girard et al., 2004). This study is a striking example of the compounding effects of distinct mutational changes in a protein and provides a framework for considering the impact of multiple polymorphisms, where the level of residual activity may be greater and the impact may lie not in cancer development, but in cancer predisposition. Another interesting example is the single point mutation (R57G) of *XLF* that impairs its nuclear import and hence fails to stimulate ligation as mentioned in Section 1.3.2.2.5. It will be interesting to find if there are associated polymorphisms that could modulate the impact of such single point mutation.

3.2 Aims

The main aims of this part of the project:

1- SNP analysis of the newly identified key NHEJ gene (*XLF*).

2- Building up population data on coding variants i*n XLF* and the identification of alleles or combinations of alleles that may affect disease predisposition.

3.3 Results

3.3.1 SNP Analysis of *XLF*

The seven coding exons of *XLF*, which are located on chromosome 2q35 (Figure 3.1**),** with their intronic boundaries, were amplified by PCR and sequenced in a random Caucasian population sample collected as described in Section 2.1.1. PCR optimization on DNA templates from different cell lines was carried out with different concentrations of $MgCl_2$ separately and in combination with different PCR adjuvants such as DMSO, acetamide, formamide and betaine. It has been observed that using the optimal amount of primers was the key to eliminating most of the primer dimers as shown in Figure 3.2A. After PCR amplification of the seven coding exons of *XLF*, the PCR products were electrophoresed. The agarose gel electrophoresis confirmed the presence and expected size of the products as shown in Figure 3.2B, C, D, E, F, G and H. All the PCR products were purified using Exo-SAP cleaning protocol as described in Section 2.1.4. All the purified PCR products were sequenced using the dideoxy termination protocol as described in Section 2.1.7. The forward and reverse sequencing of the purified PCR products were performed using the primers listed in Table 2.1. The results were analysed using the ABI sequencing analysis v5.2 software and Bioedit alignment software in comparison to the wild sequence published in the ensembl database.

Unfortunately, no *XLF* coding SNPs were identified in the studied population sample, but two intronic SNPs already published in the NCBI dbSNP were characterized in the studied sample. The first change (rs2030452) is C→G, 29bp upstream of the 2nd coding exon of *XLF*, as shown in Figure 3.3A. The second change (rs7585742) is G→C, 59bp upstream of the 3rd coding exon of *XLF*, as shown in Figure 3.3B. Moreover, two novel noncoding SNPs were

identified in the studied sample. The first is an intronic SNP (G→A change), 28bp downstream of the 6th coding sequence as shown in Figure 3.4A. The second is a novel SNP (T→C change) in the three prime untranslated region (3' UTR), 39bp downstream of this the 7th coding exon (Figure 3.4B). The percentages of genotypes of the four SNPs observed in the studied population sample are listed in Table 3.1. The wild type sequence of the seven coding exons of *XLF* is shown in Appendices 4-10.

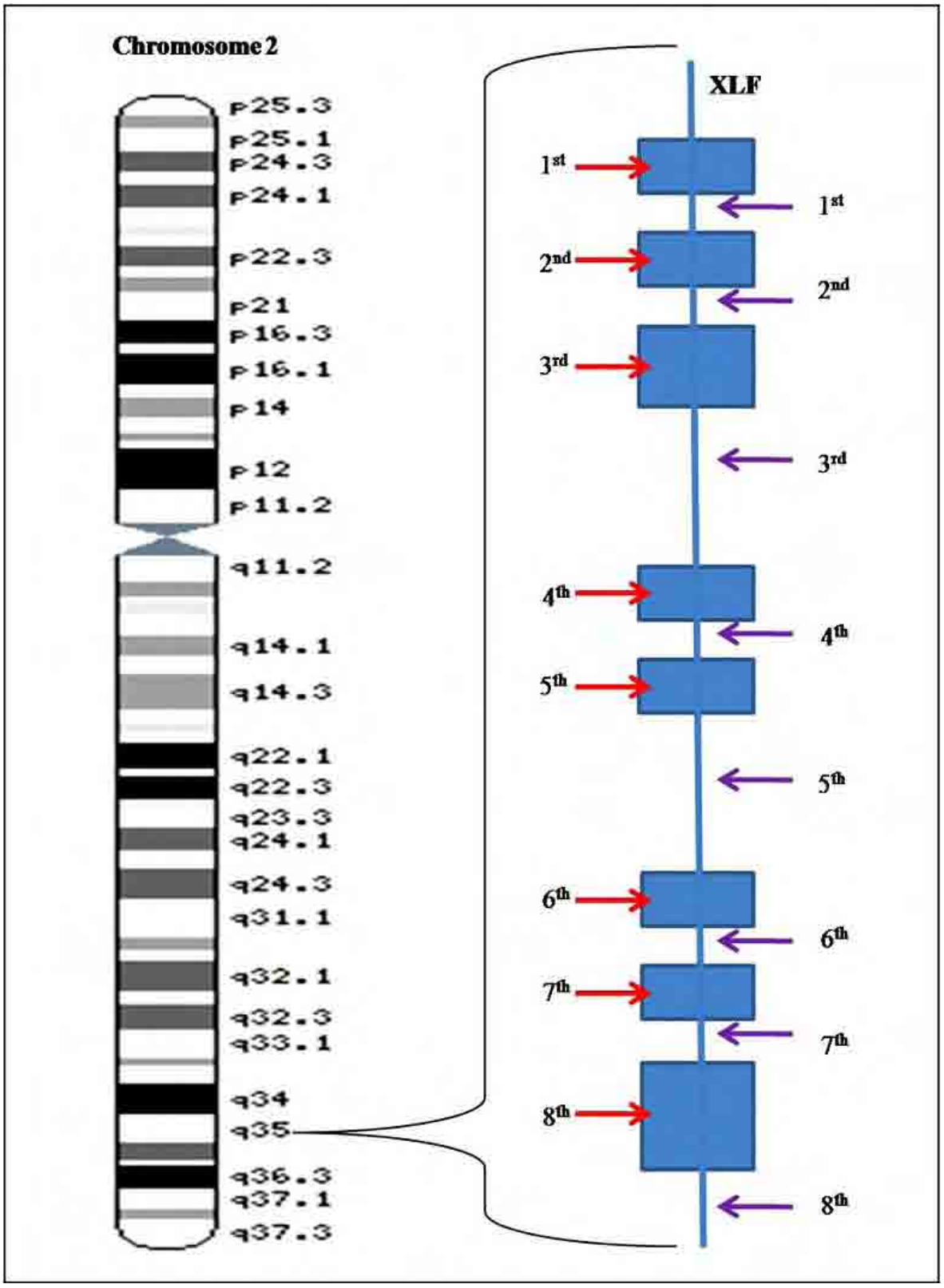

Figure 3.1: Diagrammatic representation of the structure of *XLF*
XLF consists of eight exons, as indicated by the red arrows, located on chromosome 2q35. The first exon is non-coding, whereas the 2nd, 3rd, 4th, 5th, 6th, 7th and 8th are coding exons. The introns are indicated by the purple arrows. Chromosome 2 structure has been modified from ensembl genome browser.

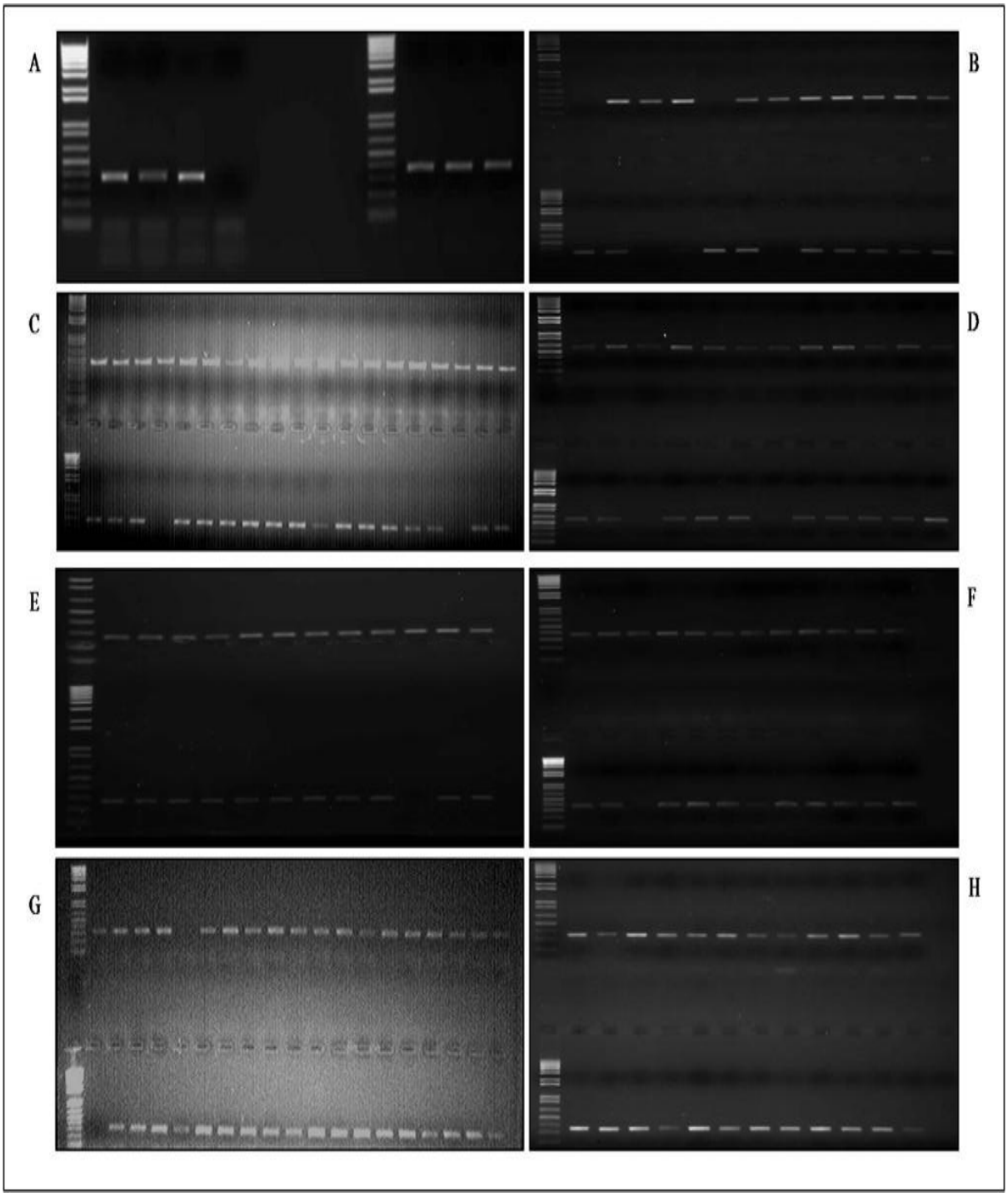

Figure 3.2: PCR optimization and PCR products of the seven coding exons of *XLF*

(A) Gel images showing the optimization of PCR by using optimal primer concentration 10picomoles of each primer on the right side alongside higher primer concentration 100picomoles of each primer on the left side. The amplified PCR products of the seven coding exons of *XLF* were electrophoresed. (B) Gel showing 24 samples of the 1st coding exon of *XLF* (product size=349bp). (C) Gel showing 38 samples of the 2nd coding exon of *XLF* (product size=492bp). (D) Gel showing 24 samples of the 3rd coding exon of *XLF* (product size=586bp). (E) Gel showing 24 samples of the 4th coding exon of *XLF* (product size=250bp). (F) Gel showing 24 samples of the 5th coding exon of *XLF* (product size=365bp). (G) Gel showing 38 samples of the 6th coding exon of *XLF* (product size=314bp). (H) Gel showing 24 samples of the 7th coding exon of *XLF* (product size=377bp).

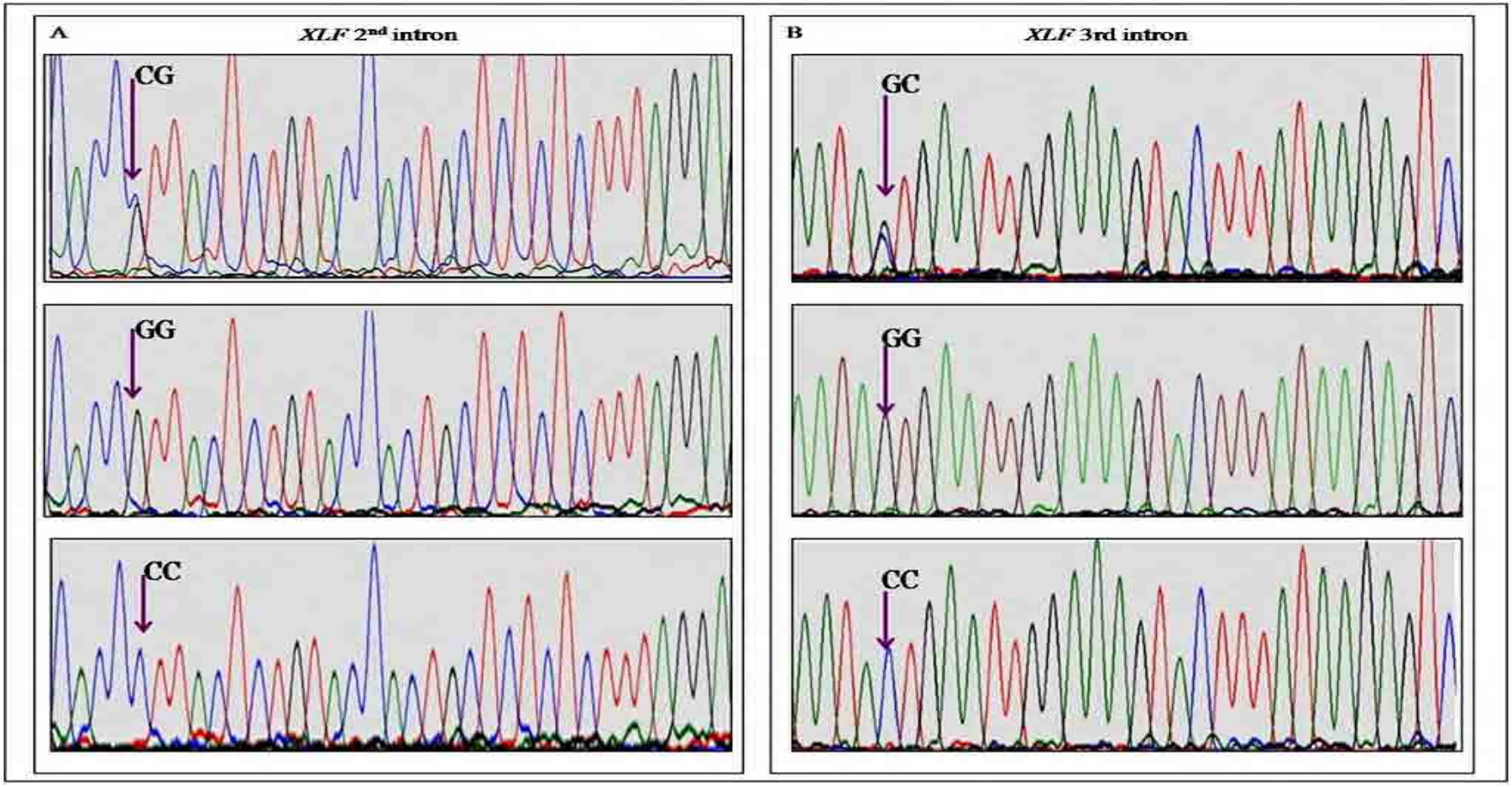

Figure 3.3: Chromatograms of the observed genotypes of the 2nd and 3rd introns of *XLF*

The green, red, blue and black peaks correspond to adenine (A), thymine (T), cytosine (C) and guanine (G) nucleobases respectively. (A) The top chromatogram shows the heterozygous CG genotype of the 2nd intron of *XLF* as indicated by the purple arrow. The middle chromatogram shows the homozygous GG genotype, whereas the bottom one shows the other homozygous CC genotype of the 2nd intron of *XLF* as indicated by the purple arrows. (B) The top chromatogram shows the heterozygous GC genotype of the 3rd intron of *XLF* as indicated by the purple arrow. The middle chromatogram shows the homozygous GG genotype, whereas the bottom one shows the other homozygous CC genotype of the 3rd intron of *XLF* as indicated by the purple arrows.

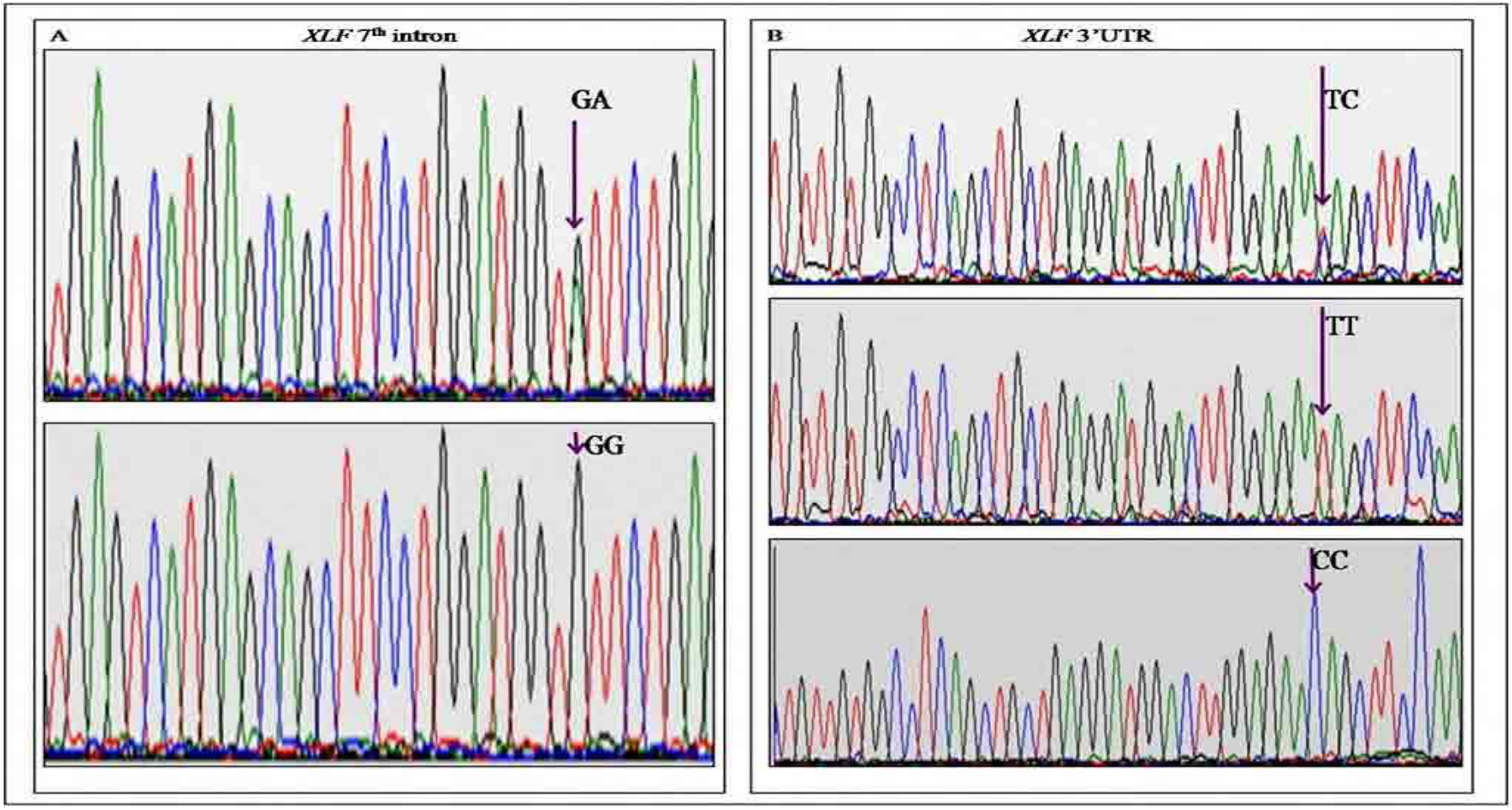

Figure 3.4: Chromatograms of the observed genotypes of the novel noncoding SNPs of *XLF*

The green, red, blue and black peaks correspond to A, T, C and G nucleobases respectively. (A) The top chromatogram shows the heterozygous GA genotype, whereas the bottom chromatogram shows the homozygous GG genotype of the 7th intron of *XLF* as indicated by the purple arrows. The homozygous GG genotype was not characterized in the studied population sample. (B) The top chromatogram shows the heterozygous TC genotype of the 3'UTR SNP of *XLF*. The middle chromatogram shows the homozygous TT genotype, whereas the bottom one shows the other homozygous CC genotype of the 3'UTR SNP of *XLF* as indicated by the purple arrows.

	Observed Genotypes		
***XLF* 2nd Intron SNP (**rs2030452) **Location**: 29bp upstream of the 2nd coding exon **Percentage of observed genotypes**	CG 23.6%	GG 37.1%	CC 39.3%
***XLF* 3rd Intron SNP** (rs7585742) **Location**: 59bp upstream of the 3rd coding exon **Percentage of observed genotypes**	GC 42.7%	GG 33.7%	CC 23.6%
***XLF* 7th Intron SNP** **Location**: 28bp downstream of the 7th exon **Percentage of observed genotypes**	GA 4.5%	GG 95.5%	AA 0 %
***XLF* 3'UTR SNP** **Location**: 39bp downstream of the 8th exon **Percentage of observed genotypes**	TC 44%	TT 55%	CC 1%

Table 3.1: Percentages of the observed *XLF* SNP genotypes in the studied population sample

3.3.2 Restriction Fragment Length Polymorphism (RFLP) Analysis of *XLF*

The 2nd coding exon of *XLF* produced a readable sequence, yet with a lot of background noise which interfered with the interpretation of base changes. In spite of the sequence noise, a potential coding SNP was found in the forward sequence of a few samples and appeared even on reverse sequencing of the same samples. It appeared as a G→A change, 15bp upstream of the 2nd coding exon, as shown in Figure 3.5A.

BsrI restriction enzyme was selected to perform RFLP analysis on these samples to verify whether this is a true polymorphism, as the reverse sequence of the same samples showed the same background noise and was not conclusive. Figure 3.5C shows one gel alongside a diagrammatic representation of the expected band pattern in Figure 3.5B. Although, it appears that the digestion is not complete, it has been concluded that only the wild genotype is present in these samples and this change is not an actual polymorphism, but mostly sequence artefact. The forward sequencing of this exon was repeated, after using fresh enzymes to clean up the PCR products. Although, the forward sequence was of good quality, it showed rapid signal loss and the full coding sequence of this exon could not be analysed. So the reverse sequence was performeed to analyse it, however no coding SNPs were identified in this exon.

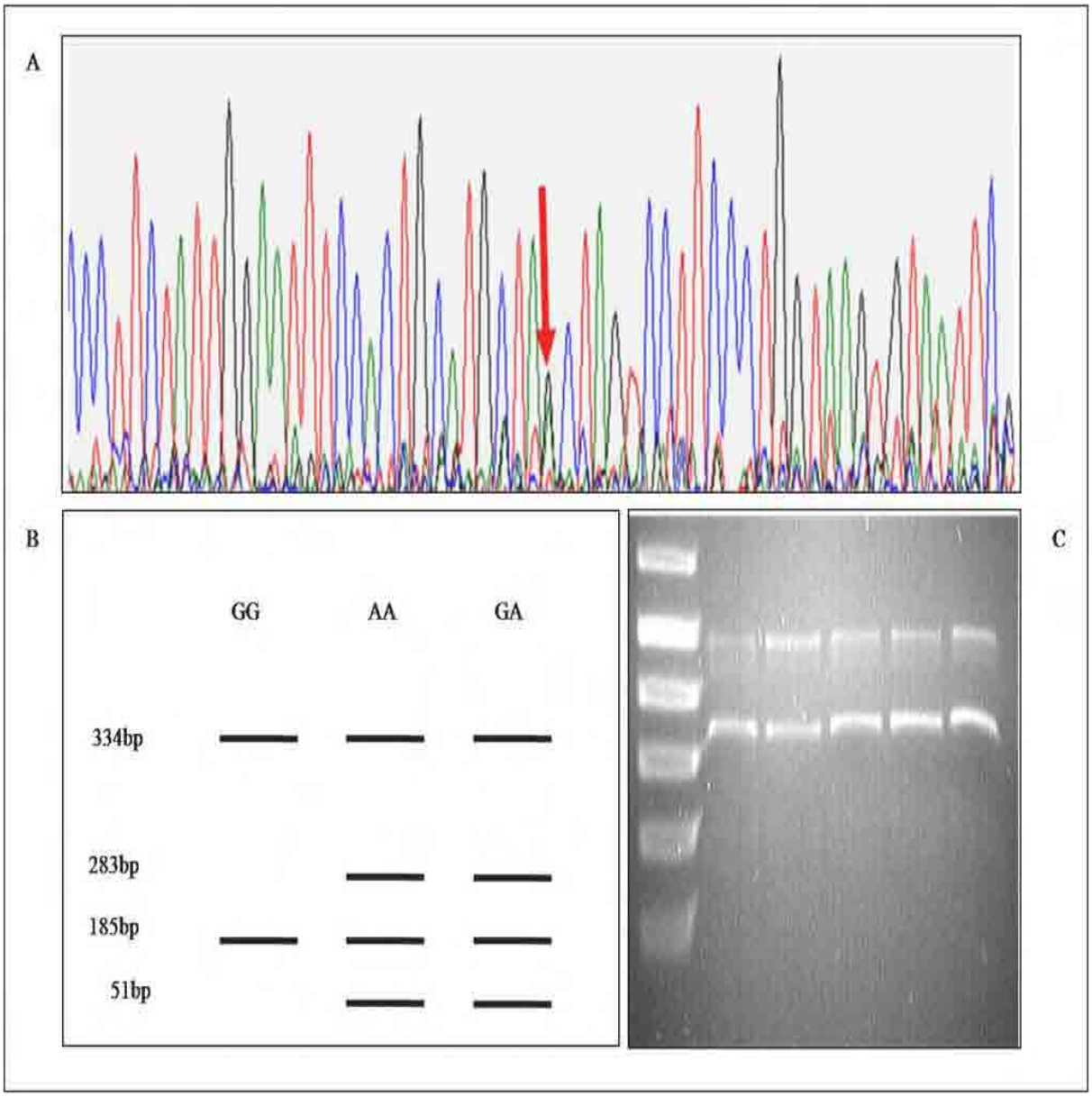

Figure 3.5: Potential coding SNP of the 2nd coding exon of *XLF* and RFLP
(A) Sequence chromatogram of the 2nd coding exon of one sample showing a potential coding SNP as indicated by the red arrow. The green, red, blue and black peaks correspond to A, T, C and G nucleobases respectively. (B) The diagrammatic representation of the expected band pattern upon digestion of the PCR product of the 2nd coding exon of *XLF* by BsrI enzyme. (C) RFLP analysis of 5 samples containing the potential coding SNP of the 2nd coding exon of *XLF* using BsrI enzyme was performed and the products were electrophoresed. The band pattern on the gel is mostly of wild type as shown in comparison to the diagrammatic representation of the expected digestion pattern.

3.3.3 *XLF* Exonic Deletion

Interestingly, PCR amplification resulted in no products in the seven amplified exons of one sample, but only truncated product in the 2nd coding exon, which appeared on the agarose gel to be of about 250bp in length, whereas the expected size was 492bp as shown in Figure 3.6A. This truncated product was cloned into pGEM-T-Easy vector and transformed into E coli. Ten white colonies were selected and minipreped. After EcoRI digestion, 3 out of 10 were found to contain the truncated insert as shown in Figure 3.6B. Sequencing of these minipreps revealed 2 different clones as shown in Figure 3.6C and D. Blast searches for these two clones showed that one of them matches part of chromosome 6 and the other matches part of chromosome 7. Amplification of the 1st two coding exons of this sample in one PCR using the forward primer of the 1st coding exon and the reverse primer of the 2nd coding exon resulted in no products, however the control samples produced an approximately 2kb product, which was expected, as shown in Figure 3.6E. Also, amplifying the 3rd and 4th coding exons of this sample in one PCR using the forward primer of the 3rd coding exon and the reverse of the 4th coding exon did not produce the expected 2kb product, although it did in the control samples, as shown in Figure 3.6F. Surprisingly, using the forward primer of the 5th coding exon in conjunction with the reverse one of the 7th coding exon for PCR amplification of this sample as well as the control produced 3kb products as expected (Figure 3.6F). This case will be discussed in more detail in the discussion. It is to be noted that 2 samples in the 96 well plates were confirmed to be negative by PCR and electrophoresis. Also, 4 samples resulted in no PCR products in the seven amplified exons, mostly due to the fact that there was not enough DNA template in these samples for the PCR to amplify.

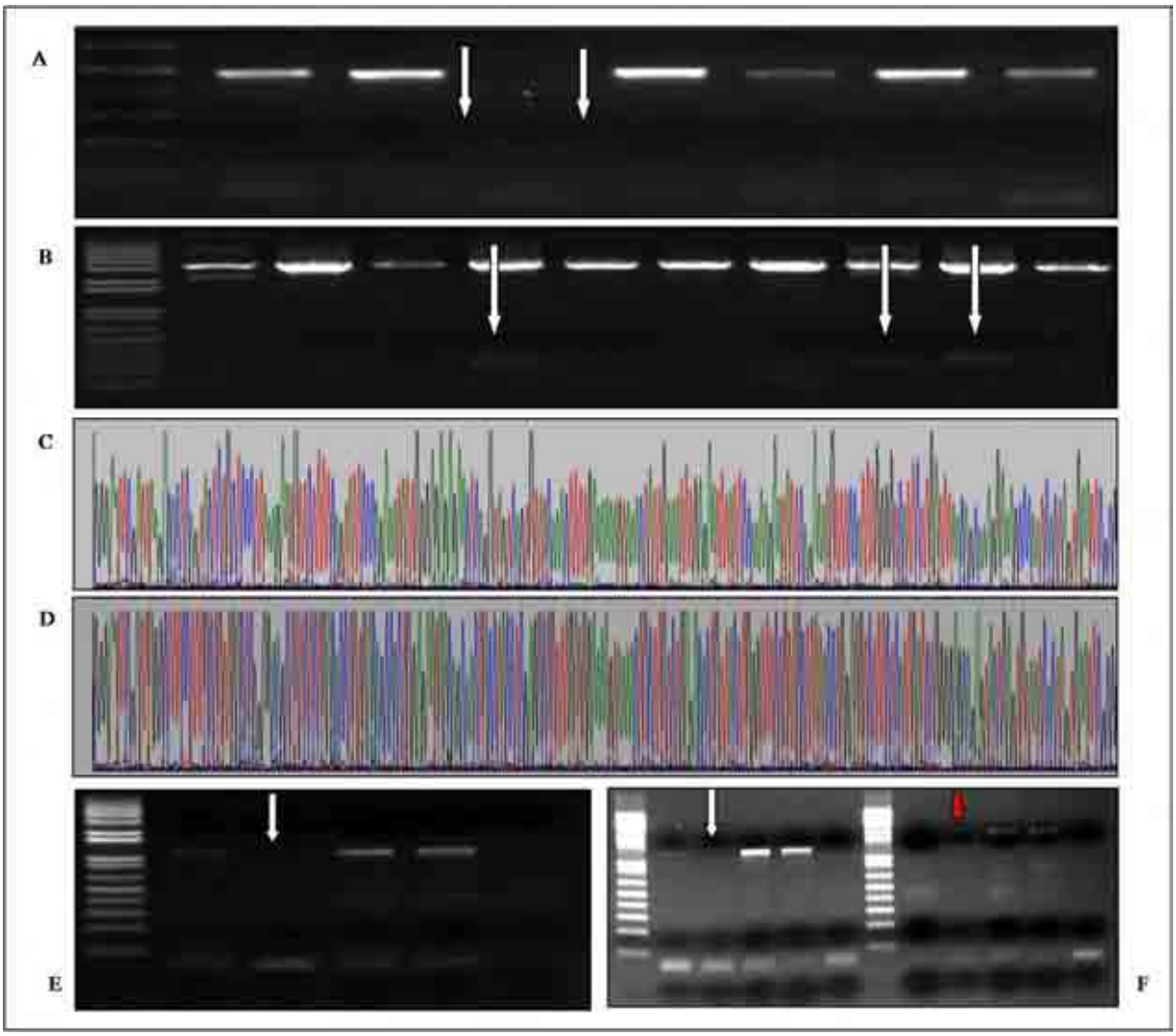

Figure 3.6: *XLF* potential exonic deletion
(A) As indicated by the white arrow a sample shows a truncated PCR product of the 2nd coding exon of *XLF* of 250bp size alongside 6 samples of 492bp wild type size. (B) Three out of the ten minipreps, as indicated by the white arrows, were found to have an insert with the expected size of 250bp. The three minipreps were sequenced and showed two completely different sequences ((C) and (D) chromatograms). (E) PCR amplification of the 1st and 2nd coding exons and in between the 1st intron, this sample did not result in any amplification product as indicated by the arrows alongside 2kb products in the control samples. (F) PCR amplification of the 3rd, 4th coding exons and the 3th intron (on the left side as indicated by the white arrow), this sample did not result in any amplification product compared to 2kb products in the control, whereas on the right side of the gel the PCR amplification of the 5th, 6th, and 7th coding exons including the 5th and 6th introns resulted in 3kb product in this sample as well as the control.

3.3.4 Double Line Sequence of the 7th Coding Exon of *XLF*

Although the PCR amplification of the 7th coding exon produced a single band on the gel which was 458bp as expected, the forward sequence of one third of the samples was of good quality and readable, whereas the other two thirds resulted in double line sequence **(**Figure 3.7). Surprisingly, reverse sequencing of these samples showed that the sequences which were readable on the forward started to be double lined on the reverse and vice versa. To rule out the suspicion of contamination and mixing up of samples, two samples, one with a readable forward sequence and the other one with a double line forward sequence, were cloned into pGEM-T-Easy vector and transformed into competent E. coli. Then, ten colonies per sample were selected, minipreped and sequenced. The sequence of these minipreps revealed nothing, but *XLF* sequence and hence the possibility of contamination had been excluded. Then, fresh PCR product of the 7th coding exon was amplified, gel purified and sequenced, however the sequence showed rapid signal loss, possibly because the gel purification decreases the yield of the purified products. Finally, to overcome this problem, nested forward and nested reverse primers were designed and ordered from Invitrogen. Using these nested primers, fresh PCR products (377bp in length) were amplified (Figure 3.2H), sequenced and the sequence analysis only showed the 3' UTR SNP as mentioned in Section 3.3.1.

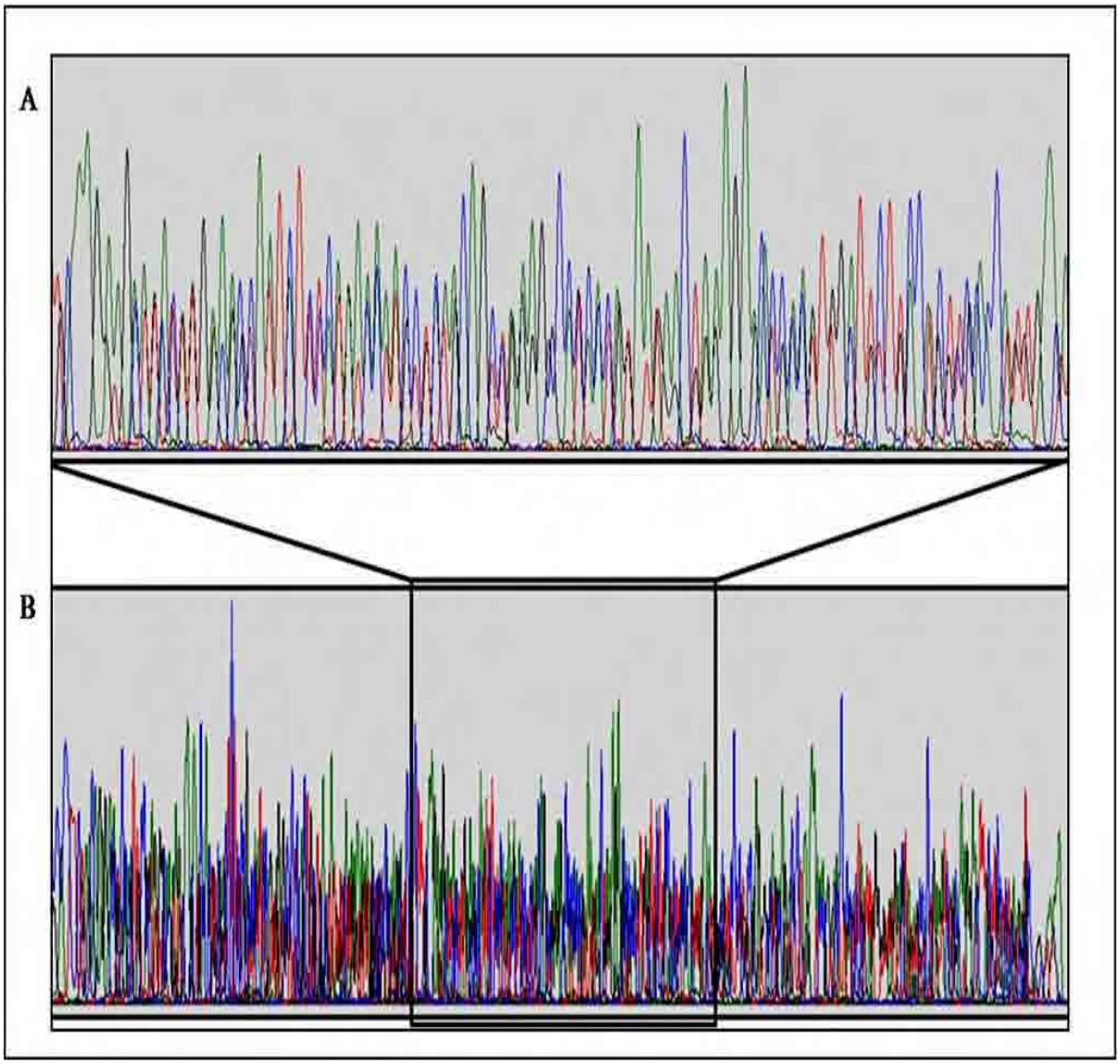

Figure 3.7: Double line sequence of the 7th coding exon of *XLF*
(A) A zoomed in section with clear double line sequence. (B) The full length of the sequence of the 7th coding exon of *XLF* in between the forward and the reverse primers shows the double pattern.

3.4 Discussion

During the initial stage of the project, a random Caucasian population sample was screened, looking for the identification of possible coding variants in *XLF*. Primer pairs were designed for PCR amplification and sequencing the seven coding exons of *XLF* including their intronic boundaries. The SNP analysis characterized two intronic SNPs, already published in the dbSNP, with the three genotypes represented in the studied population sample. The first is an intronic SNP (C→G) 29bp upstream of the 2nd coding exon (NCBI dbSNP, rs2030452) as shown in Figure 3.3A. The second is an intronic SNP (G→C) 59bp upstream of the 3rd coding exon (NCBI dbSNP, rs7585742) as shown in (Figure 3.3B). In addition, two novel noncoding SNPs have been identified in the studied random population sample. The first is an intronic (G→A change) 28bp downstream of the 6th coding exon as shown in Figure 3.4A. The second is a novel 3' UTR SNP (T→C change) 39bp downstream of the 7th coding exon as shown in Figure 3.4B.

It could be envisaged that failure to identify coding SNPs of *XLF* in the relatively small random population sample studied emphasizes its high degree of evolutionary conservation and highlights its important role in NHEJ to maintain the genomic stability as mentioned in Section 1.5.1. Although the initial plan was to extend these studies to a larger population sample and also to some tumour samples that were supposed to be collected in my home country (Egypt), this was proven not to be feasible within the time limits of this project due to organizational problems with the collection of these samples. As a future recommendation, it would be interesting if such coding variants could be identified in tumour samples.

It is noteworthy that the intronic SNPs, despite being noncoding, might be helpful for gene mapping. They can also influence the control of gene activation and its rate of transcription (Chen et al., 2010; Pastinen et al., 2004; Serre et al., 2008). In addition, they may affect splicing and the stability of the transcripts (Hull et al., 2007).

Referring to the sample discussed in Section 3.3.3 that resulted in a shifted band in the 2nd coding exon, as shown in Figure 3.6A, it was difficult to find a simple explanation and one of two scenarios could be envisaged: either a bad quality template or very long deletion spanning chromosome 2q35. Failure to amplify the 1st and 2nd coding exons together in one PCR and failure to amplify the 3rd and 4th coding exons as one product in another PCR, whereas the amplification of the last 3 coding exons resulted in 3kb product as the control samples in one PCR as shown in Figure 3.6E and F, would seem to argue against bad quality DNA as a cause. Moreover, Dr. Emma Woodward, a colleague who was working on the same samples at the same time to sequence another gene, confirmed that sequencing the PCR products of the gene she was amplifying (specifically, in this sample) produced a readable sequence. Hence the possibility of bad quality DNA as a cause was excluded. Finally, four forward primers 2kb upstream of the 1st coding exon were designed to be used individually in conjunction with the reverse primer of the 5th coding exon to identify an *XLF* deletion in this sample, however the PCR did not amplify any products. It was expected to see a 2kb short product in this particular sample in case there was a deletion in between the primer pair used as the actual wild type length is too long to be amplified with the taq DNA polymerase used in the amplification reaction. The use of proofreading polymerase as well as multiplex PCR was recommended to work out whether there was a deletion in this sample, however there

was not enough template DNA left. No history data was available and hence the diagnosis of an *XLF* deletion in this sample could not be confirmed.

It is important to mention that exon deletions, which are among the various types of mutation that exert an effect on the normal function of a gene, often remain unnoticed in initial mutation screening (Hoebeeck et al., 2005). It is also noteworthy that a recent study, published during the course of this project, identified two large *XLF* deletions of 1.9kb and 6.9kb genomic sequence in two patients of German and Malaysian origins, respectively. This study reported that patients with an NBS-like phenotype can have mutations in *XLF*, including multi-exon deletions and that analysis of *XLF* must be considered for patients for whom molecular diagnosis of *NBS* and *LIG4* deficiency has been excluded. It also highlighted that the high degree of phenotypic variability observed in the affected children of one family might be associated with *XRCC4* polymorphisms (Dutrannoy et al., 2010).

This project was originally set up to investigate the impact of possible polymorphic changes and PTMs on the function of XLF. Our preliminary data indicated that XLF is very efficiently phosphorylated by DNA-PK (Dr. Boris Kysela – unpublished observation). During the course of this project, the paper was published where XLF was found to be phosphorylated *in vitro* at its serine residues S245 and S251 in response to IR (Yu et al., 2008). Moreover, IR-induced phosphorylation of S245 is largely DNA-PK dependent, while that of S251 is ATM-dependent. Curiously, these modifications on the XLF extreme C-terminus have absolutely no effect on the ability of XLF to interact with DNA or on the *in vivo* repair of IR-induced DSBs (Yu et al., 2008). This unexpected observation is in line with other recently published data that the phosphorylation of KU (Douglas et al., 2005a), XRCC4 (Yu et al., 2003) and LIG4 (Wang et al., 2004) by DNA-PK are not required for NHEJ. Taken together, these data

indicate that although all NHEJ core components are efficiently phosphorylated *in vitro*, their phosphorylation is completely dispensable for their function *in vivo*, whereas the only notable exception is autophosphorylation of DNA-PK itself (Block et al., 2004; Chan et al., 2002; Reddy et al., 2004). Moreover, this highlights the possibility that another PTM or a combination of PTMs may play a key role in the regulation of XLF function. Hence, the characterization of the acetylation status of XLF and *in vitro* mapping of XLF acetylation sites by mass spectrometry will be the subject of Chapter Four.

CHAPTER FOUR: CHARACTERIZATION OF XLF ACETYLATION STATUS (XLF ACETYLOME)

4.1 Introduction

Protein acetylation is one of the most frequent PTMs among eukaryotes. Although co-translational N^{α}-terminal acetylation is the most common, occurring on approximately 85% of eukaryotic proteins, the less common post-translational acetylation of ε-amino group of lysine amino acid seems to be more important for functional regulation (Polevoda and Sherman, 2000). The addition of an acetyl group on lysine amino acids neutralizes the positive charge of the lysine side chain and as a result it has a significant impact on the electrostatic properties of the protein. Early studies suggested that many histones' lysine residues are acetylated abundantly and that acetylation of histones plays a role in the regulation of transcription in the context of chromatin (Allfrey et al., 1964; Clayton et al., 2006; Nightingale et al., 1998; Vidali et al., 1968).

The first histone acetyltransferase enzyme, HAT A, was identified in Tetrahymena. HAT A shares significant similarity with the yeast protein GCN5, which also catalyzes histone acetylation, in terms of their amino acid sequence (Brownell et al., 1996). Subsequently, about 30 proteins have been found to exhibit HAT activity. Each of these HATs may have histone specificity and different HATs are specific with regard to which histone amino acids they will acetylate. Interestingly, HATs target a wide range of non-histone protein substrates in addition to histones. Unlike N^{α}-terminal acetylation, post-translational ε-amino lysine acetylation of proteins is highly reversible. In humans, 18 histone deacetylase enzymes (HDACs) have been identified so far, HDAC1 to HDAC11 and SIRT1 to SIRT7, which remove the acetyl group and keep the balance of lysine acetylation in histones. Like HATs, HDACs also possess substrate specificity and accumulating evidence suggests that many, if not all, HDACs can target non-histone proteins at least *in vitro* as well (Glozak et al., 2005).

Lysine acetylation targets proteins in every cellular compartment from the nucleus to the plasma membrane. Hence, it plays a key role in diverse cellular processes, such as chromatin remodelling, cell cycle, splicing, nuclear transport and actin nucleation. High-resolution mass spectrometry has recently identified 3600 lysine acetylation sites on 1750 proteins, among them 167 acetylation sites on 72 DNA damage and repair proteins (Choudhary et al., 2009). Although, fewer DNA repair proteins such as p53, KU70, FEN1 and WRN were known to be acetylated (Yang and Seto, 2008), Choudhary and colleagues found that many other DNA damage repair proteins, such as KU80, MDC1, DDB1/2, RAD50, PCNA, MSH2, BLM and RAD54, are acetylated (Choudhary et al., 2009).

The patterns of protein acetylation and their mechanism of action vary from one protein to another and can be generally classified into three groups. First, acetylation of one or few residues can act as a simple on/off switch. Second, acetylation of lysine residue clusters can form charged patches which exert gauge-like effects or provide a failsafe mechanism. The number of acetylated residues rather than acetylation of an individual lysine will be in such cases critical for the functional impact. Third, acetylation crosstalks with other PTMs in a site-specific manner (Yang and Seto, 2008).

4.2 Acetylation Switches

It is important to mention that various PTMs can target lysine residues (Figure 4.1). This provides the basis of modification-based switches, where the targeted replacement of one modification by another regulates protein functions. For instance, alternative acetylation/ubiquitination determines protein stability, whereas competing acetylation/sumoylation likely regulates protein activity with sumoylation of transcription

factors being often linked to transcriptional repression (Spange et al., 2009; Geiss-Friedlander and Melchior, 2007). Moreover, acetylation of some nonhistone proteins occurs at multiple sites and crosstalks with phosphorylation, methylation, sumoylation, ubiquitination and other PTMs to form dynamic regulatory programs. This diversifies cellular signaling networks and indicates that an orchestra of phosphorylation, acetylation and other PTMs controls cellular signalling networks and not only one PTM (Yang and Seto, 2008).

Interestingly, the term protein modification code (PTM code) or protein code much like the histone code, has been used to describe proteins with multisite PTMs (Schreiber and Bernstein, 2002; Kouzarides, 2007; Ruthenburg et al., 2007; Turner, 2007). It is clearly much more complex than the genetic code and recent studies clearly indicate that multisite PTMs are somewhat codified and act in sequential and combinatory manners (Corden, 2007; Kurash et al., 2008; Sampath et al., 2007; Walter et al., 2008; Winter et al., 2008). So, lysine acetylation could interplay agonistically or antagonistically with other PTMs. The complexity of such interplay in a given protein correlates with the biological complexity of the corresponding organism.

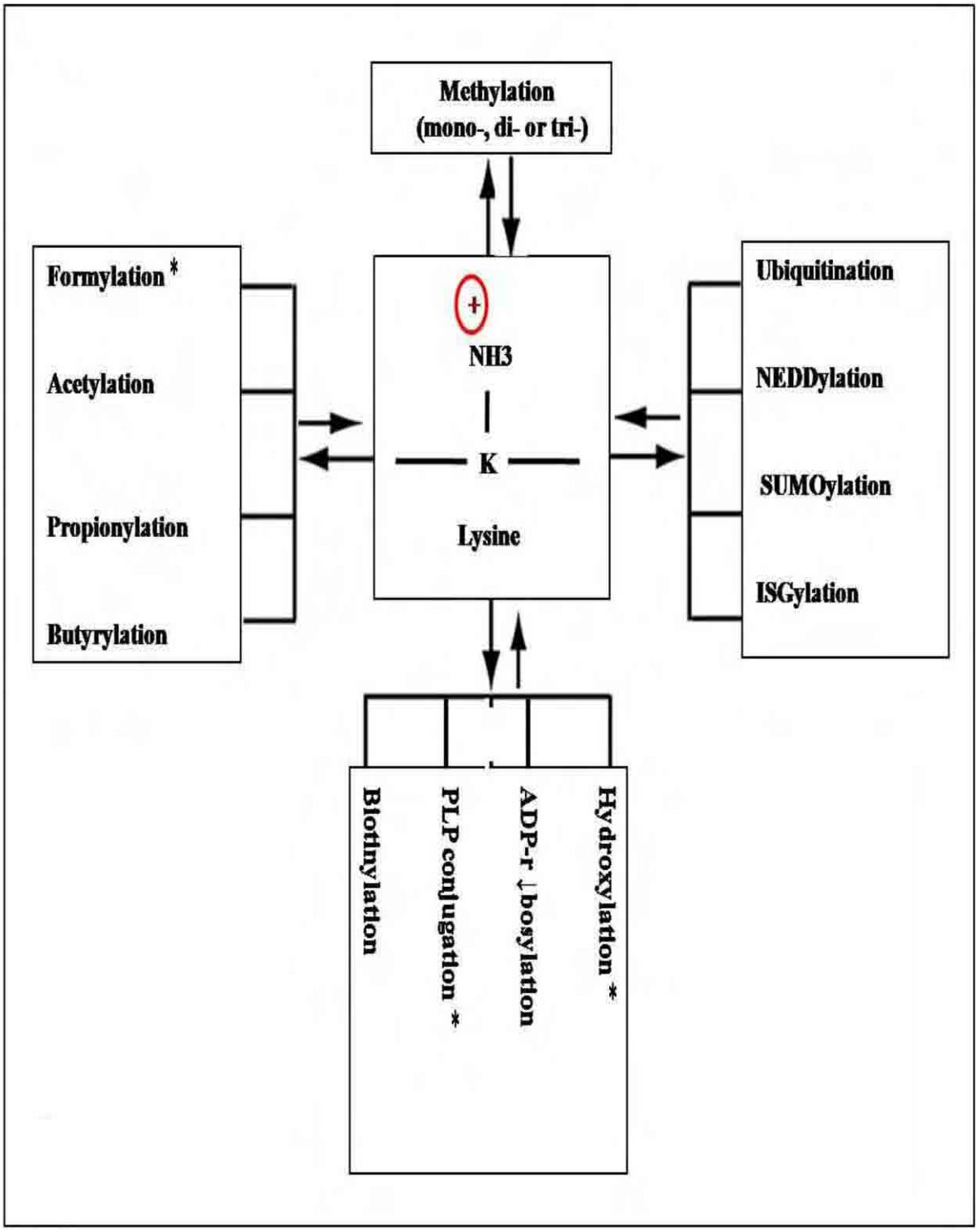

Figure 4.1: Lysine side chain modifications
This diagram summarizes all the covalent modifications of the lysine side chain. All the listed modifications are reversible except (those indicated by black star) formylation, hydroxylation, and pyridoxal 5' phosphate (PLP, a vitamin B6 derivative) conjugation. All the modifications occur enzymatically except formylation and all are mutually exclusive: one modification precludes further modifications by others and vice versa (Yang and Seto, 2008)**.**

4.3 Acetylation and NHEJ Repair Pathway

The only core component of the NHEJ pathway that has been studied in the context of acetylation is the multi-functional protein KU70 (Cohen et al., 2004a). It has been demonstrated that SIRT1 deacetylates KU70, allowing it to sequester BAX away from the mitochondria, ultimately inhibiting apoptosis (Cohen et al., 2004b). Furthermore, the preliminary work in our laboratory has shown that KU70 (but not KU80) coprecipitates with HDAC3 (personal communication with Dr. Chris Bruce). Interestingly, additional evidence suggests that TIP60 targets DNA-PK (Jiang et al., 2006a; Sun et al., 2005) besides ATM (Sun et al., 2005). Also, DNA-PKcs has been shown to phosphorylate HDAC3 and this phosphorylation is accompanied by a significant enhancement of the HDAC3 activity (Jeyakumar et al., 2007). Although KU70, an important regulator of DNA-PK, has been shown to be acetylated (Cohen et al., 2004a; Chen et al., 2007), it remains unclear whether KU70 acetylation plays a role in the regulation of DNA-PK. The effect of such modulation on cell survival and DSBR in response to IR will be investigated in Chapter Five.

The emerging picture at present is that XLF may have a much more complex role than originally proposed. A recent *in vivo* study has found that XLF accumulates (within a few seconds), in a KU-dependent but XRCC4-independent manner, at the sites of IR-induced DSBs. This finding indicated that XLF bridges the sensor and ligation complexes of the NHEJ machinery and highlights the flexibility of the assembly of the NHEJ factors on DSBs (Mari et al., 2006; Yano and Chen, 2008; Yano et al., 2008). Also, it has been demonstrated recently that XLF, ATM and H2AX all have fundamental roles in processing and joining DNA ends during VDJ recombination, but these roles have been covered by unexpected functional redundancies (Zha et al., 2011). This highlights the possibility that XLF might play

a role in damage signalling, in addition to the above mentioned roles in NHEJ. Taken together, these XLF complex interactions with many additional partners strongly suggest the possibility that, in the absence of the requirement for the phosphorylation of XLF for its function *in vivo* (which is usually the primary regulatory modification), another PTM or a combination of PTMs may play a key role in the regulation of XLF function. In fact, several lines of preliminary evidence focused our attention on the possibility that acetylation/deacetylation of the core NHEJ proteins themselves (for the importance of chromatin acetylation in DNA repair, interested readers are referred to (Averbeck and Durante, 2011; Bird et al., 2002; Downs et al., 2004; Tamburini and Tyler, 2005)), may play an important role in the regulation of their functions. First, the previous work in the group has established good evidence that all core NHEJ proteins are specifically acetylated by HATs *in vitro* (Dr. Boris Kysela – unpublished). Second, it has recently been shown that the modulation of KU70 acetylation (the main functional interacting partner of XLF *in vivo*) mediates HDAC inhibitor-induced chemosensitization of cancer cells (Chen et al., 2007). Third, the acetylation of KU70 has also been shown to regulate its apoptotic function (Cohen et al., 2004a).

4.4 Aims

The main aims of this part of the project:

1- *In vitro* expression and purification of recombinant GST-XLF in E. coli as a substrate for the *in vitro* acetylation studies

2- *In vitro* XLF acetylation mapping using mass spectrometry.

3- *In vivo* acetylation study in human cells overexpressing pFLag-XLF, pFLag-XRCC4 and pFLag-HDAC3.

4.5 Results

4.5.1 Cloning, Overexpression and Purification of GST-XLF in E. coli

Miniprep of pGEX-2TK-p plasmid with *XLF* cloned between EcoRI and XhoI restriction sites were double-digested using EcoRI and XhoI restriction enzymes and the products were resolved on an agarose gel to check for the presence of the insert as shown in Figure 4.2A. The extracted plasmid DNA was used to transform competent E. coli capable of protein expression as described in Section 2.3.8. Colonies were screened by colony PCR using pGEX forward and reverse primers for the presence of *XLF* as shown in Figure 4.2B. Positive colony was used to generate recombinant protein. Protein expression and induction were performed as described in Section 2.3.8.1, and GST-XLF was purified as described in Section 2.3.8.2. The recombinant protein was then eluted in GST-tag elution buffer and analysed by SDS-PAGE as shown in Figure 4.3. The two bands were cut out of the gel and sent for mass spectrometry. Mass spectrometry confirmed that the two bands were XLF. As the molecular weights of GST-tag and XLF are 25kDa and 33kDa respectively, it is expected that the fusion protein GST-XLF runs at a higher level as shown in Figure 4.3 (top band in the red box). In agreement with this, it has been previously shown that the fusion protein GST-XLF runs at a level higher than 55kDa (Jayaram et al., 2008). As the bottom band in the red box (Figure 4.3) was confirmed to be XLF by mass spectrometry, it is possible that the GST-tag undergoes spontaneous cleavage and leaves XLF to run at a lower level than GST-XLF or part of the XLF C-terminus degrades.

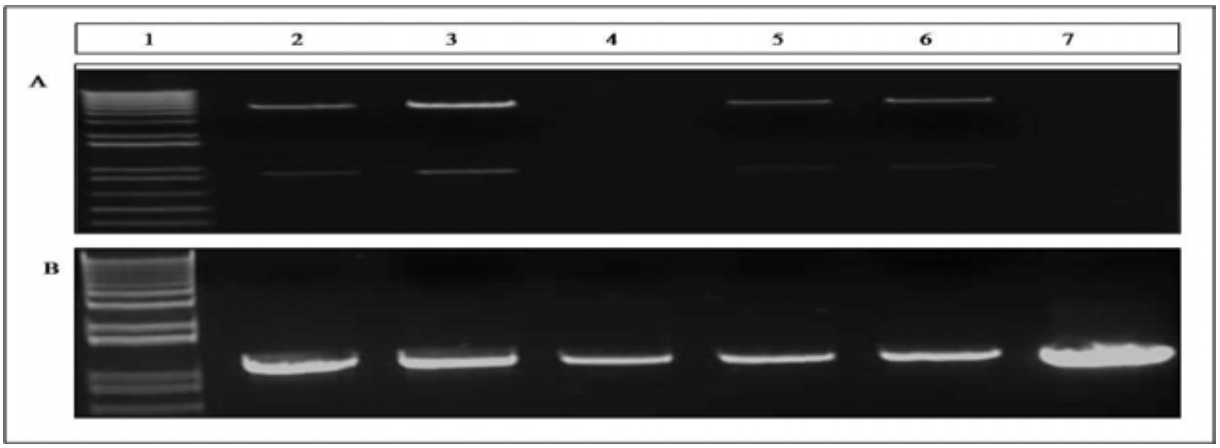

Figure 4.2: pGEX-2TKp-*XLF* double digestion and colony PCR
(A) Minipreps of pGEX-2TKp-*XLF* were double digested with EcoRI and XhoI, the bottom bands (lanes 2, 3, 5 and 6) corresponds to *XLF*. (B) Bacteria were transformed with pGEX-2TKp- *XLF* and five colonies were selected and minipreped. Colony PCR of the five minipreps were positive (lanes 2, 3, 4, 5 and 6). Lane 7 represent a positive control. The first clone was used for induction of recombinant XLF protein expression.

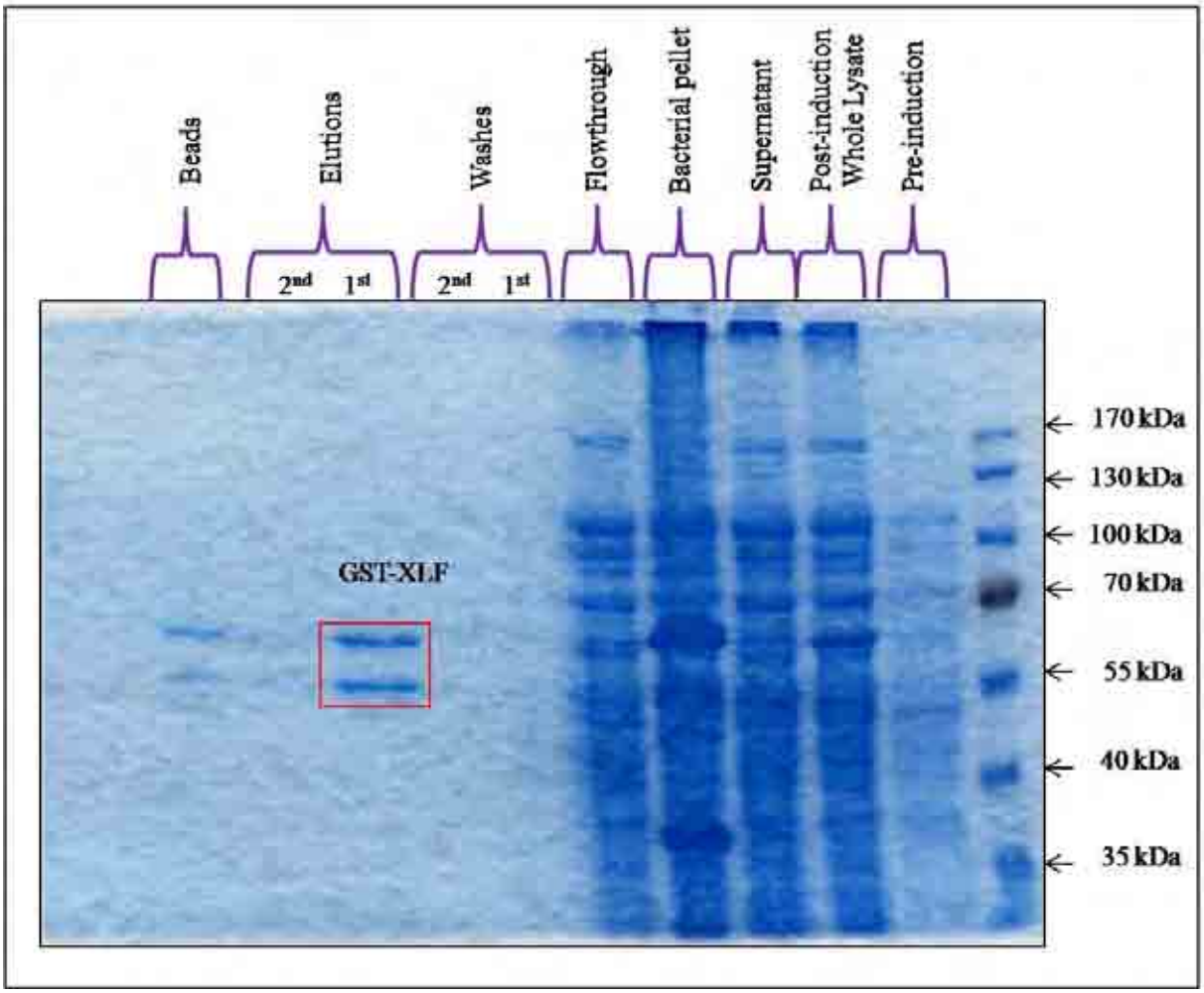

Figure 4.3: GST-XLF purification in E. coli
PGEX-2TKp expression vector with *XLF* cloned into EcoRI-XhoI restriction sites of the multiple cloning site was used to transform E. coli capable of protein expression. IPTG was used for induction of recombinant protein expression. After lysis, the GST-XLF recombinant protein was eluted in 500µL aliquots from affinity beads by glutathione. The first elution contains the most protein (red box) and very little protein remained on the beads.

4.5.2 Analysis of XLF Acetylation Sites

4.5.2.1 Bioinformatics-based Prediction of XLF Acetylation Sites

Four prediction software packages were used to predict which lysine residues of XLF undergo acetylation (Table 4.1). They all apply algorithms and support vector machines to predict protein acetylation based on the sequence characteristics of acetylated lysines within histones and nonhistone proteins (Basu et al., 2009; Li et al., 2006; Li, 2009; Xu et al., 2010). All the four packages predicted that 9 lysine residues of XLF undergo acetylation (Table 4.2).

Prediction Software	URL
PAIL: Prediction of Acetylation on Internal Lysines	http://bdmpail.biocuckoo.org/prediction.php
LysAcet: Lysine Acetylation Prediction	http://www.biosino.org/LysAcet/predict.jsp
PredMod	http://ds9.rockereller.edu/basu/redmod.html
EnsemblePail	http://www.aporc.org/EnsemblePail/index.html

Table 4.1: Acetylation prediction software packages

Peptide	Position
VVSQRAKELNKRL	59
RAKELNKRLTAPP	63
ATLLHMKDLEIQD	160
EVQVGQKHQGAGD	231
TLSAPEKESTGTS	272
QRPQLSKVKRKKP	288
PQLSKVKRKKPRG	290
LSKVKRKKPRGLF	292
SKVKRKKPRGLFS	293

Table 4.2: Prediction of XLF acetylated lysine residues
The XLF lysine residues that have been predicted to be acetylated by all the four packages are highlighted in red.

4.5.2.2 Mapping *in vitro* Acetylation Sites of XLF and XRCC4

The overall strategy implemented for studying XLF acetylation 0is outlined in a simplified flowchart as shown in Figure 4.4. This part of the project had been undertaken in collaboration with other members of the group (Dr. Darren Arbon and Diana Walsh) as part of a larger effort to study the functional significance of acetylation of the core members of NHEJ by Dr. Kysela's group.

In order to examine acetylation *in vitro*, recombinant XLF and XRCC4 proteins were individually acetylated *in vitro* using recombinant HATs domains (PCAF, P300, CBP and GCN5) and non-radioactive acetyl CoA as described in Section 2.3.9. The proteins were also tested for the basal levels of acetylation which may present before *in vitro* acetylation reaction, since some acetylation is known to take place in the *in vitro* overexpression systems, from which the proteins were purified (Huq and Wei, 2005).

Indeed, mass spectrometry showed that XLF-K160 is acetylated by both PCAF and CBP, whereas XLF-K63 and XLF-K290 are acetylated by P300. Interestingly, XLF-K197 has been found to be acetylated basally in the absence of HATs (Table 4.3). Moreover, it has been found that XRCC4-K102 is acetylated by P300 and GCN5, whereas XRCC4-K169 is acetylated by PCAF and P300 (Table 4.4). Furthermore, PCAF, CBP and P300 have been found to acetylate XRCC4 lysine residues K188, K197 and K309 (Table 4.4). It has also been found that XRCC4 lysine residues K187 and K188 are basally acetylated in the absence of HATs (Table 4.4).

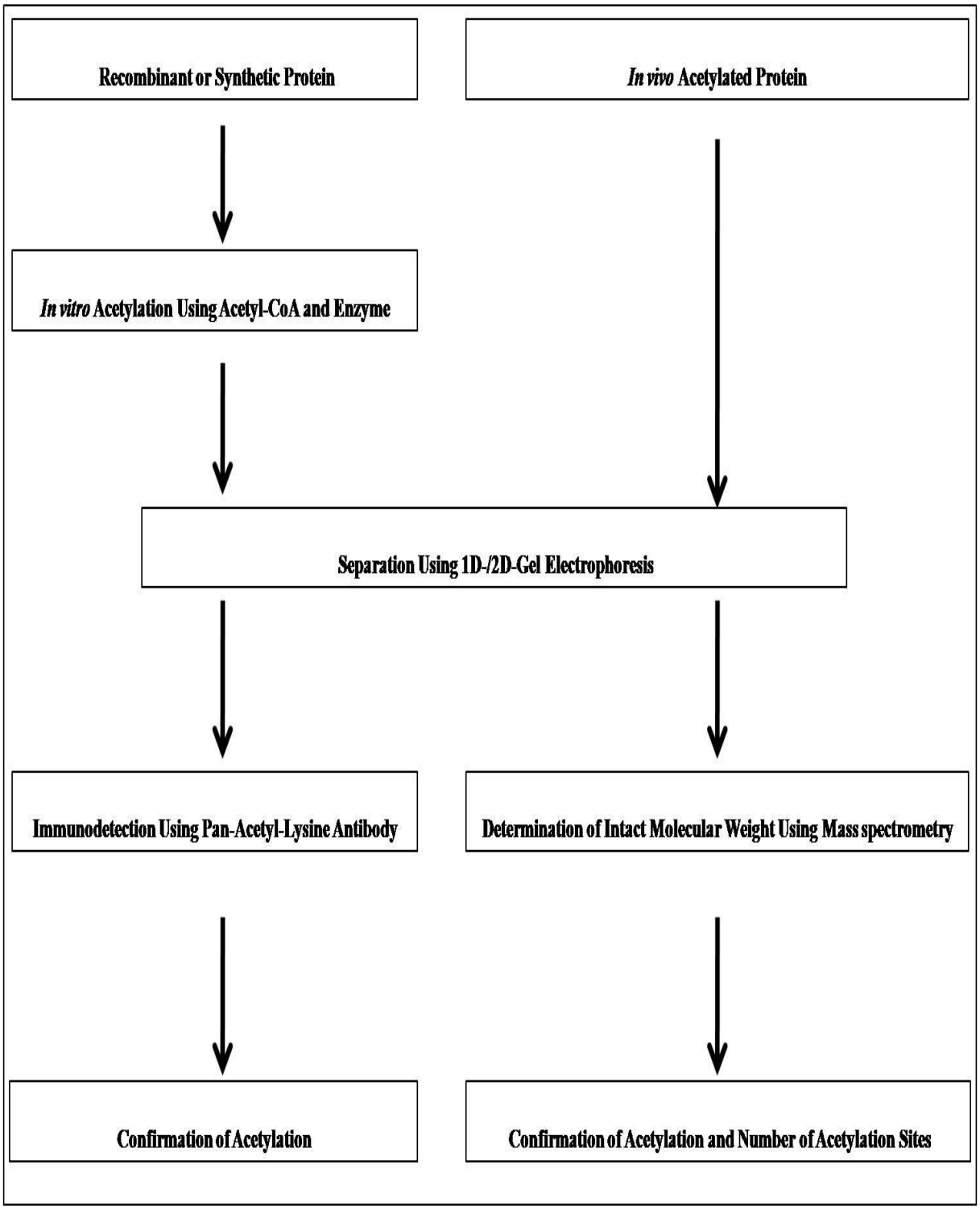

Figure 4.4: Strategy for studying protein acetylation
After enzymatic *in vitro* acetylation of recombinant proteins using [^{14}C] AcCoA, the proteins are separated from radioactive AcCoA and other by-products by one-dimensional gel electrophoresis and the acetylated proteins are detected by autoradiographic imaging. Immunodetection using acetylation-specific antibodies can be performed with *in vivo* and *in vitro* acetylated proteins using [^{12}C]AcCoA. However, both radioactive detection and immunodetection provide evidence for acetylation but do not give information about the number of acetylation sites in a protein. Mass spectrometry characterizes acetylation status of the protein and identifies the number of acetyl groups attached to the protein (Dormeyer et al., 2005).

Lysine	PCAF	P300	CBP	GCN5	XLF Alone
63		(low)			
160	(high)		(low)		
197	(low)	(low)	(low)		(low)
290		(low)			

Table 4.3: *In vitro* acetylation sites of XLF by mass spectrometry
The XLF lysine residues that undergo acetylation by PCAF, P300 and CBP are listed. In the absence of HATs, XLF is basally acetylated at K197. High and low indicate the level of acetylation. XLF-K160 is the only apparent highly acetylated residue with PCAF.

Lysine	PCAF	P300	CBP	GCN5	XRCC4 Alone
102		(low)		(low)	
169	(low)	(high)			
187	(high)	(med)		(high)	(high)
188	(high)	(med)	(low)	(high)	(high)
197	(low)	(high)	(high)		
309	(low)	(high)	(high)		

Table 4.4: *In vitro* acetylation sites of XRCC4 by mass spectrometry
The XRCC4 lysine residues that undergo acetylation by PCAF, P300, CBP and GCN5 are listed. Although K187 and K188 are highly acetylated with PCAF and GCN5 their acetylation is most likely not due to the presence of the HATs as they are also acetylated in the absence of HATs. XRCC4 shows high levels of acetylation at K197 and K309 in the presence of P300 and CBP.

4.5.3 *In vivo* Acetylation Study

First, Western blot was performed as shown in Figure 4.5, to check the expression status of pFlag-XLF, pFlag-XRCC4 and pFlag-HDAC3 overexpressing cell lines alongside MRC5VA cell line as a negative control. In order to test the Pan-Ac-K Ab, whole cell lysates from the four cell lines were prepared as described in Section 2.3.1 and probed with Pan-A-K Ab as shown in Figure 4.6. This blot showed a number of promising potential findings. It demonstrates that a 70kDa protein in MRC5VA control cells is basally acetylated, it becomes hyperacetylated one hour after exposure to IR, and its acetylation level drops again to the basal level two hours after exposure to IR. Interestingly, this 70kDa protein could not be seen in the pFlag-HDAC3 overexpressing cell lines, indicating that its deacetylation is HDAC3-dependent. Moreover, as the bands between 70kDa and 40kDa including the 55kDa appeared to be acetylated, it could be speculated that XLF and XRCC4 might potentially undergo acetylation *in vivo*, their acetylation might change in response to IR and their deacetylation might be HDAC3-dependent. However, it is recommended that coimmunoprecipitation and mass spectrometry have to be done for verification of these potential finding. Furthermore, the blot also shows that the acetylation patterns of both pFlag-XLF and pFlag-XRCC4 overexpressing cell lines looked different compared to the acetylation patterns of both MRC5VA control and pFlag-HDAC3 overexpressing cell lines.

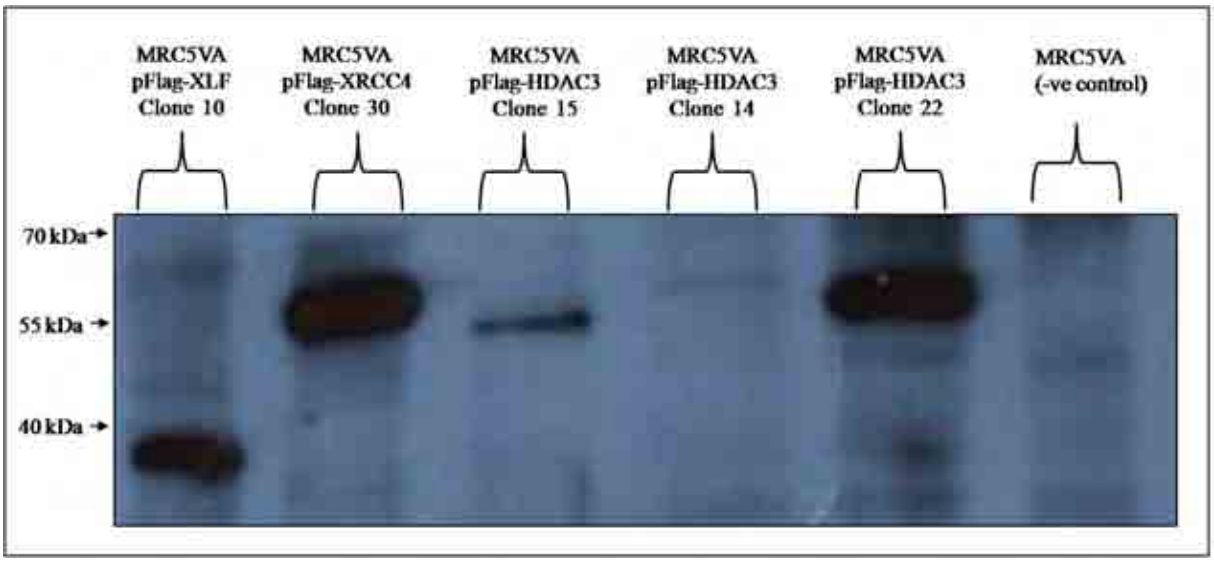

Figure 4.5: Expression status of pFlag-XLF, pFlag-XRCC4 and pFlag-HDAC3 cell lines
The Western blot shows that pFlag-XLF clone 10, pFlag-XRCC4 clone 30 and pFlag-HDAC3 clone 22 were expressing whereas pFlag-HDAC3 clone 14 and clone 15 were not. MRC5VA was used as a negative control.

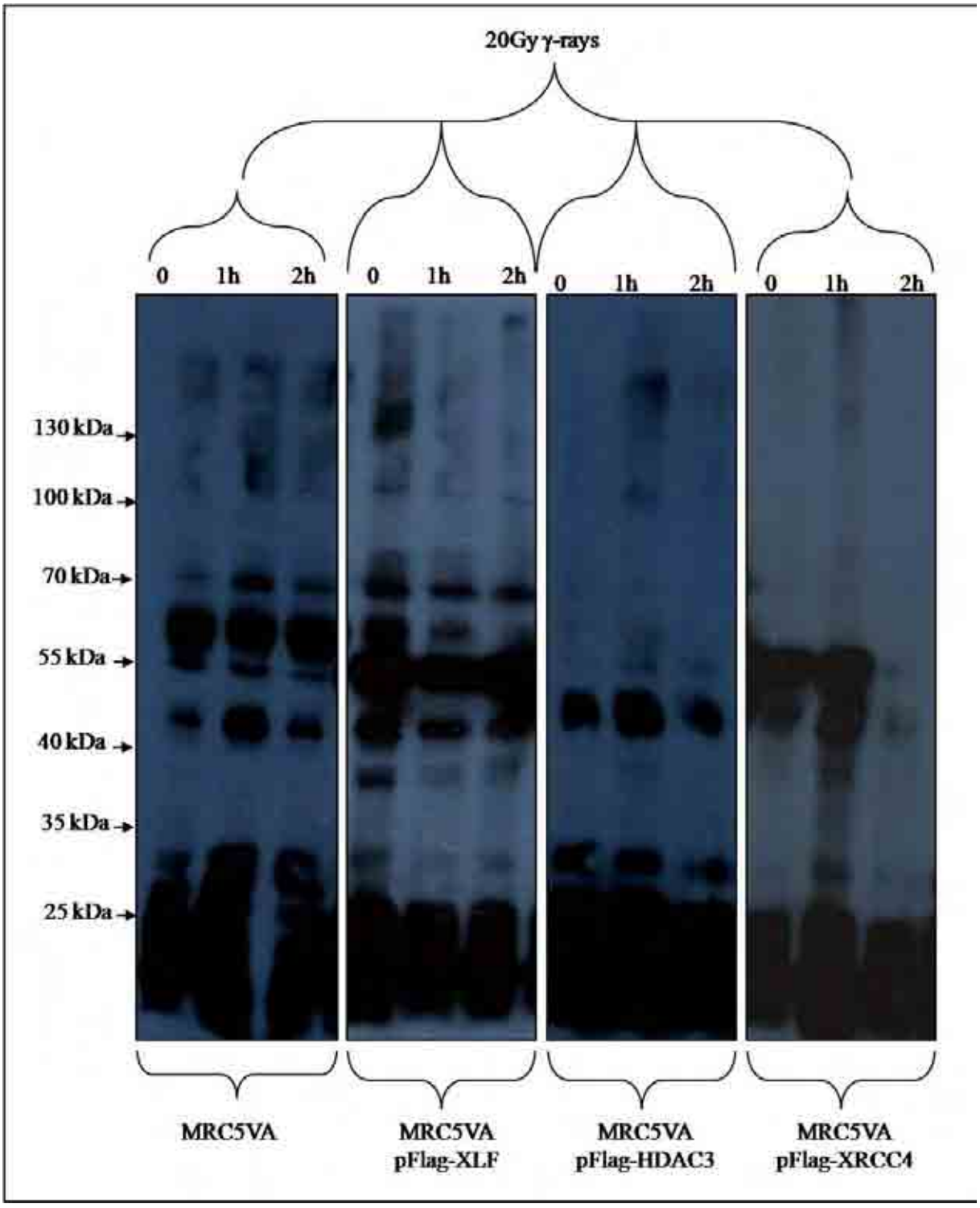

Figure 4.6: Pan-Ac-K antibody Western blot
Protein extracts from MRC5VA control cells, pFlag-XLF, pFlag-XRCC4 and pFlag-HDAC3 overexpressing cell lines non-irradiated, 1 hour and 2 hours after exposure to 20Gy of IR were separated on 9% SDS gel and probed with Pan-A-K Ab. The acetylation pattern of each cell line was different in comparison to the other cell lines, indicating that overexpressing pFlag-XLF, pFlag-XRCC4 and pFlag-HDAC3 changes the acetylation pattern. The density of the 70kDa bands in the 1st blot (MRC5VA cell line), the 55kDa bands in the 4th blot (pFlag-XRCC4 cell line) and the 40kDa bands in the four blots changes in response to IR reflecting acetylation changes in response to IR.

4.6 Discussion

Although KU70 was the only known core NHEJ member to be acetylated (Chen et al., 2007), Choudhary and colleagues recently reported that KU80 is acetylated as well (Choudhary et al., 2009). Taken together, the logical assumption that the other core NHEJ members could be acetylated as well holds true. In order to validate this assumption, a strategic plan to verify the acetylation status of XLF and map the acetylation sites of XLF and XRCC4 both *in vivo* and *in vitro* has been implemented as outlined above in Figure 4.4. The effects of XLF acetylation on the efficiency of DSBR will be the focus of future work.

Preliminary acetylation experiments using radioactive Acetyl-CoA proved that XLF is acetylated *in vitro* by PCAF HAT (personal communication with Dr. Boris Kysela). Afterwards, *in vitro* acetylation was performed by both Dr. Darren Arbon and Diana Walsh as described in Section 2.3.9. Mass spectrometry analysis showed that XLF is basally acetylated at K197 and PCAF acetylates XLF at K160 (Table 4.3). It is important to mention that the basal acetylation of recombinant proteins might have originated in the *in vitro* overexpression systems from which the proteins were purified as it does exist in the absence of HATs (Huq and Wei, 2005).

Interestingly, it has been suggested that XLF mediates its functional interactions via both its head-domain and coiled-coil areas. Moreover, the region surrounding the conserved K160 of XLF coiled-coil region is unlikely to be a DNA-binding region or a ligase-binding site, however it could be a conserved site of PTM, such as ubiquitination. Also, K197 might be critical for maintaining the folded architecture of XLF C-terminus (Li et al., 2008). This

highlights the importance of the two XLF lysine residues, K160 and K197, that have been found to be acetylated *in vitro* and the need for investigating them further.

Although the two XLF lysine residues (K197 and K160) were not predicted by the online acetylation prediction software packages used, XLF lysine residues: K290, K292 and K293 are among the residues that have been predicted by the software packages (Table 4.2). These three lysine residues reside in the highly conserved XLF extreme C-terminus. Interestingly, the last 10 amino acids of the highly conserved XLF C-terminus were found to be indispensible for the recruitment of XLF to KU complex (Yano et al., 2011). Taken together, these three lysine residues, K290, K292 and K293, being highly conserved and in the extreme C-terminus of XLF, which has been proven to be critical for DNA dependent XLF-KU interaction, might play a regulatory role in XLF function that would warrant further careful investigation.

The mass spectrometry analysis also showed that XRCC4 K169 is basally acetylated and P300 and CBP acetylate both K197 and K309 (Table 4.4). Interestingly, the XRCC4 coiled-coil includes the LIG4 binding region, which spans residues 173-195 in both chains of the XRCC4 dimer that binds the inter-BRCT domain linker region of LIG4 (Sibanda et al., 2001). Again this highlights the importance of the two XRCC4 lysine residues K169 and K197 that have been found to be acetylated *in vitro* and the need for investigating their role further. It will be interesting to examine the effects of both XLF and XRCC4 acetylation sites identified on the interactions between XLF, XRCC4 and LIG4 and the regulation of the final ligation step of NHEJ.

Although the prediction of XLF acetylation and the *in vitro* data presented here seemed a little contradictory, caution is necessary when examining the data leading to conclusions that HAT or HDAC is responsible for any given acetylation or deacetylation event. For example, optimal conditions to assay non-histone protein deacetylation have not yet been fully investigated in many cases (Glozak et al., 2005). Also, it is very important to consider that the use of only the catalytic domain of a HAT and not the full length protein can lead to different results. Removal of the non-catalytic domains can eliminate sites of protein-protein interaction as well as influence secondary structure (Polesskaya and Harel-Bellan, 2001). This highlights the importance of mass spectrometry for the identification of acetylation sites both *in vitro* and *in vivo*. In fact, the Pan-Ac-K Ab was chosen for probing co-immunoprecipitates of overexpressed pFlag-XLF, pFlag-XRCC4 and pFlag-HDAC3. This will help in confirming the interactions of the individual members of NHEJ with HDAC3 and identifying *in vivo* acetylation sites using mass spectrometry.

For the verification of the XLF acetylation status *in vivo*, the Pan-Ac-K Ab was used to probe protein extracts from MRC5VA control cells, pFlag-XLF, pFlag-XRCC4 and pFlag-HDAC3 overexpressing cell lines as described in Section 2.3.1. This pilot experiment demonstrated that KU70 is not the only core member of the NHEJ to be acetylated but that also XLF and XRCC4 potentially undergo acetylation *in vivo* and their deacetylation might be HDAC3-dependent as most of the acetylated bands seen in the three cell lines are not present in the pFlag-HDAC3 overexpressing cell line again, as shown in Figure 4.6. Moreover, their acetylation might change in response to IR, indicating that their acetylation might regulate NHEJ and/or heterochromatin structure in response to IR-induced DNA damage.

Interestingly, although Cohen and colleagues using UV treated 293T cells demonstrated that the levels of KU70 acetylation increased between 3 and 6 hours after UV treatment, which correlates with BAX activation (Cohen et al., 2004a) and migration of CBP to the cytoplasm (Sawada et al., 2003b), the 70kDa protein acetylation increased after 1 hour and returned to its basal acetylation level 2 hours post-irradiation. The contradiction between the two observations might be due to the differences between the two treatments and the two cell lines.

It is noteworthy that the acetylated-lysine specific antibodies should not be used alone to provide the sole evidence of acetylation, as it is possible to obtain both undesirable false positives and false negatives when using these antibodies (Glozak et al., 2005). Hence, this analysis could be repeated with the addition of HDAC inhibitor, as the acetylation is a reversible modification. In fact, it has been noticed that the cell lines seem to be losing the expression especially pFlag-XLF and pFlag-HDAC3 cell lines. This, in addition to the reversibility of the acetylation and the low stability of the antibody in use, could explain the technical difficulties experienced with the reproducibility of this experiment.

In conclusion, this part of the project provided good preliminary evidence that XLF and XRCC4 are acetylated and identified their acetylated lysine residues *in vitro*. The effect of acetylation of these residues on the regulation and functional interactions of both XLF and XRCC4 needs to be investigated, as this might help identifying new targets for cancer treatment.

CHAPTER FIVE: *IN VIVO* ANALYSIS OF THE IMPACT OF ACETYLATION/DEACETYLATION OF KU70 LYSINE RESIDUES K317, K331 AND K338 ON THE REPAIR OF IR-INDUCED DSBS

5.1 Introduction

KU70 is a multifunctional protein that orchestrates both DNA repair and apoptosis in response to cellular stress (Chou et al., 1992; Wang et al., 1998a; Wang et al., 1998b; Wu and Lieber, 1996). The eight lysine residues of KU70, that undergo acetylation by either CBP or pCAF: five in its C-terminus (K539, K542, K544, K553, and K556) and three in its N-terminal DNA binding domain (K317, K331 and K338), were identified. The acetylation of K539 and K542 has been found to be critical for the regulation of BAX-mediated apoptosis. Interestingly, the KU70 N-terminal K317, K331 and K338 have been suggested to play a role in DNA repair however, this role has not been fully investigated yet (Cohen et al., 2004a; Sawada et al., 2003a; Sawada et al., 2003b). The dual role of KU70 might be regulated at both transcriptional and posttranslational levels in response to apoptotic stimuli. Interestingly, targeted acetylation and deacetylation by HATs and HDACs is likely to play a role in this regulation. Moreover, increased KU70 acetylation as a result of HDAC inhibition has been shown to abolish its ability to bind BAX and suppress BAX-mediated apoptosis (Cohen et al., 2004a; Cohen et al., 2004b; Subramanian et al., 2005).

The dynamic balance between both HDACs and HATs regulates gene transcription and their imbalance can result in disordered cell cycle, proliferation and differentiation in normal cells and then lead to carcinogenesis (Kouzarides, 1999; Bi and Jiang, 2006). In fact, HDAC inhibitors act as an adjuvant, sensitizing cancer cells to radio-/chemotherapy via various mechanisms. They induce hyperacetylation of histones, remodelling chromatin structure and promoting transcription of tumour suppressor genes (Brown and Strathdee, 2002). In addition, they modulate the acetylation of many non-histone proteins, including p53, HSP90, KU70 (Lin et al., 2006) and alpha serine/threonine protein kinase (AKT) (Chen et al., 2005), thus

affecting cell proliferation and survival. Interestingly, the HDAC inhibitor sodium butyrate has been shown to reduce the expression of both *KU70* and *KU80* in human melanoma cells (Munshi et al., 2005), however Chen and colleagues found that treatment of DU-145 cells with HDAC inhibitors increases the acetylation level of KU70. Moreover, the acetylation of KU70 did not affect its complex formation with KU80 (Chen et al., 2007). This contradiction might be due to differences in the transcriptional regulation of KU proteins among different cell lines. Also, phenylbutyrate, but not sodium butyrate, has been found to sensitize multidrug resistant cancer cells to doxorubicin by suppressing the antioxidant enzymes superoxide dismutase and glutathione reductase (Shack et al., 1996). These observations highlight the varied mechanisms of action of HDAC inhibitors at both the epigenetic and cellular levels.

Surprisingly, Chen and colleagues have recently investigated a unique histone acetylation-independent mechanism by which HDAC inhibitors act as chemosensitizers in cancer cells through the modulation of KU70 acetylation. They noticed that pretreatment with HDAC inhibitors sensitizes prostate cancer cells (DU-145 cells that lack both BAX and functional p53) to bleomycin, doxorubicin and etoposide (Chen et al., 2007). However, this effect was less prominent when chemotherapy treatment preceded HDAC inhibitor treatment (Kim et al., 2003). Based on this finding they proposed that the chemosensitizing effect of HDAC inhibitors could be attributed to its ability to suppress DNA DSBR activity. As the KU heterodimer interacts with DNA through electrostatic interactions between its positively charged residues and the sugar phosphate backbone of DNA (Walker et al., 2001; Zhang et al., 2006), Chen and colleagues assumed that acetylation of lysine residues would diminish the DNA-binding activity of KU70. To test this assumption, they used SDM to replace each

of the KU70 lysine residues K317, K331 and K338 in the ring region with glutamine to mimic constitutive acetylation (Chen et al., 2007). They found that constitutive acetylation at K338 reduces the DNA-binding activity, whereas substitution of K317 or K331 with glutamine has no significant effect. Thus, they concluded that neither K317 nor K331 plays a role in DNA binding. Moreover, DNA docking analysis showed that both K317 and K331 are pointed outward from the DNA-binding ring, indicating that they are not within the effective range of electrostatic interactions with the DNA. Furthermore, transient overexpression of K338Q rendered cells more susceptible to doxorubicin in terms of γH2AX foci and clonogenic survival. This study highlighted the possibility of exploiting the modulators of KU70 acetylation in clinical trials for the treatment of prostatic cancer. These studies also suggested that acetylation/deacetylation of KU70 N-terminal lysines can play a more general role in the DNA damage responses to IR.

As radiotherapy is the major clinical modality in cancer management, studying the effects of acetylayion/deacetylation of KU70 lysine residues K317, K331 and K338 on cell survival and DSBR in response to IR would provide a rationale for designing cancer treatment strategies including different combinations of chemotherapy, radiotherapy and acetylation/deacetylation modulators to achieve optimal therapeutic benefits.

5.2 Aims

The main aims of this part of the project:

1- Establishing pFlag-*KU70*/wt and pFlag-*KU80*/wt overexpression constructs.

2- Site-directed mutagenesis to create pFlag-*KU70* aceto-blocking and aceto-mimicking mutants at the positions K317, K331 and K338 in the mammalian overexpression systems.

3- Establishing stable cell lines overexpressing pFlag-*KU70*/wt, pFlag-*KU80*/wt and pFlag-*KU70* aceto-blocking and aceto-mimicking mutant proteins.

4- Establishing his-tag overexpression systems for KU70/wt, KU80/wt and KU70 mutants for *in vitro* production of recombinant proteins in E. coli and baculovirus expression system.

5- Trial purification of his-KU70/wt and his-KU80/wt.

6- Functional analyses to investigate the effects of pFlag-KU70 aceto-blocking and aceto-mimicking mutants on DDR to IR.

5.3 Results

5.3.1 Making pFlag-*KU70*/wt and pFlag-*KU80*/wt Constructs

The wild type cDNAs of both *KU70* and *KU80* were amplified by proofreading PCRs and the products were electrophoresed as shown in Figure 5.1A. The bands were gel purified and ligated into pGEM-T-Easy vector, transformed into E. coli as shown in Figure 5.1B and C. The positive clones containing the expected size of *KU70* and *KU80* inserts were sequenced. The two clones containing the wild type sequence of both *KU70* and *KU80* were double digested as shown in Figure 5.1D. The digested bands were gel purified and ligated into Empty pFlag vector as shown in Figure 5.1E and transformed into E. coli. Then, minipreps were double digested again to excise the insert as shown in Figure 5.1F and G.

5.3.2 Creating pFlag-KU70 Mutants by SDM

The pFlag-*KU70*/wt cDNA constructed in the previous step was used as a template for SDM PCRs to change *KU70* lysine residues K317, K331 and K338 to either arginine or glutamine Replacement of lysine with arginine mimics deacetylation, whereas replacement of lysine with glutamine mimics acetylation (Cohen et al., 2004a; Li et al., 2002). The SDM PCR products were electrophoresed as shown in Figure 5.2A and B. Following Dpn I digestion the mutants plasmids were transformed into supercompetent E. coli. All the minipreps were sequenced to check that the desired mutations were incorporated in the right position as shown in Figure 5.3 and that the inserts were still in frame. The inserts containing the desired mutation were religated into fresh pFlag vector to take away any unsequenced mutations that might have been introduced into the vector backbone during the SDM PCR as shown in Figure 5.3C, D and E.

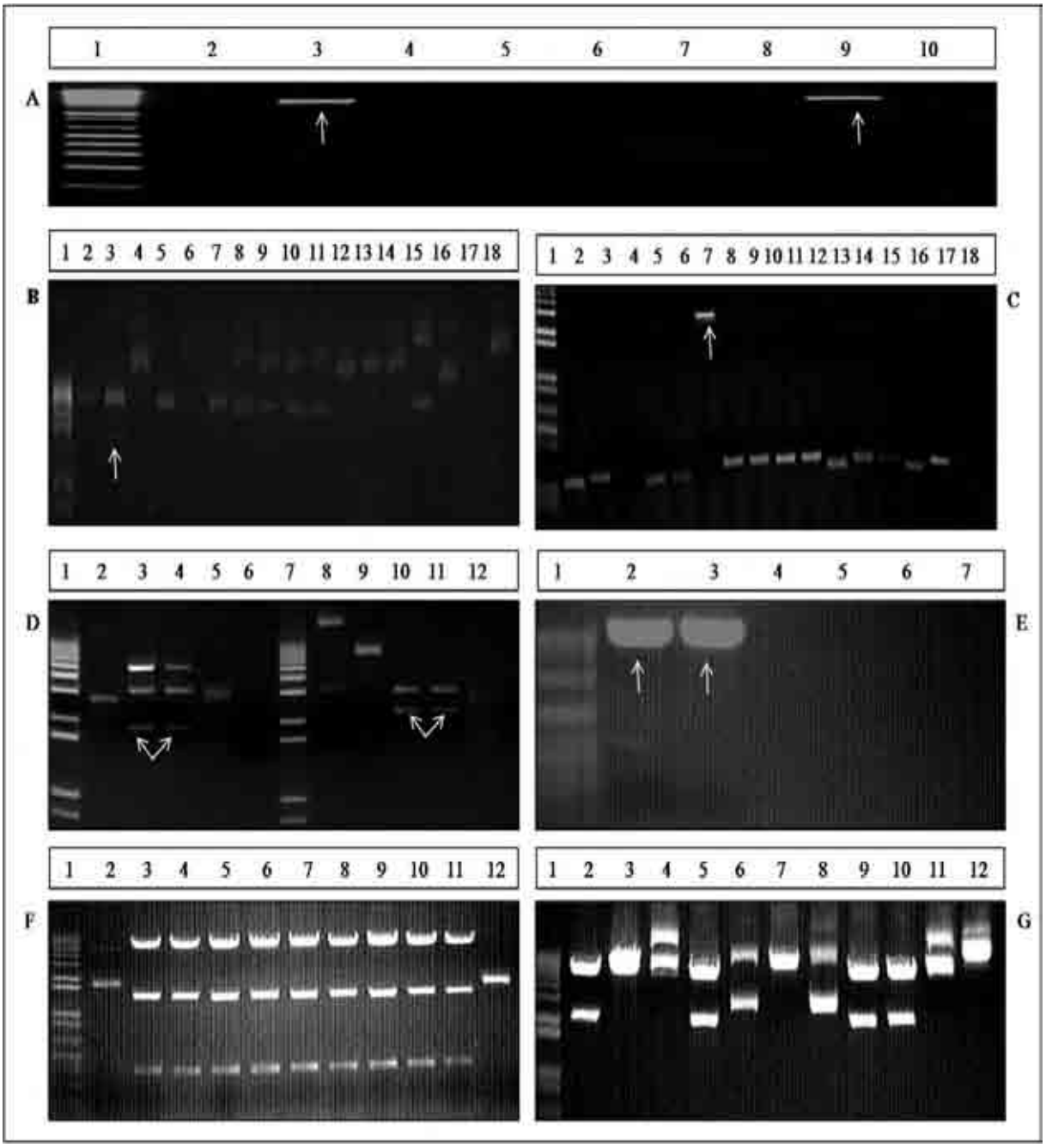

Figure 5.1: pFlag-*KU70*/wt and pFlag-*KU80*/wt constructs
(A) Agarose gel electrophoresis showing the cDNA of both *KU70* (lane 3) and *KU80* (lane 9) amplified by proofreading PCR, as indicated by the white arrows. (B) Minipreps were digested with EcoRI to drop *KU70* insert, one (lane 3) out of 17 minipreps contained the expected size insert as indicated by the white arrow. (C) Screening minipreps for *KU80* insert by PCR using M13 forward and reverse primers. Again, one (lane 7) out of 17 minipreps contained the expected size insert as indicated by the white arrow. (D) The *KU70* (lane 3 in panel (B)) and *KU80* (lane 7 in panel (C)) were digested out of pGEM-T-Easy with the restriction enzymes designed to clone both of them in frame into pFlag vector. The bottom bands in lanes 3 and 4 corresponding to *KU70* and those in lanes 10 and 11 corresponding to *KU80* as indicated by white arrows were cut and gel purified. (E) pFlag vector was treated with the same sets of enzymes to create sticky ends for both *KU70* and *KU80* as shown in lanes 2 and 3 respectively. The pFlag with ligated inserts were transformed into E. coli and the minipreps were double digested again to check the *KU70* insert as in (F) and the *KU80* insert as in (G). (F) The nine positive clones contained *KU70* (lanes 3-11) were labelled and stored as glycerol stocks. (G) The positive clones contained *KU80* (lanes 2, 5, 9 and 10) were labelled and stored as glycerol stocks.

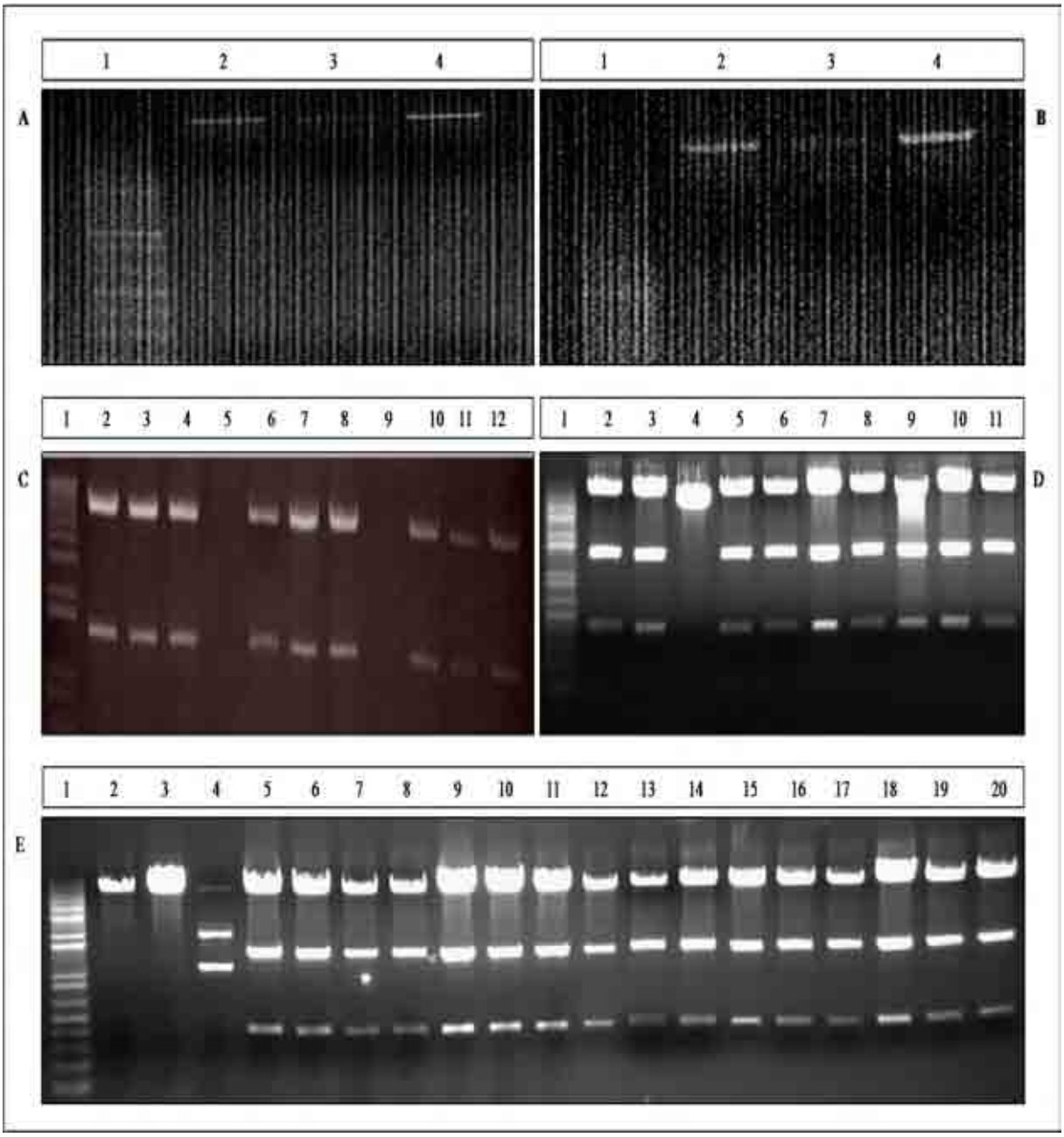

Figure 5.2: pFlag-*KU70* mutant constructs
(A) Agarose gel electrophoresis showing site-directed mutagenesis PCR products of *KU70-K317R, KU70-K331R* and *KU70-K338R* in lanes number 2, 3 and 4 respectively. (B) Agarose gel electrophoresis showing site-directed mutagenesis PCR products of *KU70-K317Q, KU70-K331Q* and *KU70-K338Q* in lanes number 2, 3 and 4 respectively. Following Dpn I digestion the plasmids with the incorporated mutations were transformed into supercompetent E. coli. The minipreps were sequenced to check that the desired mutations were incorporated in the right position and that the inserts were still in frame. The inserts containing the desired mutation and still in frame were double digested with NotI and BamHI, gel purified, religated into fresh pFlag vector treated with the same enzymes and transformed into E. coli. The minipreps were double digested to drop the inserts. (C) Agarose gel electrophoresis showing three positive clones of each *KU70* lysine to arginine mutants: three clones of *KU70-K317R* (lanes number 2, 3 and 4), three clones of *KU70-K331R* (lanes number 6, 7 and 8) and three clones of *KU70-K338R* (lanes number 10, 11 and 12). (D) Agarose gel electrophoresis showing the positive clones of *KU70-K317Q* (lanes number 2-11 except lane number 4). (E) Agarose gel electrophoresis showing the positive clones of *KU70-K331Q* (lanes number 5-11) and the positive clones of *KU70-K338Q* (lanes number 12-20). All the positive clones in C, D and E were used to make glycerol stocks.

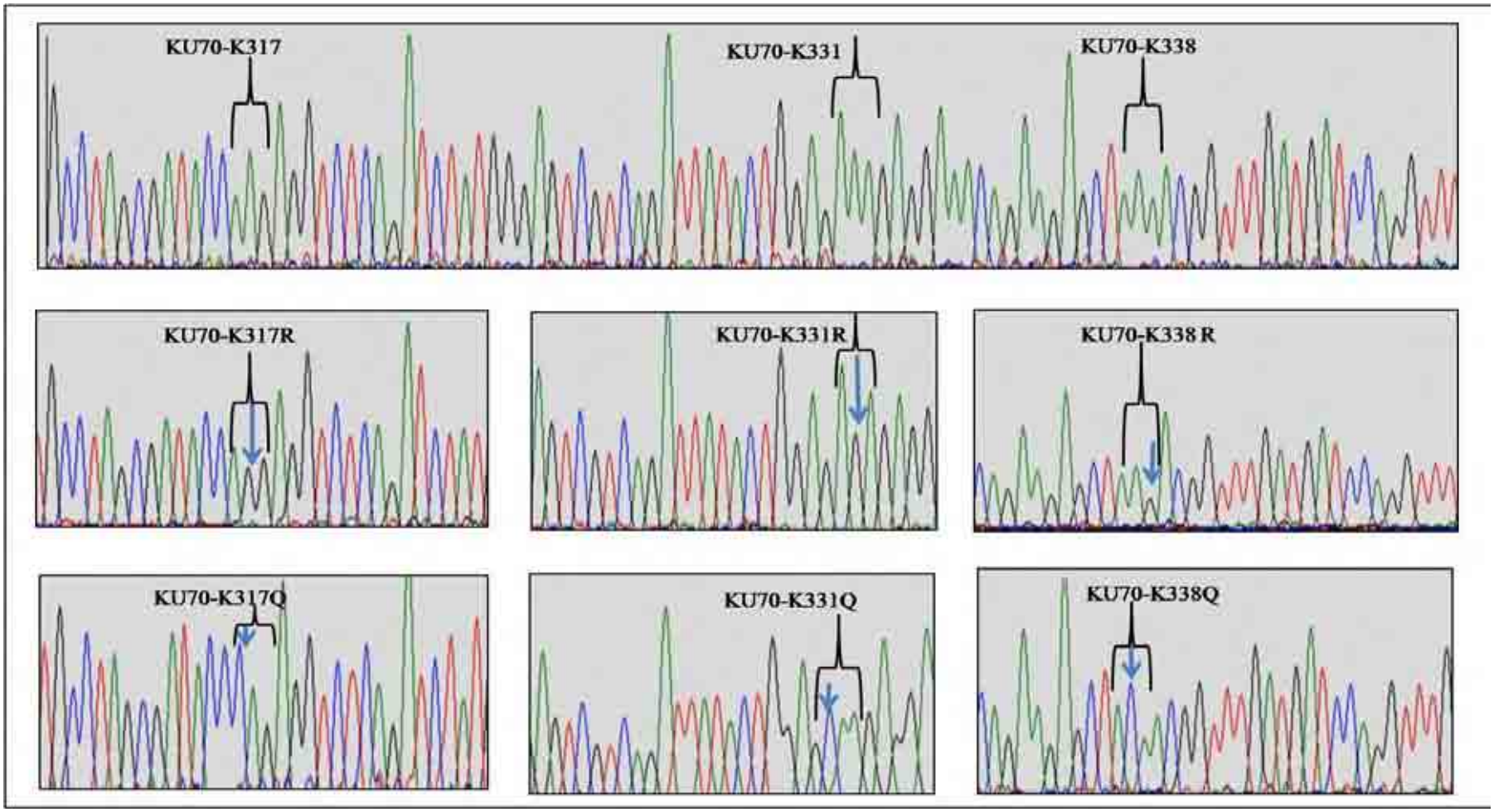

Figure 5.3: Sequence chromatograms of pFlag-*KU70*/wt and pFlag-*KU70* mutant constructs
The top chromatogram is a part of the *KU70*/wt sequence showing the three lysine residues: K317, K331 and K338. The middle panel represents three partial sequences showing the pFlag-*KU70* aceto-blocking mutants: *KU70-K317R*, *KU70-K331R* and *KU70-K338R* and the mutated bases are indicated by blue arrows. The bottom panel represents three partial sequences showing the pFlag-*KU70* aceto-mimicking mutants: *KU70-K317Q*, *KU70-K331Q* and *KU70-K338Q* and the mutated bases are indicated by blue arrows.

5.3.3 Establishing Stable Cell Lines Overexpressing pFlag-KU70/wt, pFlag-KU80/wt and pFlag-KU70 Mutants

Using both Lipofectamine 2000 and Fugene HD transfection reagents, all the constructed plasmids, pFlag-*KU70*/wt, pFlag-*KU80*/wt, pFlag-*KU70* aceto-blocking mutants (pFlag-*KU70-K317R*, pFlag-*KU70-K331R* and pFlag-*KU70-K338R*) and pFlag-KU70 aceto-mimicking mutants (pFlag-*KU70-K317Q*, pFlag-*KU70-K331Q* and pFlag-*KU70-K338Q*), were transfected into MRC5VA cells to create stable cell lines overexpressing pFlag-KU70/wt, pFlag-KU80/wt and pFlag-KU70 aceto-blocking and aceto-mimicking mutants. The cells were harvested and protein extracts were used to check the expression of pFlag-KU70/wt, pFlag-KU80/wt and pFlag-KU70 aceto-blocking and aceto-mimicking mutant proteins by Western blots as shown in Figure 5.4A, B and C.

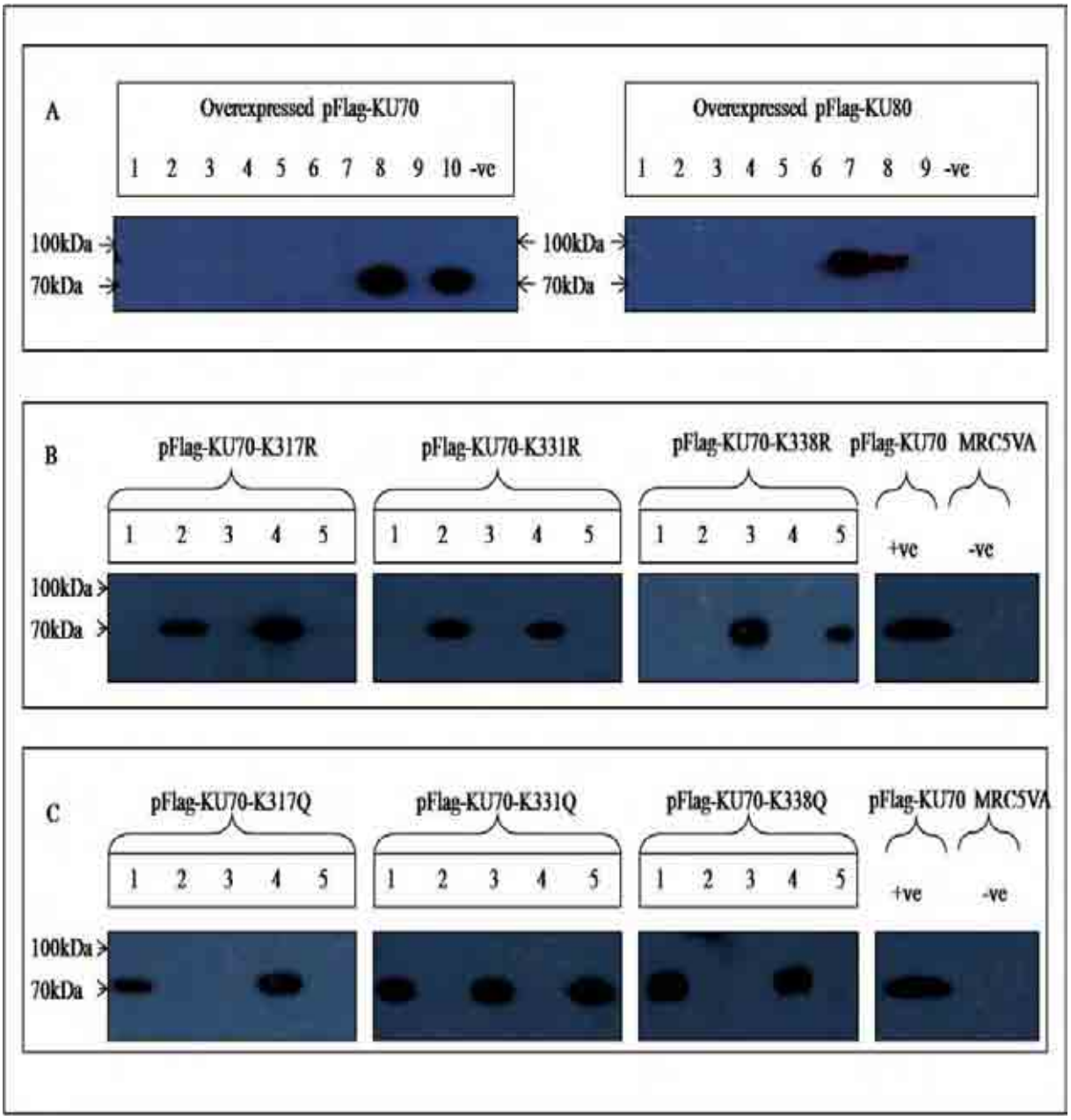

Figure 5.4: Overexpression of pFlag-KU70/wt, pFlag-KU80/wt and pFLag-KU70 mutants
Western blots were used to check the expression of all the stably transfected cell lines. (A) Western blots showing the overexpression of pFlag-KU70/wt transfected cell line on the left side (2 clones were overexpressing, lanes 8 and 10) and pFlag-KU80/wt transfected cell line on the right side (2 clones were overexpressing, lanes 7 and 8). MRC5VA was used as a negative control. Panel (B) shows 3 Western blots for pFlag-KU70-K317R, pFlag-KU70-K331R and pFlag-KU70-K338R transfected cell lines along MRC5VA as a negative control and pFlag-KU70/wt as a positive control. The Western blot for pFlag-KU70-K317R transfected cell line shows 2 clones overexpressing (lanes 2 and 4). The Western blot for pFlag-KU70-K331R transfected cell line shows 2 clones overexpressing (lanes 2 and 4). The Western blot for pFlag-KU70-K338R transfected cell line shows 2 clones overexpressing (lanes 3 and 5). Panel (C) shows 3 Western blots for pFlag-KU70-K317R, pFlag-KU70-K331R and pFlag-KU70-K338R transfected cell lines along MRC5VA as a negative control and pFlag-KU70/wt as a positive control. The Western blot for pFlag-KU70-K317Q transfected cell line shows 2 clones overexpressing (lanes 1 and 4). The Western blot for pFlag-KU70-K331Q transfected cell line shows 3 clones overexpressing (lanes 1, 3 and 5). The Western blot for pFlag-KU70-K338Q transfected cell line shows 2 clones overexpressing (lanes 1 and 4).

5.3.4 Establishing His-tag Overexpression Systems for *KU70*/wt, *KU80*/wt and *KU70* Mutants

In order to purify the recombinant proteins in E. coli with the aim of testing the effect of the individual KU70 mutant both in the *in vitro* ligation assay, kinase assay and *in vitro* acetylation assays (to identify which HAT is responsible for their acetylation), the his-tag overexpression systems were established by subcloning all the constructs into pET-28a. The pET-28a vector with the inserts was transformed into E. coli and minipreps were double digested again to check for the presence the inserts as shown in Figure 5.5A, B, C, D and E.

Competent E. coli capable of protein expression were transformed with the extracted plasmid DNA and individual colonies were assessed for the presence of the inserts by colony PCR as shown in (Figure 5.5F, G and H). The induction and expression of his-KU70/wt and his-KU80/wt were carried out as described in Section 2.3.8.1.

The purification was performed as described in Section 2.3.8.3. The recombinant proteins were analysed by SDS-PAGE as shown in Figure 5.6A, B and C. The overexpressed his-KU70/wt and his-KU80/wt were not soluble as most of it remained in the bacterial pellet as shown in Figure 5.6A and B. Also, a small soluble fraction did not bind to the beads and was lost in the flowthrough and the first wash as shown in Figure 5.6B and C. Moreover, a faint band was observed at 40kDa, which might be either degradation product or bacterial proteins nonspecifically bound to the beads. In agreement with this, it has been found that soluble KU could not be produced by independently expressing the two subunits (Hanakahi, 2007). Hence, all the constructs were switched to baculovirus overexpression system (Section 2.1.14) as shown in Figure 5.7A and B for purification of the recombinant proteins in insect cells, as Dr. Kysela previously purified the complex in insect cells (Kysela et al., 2003).

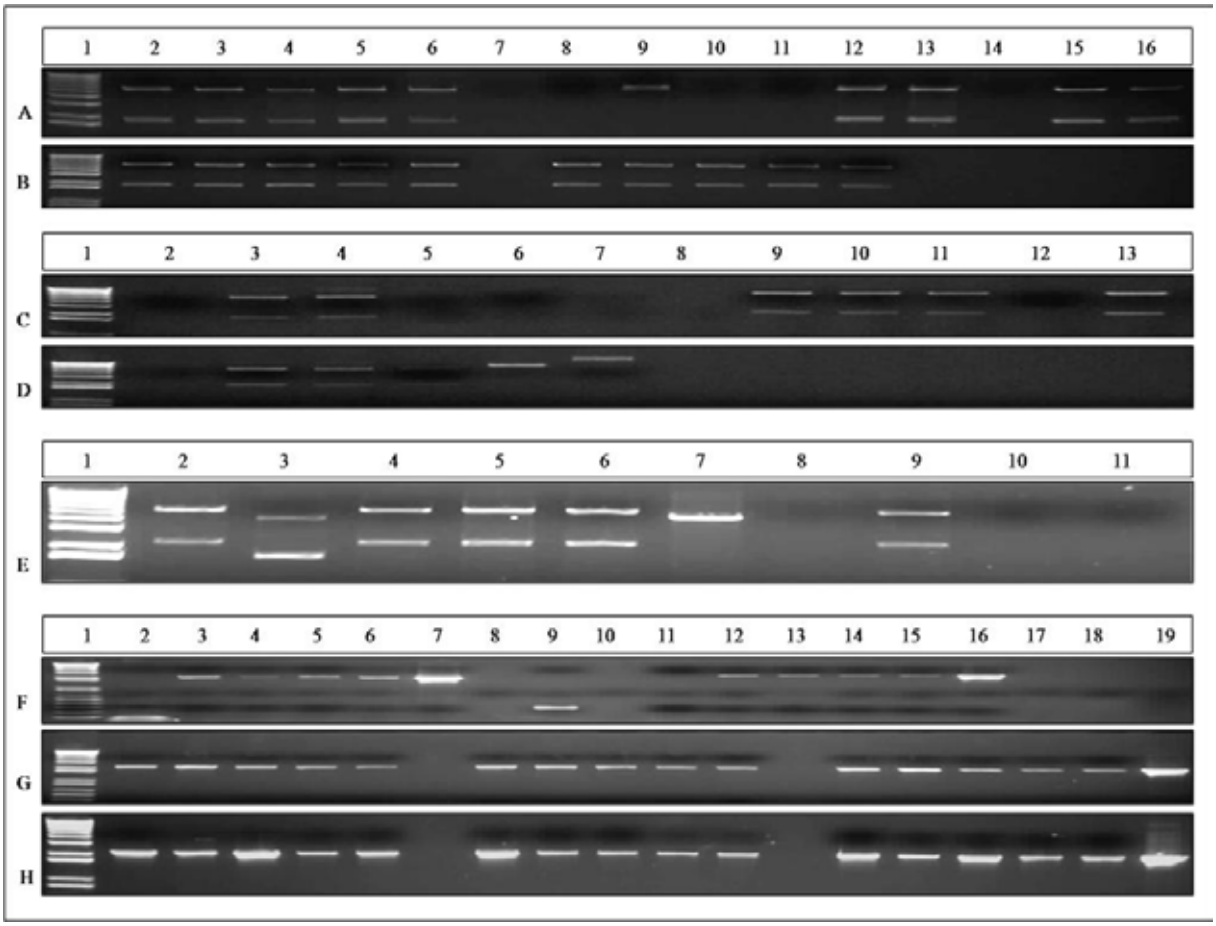

Figure 5.5: pET-28a double digestion and colony PCR
The selected minipreps of pET-28a with *KU70*/wt and *KU70* mutant inserts were double digested with BamHI and XhoI. The digested products were run on agarose gel electrophoresis. (A) The bottom bands of lanes 2, 3, 4, 5 and 6 represent 5 clones of *KU70*/wt, whereas the bottom bands of lanes 12, 13, 15 and 16 represent 4 clones of *KU70-K317R*. Empty pET-28a was double digested with BamHI and XhoI as a negative control as shown in lane 9. (B) the bottom bands of lanes 2, 3, 4, 5 and 6 represent 5 clones of *KU70-K331R*, whereas the bottom bands of lanes 8, 9, 10 , 11 and 12 represent 5 clones of *KU70-K338R*. (C) The bottom bands of lanes 3 and 4 represent 2 clones of *KU70-K317Q*, whereas the bottom bands of lanes 9,10, 11 and 13 represent 4 clones of *KU70-K331Q*. (D) The bottom bands of lanes 3, 4 and 5 represent 3 clones of *KU70-K338Q*. (E) The selected minipreps of pET-28a with *KU80*/wt inserts were double digested with BamHI and HindIII. The digested products were run on agarose gel electrophoresis. The bottom bands of lanes 2, 4, 5, 6 and 9 represent 5 clones of *KU80*/wt. All the positive clones in A, B, C, D and E were used to make glycerol stocks. Then, for protein expression, bacteria were transformed with pET-28a containing *KU70*/wt and each *KU70* mutant cloned into BamHI and XhoI restriction sites, whereas, *KU80*/wt inserts was cloned into BamHI and HindIII restriction sites. Five colonies of each were selected and minipreped. (F) Agarose gel electrophoresis showing the products of colony PCR of the minipreps of his-*KU70*/wt and his-*KU80*/wt. Lanes 3, 4, 5 and 6 represent 4 positive colonies of his-*KU70*/wt, whereas lanes 12, 13, 14 and 15 represent 4 positive colonies of his-*KU80*/wt. Lanes 7 and 16 represent PCR products of his-*KU70*/wt and his-*KU*80/wt as postive controls respectively, whereas lanes 8 and 9 (negative controls) are PCR control and PCR product of empty pET-28a respectively. (G) Colony PCR of the minipreps of his-*KU70-K317R*, his-*KU70-K331R* and his-*KU70-K338R*. Lanes 2, 3, 4, 5 and 6 represent positive colonies of his-*KU70-K317R*, whereas lanes 8, 9, 10, 11, and 12 represent 5 positive colonies of his-*KU70-K331R*. Also, lanes 8, 9, 10, 11, and 12 represent 5 positive colonies of his-*KU70-K338R*. (H) Colony PCR of the minipreps of his-*KU70-K317Q*, his-*KU70-K331Q* and his-*KU70-K338Q*. Lanes 2, 3, 4, 5 and 6 represent positive colonies of his-*KU70-K317Q*, whereas lanes 8, 9, 10, 11, and 12 represent 5 positive colonies of his-*KU70-K331Q*. Also, lanes 8, 9, 10, 11, and 12 represent 5 positive colonies of his-*KU70-K338Q*. All the postive clones in F, G and H were used to make glycerol stocks. One positive colony of his-KU70/wt and one positive colony of his-KU80/wt were used for induction of recombinant protein expression and trial purification.

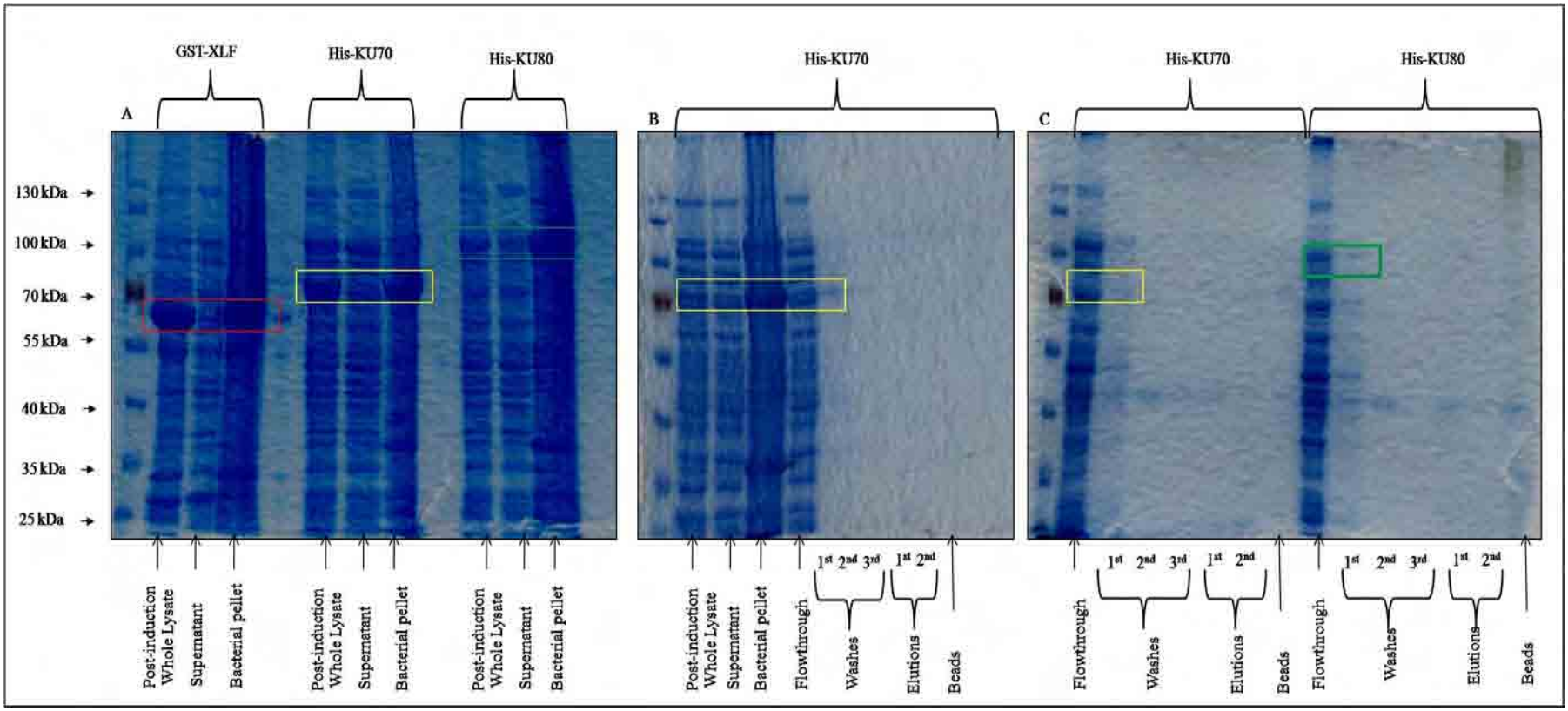

Figure 5.6: Trial purification of his-KU70/wt and his-KU80/wt in E. coli

KU70/wt and *KU80*/wt were cloned into BamHI-XhoI and BamHI-HindIII restriction sites of pET-28a expression vector respectively. Plasmid DNA was used to transform bacteria. IPTG was used for induction of recombinant protein expression. After lysis the recombinant proteins were eluted in 500µL aliquots from affinity beads by glutathione. (A) Protein gel shows the expression of GST-XLF (red box) alongside the expression of his-KU70/wt (yellow box) and the expression of his-KU80/wt (green box). (B) His-KU70/wt was insoluble and retained in the pellet. A small soluble fraction did bind to the beads and almost all the protein was lost in the flowthrough and first wash (yellow box). (C) His-KU70/wt (yellow box) and his-KU80/wt (green box) were insoluble and retained in the pellets. Small soluble fractions did bind to the beads and almost all the protein was lost in the flowthrough and first wash. These are bands at 40kDa which are either degradation products or non-specific bacterial proteins bound to the beads.

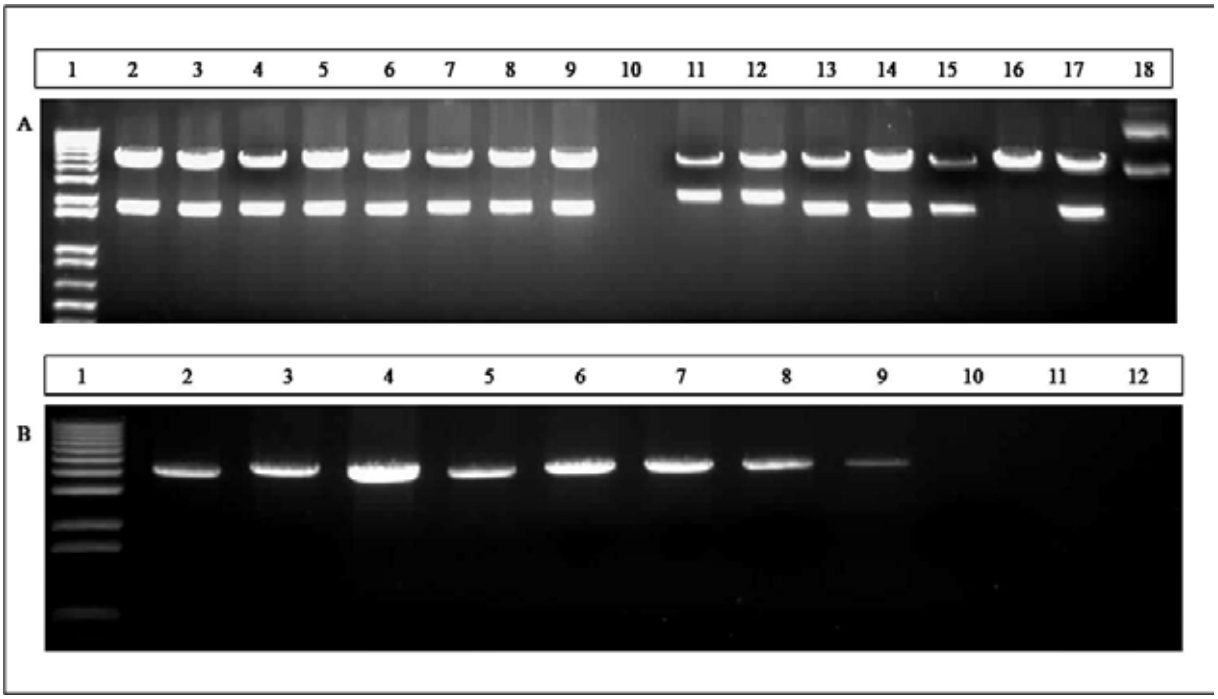

Figure 5.7: pFast-bac-HTb double digestion and PCR of Bacmids
(A) Minipreps of pFast-bac-HTb with *KU70*/wt, *KU80*/wt, *KU70-K317R*, *KU70-K331R*, *KU70-K338R*, *KU70-K317Q*, *KU70-K331Q* and *KU70-K338Q* inserts cloned into BamHI and XhoI restriction sites were double digested with BamHI and XhoI. The bottom bands of lanes 2 and 3 represent 2 postive clones of KU70/wt, whereas the bottom bands of lanes 4 and 5 represent 2 postive clones of *KU70-K317R*. The bottom bands of lanes 6 and 7 represent 2 postive clones of *KU70-K331R*, whereas the bottom bands of lanes 8 and 9 represent 2 postive clones of *KU70-K338R*. The bottom bands of lanes 11 and 12 represent 2 postive clones of Ku80/wt whereas, the bottom bands of lanes 13 and 14 represent 2 postive clones of *KU70-K317Q*. The bottom band of lane 15 represents one postive clone of *KU70-K331Q* whereas, the bottom band of lane 17 represents one postive clone of *KU70-K331Q*. (B) DH10Bac competent cells were transformed with pFast-bac-HTb containing *KU70*/wt, *KU80*/wt and *KU70* mutant inserts cloned into BamHI and XhoI restriction sites of pFast-bac-HTb to generate bacmids of the eight inserts. The bacmids were isolated and PCR verified the presence of the eight inserts. Lanes 2-9 represent the PCR products of *KU70*/wt, *KU80*/wt, *KU70-K317R*, *KU70-K331R*, *KU70-K338R*, *KU70-K317Q*, *KU70-K331Q* and *KU70-K338Q* bacmids respectively. M13 forward and M13 reverse primers were used for the PCR and the expected size of the product was around 4kb.

5.3.5 *In Vivo* Analysis of the Impact of Overexpression of KU70 Mutants on DDR in Response to IR

5.3.5.1 Clonogenic Survival Assay

5.3.5.1.1 Clonogenic Survival Assay of pFlag-KU70 Aceto-Blocking Mutants

In order to assess the effects of pFlag-KU70 aceto-blocking mutants on cell survival following exposure to IR, all the pFlag-KU70 aceto-blocking (pFlag-KU70-K317R, pFlag-KU70-K331R and pFlag-KU70-K338R) mutant cell lines and the control cells MRC5VA, MRC5VA with Empty-Flag vector, pFlag-KU70/wt and pFlag-KU80/wt were exposed to increasing doses of IR and their survival rates plotted (Figure 5.8A and B). The three pFlag-KU70 aceto-blocking mutant cell lines were more radiosensitive than the control cell lines. At 8Gy, the differences between the surviving fractions of pFlag-KU70 aceto-blocking mutant cells pFlag-KU70-K317R, pFlag-KU70-K331R and pFlag-KU70-K338R and that of MRC5VA control cells were statistically significant with p-values: p=0.02, p=0.02 and p=0.02 respectively (Figure 5.9A and B and Appendix 11). At 8Gy, the differences between the surviving fractions of pFlag-KU70 aceto-blocking mutant cells pFlag-KU70-K317R, pFlag-KU70-K331R and pFlag-KU70-K338R and that of MRC5VA with Empty-Flag vector were statistically significant with p-values: p=0.02, p=0.02 and p=0.02 respectively (Figure 5.9A and B and Appendix 11). At 8Gy, the differences between the surviving fractions of pFlag-KU70 aceto-blocking mutant cells pFlag-KU70-K317R, pFlag-KU70-K331R and pFlag-KU70-K338R and that of pFlag-KU70/wt were statistically significant with p-values: p=0.04, p=0.04 and p=0.04 respectively (Figure 5.9A and B and Appendix 11).

5.3.5.1.2 Clonogenic Survival Assay of pFlag-KU70 Aceto-Mimicking Mutants

As shown in Figure 5.9A and B, the three pFlag-KU70 aceto-mimicking mutant cell lines were more radiosensitive than the control cell lines. At 8Gy, the differences between the surviving fractions of pFlag-KU70 aceto-mimicking mutant cells pFlag-KU70-K317Q, pFlag-KU70-K331Q and pFlag-KU70-K338Q and that of MRC5VA control cells were statistically significant with p-values: p=0.02, p=0.02 and p=0.02 respectively (Figure 5.9A and B and Appendix 11). At 8Gy, the differences between the surviving fractions of pFlag-KU70 aceto-mimicking mutant cells pFlag-KU70-K317Q, pFlag-KU70-K331Q and pFlag-KU70-K338Q and that of MRC5VA with Empty-Flag vector were statistically significant with p-values: p=0.02, p=0.02 and p=0.02 respectively (Figure 5.9A and B and Appendix 11). At 8Gy, the differences between the surviving fractions of pFlag-KU70 aceto-mimicking mutant cells pFlag-KU70-K317Q, pFlag-KU70-K331Q and pFlag-KU70-K338Q and that of pFlag-KU70/wt were statistically significant with p-values: p=0.04, p=0.04 and p=0.04 respectively (Figure 5.9A and B and Appendix 11).

5.3.5.2 Expression and Cellular Localization of the pFlag-KU70 Mutants

Since the impact of both pFlag-KU70 aceto-blocking and aceto-mimicking mutants on the survival was clear in response to IR, especially at 8Gy, this would suggest that their radiosensitising effect might be due to DSBR defect. However, as the mutants might be exclusively segregated either to the nucleus or to the cytoplasm, immunofluorescence was done to check the expression and the cellular localization of pFlag-KU70 aceto-blocking mutants, pFlag-KU70 aceto-mimicking mutants alongside pFlag-KU70/wt as a positive control and MRC5VA as a negative control. Figure 5.10 shows that all the mutants were expressing, behaved like the positive control pFlag-KU70/wt and localized to the nucleus.

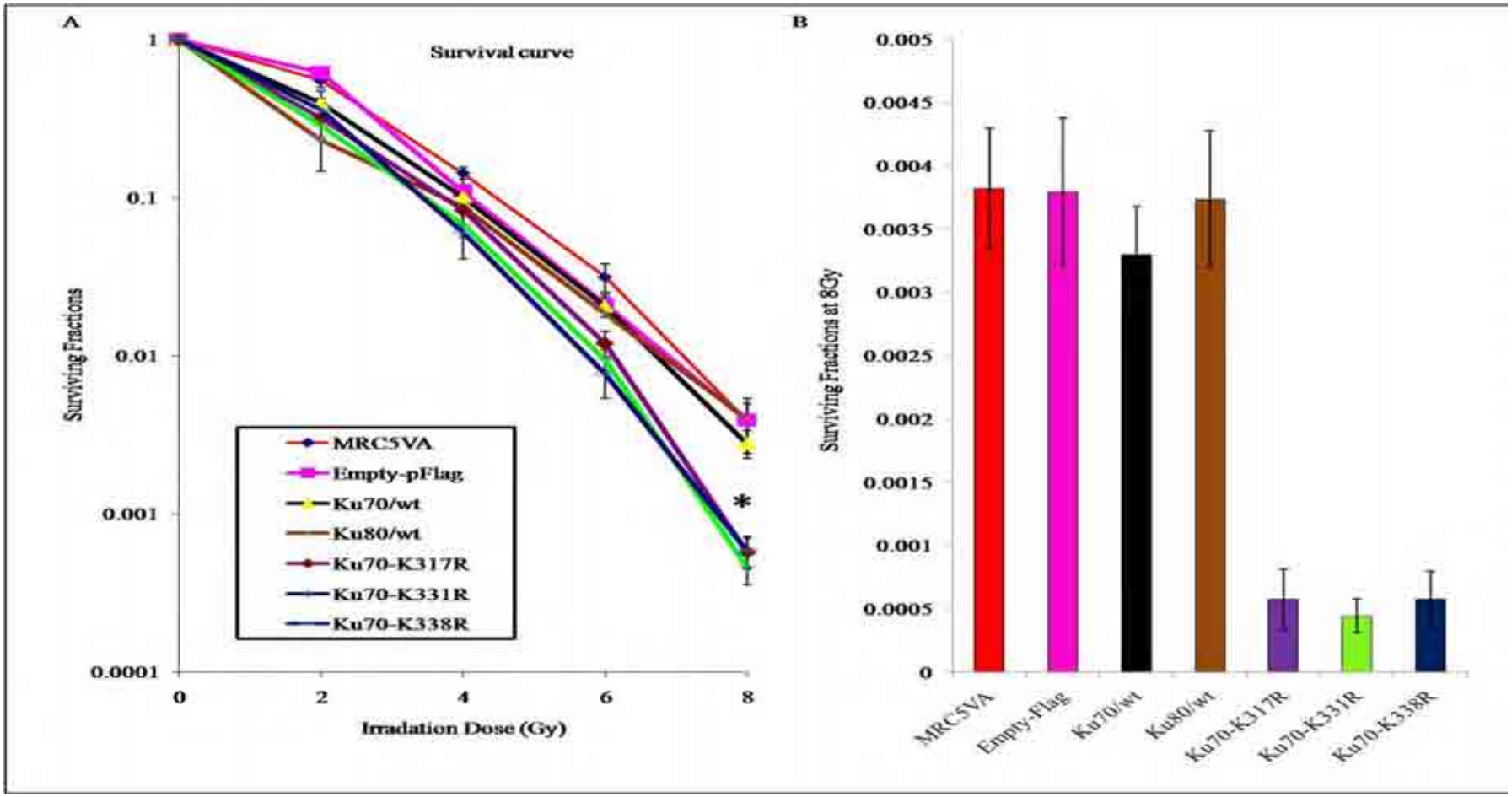

Figure 5.8: Clonogenic survival of pFlag-KU70 aceto-blocking mutant cell lines in response to IR

(A) The clonogenic survival curves show that the pFlag-KU70 aceto-blocking mutant: pFlag-KU70-K317R, pFlag-KU70-K331R and pFlag-KU70-K338R cell lines are more sensitive than the control cell lines (MRC5VA, Empty-pFlag Vector, pFlag-KU70/wt and pFlag-KU80/wt), especially at 8Gy. (B) The bar graph shows that the surviving fractions of pFlag-KU70 aceto-blocking mutant pFlag-KU70-K317R, pFlag-KU70-K331R and pFlag-KU70-K338R cell lines at 8Gy are significantly lower than those of the control cell lines (MRC5VA, Empty-pFlag Vector, pFlag-KU70/wt and pFlag-KU80/wt). The black star represents the statistically significant difference of $p<0.05$ as measured by Students' two tailed t-test. (n=3 independent experiments) and error bars represent ± standard error of the mean.

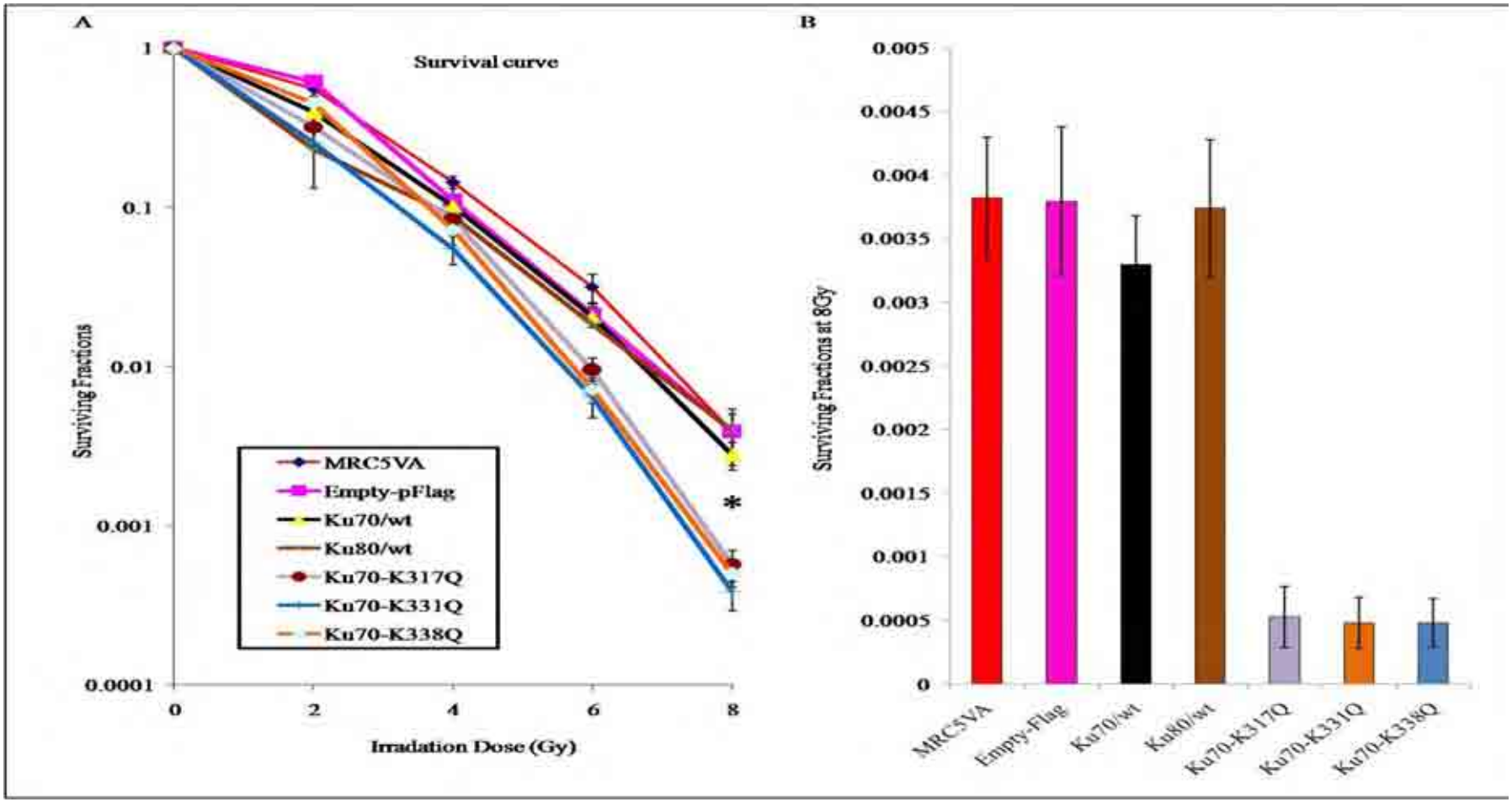

Figure 5.9: Clonogenic survival of pFlag-KU70 aceto-mimicking mutant cell lines in response to IR

(A) The clonogenic survival curves show that the pFlag-KU70 aceto-mimicking mutant: pFlag-KU70-K317Q, pFlag-KU70-K331Q and pFlag-KU70-K338Q cell lines are more sensitive than the control cell lines (MRC5VA, Empty-pFlag Vector, pFlag-KU70/wt and pFlag-KU80/wt) at 8Gy. (B) The bar graph shows that the surviving fractions of pFlag-KU70 aceto-mimicking mutant pFlag-KU70-K317Q, pFlag-KU70-K331Q and pFlag-KU70-K338Q cell lines are at 8Gy are significantly lower than those of the control cell lines (MRC5VA, Empty-pFlag Vector, pFlag-KU70/wt and pFlag-KU80/wt) at 8Gy. The black star represents the statistically significant difference of $p<0.05$ as measured by Students' two tailed t-test. (n=3 independent experiments) and error bars represent ± standard error of the mean.

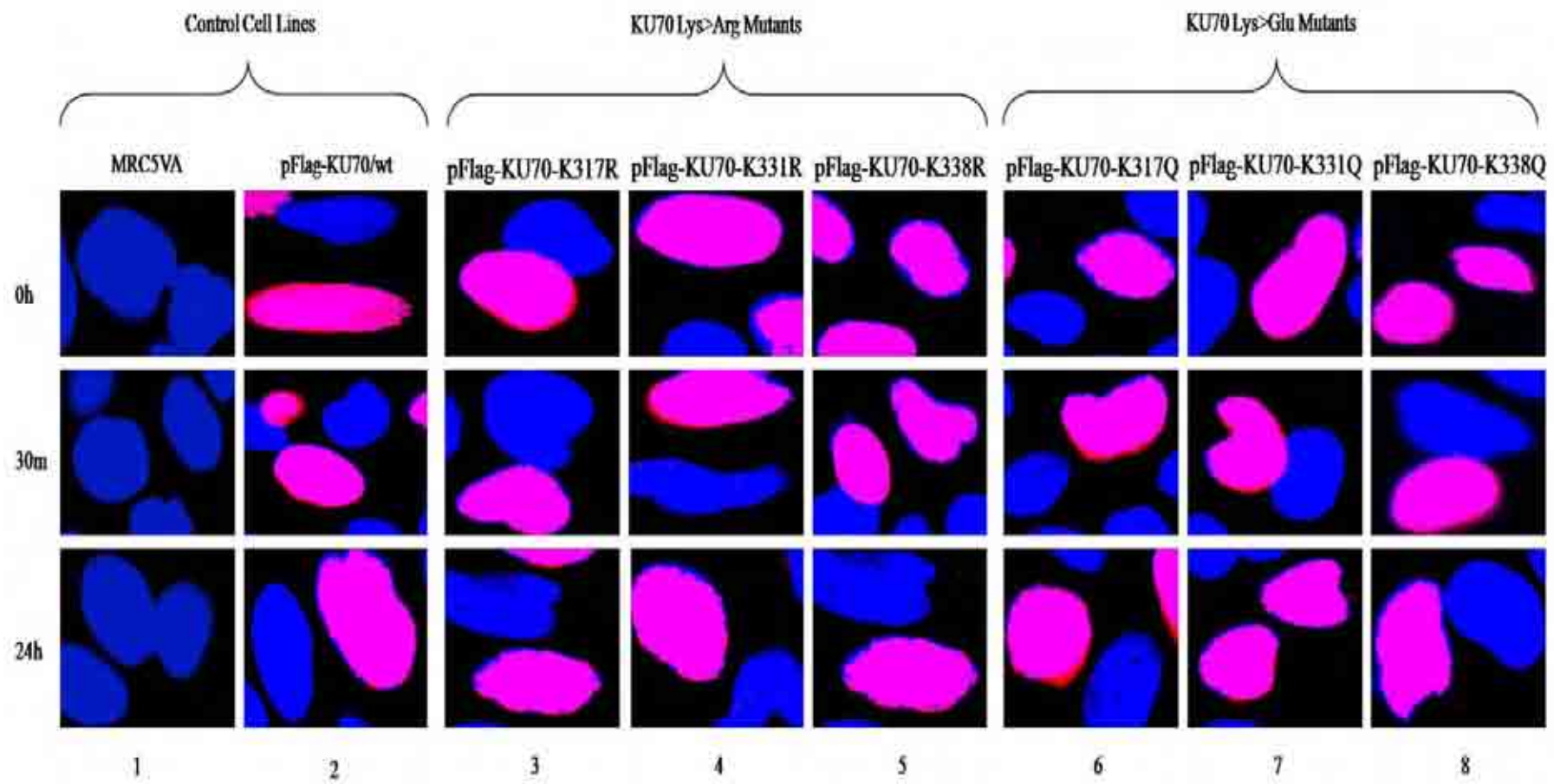

Figure 5.10: Expression and cellular localization of the pFlag-KU70 mutants
The expression of the pFlag-KU70/wt, pFlag-KU70 aceto-blocking and aceto-mimicking mutant cell lines was checked with immunofluorescence using primary pFlag and secondary fluorescent antibody. Immunofluorescence shows nuclear red staining of pFlag-KU70 aceto-blocking mutant pFlag-KU70-K317R, pFlag-KU70-K331R and pFlag-KU70-K338R (lanes 3, 4 and 5 respectively) and aceto-mimicking mutant pFlag-KU70-K317Q, pFlag-KU70-K331Q and pFlag-KU70-K338Q (lanes 6, 7 and 8) cell lines along both the pFlag-KU70/wt cell line (lane 2) as a positive control and the MRC5VA cell line (lane 1) as a negative control. This indicates that both the KU70/wt, aceto-blocking and aceto-mimicking mutants localized to the nucleus.

5.3.5.3 γH2AX DNA Repair Foci Assay

γH2AX is a sensitive and early marker of DSBs (Rogakou et al., 2000; Rogakou et al., 1998), which can sense low levels of DNA damage much better than other methods (Banath et al., 2004). It has been reported that it can detect doses of radiation down to 1 mGy (Martin et al., 2003). Briefly, using primary γH2AX antibody and fluorescent secondary antibody to stain the cells allows the visualization and quantification of DNA damage within cells under the epifluorescent microscope (Huang et al., 2003; Lowndes and Toh, 2005). Residual γH2AX can reflect either the radiosensitivity of cells or their repair efficiency (Klokov et al., 2006). Hence, the γH2AX assay became the most popular technique for detecting DSBs.

5.3.5.3.1 γH2AX Foci Assay of pFlag-KU70 Aceto-Blocking Mutants

As the clonogenic survival assays revealed that all the mutant cells were more radiosensitive compared to the control cells, and in order to address the effects of pFlag-KU70 aceto-blocking mutants on DSBR, the levels of γH2AX were studied in the three pFlag-KU70 aceto-blocking mutant cell lines alongside the four control cell lines after exposure to 5Gy of IR. The γH2AX foci were quantified in un-irradiated cells to determine the background level, 30 minutes following IR to determine the peak of DNA damage and 24 hours post-irradiation when, under normal conditions, the majority of DSBs should be repaired. Figure 5.11 shows the foci seen in the three pFlag-KU70 aceto-blocking mutant cell lines alongside the four control cells (un-irradiated, 30 minutes post-irradiation and 24 hours post-irradiation). All the pFlag-KU70 aceto-blocking mutant cell lines and the control cell lines had an average of four foci per nucleus as a basal background in non-irradiated cells. At 30 minutes post IR, all the mutants and control cell lines displayed comparably high amounts of γH2AX foci, an average of 50 large foci per nucleus. Twenty four hours post-irradiation, the majority, if not all, of the

γH2AX foci have disappeared in the control cell lines, with eight foci on average per nucleus. The pFlag-KU70 aceto-blocking mutant cell lines retained a higher amount of γH2AX foci after 24 hours, on average 16 foci per nucleus. Plotting the number of unrepaired breaks as a percentage of the total breaks seen at 30 minutes, termed the residual foci, clearly shows the difference between the pFlag-KU70 aceto-blocking mutant cell lines and the control cell lines (Figure 5.13A). The differences between the residual foci of pFlag-KU70 aceto-blocking mutant cells pFlag-KU70-K317R, pFlag-KU70-K331R and pFlag-KU70-K338R and that of MRC5VA were statistically significant with p-values of p=0.02, p=0.03 and p=0.04 respectively (Appendix 12). The differences between the residual foci of pFlag-KU70 aceto-blocking mutant cells pFlag-KU70-K317R, pFlag-KU70-K331R and pFlag-KU70-K338R and that of MRC5VA with Empty-Flag vector were statistically significant with p-values of p=0.02, p=0.03 and p=0.04 respectively (Appendix 12). The differences between the residual foci of pFlag-KU70 aceto-blocking mutant cells pFlag-KU70-K317R, pFlag-KU70-K331R and pFlag-KU70-K338R and that of pFlag-KU70/wt were statistically significant with p-values of p=0.02, p=0.03 and p=0.04 respectively (Appendix 12). This indicates that overexpressing the individual pFlag-KU70 aceto-blocking mutants pFlag-KU70-K317R, pFlag-KU70-K331R and pFlag-KU70-K338R compromised DSBR.

5.3.5.3.2 γH2AX Foci Assay of pFlag-KU70 Aceto-Mimicking Mutants

The levels of γH2AX were studied in the three pFlag-KU70 aceto-mimicking mutant cell lines alongside the four control cell lines after exposure to 5Gy of IR (Figure 5.12). Plotting the number of unrepaired breaks as a percentage of the total breaks seen at 30 minutes, termed the residual foci, clearly shows the difference between the pFlag-KU70 aceto-mimicking mutant cell lines and the control cell lines (Figure 5.13B). The differences between the

residual foci of pFlag-KU70 aceto-mimicking mutant cells pFlag-KU70-K317Q, pFlag-KU70-K331Q and pFlag-KU70-K338Q and that of MRC5VA control cells were statistically significant with p-values of p=0.02, p=0.02 and p=0.04 respectively (Appendix 12). The differences between the residual foci of pFlag-KU70 aceto-mimicking mutant cells pFlag-KU70-K317Q, pFlag-KU70-K331Q and pFlag-KU70-K338Q and that of MRC5VA with Empty-Flag vector were statistically significant with p-values of p=0.02, p=0.03 and p=0.04 respectively (Appendix 12). The differences between the residual foci of pFlag-KU70 aceto-mimicking mutant cells pFlag-KU70-K317Q, pFlag-KU70-K331Q and pFlag-KU70-K338Q and that of pFlag-KU70/wt were statistically significant with p-values of p=0.02, p=0.03 and p=0.04 respectively (Appendix 12). This indicates that overexpressing the individual pFlag-KU70 aceto-blocking mutants pFlag-KU70-K317Q, pFlag-KU70-K331Q and pFlag-KU70-K338Q compromised DSBR.

Although the differences between the surviving fractions of the aceto-blocking (Figure 5.8A and B) and the aceto-mimicking (Figure 5.9A and B) mutant cell lines at 8Gy were minimal, the noticeable differences between the residual γH2AX foci of pFlag-KU70-K338R (Figure 5.13A) and pFlag-KU70-K338Q mutant cell lines (Figure 5.13B) and those of the other mutant cell lines could be attributed to changes in the levels of expression of the mutant proteins, as the pFlag-KU70-K338R mutant cell line seemed to be losing the expression.

5.3.5.4 γH2AX Pan-nuclear Staining

Few nuclei of the mutants cell lines of both the aceto-blocking and the aceto-mimicking showed a characteristic pan-nuclear γH2AX staining pattern as shown in Figure 5.14, compared to foci pattern in the four control cell lines.

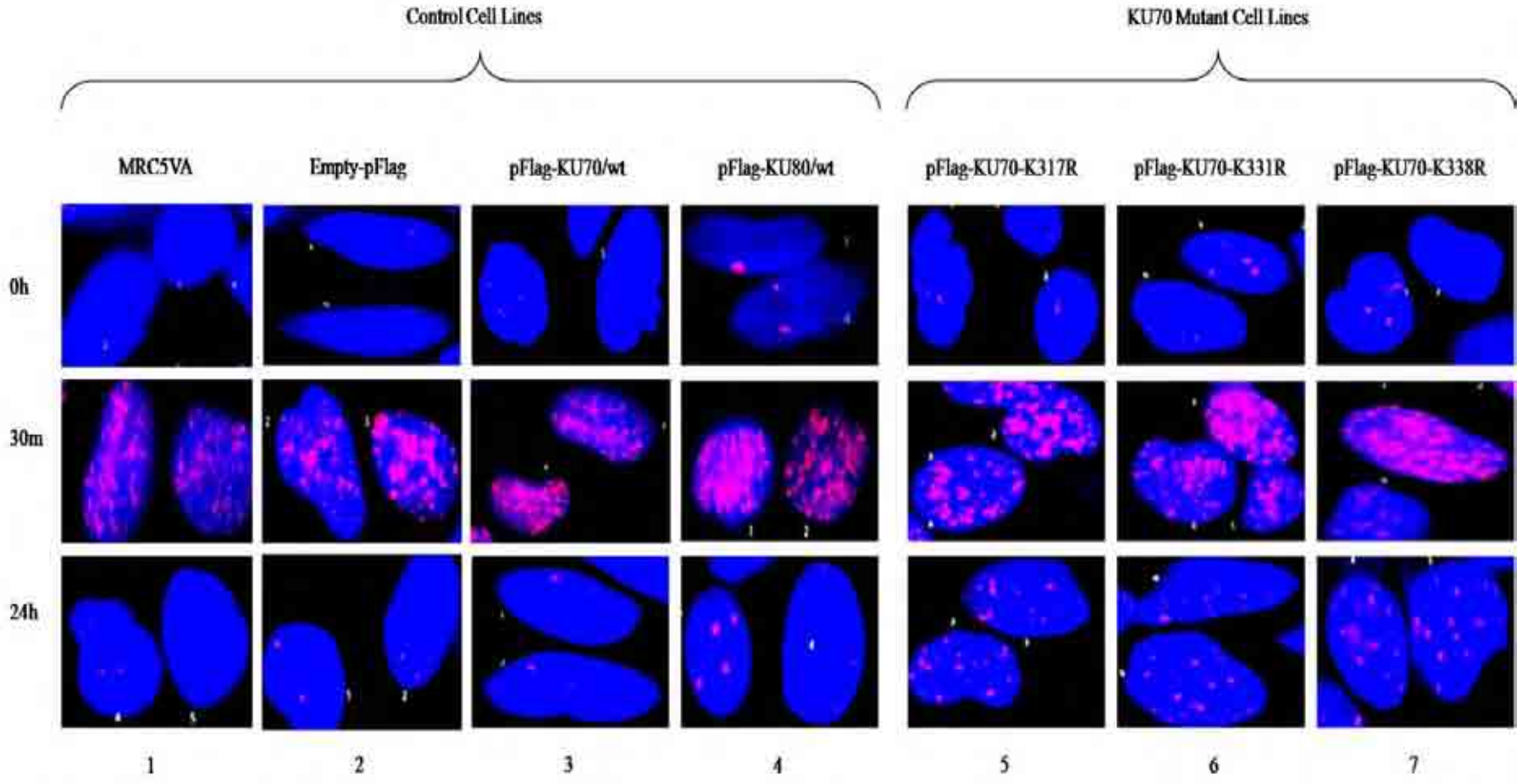

Figure 5.11: γH2AX foci of the pFlag-KU70 aceto-blocking mutant cell lines

Lanes number 1, 2, 3 and 4 show the control cells MRC5VA, Empty-pFlag Vector, pFlag-KU70/wt and pFlag-KU80/wt respectively. The un-irradiated (0h) control cell lines show no, or very low, γH2AX foci which are representative of DSBs and 30 minutes post-irradiation show the peak of γH2AX signal with the majority of these being repaired 24 hours post IR. Lanes number 5, 6 and 7 show the pFlag-KU70 aceto-blocking mutant pFlag-KU70-K317R, pFlag-KU70-K331R and pFlag-KU70-K338R cell lines. The un-irradiated mutant cells show very similar levels of γH2AX foci at 0 hour and 30 minutes to those of the control cell lines, however, there are considerably more foci remaining 24 hours post-irradiation indicating slower repair in comparison with the control cell lines.

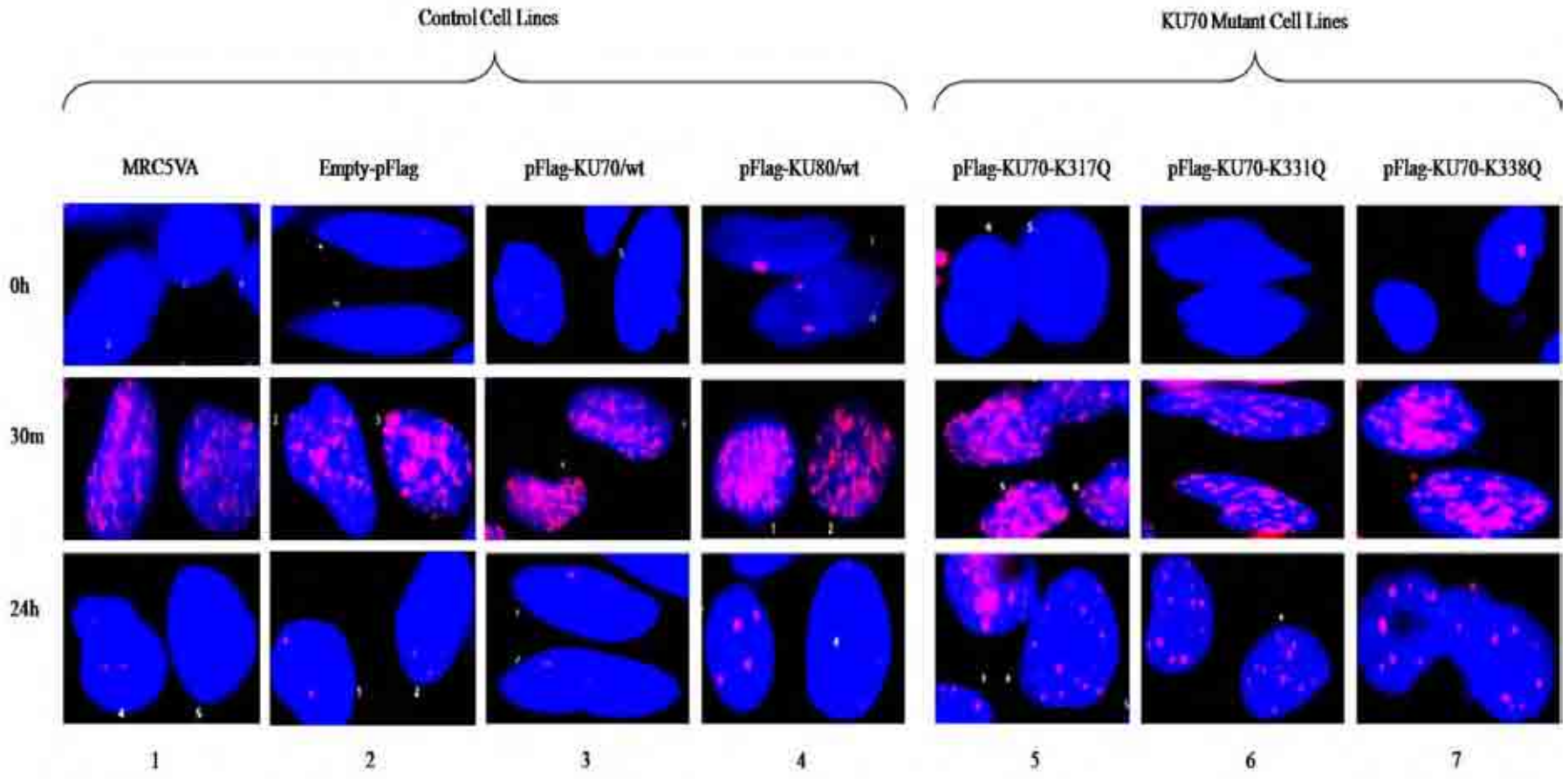

Figure 5.12: γH2AX foci of the pFlag-KU70 aceto-mimicking mutant cell lines
Lanes number 1, 2, 3 and 4 show the control cells MRC5VA, Empty-pFlag Vector, pFlag-KU70/wt and pFlag-KU80/wt respectively. The un-irradiated (0h) control cell lines show no, or very low, γH2AX foci which are representative of DSBs and 30 minutes post-irradiation show the peak of γH2AX signal, with the majority of these being repaired 24 hours post IR. Lanes number 5, 6 and 7 show the aceto-mimicking mutant pFlag-KU70-K317Q, pFlag-KU70-K331Q and pFlag-KU70-K338Q cell lines. The un-irradiated mutant cells show very similar levels of γH2AX foci at 0 hour and 30 minutes to that of the control cell lines, however, there are considerably more foci remaining 24 hours post-irradiation indicating slower repair in comparison with the control cell lines.

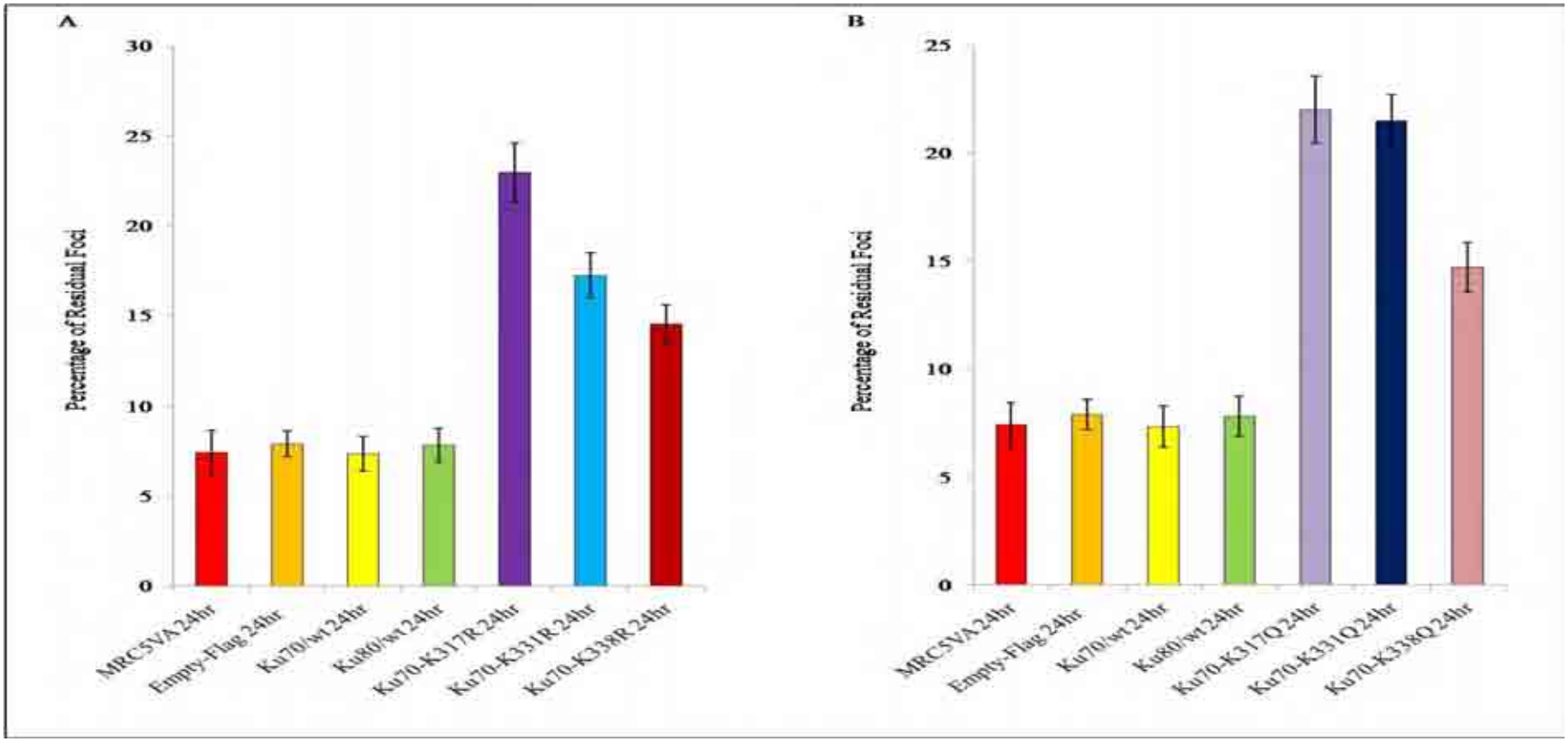

Figure 5.13: γH2AX residual foci of the pFlag-KU70 mutant cell lines 24 hours post-irradiation
Foci counted at 30 minutes and 24 hours post -irradiation were normalised against the un-irradiated counts. Residual foci were calculated as the percentage of foci remaining after 24 hours against the foci counted at 30 minutes post-irradiation. (A) The control cell lines (MRC5VA, Empty-pFlag Vector, pFlag-KU70/wt and pFlag-KU80/wt) all displayed comparable levels of residual foci at 24 hours post-irradiation, on average 7%, whereas the aceto-blocking mutant pFlag-KU70-K317R, pFlag-KU70-K331R and pFlag-KU70-K338R cell lines displayed a much higher amount of residual foci at 24 hours post-irradiation, on average 18%. (B) The control cell lines (MRC5VA, Empty-pFlag Vector, pFlag-KU70/wt and pFlag-KU80/wt) all displayed comparable levels of residual foci at 24 hours post-irradiation, on average 7%, whereas the aceto-mimicking mutant pFlag-KU70-K317Q, pFlag-KU70-K331Q and pFlag-KU70-K338Q cell lines displayed a much higher number of residual foci at 24 hours post-irradiation, on average 19%.

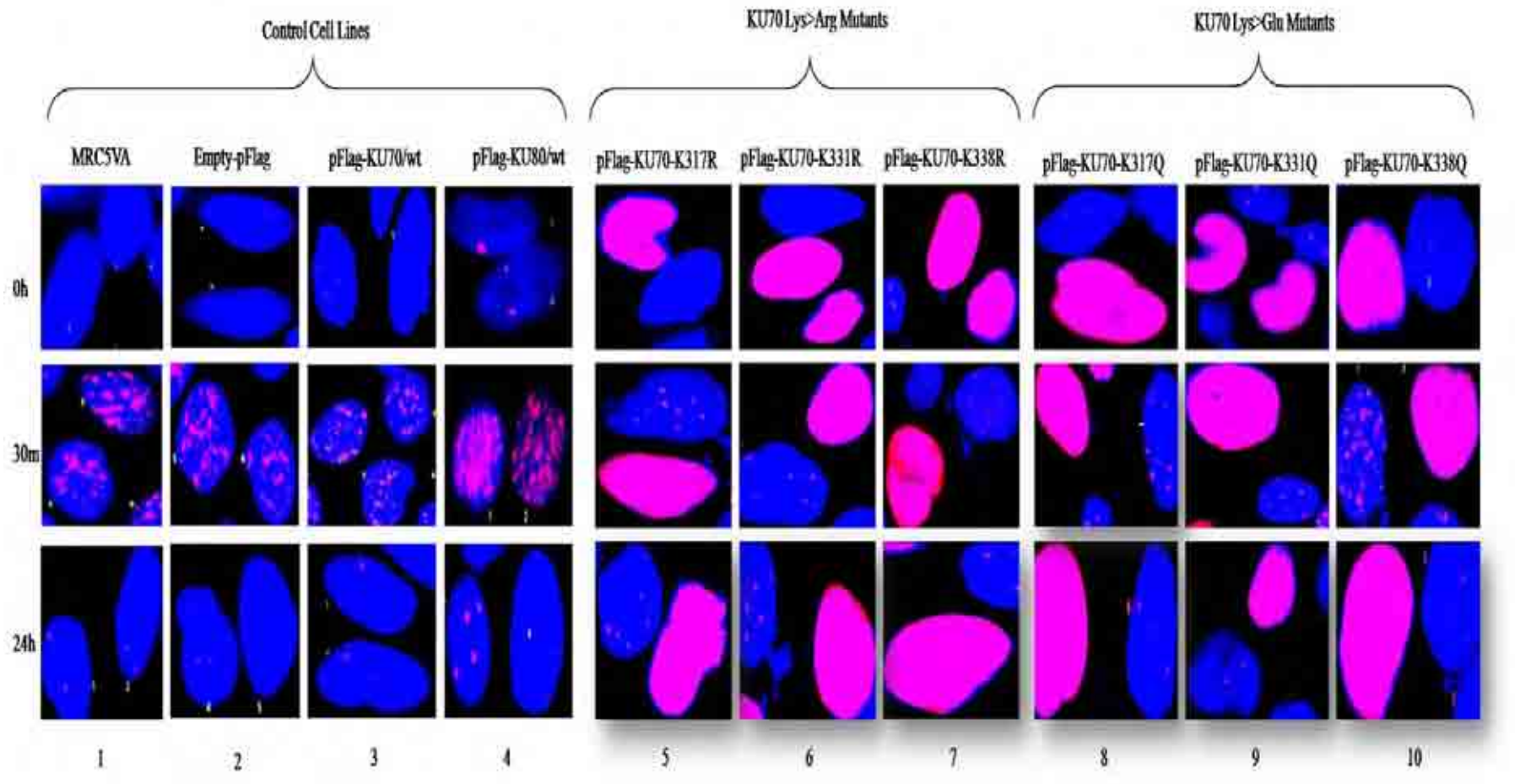

Figure 5.14: Pan-nuclear γH2AX staining of the pFlag-KU70 mutant cell lines
The control cells (lanes number 1, 2, 3 and 4 represent MRC5VA, Empty-pFlag Vector, pFlag-KU70/wt and pFlag-KU80/wt respectively) show foci staining pattern of γH2AX, whereas the pFlag-KU70 aceto-blocking mutant pFlag-KU70-K317R, pFlag-KU70-K331R and pFlag-KU70-K338R cell lines (lanes 5, 6, and 7 respectively) and the pFlag-KU70 aceto-mimicking mutant pFlag-KU70-K317Q, pFlag-KU70-K331Q and pFlag-KU70-K338Q (lanes 8, 9, and 10 respectively) show a mix of characteristic pan-nuclear staining pattern and foci staining pattern of γH2AX.

5.4 Discussion

In order to address the functional consequences of altering the KU70 lysine residues KU70-K317, KU70-K331 and KU70-K338, they have been replaced by arginine, which is charge-conserving (mimicking deacetylation), and by glutamine, which is non-charged (mimicking acetylation). After creating the wild type and mutant constructs and establishing stable cell lines overexpressing these mutant proteins, clonogenic survival assays revealed that both the aceto-blocking (Figure 5.8A and B) and the aceto-mimicking mutants (Figure 5.9A and B) of these three lysine residues render the cells sensitive to IR compared to the control cell lines. This effect was statistically significant at 8Gy of IR (Figure 5.8B and Figure 5.9B and Appendix 11). The radiosensitizing effect was not quite obvious at lower radiation doses, for p-values at 6Gy see Appendix 11. One possible explanation is that the cells retain the wild type *KU70* and *BAX* which might be sufficient for the repair of the damage induced at lower doses of IR. Similar observations have been previously reported for the *LIG4* hypomorphic mutation in a 12 years old leukaemia patient who was developmentally normal until the onset of leukaemia but dramatically over-responded to radiotherapy. In fact, it has been suggested that the residual ligase activity present in 180BR cells may be sufficient to efficiently handle a few but not excessive DSBs (Girard et al., 2004; Riballo et al., 2001).

As the effect of both pFlag-KU70 aceto-blocking and aceto-mimicking mutants on the cell survival was clear in response to IR especially at 8Gy, this prompted us to test whether this radiosensitivity is due to DSBR defect by the γH2AX foci assay. However, it was necessary to check the expression and the cellular localization of these mutants as mislocalization might disturb the function of the protein. The localization analysis showed that all the mutant cell

lines as well as the pFlag-KU70/wt cell line are expressing and the tagged proteins are localized to the nucleus (Figure 5.10). This will be discussed at the end.

To evaluate the impact of both pFlag-KU70 aceto-blocking and aceto-mimicking mutants on the efficacy of DSBR, the γH2AX foci assay was performed in both pFlag-KU70 aceto-blocking (Figure 5.11) and aceto-mimicking (Figure 5.12) mutant cell lines alongside the control cell lines. The percentage of γH2AX residual foci was quantified in all the mutant cell lines in response to 5Gy IR and compared to those of the control cell lines. Both the pFlag-KU70 aceto-blocking (Figure 5.13A) and aceto-mimicking mutants (Figure 5. 13B) retained statistically significant higher percentages of residual foci 24 hours post irradiation than the control cell lines (Appendix 12). This strongly suggests that both the pFlag-KU70 aceto-blocking and aceto-mimicking mutants compromised the DSBR. Although γH2AX foci assay is a reliable marker for the quantification of DSBs, recent evidence indicates that the number of γH2AX may not represent true DSBs induced by different damaging agents (Bouquet et al., 2006). Hence, another independent DSB measuring method is necessary to verify this conclusion and pulse field gel electrophoresis experiments are in progress to do so.

Based on the clonogenic survival data (Figure 5.8A and B and Figure 5.9A and B) and γH2AX data (Figure 5.11 and Figure 5.12) that the pFlag-KU70 aceto-blocking and aceto-mimicking mutant cell lines are radiosensitive and DSBR defective, it has been concluded that the original non-modified wild type lysine residues KU70-K317, KU70-K331 and KU70-K338 are critical for the DSBR role of the holoenzyme DNA-PK. Taken together, these data strongly indicate that a dynamic equilibrium of the acetylation status of these three lysine residues is needed for regulating DNA-PK in response to IR. In agreement with this, the data

collected so far on HATs and HDACs inhibition highlights the need and importance of maintaining the acetylation equilibrium inside the cell (Averbeck and Durante, 2011).

Although the data presented here show that dynamic equilibrium of acetylation status of KU70-K317, KU70-K331 and KU70-K338 is critical for DSBR in response to IR, alternatively the original non-modified wild type lysine residues are required for the optimal repair of DSBs, Chen and colleagues found that mimicking acetylation of K338 suppresses the DNA-binding of KU70 and sensitizes cells to doxorubicin, whereas mimicking acetylation of K317 or K331 does not. Furthermore, their docking analysis showed that both K317 and K331 were pointed outward from the DNA-binding ring and they were not within the effective range of electrostatic interactions with the DNA (Chen et al., 2007). However, it has to be mentioned that Chen and colleagues did not study the aceto-blocking effect of these lysine residues.

Surprisingly, in contrast to the above study, Lehman and colleagues, using chemical modification of lysine combined with mass spectrometry found that K317 is biotinylated in both free and DNA-bound KU. Examination of the crystal structure of the KU-DNA complex revealed that the R-group of lysine K317 is completely solvent accessible for biotinylation. Moreover, they found that the R-group of K331, which is also present on the pillar and points into the central cavity where DNA is threading through KU, is always biotinylated when KU is free and not modified in DNA-bound KU indicating that the presence of DNA blocks chemical modification of this residue. Thus, K331 sits in the bridge-pillar region of KU70 and is in close proximity to the duplex DNA, likely making contact to sugar or phosphate. Interestingly, they also reported that K338, which was reported to make contact with a sugar in the crystal structure (Walker et al., 2001), biotinylation is variable in both free and DNA-

bound KU. This may be due to the dynamic nature of the DNA binding process or equilibrium of bound and unbound KU (Lehman et al., 2008).

Although the above two studies and the data presented here seem to be partially contradicting, the differences could plausibly be explained on the basis of the dynamic nature of KU-DNA binding. The dynamic nature of KU-DNA binding suggests the potential for KU conformational changes to accompany DNA binding and its very interesting structure facilitates its role in DNA binding (Lehman et al., 2008). Moreover, our prediction is that the three lysine residues K317, K331 and K338 of the KU70 DNA-binding domain could sequentially make contact with the DNA backbone assuming that the KU inward movement on broken ends is rotational or oscillatory, as this kind of movement is the only possible one that could make the three lysine residues sequentially approach the DNA backbone either directly contacting it or entering into the effective range of electrostatic interactions with the DNA backbone. Within this effective electrostatic range, the DNA sterically blocks any kind of lysine modifications. Moreover, the rotational movement could bring the residues that are pointed outward from the DNA-binding ring into the effective range of electrostatic interactions with the DNA, forcing them inward towards the DNA backbone. With continued KU rotation, if needed, depending on the structure of the lesion, the lysine that moved inward and contacted the DNA backbone might move outwards again and become accessible for modification. Then, this lysine might provide a docking site for interacting proteins or regulate post-kinase activities which include facilitating the binding of other NHEJ components and the release of KU and DNA-PKcs from the termini prior to ligation. Then the next lysine residue follows the same sequence of events.

Interestingly, although studying the effect of both the aceto-mimicking and the aceto-blocking mutants of KU70-K317, KU70-K331 and KU70-K338 on apoptosis was beyond the time scope of this project, it is important to mention that the characteristic pan-nuclear γH2AX staining observed in the aceto-mimicking and the aceto-blocking mutant cell lines (Figure 5.14) might represent a pre-apoptotic signal. This highlights the possibility that the acetylation and deacetylation of these lysine residues might be important for the apoptotic function of KU70, or that the acetylation/deacetylation equilibrium between these N-terminal lysine residues, together with K539 and K542 in its C-terminus (Cohen et al., 2004a), may be required for the regulation of apoptosis. It is noteworthy that it has been suggested that pan-nuclear γH2AX staining might represent a pre-apoptotic signal associated with early nuclear-wide conformational chromatin changes in primary human fibroblasts in response to UV treatment. Also, it has been demonstrated that this pattern is DSB-independent and NER-dependent (Halicka et al., 2005; Mari et al., 2006). Moreover, it has been found that inhibition of ATM or c-Jun N-terminal kinase (JNK) reduces the levels of both UV-induced pan-nuclear γH2AX and S phase apoptosis, whereas inhibition of ATR by caffeine dramatically increased both of them (de Feraudy et al., 2010). Also, JNK-mediated phosphorylation of H2AX was essential for caspase-activated DNase (CAD)-mediated nucleosomal DNA fragmentation during apoptosis, which suggests that UV-induced pan-nuclear γH2AX may be essential for early steps before CAD-mediated nucleosomal DNA fragmentation (Lu et al., 2006). Interestingly, similar high levels of pan-nuclear γH2AX have been observed as a result of activation of the tumor necrosis factor-related apoptosis-inducing ligand (TRAIL) pathway in response to UV irradiation (Solier et al., 2009). Furthermore, it has been shown that this pan-nuclear γH2AX is replication helicase cofactor CDC45-dependent (Gagou et al., 2010). CDC45 is involved in DNA replication initiation (Aparicio et al., 2009; Bauerschmidt et al.,

2007) and in combination with p21 has an effect on apoptosis (Rodriguez et al., 2008). These findings highlight the role of the three KU70 lysine residues in apoptosis and replication.

Despite the fact that the γH2AX foci assay was performed on G1/G0 cells, the minority of cells with pan-nuclear staining which were observed in non-irradiated cells as well as after 30 minutes and 24 hours post IR (Figure 5.14) might represent S-phase cells. This finding suggests that the three lysine residues might play a critical role in both cell cycle regulation and induction of apoptosis in the S-phase. In line with the latter, the staining pattern was noticed once in the control cell line MRC5VA, which was late passage, and indeed the cells in the original passaged flask died just three days (one passage) after the cells were seeded in 6-well plates fixed for γH2AX staining. Moreover, this finding indicates that DNA-PK might be the kinase responsible for this phosphorylation pattern. However, to verify this, the work needs to be repeated in KU70$^{-/-}$ cell line, which was not available when the project started. Although, the presence of wild type KU70 might not be optimal, it is possible that its presence enabled us to test the effect of the mutants in response to IR, and that knocking it down, which is technically difficult and complicated, might have killed the cells due to KU complex dual role in both DNA repair (as shown by γH2AX residual foci) and apoptosis (as shown by the pan-nuclear γH2AX staining pattern).

Although KU70 is well known to be cytoplasmic, all the pFlag-tagged mutants, as well as the pFlag-KU70/wt, appeared to be exclusively localized to the nucleus by using the primary pFlag and secondary fluorescent antibodies (Figure 5.10). It is possible that the pFlag-tagged wild and mutant proteins undergo different conformational changes in the cytoplasm, hiding the tag, hence the pFlag antibody failed to detect it in the cytoplasm. In fact, this highlights the possibility that aceto-mimicking and aceto-blocking mutants of KU70-K317, KU70-

K331and KU70-K338 might undergo another different conformational change that disturbs the KU70-BAX complex. This could plausibly explain the apoptotic pan-nuclear staining of γH2AX observed in the mutant cell lines, on the assumption that there is a dynamic balance between the lysine residues of both N-terminus and C-terminus of KU70 that regulates KU70-BAX apoptotic function. Interestingly, Castle and colleagues have recently shaken the notion of KU70 cytoplasmic localization as they found that the role of BAX-KU70 complex is distinct to neuroblastoma, whereas knocking out KU70 in ovarian cancer cells or breast cancer cells did not affect their survival (Castle et al., 2010). They hypothesized that in healthy neural stem cells, BAX is not complexed to KU70 and is free to respond to death-inducing stimuli that are important during neural development, whereas in neuroblastoma the cytoplasmic BAX-KU70 complex prevent apoptosis and increase chromosomal aberrations (Ouyang et al., 1997; Stallings et al., 2007) owing to inaccurate NHEJ, as the presence of KU70 outside the nucleus may further interfere with the normal DNA repair ability (Takata et al., 1998). As KU70 is a universal protein and there is no doubt about its cytoplasmic existence, it would be interesting to try different permeabilization buffers that might help fluorescent visualization of the cytoplasmic fractions of pFlag-tagged wild and mutant proteins by the pFlag antibody.

CHAPTER SIX: SUMMARY AND RECOMMENDATIONS

The work undertaken in this thesis identified two novel intronic SNPs of *XLF* in the studied random Caucasian population sample. The first is an intronic SNP (G→A change) 28bp downstream of the 6th coding exon of *XLF* (Figure 3.7). The second is a novel 3' UTR SNP (T→C change) 39bp downstream of the 7th coding exon of *XLF* (Figure 3.9). Moreover, it has characterised two intronic SNPs already published in the dbSNP with the three genotypes represented in the studied population sample (Figure 3.4 and Figure 3.6). It would be interesting to characterize the effects of these novel SNPs on *XLF* transcription and expression and whether they affect splicing or stability of its transcripts. Also, using high-throughput sequencing techniques is likely to help in identifying genetic variations of the different genes from the same pathway and hence facilitates pathway-based analysis of multiple genetic polymorphisms in the risk assessment of cancer and complex diseases.

Interestingly the data presented here identified XLF and the other core NHEJ members as potential candidates for acetylation/decacetylation mediated functional regulation. It would be useful to investigate the acetylation status of the core members of the NHEJ further, as this will definitely help in deciphering how acetylation of these proteins regulates this pathway and coordinates, via crosstalk with other PTMs, the interplay of not only repair but also pre-repair and post-repair events as well. This in turn may help fine-tune the design of cancer treatment strategies using modulators of HDACs and HATs in combination with modulators of other PTMs, chemotherapy and/or radiotherapy.

In addition, it would be interesting to study the effect of acetylation of XLF-K160, as it has been previously suggested to be a conserved site of PTM, such as ubiquitination. This indicates that this residue might represent an acetylation switch where acetylation and ubiquitination might regulate XLF interactions and function. Also, studying the effect of

acetylation of XLF-K197 on the structure of XLF might help identify the mode of XLF interaction with XRCC4/LIG4 complex and stimulation of the ligation. Furthermore, it would be very interesting to test whether the XLF C-terminus lysine residues K290, K292 and K293, which are highly conserved and predicted to be acetylated, are critical for DNA-dependent XLF-KU interaction or regulation of XLF function.

Interestingly, the two XRCC4 lysine residues K169 and K197 (Table 4.4), that have been found to be acetylated *in vitro*, lie on both sides of the LIG4-binding region of XRCC4 which spans residues 173-195. This indicates that the acetylation of these two XRCC4 lysine residues, K169 and K197, might be critical for the interactions between XRCC4, LIG4 and XLF and the regulation of the final ligation step of NHEJ.

Also, the work undertaken in this thesis has provided evidence that maintaining the dynamic equilibrium of acetylation of KU70 lysine residues: K317, K331 and K338 is critical for its function in DSBR. It has also suggested the possibility that other related regulatory PTMs of these residues might play a role in DSBR, as the radio-sensitisation seen in our study may be due to abolition of any other PTMs that might possibly take place on these residues. Future studies should address the question of how these residues impact on all previously identified enzymatic activities of KU70 protein.

Interestingly, a recent study has provided evidence that amphiregulin (AREG) mediates gefitinib resistance in non-small cell lung cancer (NSCLC), as it reduces KU70 acetylation, therefore suppressing BAX-mediated apoptosis. This highlights the importance of including the HDAC inhibitors in combination with tyrosine kinase inhibitor (TKI) of epidermal growth factor receptor (EGFR) especially in EGFR-TKI-resistant patients (Busser et al., 2010a).

Moreover, they demonstrated that the use of small interfering RNAs of AREG (AREG siRNAs) might enhance the cytotoxicity of gefitinib (Busser et al., 2010b).

In conclusion, the data presented here in the context of the present status of our knowledge about DDR mechanisms highlights the need for more extensive studies to dissect the roles of acetylation/deacetylation mediated regulation of NHEJ and other DNA repair pathways. Such studies are likely to facilitate designs of new biological cancer therapies to be used with standard chemotherapy and radiotherapy, resulting in a better therapeutic outcome for cancer patients.

CHAPTER SEVEN: APPENDICES

Appendix 1: Human XLF wild sequence

1- Human *XLF* wild nucleotide sequence (900 nt)

ATGGAAGAACTGGAGCAAGGCCTGTTGATGCAGCCATGGGCGTGGCTACAGCTTGCAGAGAACTCCCT
CTTGGCCAAGGTTTTTATCACCAAGCAGGGCTATGCCTTGTTGGTTTCAGATCTTCAACAGGTGTGGC
ATGAACAGGTGGACACTAGTGTGGTCAGCCAGCGAGCCAAGGAGCTGAACAAGCGGCTCACTGCTCCT
CCTGCAGCTTTCCTCTGTCATTTGGATAATCTCCTTCGCCCATTGTTGAAGGACGCTGCTCACCCTAG
CGAAGCTACCTTCTCCTGTGATTGTGTGGCAGATGCACTGATTCTACGGGTGCGAAGTGAGCTCTCTG
GCCTCCCCTTCTATTGGAATTTCCACTGCATGCTAGCTAGTCCTTCCCTGGTCTCCCAACATTTGATT
CGTCCTCTGATGGGCATGAGTCTGGCATTACAGTGCCAAGTGAGGGAGCTAGCAACGTTACTTCATAT
GAAAGACCTAGAGATCCAAGACTACCAGGAGAGTGGGGCTACGCTGATTCGAGATCGATTGAAGACAG
AACCATTTGAAGAAAATTCCTTCTTGGAACAATTTATGATAGAGAAACTGCCAGAGGCATGCAGCATT
GGTGATGGAAAGCCCTTTGTCATGAATCTGCAGGATCTGTATATGGCAGTCACCACACAAGAGGTCCA
AGTGGGACAGAAGCATCAAGGCGCTGGAGATCCTCATACCTCAAACAGTGCTTCCCTGCAAGGAATCG
ATAGCCAATGTGTAAACCAGCCAGAACAACTGGTCTCCTCAGCCCCAACCCTCTCAGCACCTGAGAAA
GAGTCCACGGGTACTTCAGGCCCTCTGCAGAGACCTCAGCTGTCAAAGGTCAAGAGGAAGAAGCCAAG
GGGTCTCTTCAGTTAA

2- Human XLF wild amino acid sequence (299 aa)

MEELEQGLLMQPWAWLQLAENSLLAKVFITKQGYALLVSDLQQVWHEQVDTSVVSQRAKELNKRLTAP
PAAFLCHLDNLLRPLLKDAAHPSEATFSCDCVADALILRVRSELSGLPFYWNFHCMLASPSLVSQHLI
RPLMGMSLALQCQVRELATLLHMKDLEIQDYQESGATLIRDRLKTEPFEENSFLEQFMIEKLPEACSI
GDGKPFVMNLQDLYMAVTTQEVQVGQKHQGAGDPHTSNSASLQGIDSQCVNQPEQLVSSAPTLSAPEK
ESTGTSGPLQRPQLSKVKRKKPRGLFS

3- GST-*XLF*

GST-XLF is a generous gift from Professor Steve Jackson laboratory. Plasmid pGEX-2TK-p was derived from pGEX-2TK plasmid (Amersham) by insertion of the sequence AATTCTAGACTCCATGGGTCGACTGAGCTCAAGCT at the EcoRI site. The XLF gene was cloned into pGEX 2TK-p inbetween EcoRI and XhoI as follows:

GaattctaATGGAAGAACTGGAGCAAGGCCTGTTGATGCAGCCATGGGCGTGGCTACAGCTTGCAGAGAA
CTCCCTCTTGGCCAAGGTTTTTATCACCAAGCAGGGCTATGCCTTGTTGGTTTCAGATCTTCAACAGG
TGTGGCATGAACAGGTGGACACTAGTGTGGTCAGCCAGCGAGCCAAGGAGCTGAACAAGCGGCTCACT
GCTCCTCCTGCAGCTTTCCTCTGTCATTTGGATAATCTCCTTCGCCCATTGTTGAAGGACGCTGCTCA
CCCTAGCGAAGCTACCTTCTCCTGTGATTGTGTGGCAGATGCACTGATTCTACGGGTGCGAAGTGAGC
TCTCTGGCCTCCCCTTCTATTGGAATTTCCACTGCATGCTAGCTAGTCCTTCCCTGGTCTCCCAACAT
TTGATTCGTCCTCTGATGGGCATGAGTCTGGCATTACAGTGCCAAGTGAGGGAGCTAGCAACGTTACT
TCATATGAAAGACCTAGAGATCCAAGACTACCAGGAGAGTGGGGCTACGCTGATTCGAGATCGATTGA
AGACAGAACCATTTGAAGAAAATTCCTTCTTGGAACAATTTATGATAGAGAAACTGCCAGAGGCATGC
AGCATTGGTGATGGAAAGCCCTTTGTCATGAATCTGCAGGATCTGTATATGGCAGTCACCACACAAGA
GGTCCAAGTGGGACAGAAGCATCAAGGCGCTGGAGATCCTCATACCTCAAACAGTGCTTCCCTGCAAG
GAATCGATAGCCAATGTGTAAACCAGCCAGAACAACTGGTCTCCTCAGCCCCAACCCTCTCAGCACCT
GAGAAAGAGTCCACGGGTACTTCAGGCCCTCTGCAGAGACCTCAGCTGTCAAAGGTCAAGAGGAAGAA
GCCAAGGGGTCTCTTCAGTTAA**ctcgag**

Appendix 2: Human KU80 wild sequence

1- Human *KU80* wild nucleotide sequence (2199 nt)

ATGGTGCGGTCGGGGAATAAGGCAGCTGTTGTGCTGTGTATGGACGTGGGCTTTACCATGAGTAACTC
CATTCCTGGTATAGAATCCCCATTTGAACAAGCAAAGAAGGTGATAACCATGTTTGTACAGCGACAGG
TGTTTGCTGAGAACAAGGATGAGATTGCTTTAGTCCTGTTTGGTACAGATGGCACTGACAATCCCCTT
TCTGGTGGGGATCAGTATCAGAACATCACAGTGCACAGACATCTGATGCTACCAGATTTTGATTTGCT
GGAGGACATTGAAAGCAAAATCCAACCAGGTTCTCAACAGGCTGACTTCCTGGATGCACTAATCGTGA
GCATGGATGTGATTCAACATGAAACAATAGGAAAGAAGTTTGAGAAGAGGCATATTGAAATATTCACT
GACCTCAGCAGCCGATTCAGCAAAAGTCAGCTGGATATTATAATTCATAGCTTGAAGAAATGTGACAT
CTCCCTGCAATTCTTCTTGCCTTTCTCACTTGGCAAGGAAGATGGAAGTGGGGACAGAGGAGATGGCC
CCTTTCGCTTAGGTGGCCATGGGCCTTCCTTTCCACTAAAAGGAATTACCGAACAGCAAAAAGAAGGT
CTTGAGATAGTGAAAATGGTGATGATATCTTTAGAAGGTGAAGATGGGTTGGATGAAATTTATTCATT
CAGTGAGAGTCTGAGAAAACTGTGCGTCTTCAAGAAAATTGAGAGGCATTCCATTCACTGGCCCTGCC
GACTGACCATTGGCTCCAATTTGTCTATAAGGATTGCAGCCTATAAATCGATTCTACAGGAGAGAGTT
AAAAAGACTTGGACAGTTGTGGATGCAAAAACCCTAAAAAAAGAAGATATACAAAAAGAAACAGTTTA
TTGCTTAAATGATGATGATGAAACTGAAGTTTTAAAAGAGGATATTATTCAAGGGTTCCGCTATGGAA
GTGATATAGTTCCTTTCTCTAAAGTGGATGAGGAACAAATGAAATATAAATCGGAGGGGAAGTGCTTC
TCTGTTTTGGGATTTTGTAAATCTTCTCAGGTTCAGAGAAGATTCTTCATGGGAAATCAAGTTCTAAA
GGTCTTTGCAGCAAGAGATGATGAGGCAGCTGCAGTTGCACTTTCCTCCCTGATTCATGCTTTGGATG
ACTTAGACATGGTGGCCATAGTTCGATATGCTTATGACAAAAGAGCTAATCCTCAAGTCGGCGTGGCT
TTTCCTCATATCAAGCATAACTATGAGTGTTTAGTGTATGTGCAGCTGCCTTTCATGGAAGACTTGCG
GCAATACATGTTTTCATCCTTGAAAAACAGTAAGAAATATGCTCCCACCGAGGCACAGTTGAATGCTG
TTGATGCTTTGATTGACTCCATGAGCTTGGCAAAGAAAGATGAGAAGACAGACACCCTTGAAGACTTG
TTTCCAACCACCAAAATCCCAAATCCTCGATTTCAGAGATTATTTCAGTGTCTGCTGCACAGAGCTTT
ACATCCCCGGGAGCCTCTACCCCCAATTCAGCAGCATATTTGGAATATGCTGAATCCTCCCGCTGAGG
TGACAACAAAAAGTCAGATTCCTCTCTCTAAAATAAAGACCCTTTTTCCTCTGATTGAAGCCAAGAAA
AAGGATCAAGTGACTGCTCAGGAAATTTTCCAAGACAACCATGAAGATGGACCTACAGCTAAAAAATT
AAAGACTGAGCAAGGGGGAGCCCACTTCAGCGTCTCCAGTCTGGCTGAAGGCAGTGTCACCTCTGTTG
GAAGTGTGAATCCTGCTGAAAACTTCCGTGTTCTAGTGAAACAGAAGAAGGCCAGCTTTGAGGAAGCG
AGTAACCAGCTCATAAATCACATCGAACAGTTTTTGGATACTAATGAAACACCGTATTTTATGAAGAG
CATAGACTGCATCCGAGCCTTCCGGGAAGAAGCCATTAAGTTTTCAGAAGAGCAGCGCTTTAACAACT
TCCTGAAAGCCCTTCAAGAGAAAGTGGAAATTAAACAATTAAATCATTTCTGGGAAATTGTTGTCCAG
GATGGAATTACTCTGATCACCAAAGAGGAAGCCTCTGGAAGTTCTGTCACAGCTGAGGAAGCCAAAAA
GTTTCTGGCCCCCAAAGACAAACCAAGTGGAGACACAGCAGCTGTATTTGAAGAAGGTGGTGATGTGG
ACGATTTATTGGACATGATATAG

2- Human KU80 wild amino acid sequence (732 aa)

MVRSGNKAAVVLCMDVGFTMSNSIPGIESPFEQAKKVITMFVQRQVFAENKDEIALVLFGTDGTDNPL
SGGDQYQNITVHRHLMLPDFDLLEDIESKIQPGSQQADFLDALIVSMDVIQHETIGKKFEKRHIEIFT
DLSSRFSKSQLDIIIHSLKKCDISLQFFLPFSLGKEDGSGDRGDGPFRLGGHGPSFPLKGITEQQKEG
LEIVKMVMISLEGEDGLDEIYSFSESLRKLCVFKKIERHSIHWPCRLTIGSNLSIRIAAYKSILQERV
KKTWTVVDAKTLKKEDIQKETVYCLNDDDETEVLKEDIIQGFRYGSDIVPFSKVDEEQMKYKSEGKCF
SVLGFCKSSQVQRRFFMGNQVLKVFAARDDEAAAVALSSLIHALDDLDMVAIVRYAYDKRANPQVGVA
FPHIKHNYECLVYVQLPFMEDLRQYMFSSLKNSKKYAPTEAQLNAVDALIDSMSLAKKDEKTDTLEDL
FPTTKIPNPRFQRLFQCLLHRALHPREPLPPIQQHIWNMLNPPAEVTTKSQIPLSKIKTLFPLIEAKK
KDQVTAQEIFQDNHEDGPTAKKLKTEQGGAHFSVSSLAEGSVTSVGSVNPAENFRVLVKQKKASFEEA
SNQLINHIEQFLDTNETPYFMKSIDCIRAFREEAIKFSEEQRFNNFLKALQEKVEIKQLNHFWEIVVQ
DGITLITKEEASGSSVTAEEAKKFLAPKDKPSGDTAAVFEEGGDVDDLLDMI

Appendix 3: Human KU70 wild sequence

1- Human *KU70* wild nucleotide sequence (1830 nt)

ATGTCAGGGTGGGAGTCATATTACAAAACCGAGGGCGATGAAGAAGCAGAGGAAGAACAAGAAGAGAA
CCTTGAAGCAAGTGGAGACTATAAATATTCAGGAAGAGATAGTTTGATTTTTTTGGTTGATGCCTCCA
AGGCTATGTTTGAATCTCAGAGTGAAGATGAGTTGACACCTTTTGACATGAGCATCCAGTGTATCCAA
AGTGTGTACATCAGTAAGATCATAAGCAGTGATCGAGATCTCTTGGCTGTGGTGTTCTATGGTACCGA
GAAAGACAAAAATTCAGTGAATTTTAAAAATATTTACGTCTTACAGGAGCTGGATAATCCAGGTGCAA
AACGAATTCTAGAGCTTGACCAGTTTAAGGGGCAGCAGGGACAAAAACGTTTCCAAGACATGATGGGC
CACGGATCTGACTACTCACTCAGTGAAGTGCTGTGGGTCTGTGCCAACCTCTTTAGTGATGTCCAATT
CAAGATGAGTCATAAGAGGATCATGCTGTTCACCAATGAAGACAACCCCCATGGCAATGACAGTGCCA
AAGCCAGCCGGGCCAGGACCAAAGCCGGTGATCTCCGAGATACAGGCATCTTCCTTGACTTGATGCAC
CTGAAGAAACCTGGGGGCTTTGACATATCCTTGTTCTACAGAGATATCATCAGCATAGCAGAGGATGA
GGACCTCAGGGTTCACTTTGAGGAATCCAGCAAGCTAGAAGACCTGTTGCGGAAGGTTCGCGCCAAGG
AGACCAGGAAGCGAGCACTCAGCAGGTTAAAGCTGAAGCTCAACAAAGATATAGTGATCTCTGTGGGC
ATTTATAATCTGGTCCAGAAGGCTCTCAAGCCTCCTCCAATAAAGCTCTATCGGGAAACAAATGAACC
AGTGAAAACCAAGACCCGGACCTTTAATACAAGTACAGGCGGTTTGCTTCTGCCTAGCGATACCAAGA
GGTCTCAGATCTATGGGAGTCGTCAGATTATACTGGAGAAAGAGGAAACAGAAGAGCTAAAACGGTTT
GATGATCCAGGTTTGATGCTCATGGGTTTCAAGCCGTTGGTACTGCTGAAGAAACACCATTACCTGAG
GCCCTCCCTGTTCGTGTACCCAGAGGAGTCGCTGGTGATTGGGAGCTCAACCCTGTTCAGTGCTCTGC
TCATCAAGTGTCTGGAGAAGGAGGTTGCAGCATTGTGCAGATACACACCCCGCAGGAACATCCCTCCT
TATTTTGTGGCTTTGGTGCCACAGGAAGAAGAGTTGGATGACCAGAAAATTCAGGTGACTCCTCCAGG
CTTCCAGCTGGTCTTTTTACCCTTTGCTGATGATAAAAGGAAGATGCCCTTTACTGAAAAAATCATGG
CAACTCCAGAGCAGGTGGGCAAGATGAAGGCTATCGTTGAGAAGCTTCGCTTCACATACAGAAGTGAC
AGCTTTGAGAACCCCGTGCTGCAGCAGCACTTCAGGAACCTGGAGGCCTTGGCCTTGGATTTGATGGA
GCCGGAACAAGCAGTGGACCTGACATTGCCCAAGGTTGAAGCAATGAATAAAAGACTGGGCTCCTTGG
TGGATGAGTTTAAGGAGCTTGTTTACCCACCAGATTACAATCCTGAAGGGAAAGTTACCAAGAGAAAA
CACGATAATGAAGGTTCTGGAAGCAAAAGGCCCAAGGTGGAGTATTCAGAAGAGGAGCTGAAGACCCA
CATCAGCAAGGGTACGCTGGGCAAGTTCACTGTGCCCATGCTGAAAGAGGCCTGCCGGGCTTACGGGC
TGAAGAGTGGGCTGAAGAAGCAGGAGCTGCTGGAAGCCCTCACCAAGCACTTCCAGGACTGA

2- Human KU70 wild amino acid sequence (609 aa)

MSGWESYYKTEGDEEAEEEQEENLEASGDYKYSGRDSLIFLVDASKAMFESQSEDELTPFDMSIQCIQ
SVYISKIISSDRDLLAVVFYGTEKDKNSVNFKNIYVLQELDNPGAKRILELDQFKGQQGQKRFQDMMG
HGSDYSLSEVLWVCANLFSDVQFKMSHKRIMLFTNEDNPHGNDSAKASRARTKAGDLRDTGIFLDLMH
LKKPGGFDISLFYRDIISIAEDEDLRVHFEESSKLEDLLRKVRAKETRKRALSRLKLKLNKDIVISVG
IYNLVQKALKPPPIKLYRETNEPVKTKTRTFNTSTGGLLLPSDTKRSQIYGSRQIILEKEETEELKR
FDDPGLMLMGFKPLVLLKKHHYLRPSLFVYPEESLVIGSSTLFSALLIKCLEKEVAALCRYTPRRNIP
PYFVALVPQEEELDDQKIQVTPPGFQLVFLPFADDKRKMPFTEKIMATPEQVGKMKAIVEKLRFTYRS
DSFENPVLQQHFRNLEALALDLMEPEQAVDLTLPKVEAMNKRLGSLVDEFKELVYPPDYNPEGKVTKR
KHDNEGSGSKRPKVEYSEEELKTHISKGTLGKFTVPMLKEACRAYGLKSGLKKQELLEALTKHFQD

Appendix 4

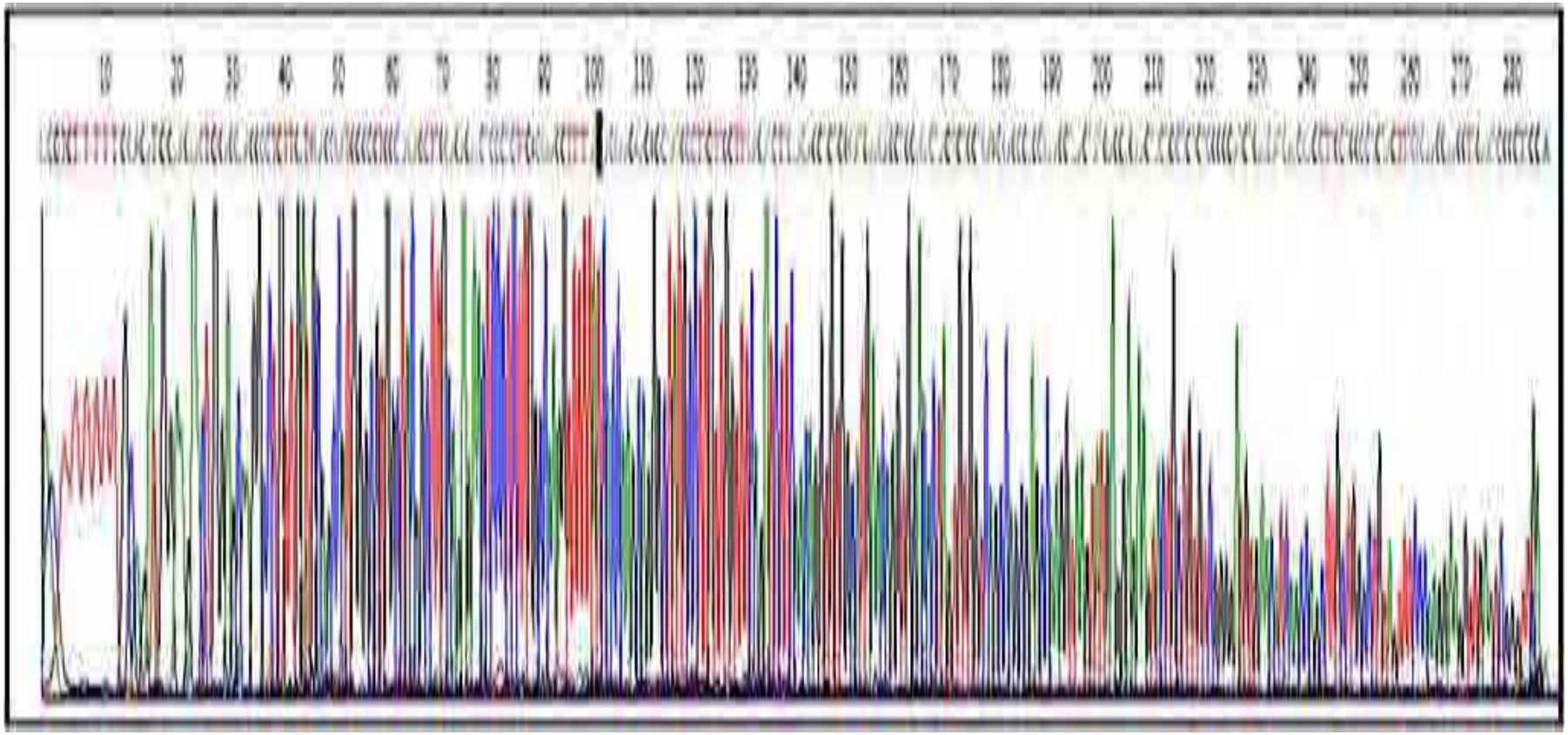

Chromoatogram of wild sequence of the 1st coding exon of *XLF*

Appendix 5

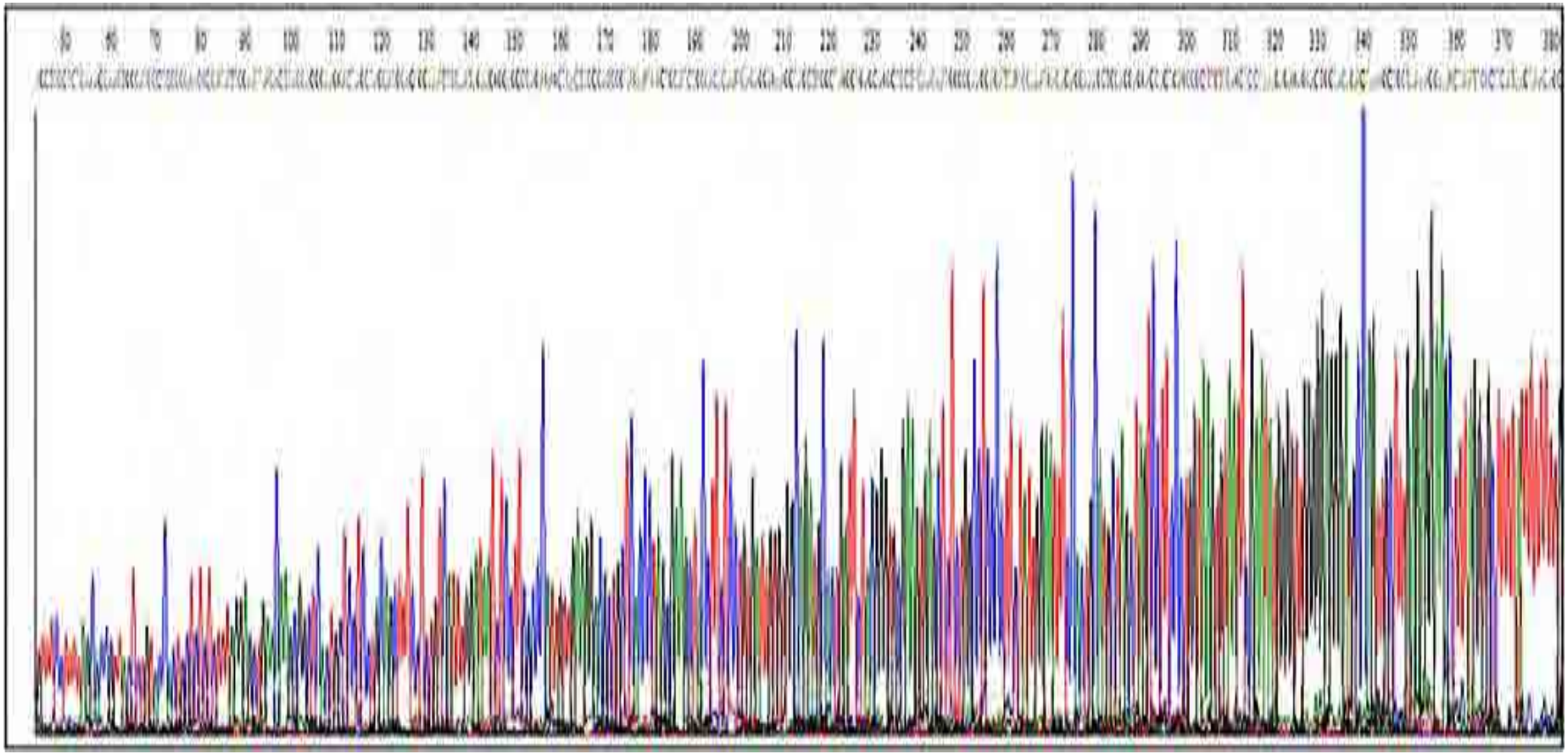

Chromoatogram of wild sequence of the 2nd coding exon of *XLF*

Appendix 6

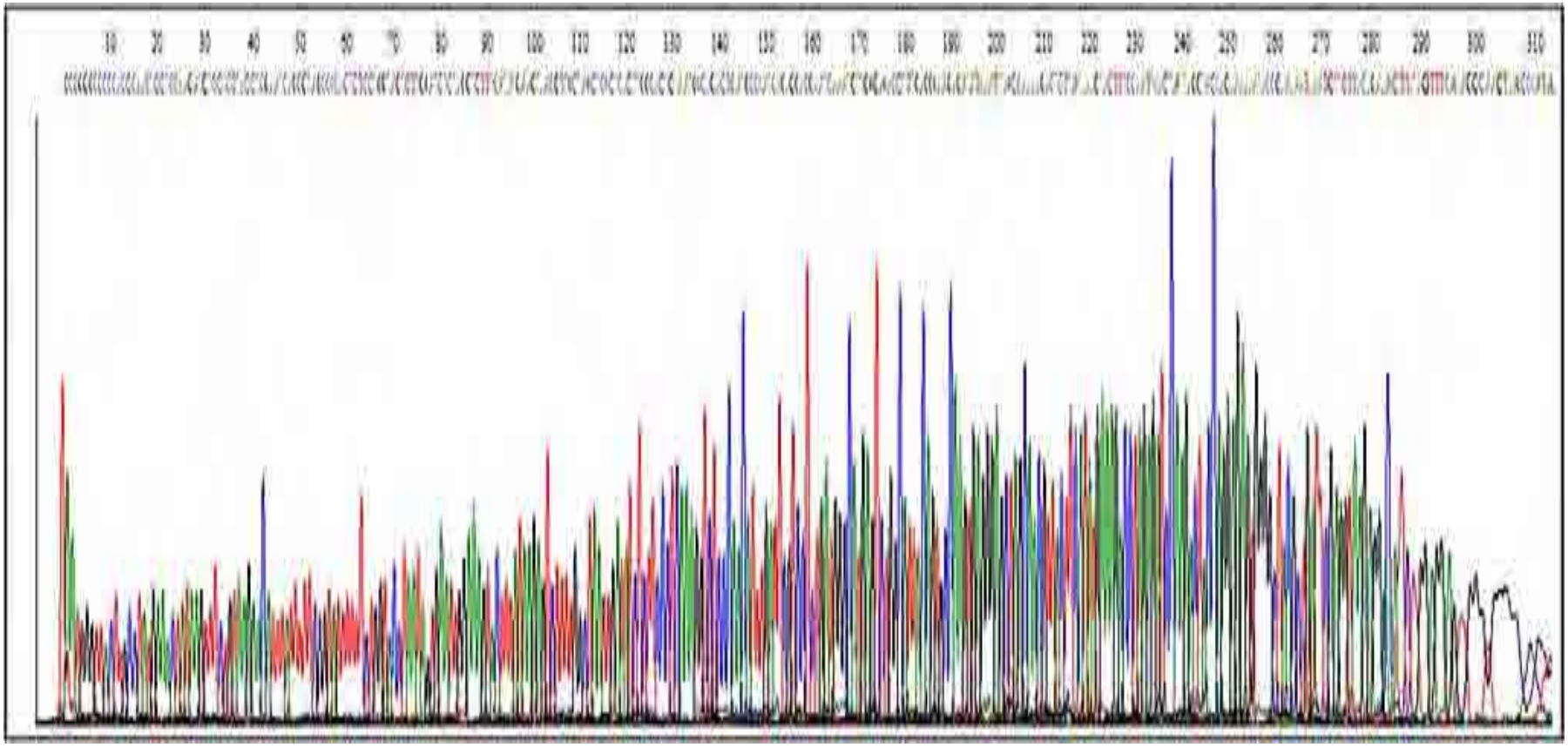

Chromoatogram of wild sequence of the 3rd coding exon of *XLF*

Appendix 7

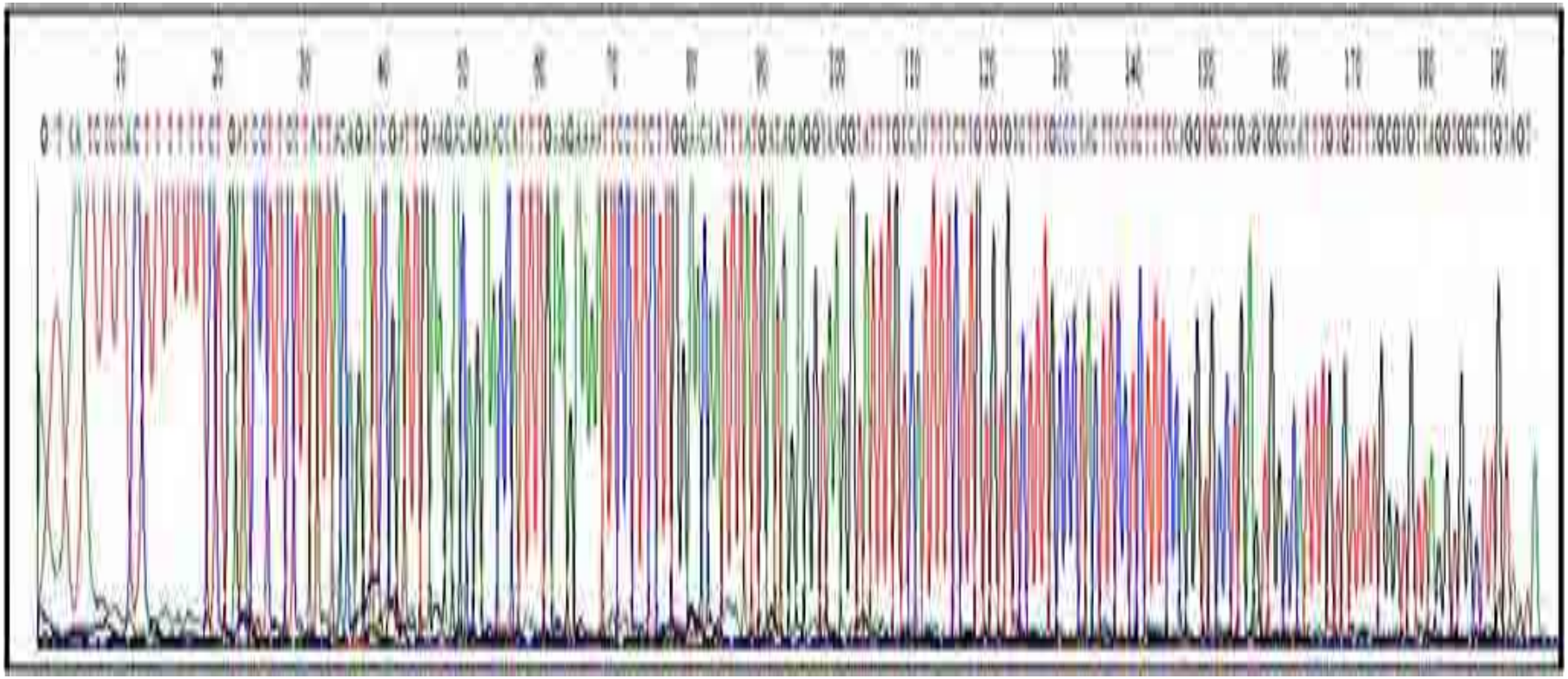

Chromoatogram of wild sequence of the 4th coding exon of *XLF*

Appendix 8

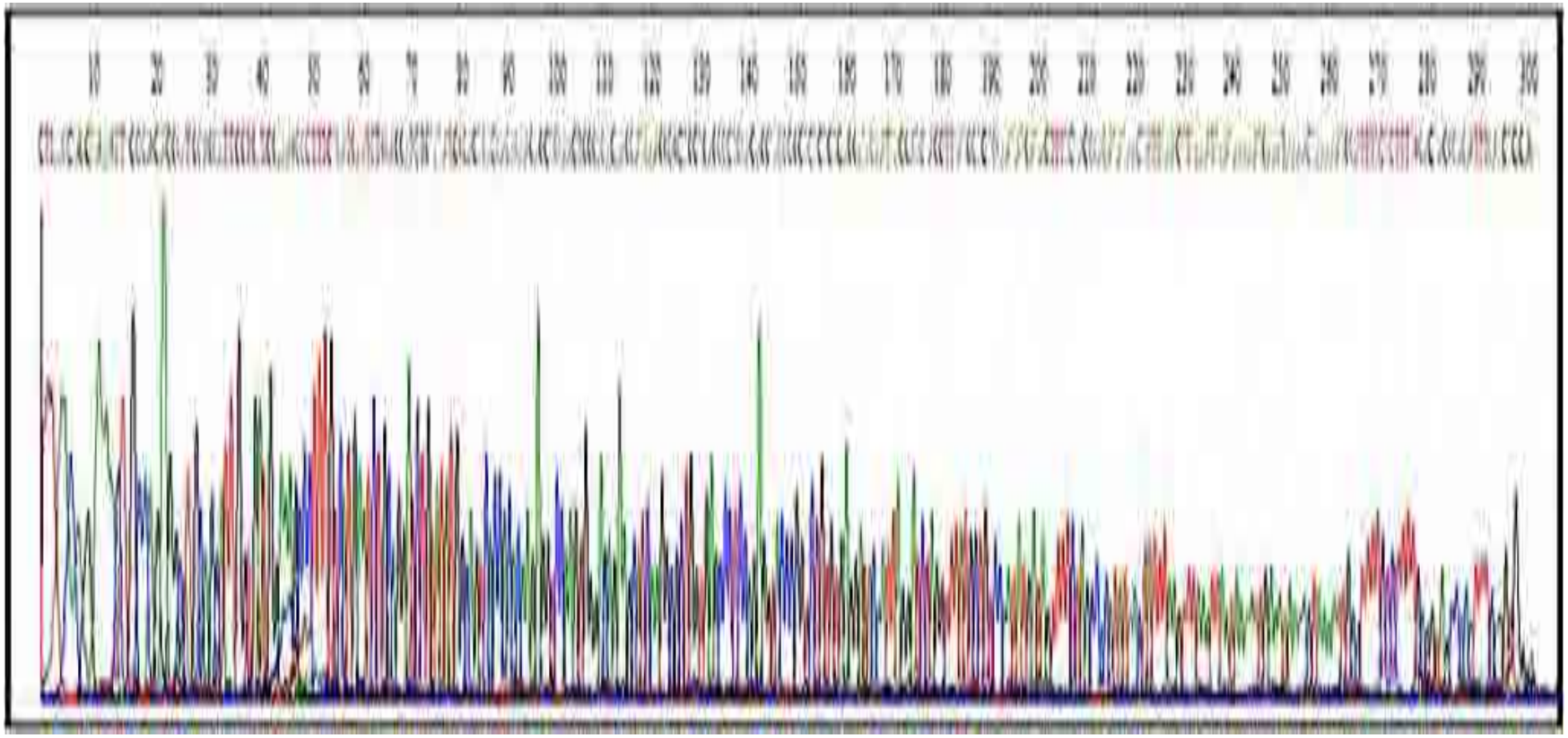

Chromoatogram of wild sequence of the 5th coding exon of *XLF*

Appendix 9

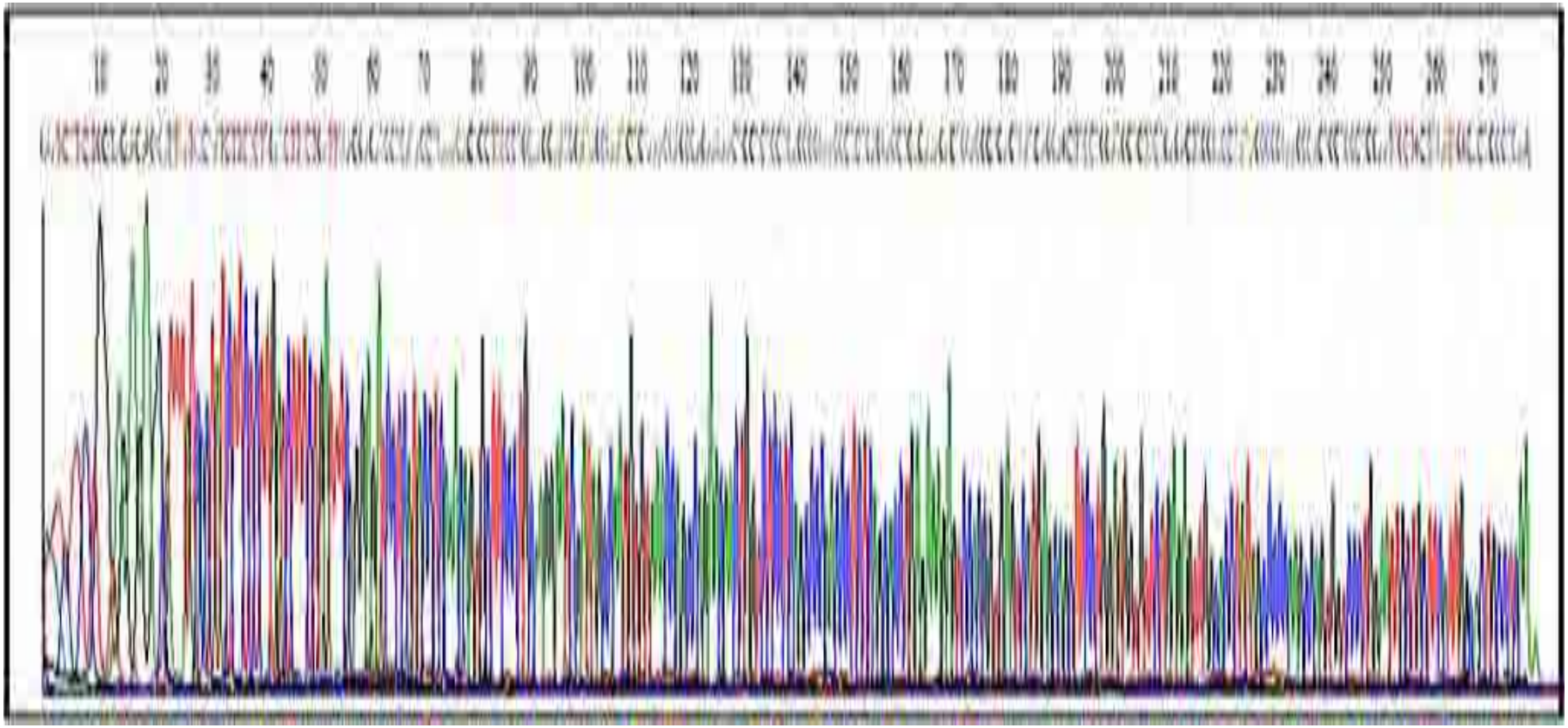

Chromoatogram of wild sequence of the 6th coding exon of *XLF*

Appendix 10

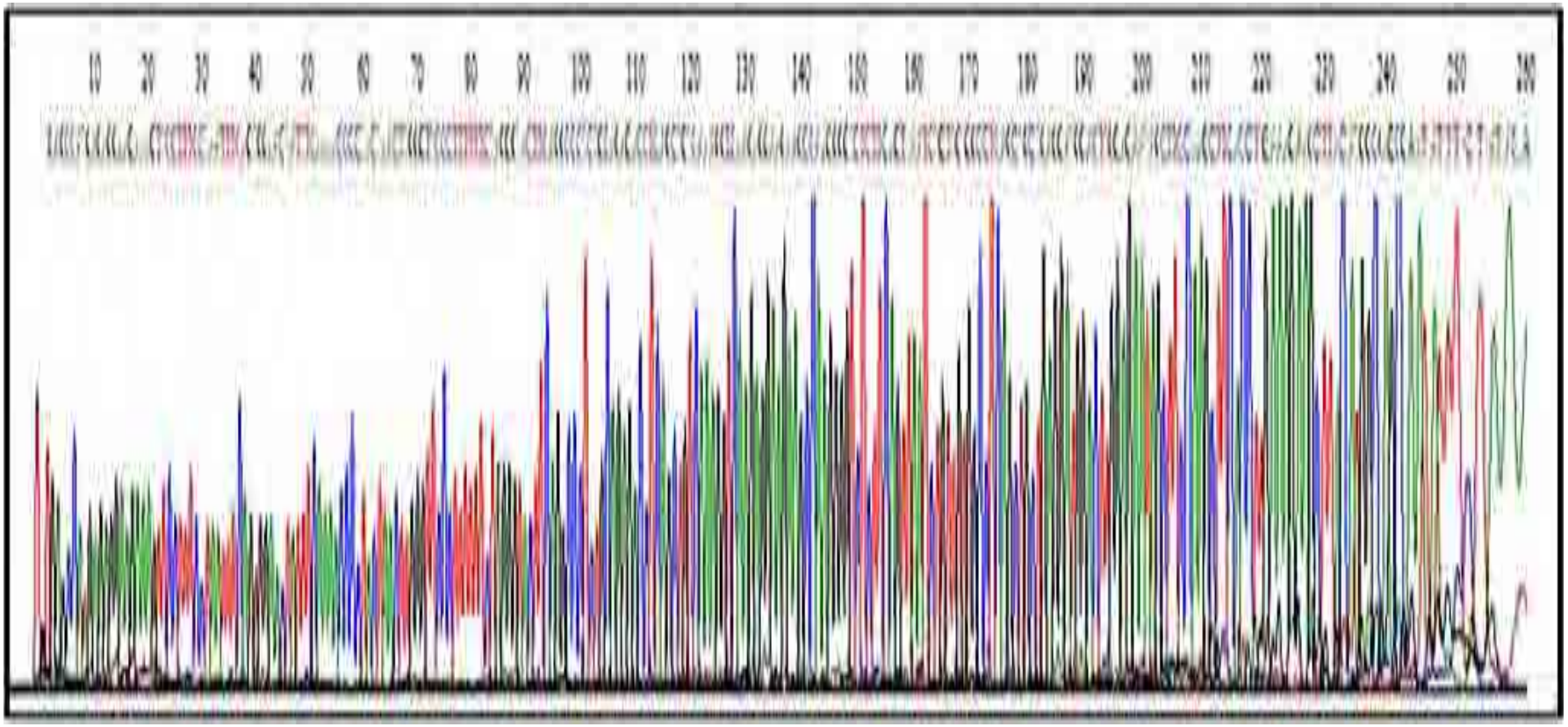

Chromoatogram of wild sequence of the 7th coding exon of *XLF*

Appendix 11

		pFlag-KU70-K317R	pFlag-KU70-K331R	pFlag-KU70-K338R	pFlag-KU70-K317Q	pFlag-KU70-K331Q	pFlag-KU70-K338Q
MRC5VA	6Gy	0.05	0.05	0.06	0.06	0.05	0.05
	8Gy	0.02	0.02	0.02	0.02	0.02	0.02
Empty-pFlag	6Gy	0.06	0.06	0.06	0.06	0.05	0.06
	8Gy	0.02	0.02	0.02	0.02	0.02	0.02
pFlag-KU70/wt	6Gy	0.06	0.06	0.06	0.06	0.05	0.06
	8Gy	0.04	0.04	0.04	0.04	0.04	0.04
pFlag-KU80/wt	6Gy	0.06	0.06	0.06	0.06	0.05	0.06
	8Gy	0.02	0.02	0.02	0.02	0.02	0.02

Table 5.1: Statistical analysis of the surviving fractions at 6Gy and 8Gy
All the clonogenic survival experiments were performed in three independent replicates. Mean value, standard deviation and standard error of the mean were calculated. Student T test was used to analyse differences between the surviving fractions of pFlag-KU70 mutant (both aceto-blocking and aceto-mimicking) and those of the control cell lines at both 6Gy and 8Gy. The table shows the p-values. Differences were considered significant if $p<0.05$.

Appendix 12

	pFlag-KU70-K317R	pFlag-KU70-K331R	pFlag-KU70-K338R	pFlag-KU70-K317Q	pFlag-KU70-K331Q	pFlag-KU70-K338Q
MRC5VA	0.02	0.03	0.04	0.02	0.02	0.04
Empty-pFlag	0.02	0.03	0.04	0.02	0.02	0.04
pFlag-KU70/wt	0.02	0.03	0.04	0.02	0.02	0.04
pFlag-KU80/wt	0.02	0.04	0.04	0.02	0.03	0.04

Table 5.2: Statistical analysis of the γH2AX residual foci at 5Gy
All the γH2AX foci experiments were performed in two independent replicates. Mean value, standard deviation and standard error of the mean were calculated. Student T test was used to analySe differences between the γH2AX residual foci of pFlag KU70 mutant (both aceto-blocking and aceto-mimicking) and those of the control cell lines ay 5Gy. The table shows the p-values. Differences were considered significant if $p<0.05$.

CHAPTER EIGHT: REFERENCES

Aaltonen, L., Johns, L., Jarvinen, H., et al. (2007) Explaining the familial colorectal cancer risk associated with mismatch repair (MMR)-deficient and MMR-stable tumors. **Clin Cancer Res**, 13: (1): 356-361.

Aas, P. A., Otterlei, M., Falnes, P. O., et al. (2003) Human and bacterial oxidative demethylases repair alkylation damage in both RNA and DNA. **Nature**, 421: (6925): 859-863.

Abraham, J., Earl, H. M., Pharoah, P. D., et al. (2006) Pharmacogenetics of cancer chemotherapy. **Biochim Biophys Acta**, 1766: (2): 168-183.

Ahnesorg, P., Smith, P. and Jackson, S. P. (2006) XLF interacts with the XRCC4-DNA ligase IV complex to promote DNA nonhomologous end-joining. **Cell**, 124: (2): 301-313.

Ali, A., Zhang, J., Bao, S., et al. (2004) Requirement of protein phosphatase 5 in DNA-damage-induced ATM activation. **Genes Dev**, 18: (3): 249-254.

Allfrey, V. G., Faulkner, R. and Mirsky, A. E. (1964) Acetylation and methylation of histones and their possible role in the regulation of RNA synthesis. **Proc Natl Acad Sci**, 51: 786-794.

Altieri, F., Grillo, C., Maceroni, M., et al. (2008) DNA damage and repair: from molecular mechanisms to health implications. **Antioxid Redox Signal**, 10: (5): 891-937.

Amsel, A. D., Rathaus, M., Kronman, N., et al. (2008) Regulation of the proapoptotic factor Bax by Ku70-dependent deubiquitylation. **Proc Natl Acad Sci**, 105: (13): 5117-5122.

Andres, S. N., Modesti, M., Tsai, C. J., et al. (2007) Crystal structure of human XLF: a twist in nonhomologous DNA end-joining. **Mol Cell**, 28: (6): 1093-1101.

Aparicio, T., Guillou, E., Coloma, J., et al. (2009) The human GINS complex associates with Cdc45 and MCM and is essential for DNA replication. **Nucleic Acids Res**, 37: (7): 2087-2095.

Arakawa, H., Moldovan, G. L., Saribasak, H., et al. (2006) A role for PCNA ubiquitination in immunoglobulin hypermutation. **PLoS Biol**, 4: (11): e366.

Araujo, S. J., Nigg, E. A. and Wood, R. D. (2001) Strong functional interactions of TFIIH with XPC and XPG in human DNA nucleotide excision repair, without a preassembled repairosome. **Mol Cell Biol**, 21: (7): 2281-2291.

Arnaudeau, C., Lundin, C. and Helleday, T. (2001) DNA double-strand breaks associated with replication forks are predominantly repaired by homologous recombination involving an exchange mechanism in mammalian cells. **J Mol Biol**, 307: (5): 1235-1245.

Averbeck, N. B. and Durante, M. (2011) Protein acetylation within the cellular response to radiation. **J Cell Physiol**, 226: (4): 962-967.

Bailey, S. M., Meyne, J., Chen, D. J., et al. (1999) DNA double-strand break repair proteins are required to cap the ends of mammalian chromosomes. **Proc Natl Acad Sci**, 96: (26): 14899-14904.

Bakalkin, G., Yakovleva, T., Hurd, Y. L., et al. (1998) Autoantigen Ku in the brain. Developmentally regulated expression and subcellular localization. **Neuroreport**, 9: (9): 2147-2151.

Bakkenist, C. J. and Kastan, M. B. (2003) DNA damage activates ATM through intermolecular autophosphorylation and dimer dissociation. **Nature**, 421: (6922): 499-506.

Banath, J. P., Macphail, S. H. and Olive, P. L. (2004) Radiation sensitivity, H2AX phosphorylation and kinetics of repair of DNA strand breaks in irradiated cervical cancer cell lines. **Cancer Res**, 64: (19): 7144-7149.

Barnes, D. E. and Lindahl, T. (2004) Repair and genetic consequences of endogenous DNA base damage in mammalian cells. **Annu Rev Genet**, 38: 445-476.

Bartek, J. and Hodny, Z. (2010) SUMO boosts the DNA damage response barrier against cancer. **Cancer Cell**, 17: (1): 9-11.

Bartek, J. and Lukas, J. (2007) DNA damage checkpoints: from initiation to recovery or adaptation. **Curr Opin Cell Biol**, 19: (2): 238-245.

Basu, A., Rose, K. L., Zhang, J., et al. (2009) Proteome-wide prediction of acetylation substrates. **PNAS**, 106: (33): 13785-13790.

Batty, D. P. and Wood, R. D. (2000) Damage recognition in nucleotide excision repair of DNA. **Gene**, 241: (2): 193-204.

Bauerschmidt, C., Pollok, S., Kremmer, E., et al. (2007) Interactions of human Cdc45 with the Mcm2-7 complex, the GINS complex, and DNA polymerases delta and epsilon during S phase. **Genes Cells**, 12: (6): 745-758.

Bennett, E. J. and Harper, J. W. (2008) DNA damage: ubiquitin marks the spot. **Nat Struct Mol Biol**, 15: (1): 20-22.

Benson, F. E., Baumann, P. and West, S. C. (1998) Synergistic actions of Rad51 and Rad52 in recombination and DNA repair. **Nature**, 391: (6665): 401-404.

Bergink, S. and Jentsch, S. (2009) Principles of ubiquitin and SUMO modifications in DNA repair. **Nature**, 458: (7237): 461-467.

Bi, G. and Jiang, G. (2006) The molecular mechanism of HDAC inhibitors in anticancer effects. **Cell Mol Immunol**, 3: (4): 285-290.

Bianchi, A. and De Lange, T. (1999) Ku binds telomeric DNA in vitro. **J Biol Chem**, 274: (30): 21223-21227.

Bird, A. W., Yu, D. Y., Pray-Grant, M. G., et al. (2002) Acetylation of histone H4 by Esa1 is required for DNA double-strand break repair. **Nature**, 419: (6905): 411-415.

Blackwell, L. J., Martik, D., Bjornson, K. P., et al. (1998) Nucleotide-promoted release of hMutSalpha from heteroduplex DNA is consistent with an ATP-dependent translocation mechanism. **J Biol Chem**, 273: (48): 32055-32062.

Block, W. D., Yu, Y., Merkle, D., et al. (2004) Autophosphorylation-dependent remodeling of the DNA-dependent protein kinase catalytic subunit regulates ligation of DNA ends. **Nucleic Acids Res**, 32: (14): 4351-4357.

Bochkareva, E., Belegu, V., Korolev, S., et al. (2001) Structure of the major single-stranded DNA-binding domain of replication protein A suggests a dynamic mechanism for DNA binding. **Embo J**, 20: (3): 612-618.

Bohgaki, T., Bohgaki, M. and Hakem, R. (2010) DNA double-strand break signaling and human disorders. **Genome Integr**, 1: (1): 15.

Bouquet, F., Muller, C. and Salles, B. (2006) The Loss of gammaH2AX Signal is a Marker of DNA Double Strand Breaks Repair Only at Low Levels of DNA Damage. **Cell Cycle**, 5: (10): 1116-1122.

Bradford, M. M. (1976) A rapid and sensitive method for the quantitation of microgram quantities of protein utilizing the principle of protein-dye binding. **Anal Biochem**, 72: (1-2): 248-254.

Bredemeyer, A. L., Huang, C. Y., Walker, L. M., et al. (2008) Aberrant V(D)J recombination in ataxia telangiectasia mutated-deficient lymphocytes is dependent on nonhomologous DNA end joining. **J Immunol**, 181: (4): 2620-2625.

Brooks, L., 3rd, Heimsath, E. G., Jr., Loring, G. L., et al. (2008) FHA-RING ubiquitin ligases in cell division cycle control. **Cell Mol Life Sci**, 65: (21): 3458-3466.

Brown, R. and Strathdee, G. (2002) Epigenomics and epigenetic therapy of cancer. **Trends Mol Med**, 8: (4 Suppl): S43-48.

Brownell, J. E., Zhou, J., Ranalli, T., et al. (1996) Tetrahymena histone acetyltransferase A: a homolog to yeast Gcn5p linking histone acetylation to gene activation. **Cell**, 84: (6): 843-851.

Buck, D., Malivert, L., De Chasseval, R., et al. (2006) Cernunnos, a novel nonhomologous end-joining factor, is mutated in human immunodeficiency with microcephaly. **Cell**, 124: (2): 287-299.

Bunick, C. G. and Chazin, W. J. (2005) Two blades of the [ex]scissor. **Structure**, 13: (12): 1740-1741.

Bunick, C. G., Miller, M. R., Fuller, B. E., et al. (2006) Biochemical and structural domain analysis of xeroderma pigmentosum complementation group C protein. **Biochemistry**, 45: (50): 14965-14979.

Busser, B., Sancey, L., Josserand, V., et al. (2010a) Amphiregulin promotes BAX inhibition and resistance to gefitinib in non-small-cell lung cancers. **Mol Ther**, 18: (3): 528-535.

Busser, B., Sancey, L., Josserand, V., et al. (2010b) Amphiregulin promotes resistance to gefitinib in non-small cell lung cancer cells by regulating Ku70 acetylation. **Mol Ther**, 18: (3): 536-543.

Cadet, J., Douki, T., Gasparutto, D., et al. (2003) Oxidative damage to DNA: formation, measurement and biochemical features. **Mutat Res**, 531: (1-2): 5-23.

Caldecott, K. W. (2001) Mammalian DNA single-strand break repair: an X-ra(y)ted affair. **Bioessays**, 23: (5): 447-455.

Callebaut, I., Malivert, L., Fischer, A., et al. (2006) Cernunnos interacts with the XRCC4 x DNA-ligase IV complex and is homologous to the yeast nonhomologous end-joining factor Nej1. **J Biol Chem**, 281: (20): 13857-13860.

Callen, E., Jankovic, M., Wong, N., et al. (2009) Essential role for DNA-PKcs in DNA double-strand break repair and apoptosis in ATM-deficient lymphocytes. **Mol Cell**, 34: (3): 285-297.

Cary, R. B., Peterson, S. R., Wang, J., et al. (1997) DNA looping by Ku and the DNA-dependent protein kinase. **Proc Natl Acad Sci**, 94: (9): 4267-4272.

Castle, V., Kwok, R., Opipari, A., et al. (2010) Ku70 acetylation in neuroblastoma pathogenesis and therapy. **Trans Am Clin Climatol Assoc**, 121: 183-191.

Chai, W., Ford, L. P., Lenertz, L., et al. (2002) Human Ku70/80 associates physically with telomerase through interaction with hTERT. **J Biol Chem**, 277: (49): 47242-47247.

Chalmers, A. J. (2004) Poly(ADP-ribose) polymerase-1 and ionizing radiation: sensor, signaller and therapeutic target. **Clin Oncol**, 16: (1): 29-39.

Chan, D. W., Chen, B. P.-C., Prithivirajsingh, S., et al. (2002) Autophosphorylation of the DNA-dependent protein kinase catalytic subunit is required for rejoining of DNA double-strand breaks. **Genes Dev**, 16: (18): 2333-2338.

Chan, D. W. and Lees-Miller, S. P. (1996) The DNA-dependent protein kinase is inactivated by autophosphorylation of the catalytic subunit. **J Biol Chem**, 271: (15): 8936-8941.

Chen, C. S., Wang, Y. C., Yang, H. C., et al. (2007) Histone deacetylase inhibitors sensitize prostate cancer cells to agents that produce DNA double-strand breaks by targeting Ku70 acetylation. **Cancer Res**, 67: (11): 5318-5327.

Chen, C. S., Weng, S. C., Tseng, P. H., et al. (2005) Histone acetylation-independent effect of histone deacetylase inhibitors on Akt through the reshuffling of protein phosphatase 1 complexes. **J Biol Chem**, 280: (46): 38879-38887.

Chen, R., Davydov, E. V., Sirota, M., et al. (2010) Non-synonymous and synonymous coding SNPs show similar likelihood and effect size of human disease association. **PLoS ONE**, 5: (10): e13574.

Chou, C. H., Wang, J., Knuth, M. W., et al. (1992) Role of a major autoepitope in forming the DNA binding site of the p70 (Ku) antigen. **J Exp Med**, 175: (6): 1677-1684.

Choudhary, C., Kumar, C., Gnad, F., et al. (2009) Lysine acetylation targets protein complexes and co-regulates major cellular functions. **Science**, 325: (5942): 834-840.

Chowdhury, D., Keogh, M. C., Ishii, H., et al. (2005) gamma-H2AX dephosphorylation by protein phosphatase 2A facilitates DNA double-strand break repair. **Mol Cell**, 20: (5): 801-809.

Chowdhury, D., Xu, X., Zhong, X., et al. (2008) A PP4-phosphatase complex dephosphorylates gamma-H2AX generated during DNA replication. **Mol Cell**, 31: (1): 33-46.

Clayton, A. L., Hazzalin, C. A. and Mahadevan, L. C. (2006) Enhanced Histone Acetylation and Transcription: A Dynamic Perspective. **Mol cell**, 23: (3): 289-296.

Cohen, H. Y., Lavu, S., Bitterman, K. J., et al. (2004a) Acetylation of the C terminus of Ku70 by CBP and PCAF controls Bax-mediated apoptosis. **Mol Cell**, 13: (5): 627-638.

Cohen, H. Y., Miller, C., Bitterman, K. J., et al. (2004b) Calorie restriction promotes mammalian cell survival by inducing the SIRT1 deacetylase. **Science**, 305: (5682): 390-392.

Coin, F., Oksenych, V., Mocquet, V., et al. (2008) Nucleotide excision repair driven by the dissociation of CAK from TFIIH. **Mol cell**, 31: (1): 9-20.

Constantin, N., Dzantiev, L., Kadyrov, F. A., et al. (2005) Human mismatch repair: reconstitution of a nick-directed bidirectional reaction. **J Biol Chem**, 280: (48): 39752-39761.

Constantinou, A., Tarsounas, M., Karow, J. K., et al. (2000) Werner's syndrome protein (WRN) migrates Holliday junctions and co-localizes with RPA upon replication arrest. **Embo Rep**, 1: (1): 80-84.

Corden, J. L. (2007) Transcription. Seven ups the code. **Science**, 318: (5857): 1735-1736.

Corneo, B., Wendland, R. L., Deriano, L., et al. (2007) Rag mutations reveal robust alternative end joining. **Nature**, 449: (7161): 483-486.

Couedel, C., Mills, K. D., Barchi, M., et al. (2004) Collaboration of homologous recombination and nonhomologous end-joining factors for the survival and integrity of mice and cells. **Genes Dev**, 18: (11): 1293-1304.

Cui, X., Yu, Y., Gupta, S., et al. (2005) Autophosphorylation of DNA-dependent protein kinase regulates DNA end processing and may also alter double-strand break repair pathway choice. **Mol Cell Biol**, 25: (24): 10842-10852.

D'amours, D. and Jackson, S. P. (2002) The Mre11 complex: at the crossroads of dna repair and checkpoint signalling. **Nat Rev Mol Cell Biol**, 3: (5): 317-327.

D'errico, M., Parlanti, E., Teson, M., et al. (2007) The role of CSA in the response to oxidative DNA damage in human cells. **Oncogene**, 26: (30): 4336-4343.

Dai, Y., Kysela, B., Hanakahi, L. A., et al. (2003) Nonhomologous end joining and V(D)J recombination require an additional factor. **Proc Natl Acad Sci**, 100: (5): 2462-2467.

Dalziel, R. G., Mendelson, S. C. and Quinn, J. P. (1992) The nuclear autoimmune antigen Ku is also present on the cell surface. **Autoimmunity**, 13: (4): 265-267.

Das, A., Wiederhold, L., Leppard, J. B., et al. (2006) NEIL2-initiated, APE-independent repair of oxidized bases in DNA: Evidence for a repair complex in human cells. **DNA Repair (Amst)**, 5: (12): 1439-1448.

Daughdrill, G. W., Buchko, G. W., Botuyan, M. V., et al. (2003) Chemical shift changes provide evidence for overlapping single-stranded DNA- and XPA-binding sites on the 70 kDa subunit of human replication protein A. **Nucleic Acids Res**, 31: (14): 4176-4183.

Davis, A. J. and Chen, D. J. (2010) A role for ATM kinase activity and Mre11 in microhomology-mediated end-joining. **Cell Cycle**, 9: (16): 3147-3148.

De Boer, J. and Hoeijmakers, J. H. (2000) Nucleotide excision repair and human syndromes. **Carcinogenesis**, 21: (3): 453-460.

De Feraudy, S., Revet, I., Bezrookove, V., et al. (2010) A minority of foci or pan-nuclear apoptotic staining of gammaH2AX in the S phase after UV damage contain DNA double-strand breaks. **Proc Natl Acad Sci**, 107: (15): 6870-6875.

Defazio, L. G., Stansel, R. M., Griffith, J. D., et al. (2002) Synapsis of DNA ends by DNA-dependent protein kinase. **Embo J**, 21: (12): 3192-3200.

Demple, B. and Sung, J. S. (2005) Molecular and biological roles of Ape1 protein in mammalian base excision repair. **DNA Repair (Amst)**, 4: (12): 1442-1449.

Denver, D. R., Swenson, S. L. and Lynch, M. (2003) An evolutionary analysis of the helix-hairpin-helix superfamily of DNA repair glycosylases. **Mol Biol Evol**, 20: (10): 1603-1611.

Deriano, L., Stracker, T. H., Baker, A., et al. (2009) Roles for NBS1 in alternative nonhomologous end-joining of V(D)J recombination intermediates. **Mol Cell**, 34: (1): 13-25.

Dibiase, S. J., Zeng, Z. C., Chen, R., et al. (2000) DNA-dependent protein kinase stimulates an independently active, nonhomologous, end-joining apparatus. **Cancer Res**, 60: (5): 1245-1253.

Dip, R., Camenisch, U. and Naegeli, H. (2004) Mechanisms of DNA damage recognition and strand discrimination in human nucleotide excision repair. **DNA Repair (Amst)**, 3: (11): 1409-1423.

Divine, K. K., Gilliland, F. D., Crowell, R. E., et al. (2001) The XRCC1 399 glutamine allele is a risk factor for adenocarcinoma of the lung. **Mutat Res**, 461: (4): 273-278.

Dizdaroglu, M. (2005) Base-excision repair of oxidative DNA damage by DNA glycosylases. **Mutat Res**, 591: (1-2): 45-59.

Doil, C., Mailand, N., Bekker-Jensen, S., et al. (2009) RNF168 binds and amplifies ubiquitin conjugates on damaged chromosomes to allow accumulation of repair proteins. **Cell**, 136: (3): 435-446.

Dormeyer, W., Ott, M. and Schnolzer, M. (2005) Probing lysine acetylation in proteins. **Mol Cell Proteomics** 4: (9): 1226-1239.

Douglas, P., Gupta, S., Morrice, N., et al. (2005a) DNA-PK-dependent phosphorylation of Ku70/80 is not required for non-homologous end joining. **DNA Repair**, 4: (9): 1006-1018.

Douglas, P., Gupta, S., Morrice, N., et al. (2005b) DNA-PK-dependent phosphorylation of Ku70/80 is not required for non-homologous end joining. **DNA Repair (Amst)**, 4: (9): 1006-1018.

Downs, J. A., Allard, S., Jobin-Robitaille, O., et al. (2004) Binding of chromatin-modifying activities to phosphorylated histone H2A at DNA damage sites. **Mol cell**, 16: (6): 979-990.

Dunand-Sauthier, I., Hohl, M., Thorel, F., et al. (2005) The spacer region of XPG mediates recruitment to nucleotide excision repair complexes and determines substrate specificity. **J Biol Chem**, 280: (8): 7030-7037.

Duncan, T., Trewick, S. C., Koivisto, P., et al. (2002) Reversal of DNA alkylation damage by two human dioxygenases. **Proc Natl Acad Sci**, 99: (26): 16660-16665.

Dunning, A. M., Chiano, M., Smith, N. R., et al. (1997) Common BRCA1 variants and susceptibility to breast and ovarian cancer in the general population. **Hum Mol Genet**, 6: (2): 285-289.

Durocher, F., Shattuck-Eidens, D., Mcclure, M., et al. (1996) Comparison of BRCA1 polymorphisms, rare sequence variants and/or missense mutations in unaffected and breast/ovarian cancer populations. **Hum Mol Genet**, 5: (6): 835-842.

Dutrannoy, V., Demuth, I., Baumann, U., et al. (2010) Clinical variability and novel mutations in the NHEJ1 gene in patients with a Nijmegen breakage syndrome-like phenotype. **Hum Mutat**, 31: (9): 1059-1068.

Dybdahl, M., Vogel, U., Frentz, G., et al. (1999) Polymorphisms in the DNA repair gene XPD: correlations with risk and age at onset of basal cell carcinoma. **Cancer Epidemiology, Biomarkers and Prevention**, 8: (1): 77-81.

Dzantiev, L., Constantin, N., Genschel, J., et al. (2004) A defined human system that supports bidirectional mismatch-provoked excision. **Mol Cell**, 15: (1): 31-41.

Efferth, T. and Volm, M. (2005) Pharmacogenetics for individualized cancer chemotherapy. **Pharmacol Ther** 107: (2): 155-176.

Errami, A., Smider, V., Rathmell, W. K., et al. (1996) Ku86 defines the genetic defect and restores X-ray resistance and V(D)J recombination to complementation group 5 hamster cell mutants. **Mol Cell Biol**, 16: (4): 1519-1526.

Evans, M. D., Dizdaroglu, M. and Cooke, M. S. (2004) Oxidative DNA damage and disease: induction, repair and significance. **Mutat Res**, 567: (1): 1-61.

Fattah, F., Lee, E. H., Weisensel, N., et al. (2010) Ku regulates the non-homologous end joining pathway choice of DNA double-strand break repair in human somatic cells. **PLoS Genet**, 6: (2): e1000855.

Feldmann, E., Schmiemann, V., Goedecke, W., et al. (2000) DNA double-strand break repair in cell-free extracts from Ku80-deficient cells: implications for Ku serving as an alignment factor in non-homologous DNA end joining. **Nucleic Acids Res**, 28: (13): 2585-2596.

Feng, L., Huang, J. and Chen, J. (2009) MERIT40 facilitates BRCA1 localization and DNA damage repair. **Genes Dev**, 23: (6): 719-728.

Fortini, P. and Dogliotti, E. (2007) Base damage and single-strand break repair: mechanisms and functional significance of short- and long-patch repair subpathways. **DNA Repair (Amst)**, 6: (4): 398-409.

Frampton, J., Irmisch, A., Green, C. M., et al. (2006) Postreplication repair and PCNA modification in Schizosaccharomyces pombe. **Mol Biol Cell**, 17: (7): 2976-2985.

Friedberg, E. C. (2001) How nucleotide excision repair protects against cancer. **Nat Rev Cancer**, 1: (1): 22-33.

Frosina, G., Fortini, P., Rossi, O., et al. (1996) Two pathways for base excision repair in mammalian cells. **J Biol Chem**, 271: (16): 9573-9578.

Fu, Y. P., Yu, J. C., Cheng, T. C., et al. (2003) Breast cancer risk associated with genotypic polymorphism of the nonhomologous end-joining genes: a multigenic study on cancer susceptibility. **Cancer Res**, 63: (10): 2440-2446.

Gagou, M. E., Zuazua-Villar, P. and Meuth, M. (2010) Enhanced H2AX phosphorylation, DNA replication fork arrest, and cell death in the absence of Chk1. **Mol Biol Cell**, 21: (5): 739-752.

Galanty, Y., Belotserkovskaya, R., Coates, J., et al. (2009) Mammalian SUMO E3-ligases PIAS1 and PIAS4 promote responses to DNA double-strand breaks. **Nature**, 462: (7275): 935-939.

Galkin, V. E., Esashi, F., Yu, X., et al. (2005) BRCA2 BRC motifs bind RAD51-DNA filaments. **Proc Natl Acad Sci**, 102: (24): 8537-8542.

Geiss-Friedlander, R. and Melchior, F. (2007) Concepts in sumoylation: a decade on. **Nat Rev Mol Cell Biol**, 8: (12): 947-956.

Genschel, J., Littman, S. J., Drummond, J. T., et al. (1998) Isolation of MutS beta from human cells and comparison of the mismatch repair specificities of MutS beta and MutS alpha. **J Biol Chem**, 273: (31): 19895-19901.

Genschel, J. and Modrich, P. (2003) Mechanism of 5'-directed excision in human mismatch repair. **Mol Cell**, 12: (5): 1077-1086.

Gervais, V., Lamour, V., Jawhari, A., et al. (2004) TFIIH contains a PH domain involved in DNA nucleotide excision repair. **Nat Struct Mol Biol**, 11: (7): 616-622.

Giffin, W., Torrance, H., Rodda, D. J., et al. (1996) Sequence-specific DNA binding by Ku autoantigen and its effects on transcription. **Nature**, 380: (6571): 265-268.

Girard, P. M., Kysela, B., Harer, C. J., et al. (2004) Analysis of DNA ligase IV mutations found in LIG4 syndrome patients: the impact of two linked polymorphisms. **Hum Mol Genet**, 13: (20): 2369-2376.

Glozak, M. A., Sengupta, N., Zhang, X., et al. (2005) Acetylation and deacetylation of non-histone proteins. **Gene**, 363: 15-23.

Goedecke, W., Eijpe, M., Offenberg, H. H., et al. (1999) Mre11 and Ku70 interact in somatic cells, but are differentially expressed in early meiosis. **Nat Genet**, 23: (2): 194-198.

Goldberg, M., Stucki, M., Falck, J., et al. (2003) MDC1 is required for the intra-S-phase DNA damage checkpoint. **Nature**, 421: (6926): 952-956.

Goodarzi, A. A., Jonnalagadda, J. C., Douglas, P., et al. (2004) Autophosphorylation of ataxia-telangiectasia mutated is regulated by protein phosphatase 2A. **Embo J**, 23: (22): 4451-4461.

Goodarzi, A. A., Yu, Y., Riballo, E., et al. (2006) DNA-PK autophosphorylation facilitates Artemis endonuclease activity. **Embo J**, 25: (16): 3880-3889.

Gradia, S., Subramanian, D., Wilson, T., et al. (1999) hMSH2-hMSH6 forms a hydrolysis-independent sliding clamp on mismatched DNA. **Mol Cell**, 3: (2): 255-261.

Gu, J., Lu, H., Tippin, B., et al. (2007a) XRCC4:DNA ligase IV can ligate incompatible DNA ends and can ligate across gaps. **Embo J**, 26: (4): 1010-1023.

Gu, J., Lu, H., Tsai, A. G., et al. (2007b) Single-stranded DNA ligation and XLF-stimulated incompatible DNA end ligation by the XRCC4-DNA ligase IV complex: influence of terminal DNA sequence. **Nucleic Acids Res**, 35: (17): 5755-5762.

Gu, Y., Seidl, K. J., Rathbun, G. A., et al. (1997) Growth retardation and leaky SCID phenotype of Ku70-deficient mice. **Immunity**, 7: (5): 653-665.

Haglund, K. and Dikic, I. (2005) Ubiquitylation and cell signaling. **Embo J**, 24: (19): 3353-3359.

Hakem, R. (2008) DNA-damage repair; the good, the bad, and the ugly. **Embo J**, 27: (4): 589-605.

Halicka, H. D., Huang, X., Traganos, F., et al. (2005) Histone H2AX phosphorylation after cell irradiation with UV-B: relationship to cell cycle phase and induction of apoptosis. **Cell Cycle**, 4: (2): 339-345.

Hammarsten, O. and Chu, G. (1998) DNA-dependent protein kinase: DNA binding and activation in the absence of Ku. **Proc Natl Acad Sci**, 95: (2): 525-530.

Han, J., Hankinson, S. E., Ranu, H., et al. (2004) Polymorphisms in DNA double-strand break repair genes and breast cancer risk in the Nurses' Health Study. **Carcinogenesis**, 25: (2): 189-195.

Han, L. and Yu, K. (2008) Altered kinetics of nonhomologous end joining and class switch recombination in ligase IV-deficient B cells. **J Exp Med**, 205: (12): 2745-2753.

Hanakahi, L. A. (2007) 2-Step purification of the Ku DNA repair protein expressed in Escherichia coli. **Protein Expr Purif**, 52: (1): 139-145.

Hanawalt, P. C. (2002) Subpathways of nucleotide excision repair and their regulation. **Oncogene**, 21: (58): 8949-8956.

Harrison, J. C. and Haber, J. E. (2006) Surviving the breakup: the DNA damage checkpoint. **Annu Rev Genet**, 40: 209-235.

Hayden, M. S. and Ghosh, S. (2008) Shared principles in NF-kappaB signaling. **Cell**, 132: (3): 344-362.

Hazra, T. K., Das, A., Das, S., et al. (2007) Oxidative DNA damage repair in mammalian cells: a new perspective. **DNA Repair (Amst)**, 6: (4): 470-480.

Healey, C. S., Dunning, A. M., Dawn Teare, M., et al. (2000) A common variant in BRCA2 is associated with both breast cancer risk and prenatal viability. **Nat Genet**, 26: (3): 362-364.

Hegde, M. L., Hazra, T. K. and Mitra, S. (2008) Early steps in the DNA base excision/single-strand interruption repair pathway in mammalian cells. **Cell Res**, 18: (1): 27-47.

Helleday, T., Lo, J., Van Gent, D. C., et al. (2007) DNA double-strand break repair: From mechanistic understanding to cancer treatment. **DNA Repair**, 6: (7): 923-935.

Helleman, J., Van Staveren, I., Dinjens, W., et al. (2006) Mismatch repair and treatment resistance in ovarian cancer. **BMC Cancer**, 6: (1): 1-10.

Hentges, P., Ahnesorg, P., Pitcher, R. S., et al. (2006) Evolutionary and functional conservation of the DNA non-homologous end-joining protein, XLF/Cernunnos. **J Biol Chem**, 281: (49): 37517-37526.

Hershko, A. and Ciechanover, A. (1998) The ubiquitin system. **Annu Rev Biochem**, 67: 425-479.

Higashiura, M., Shimizu, Y., Tanimoto, M., et al. (1992) Immunolocalization of Ku-proteins (p80/p70): localization of p70 to nucleoli and periphery of both interphase nuclei and metaphase chromosomes. **Exp Cell Res**, 201: (2): 444-451.

Hirata, H., Hinoda, Y., Tanaka, Y., et al. (2007) Polymorphisms of DNA repair genes are risk factors for prostate cancer. **Eur J Cancer**, 43: (2): 231-237.

Hitomi, K., Iwai, S. and Tainer, J. A. (2007) The intricate structural chemistry of base excision repair machinery: implications for DNA damage recognition, removal, and repair. **DNA Repair (Amst)**, 6: (4): 410-428.

Hochegger, H., Dejsuphong, D., Fukushima, T., et al. (2006) Parp-1 protects homologous recombination from interference by Ku and Ligase IV in vertebrate cells. **Embo J**, 25: (6): 1305-1314.

Hoebeeck, J., Van Der Luijt, R., Poppe, B., et al. (2005) Rapid detection of VHL exon deletions using real-time quantitative PCR. **Lab Invest**, 85: (1): 24-33.

Hoege, C., Pfander, B., Moldovan, G. L., et al. (2002) RAD6-dependent DNA repair is linked to modification of PCNA by ubiquitin and SUMO. **Nature**, 419: (6903): 135-141.

Hoeijmakers, J. H. (2001) Genome maintenance mechanisms for preventing cancer. **Nature**, 411: (6835): 366-374.

Hopfner, K. P., Karcher, A., Craig, L., et al. (2001) Structural biochemistry and interaction architecture of the DNA double-strand break repair Mre11 nuclease and Rad50-ATPase. **Cell**, 105: (4): 473-485.

Hsu, H. L., Gilley, D., Blackburn, E. H., et al. (1999) Ku is associated with the telomere in mammals. **Proc Natl Acad Sci**, 96: (22): 12454-12458.

Huang, L., Grim, S., Smith, L. E., et al. (2004) Ionizing radiation induces delayed hyperrecombination in mammalian cells. **Mol Cell Biol**, 24: (11): 5060-5068.

Huang, X., Traganos, F. and Darzynkiewicz, Z. (2003) DNA damage induced by DNA topoisomerase I- and topoisomerase II- inhibitors detected by histone H2AX phosphorylation in relation to the cell cycle phase and apoptosis. **Cell Cycle**, 2: (6): 613-618.

Huertas, P. and Jackson, S. P. (2009) Human CtIP mediates cell cycle control of DNA end resection and double strand break repair. **J Biol Chem**, 284: (14): 9558-9565.

Huffman, J. L., Sundheim, O. and Tainer, J. A. (2005) DNA base damage recognition and removal: new twists and grooves. **Mutat Res**, 577: (1-2): 55-76.

Hull, J., Campino, S., Rowlands, K., et al. (2007) Identification of common genetic variation that modulates alternative splicing. **PLoS Genet**, 3: (6): e99.

Huq, M. and Wei, L. N. (2005) Post-translational modification of nuclear co-repressor receptor-interacting protein 140 by acetylation. **Mol Cell Proteomics**, 4: (7): 975-983.

Ikura, T., Tashiro, S., Kakino, A., et al. (2007) DNA damage-dependent acetylation and ubiquitination of H2AX enhances chromatin dynamics. **Mol Biol Cell**, 27: (20): 7028-7040.

Iliakis, G. (2009) Backup pathways of NHEJ in cells of higher eukaryotes: cell cycle dependence. **Radiother Oncol**, 92: (3): 310-315.

Iliakis, G., Blocher, D., Metzger, L., et al. (1991) Comparison of DNA double-strand break rejoining as measured by pulsed field gel electrophoresis, neutral sucrose gradient centrifugation and non-unwinding filter elution in irradiated plateau-phase CHO cells. **Int J Radiat Biol**, 59: (4): 927-939.

Izumi, T., Wiederhold, L. R., Roy, G., et al. (2003) Mammalian DNA base excision repair proteins: their interactions and role in repair of oxidative DNA damage. **Toxicology**, 193: (1-2): 43-65.

Jackson, S. P. and Bartek, J. (2009) The DNA-damage response in human biology and disease. **Nature**, 461: (7267): 1071-1078.

Janezic, S. A., Ziogas, A., Krumroy, L. M., et al. (1999) Germline BRCA1 alterations in a population-based series of ovarian cancer cases. **Hum Mol Genet**, 8: (5): 889-897.

Jascur, T. and Boland, C. R. (2006) Structure and function of the components of the human DNA mismatch repair system. **Int J Cancer**, 119: (9): 2030-2035.

Jayaram, S., Ketner, G., Adachi, N., et al. (2008) Loss of DNA ligase IV prevents recognition of DNA by double-strand break repair proteins XRCC4 and XLF. **Nucleic Acids Res**, 36: (18): 5773-5786.

Jazayeri, A., Falck, J., Lukas, C., et al. (2006) ATM- and cell cycle-dependent regulation of ATR in response to DNA double-strand breaks. **Nat Cell Biol**, 8: (1): 37-45.

Jeyakumar, M., Liu, X. F., Erdjument-Bromage, H., et al. (2007) Phosphorylation of thyroid hormone receptor-associated nuclear receptor corepressor holocomplex by the DNA-dependent protein kinase enhances its histone deacetylase activity. **J Biol Chem**, 282: (13): 9312-9322.

Jiang, X., Sun, Y., Chen, S., et al. (2006a) The FATC domains of PIKK proteins are functionally equivalent and participate in the Tip60-dependent activation of DNA-PKcs and ATM. **J. Biol. Chem.**, 281: 15741-15746.

Jiang, X., Sun, Y., Chen, S., et al. (2006b) The FATC domains of PIKK proteins are functionally equivalent and participate in the Tip60-dependent activation of DNA-PKcs and ATM. **J. Biol. Chem.**, 281: 15741-15746.

Jin, S. and Weaver, D. T. (1997) Double-strand break repair by Ku70 requires heterodimerization with Ku80 and DNA binding functions. **Embo J**, 16: (22): 6874-6885.

Jiricny, J. (2006) The multifaceted mismatch-repair system. **Nat Rev Mol Cell Biol**, 7: (5): 335-346.

Jun, S. H., Kim, T. G. and Ban, C. (2006) DNA mismatch repair system. Classical and fresh roles. **Febs J**, 273: (8): 1609-1619.

Kadyrov, F. A., Dzantiev, L., Constantin, N., et al. (2006) Endonucleolytic function of MutLalpha in human mismatch repair. **Cell**, 126: (2): 297-308.

Karimi-Busheri, F., Daly, G., Robins, P., et al. (1999) Molecular characterization of a human DNA kinase. **J Biol Chem**, 274: (34): 24187-24194.

Karow, J. K., Constantinou, A., Li, J. L., et al. (2000) The Bloom's syndrome gene product promotes branch migration of holliday junctions. **Proc Natl Acad Sci**, 97: (12): 6504-6508.

Kelley, M. R. and Parsons, S. H. (2001) Redox regulation of the DNA repair function of the human AP endonuclease Ape1/ref-1. **Antioxid Redox Signal**, 3: (4): 671-683.

Kennedy, R. D. and D'andrea, A. D. (2005) The Fanconi Anemia/BRCA pathway: new faces in the crowd. **Genes Dev**, 19: (24): 2925-2940.

Keogh, M. C., Kim, J. A., Downey, M., et al. (2006) A phosphatase complex that dephosphorylates [gamma]H2AX regulates DNA damage checkpoint recovery. **Nature**, 439: (7075): 497-501.

Kim, B., Ryu, K. S., Kim, H. J., et al. (2005a) Solution structure and backbone dynamics of the XPC-binding domain of the human DNA repair protein hHR23B. **Febs J**, 272: (10): 2467-2476.

Kim, J. S., Krasieva, T. B., Kurumizaka, H., et al. (2005b) Independent and sequential recruitment of NHEJ and HR factors to DNA damage sites in mammalian cells. **J Cell Biol**, 170: (3): 341-347.

Kim, M. S., Blake, M., Baek, J. H., et al. (2003) Inhibition of histone deacetylase increases cytotoxicity to anticancer drugs targeting DNA. **Cancer Res**, 63: (21): 7291-7300.

Klaunig, J. E., Kamendulis, L. M. and Hocevar, B. A. (2010) Oxidative stress and oxidative damage in carcinogenesis. **J Toxicol Pathol**, 38: (1): 96-109.

Klokov, D., Macphail, S. M., Banath, J. P., et al. (2006) Phosphorylated histone H2AX in relation to cell survival in tumor cells and xenografts exposed to single and fractionated doses of X-rays. **Radiother Oncol**, 80: (2): 223-229.

Koike, M., Awaji, T., Kataoka, M., et al. (1999a) Differential subcellular localization of DNA-dependent protein kinase components Ku and DNA-PKcs during mitosis. **J Cell Sci**, 112: 4031-4039.

Koike, M., Ikuta, T., Miyasaka, T., et al. (1999b) Ku80 can translocate to the nucleus independent of the translocation of Ku70 using its own nuclear localization signal. **Oncogene**, 18: (52): 7495-7505.

Kolas, N. K., Chapman, J. R., Nakada, S., et al. (2007) Orchestration of the DNA-damage response by the RNF8 ubiquitin ligase. **Science**, 318: (5856): 1637-1640.

Kouzarides, T. (1999) Histone acetylases and deacetylases in cell proliferation. **Curr Opin Genet Dev**, 9: (1): 40-48.

Kouzarides, T. (2007) Chromatin modifications and their function. **Cell**, 128: (4): 693-705.

Kreklau, E. L., Limp-Foster, M., Liu, N., et al. (2001) A novel fluorometric oligonucleotide assay to measure O 6-methylguanine DNA methyltransferase, methylpurine DNA glycosylase, 8-oxoguanine DNA glycosylase and abasic endonuclease activities: DNA repair status in human breast carcinoma cells overexpressing methylpurine DNA glycosylase. **Nucleic Acids Res**, 29: (12): 2558-2566.

Krokan, H., Kavli, B. and Slupphaug, G. (2004) Novel aspects of macromolecular repair and relationship to human disease. **J Mol Med**, 82: (5): 280-297.

Krokan, H. E., Standal, R. and Slupphaug, G. (1997) DNA glycosylases in the base excision repair of DNA. **Biochem J**, 325 (Pt 1): 1-16.

Kunkel, T. A. and Erie, D. A. (2005) DNA mismatch repair. **Annu Rev Biochem**, 74: 681-710.

Kurash, J. K., Lei, H., Shen, Q., et al. (2008) Methylation of p53 by Set7/9 mediates p53 acetylation and activity in vivo. **Mol Cell**, 29: (3): 392-400.

Kuschel, B., Auranen, A., Mcbride, S., et al. (2002) Variants in DNA double-strand break repair genes and breast cancer susceptibility. **Hum Mol Genet**, 11: (12): 1399-1407.

Kusumoto, R., Masutani, C., Sugasawa, K., et al. (2001) Diversity of the damage recognition step in the global genomic nucleotide excision repair in vitro. **Mutat Res**, 485: (3): 219-227.

Kysela, B., Doherty, A. J., Chovanec, M., et al. (2003) Ku stimulation of DNA ligase IV-dependent ligation requires inward movement along the DNA molecule. **J Biol Chem**, 278: (25): 22466-22474.

Landi, S., Gemignani, F., Canzian, F., et al. (2006) DNA repair and cell cycle control genes and the risk of young-onset lung cancer. **Cancer Res**, 66: (22): 11062-11069.

Lavin, M. F. (2008) Ataxia-telangiectasia: from a rare disorder to a paradigm for cell signalling and cancer. **Nat Rev Mol Cell Biol**, 9: (10): 759-769.

Leach, C. A. and Michael, W. M. (2005) Ubiquitin/SUMO modification of PCNA promotes replication fork progression in Xenopus laevis egg extracts. **J Cell Biol**, 171: (6): 947-954.

Lee, B. I. and Wilson, D. M., 3rd (1999) The RAD2 domain of human exonuclease 1 exhibits 5' to 3' exonuclease and flap structure-specific endonuclease activities. **J Biol Chem**, 274: (53): 37763-37769.

Lee, J. H., Park, C. J., Arunkumar, A. I., et al. (2003) NMR study on the interaction between RPA and DNA decamer containing cis-syn cyclobutane pyrimidine dimer in the presence of XPA: implication for damage verification and strand-specific dual incision in nucleotide excision repair. **Nucleic Acids Res**, 31: (16): 4747-4754.

Lee, J. H. and Paull, T. T. (2005) ATM activation by DNA double-strand breaks through the Mre11-Rad50-Nbs1 complex. **Science**, 308: (5721): 551-554.

Lee, K. B., Wang, D., Lippard, S. J., et al. (2002) Transcription-coupled and DNA damage-dependent ubiquitination of RNA polymerase II in vitro. **Proc Natl Acad Sci** 99: (7): 4239-4244.

Lehman, J. A., Hoelz, D. J. and Turchi, J. J. (2008) DNA-dependent conformational changes in the Ku heterodimer. **Biochemistry**, 47: (15): 4359-4368.

Lehmann, A. R. (2006) Translesion synthesis in mammalian cells. **Exp Cell Res**, 312: (14): 2673-2676.

Levy, N., Martz, A., Bresson, A., et al. (2006) XRCC1 is phosphorylated by DNA-dependent protein kinase in response to DNA damage. **Nucleic Acids Res**, 34: (1): 32-41.

Li, A., Xue, Y., Jin, C., et al. (2006) Prediction of N epsilon-acetylation on internal lysines implemented in Bayesian Discriminant Method. **Biochem Biophys Res Communications**, 350: (4): 818-824.

Li, G. C., Yang, S. H., Kim, D., et al. (1995) Suppression of heat-induced hsp70 expression by the 70-kDa subunit of the human Ku autoantigen. **Proc Natl Acad Sci** 92: (10): 4512-4516.

Li, M., Luo, J., Brooks, C. L., et al. (2002) Acetylation of p53 inhibits its ubiquitination by Mdm2. **J Bio Chem**, 277: (52): 50607-50611.

Li, S., Li, H., Li, M., Shyr, Y., Xie, L., Li, Y. (2009) Improved prediction of lysine acetylation by support vector machines. **Protein Pept Lett**, 16: (8): 977-983.

Li, Y., Chirgadze, D. Y., Bolanos-Garcia, V. M., et al. (2008) Crystal structure of human XLF/Cernunnos reveals unexpected differences from XRCC4 with implications for NHEJ. **EMBO J**, 27: (1): 290-300.

Liang, L., Deng, L., Nguyen, S. C., et al. (2008) Human DNA ligases I and III, but not ligase IV, are required for microhomology-mediated end joining of DNA double-strand breaks. **Nucleic Acids Res**, 36: (10): 3297-3310.

Lin, H. Y., Chen, C. S., Lin, S. P., et al. (2006) Targeting histone deacetylase in cancer therapy. **Med Res Rev**, 26: (4): 397-413.

Liu, E. S. and Lee, A. S. (1991) Common sets of nuclear factors binding to the conserved promoter sequence motif of two coordinately regulated ER protein genes, GRP78 and GRP94. **Nucleic Acids Res**, 19: (19): 5425-5431.

Liu, Y., Masson, J. Y., Shah, R., et al. (2004) RAD51C is required for Holliday junction processing in mammalian cells. **Science**, 303: (5655): 243-246.

Lowndes, N. F. and Toh, G. W. L. (2005) DNA repair: the importance of phosphorylating histone H2AX. **Curr Biol**, 15: (3): 99-102.

Lu, C., Zhu, F., Cho, Y. Y., et al. (2006) Cell apoptosis: requirement of H2AX in DNA ladder formation, but not for the activation of caspase-3. **Mol Cell**, 23: (1): 121-132.

Lu, H., Pannicke, U., Schwarz, K., et al. (2007) Length-dependent binding of human XLF to DNA and stimulation of XRCC4.DNA ligase IV activity. **J Biol Chem**, 282: (15): 11155-11162.

Lukas, C., Melander, F., Stucki, M., et al. (2004) Mdc1 couples DNA double-strand break recognition by Nbs1 with its H2AX-dependent chromatin retention. **Embo J**, 23: (13): 2674-2683.

Lyndaker, A. M. and Alani, E. (2009) A tale of tails: insights into the coordination of 3' end processing during homologous recombination. **Bioessays**, 31: (3): 315-321.

Ma, J. L., Kim, E. M., Haber, J. E., et al. (2003) Yeast Mre11 and Rad1 proteins define a Ku-independent mechanism to repair double-strand breaks lacking overlapping end sequences. **Mol Cell Biol**, 23: (23): 8820-8828.

Ma, Y., Lu, H., Tippin, B., et al. (2004) A biochemically defined system for mammalian nonhomologous DNA end joining. **Mol Cell**, 16: (5): 701-713.

Ma, Y., Schwarz, K. and Lieber, M. R. (2005) The Artemis:DNA-PKcs endonuclease cleaves DNA loops, flaps, and gaps. **DNA Repair (Amst)**, 4: (7): 845-851.

Madhusudan, S. and Middleton, M. R. (2005) The emerging role of DNA repair proteins as predictive, prognostic and therapeutic targets in cancer. **Cancer Treatment Rev**, 31: (8): 603-617.

Mailand, N., Bekker-Jensen, S., Faustrup, H., et al. (2007) RNF8 ubiquitylates histones at DNA double-strand breaks and promotes assembly of repair proteins. **Cell**, 131: (5): 887-900.

Maizels, N. (2005) Immunoglobulin gene diversification. **Annu Rev Genet**, 39: 23-46.

Mallette, F. A., Gaumont-Leclerc, M. F. and Ferbeyre, G. (2007) The DNA damage signaling pathway is a critical mediator of oncogene-induced senescence. **Genes Dev**, 21: (1): 43-48.

Mansour, W. Y., Schumacher, S., Rosskopf, R., et al. (2008) Hierarchy of nonhomologous end-joining, single-strand annealing and gene conversion at site-directed DNA double-strand breaks. **Nucleic Acids Res**, 36: (12): 4088-4098.

Mao, Z., Bozzella, M., Seluanov, A., et al. (2008) Comparison of nonhomologous end joining and homologous recombination in human cells. **DNA Repair (Amst)**, 7: (10): 1765-1771.

Mari, P. O., Florea, B. I., Persengiev, S. P., et al. (2006) Dynamic assembly of end-joining complexes requires interaction between Ku70/80 and XRCC4. **Proc Natl Acad Sci**, 103: (49): 18597-18602.

Martin, G. M., Austad, S. N. and Johnson, T. E. (1996) Genetic analysis of ageing: role of oxidative damage and environmental stresses. **Nat Genet**, 13: (1): 25-34.

Martin, O. A., Pilch, D. R., Redon, C., et al. (2003) Involvement of H2AX in the DNA Damage and Repair Response. **Cancer Biol Ther**, 2: (3): 231-233.

Matsumoto, Y., Kim, K. and Bogenhagen, D. F. (1994) Proliferating cell nuclear antigen-dependent abasic site repair in Xenopus laevis oocytes: an alternative pathway of base excision DNA repair. **Mol Cell Biol**, 14: (9): 6187-6197.

Matsuoka, S., Ballif, B. A., Smogorzewska, A., et al. (2007) ATM and ATR substrate analysis reveals extensive protein networks responsive to DNA damage. **Science**, 316: (5828): 1160-1166.

Mcculloch, S. D., Gu, L. and Li, G. M. (2003) Bi-directional processing of DNA loops by mismatch repair-dependent and -independent pathways in human cells. **J Biol Chem**, 278: (6): 3891-3896.

Mckinnon, P. J. and Caldecott, K. W. (2007) DNA strand break repair and human genetic disease. **Annu Rev Genomics Hum Genet**, 8: 37-55.

Meek, K., Dang, V. and Lees-Miller, S. P. (2009) DNA-PK: the means to justify the ends? **Adv Immunol**, 99: 33-58.

Merkle, D., Douglas, P., Moorhead, G. B., et al. (2002) The DNA-dependent protein kinase interacts with DNA to form a protein-DNA complex that is disrupted by phosphorylation. **Biochemistry**, 41: (42): 12706-12714.

Metzger, L. and Iliakis, G. (1991) Kinetics of DNA double-strand break repair throughout the cell cycle as assayed by pulsed field gel electrophoresis in CHO cells. **Int J Radiat Biol**, 59: (6): 1325-1339.

Mills, K. D., Ferguson, D. O., Essers, J., et al. (2004) Rad54 and DNA Ligase IV cooperate to maintain mammalian chromatid stability. **Genes Dev**, 18: (11): 1283-1292.

Mimitou, E. P. and Symington, L. S. (2009) DNA end resection: many nucleases make light work. **DNA Repair (Amst)**, 8: (9): 983-995.

Mimori, T., Akizuki, M., Yamagata, H., et al. (1981) Characterization of a high molecular weight acidic nuclear protein recognized by autoantibodies in sera from patients with polymyositis-scleroderma overlap. **J Clin Invest**, 68: (3): 611-620.

Mo, X. and Dynan, W. S. (2002) Subnuclear localization of Ku protein: functional association with RNA polymerase II elongation sites. **Mol Cell Biol**, 22: (22): 8088-8099.

Modrich, P. (2006) Mechanisms in eukaryotic mismatch repair. **J Biol Chem**, 281: (41): 30305-30309.

Moreno-Herrero, F., De Jager, M., Dekker, N. H., et al. (2005) Mesoscale conformational changes in the DNA-repair complex Rad50/Mre11/Nbs1 upon binding DNA. **Nature**, 437: (7057): 440-443.

Morris, J. R. (2010) SUMO in the mammalian response to DNA damage. **Biochem Soc Trans**, 38: (1): 92-97.

Morris, J. R., Boutell, C., Keppler, M., et al. (2009) The SUMO modification pathway is involved in the BRCA1 response to genotoxic stress. **Nature**, 462: (7275): 886-890.

Morris, J. R., Pangon, L., Boutell, C., et al. (2006) Genetic analysis of BRCA1 ubiquitin ligase activity and its relationship to breast cancer susceptibility. **Hum Mol Genet**, 15: (4): 599-606.

Munshi, A., Kurland, J. F., Nishikawa, T., et al. (2005) Histone deacetylase inhibitors radiosensitize human melanoma cells by suppressing DNA repair activity. **Clin Cancer Res**, 11: (13): 4912-4922.

Myung, K., He, D. M., Lee, S. E., et al. (1997) KARP-1: a novel leucine zipper protein expressed from the Ku86 autoantigen locus is implicated in the control of DNA-dependent protein kinase activity. **Embo J**, 16: (11): 3172-3184.

Nakada, S., Chen, G. I., Gingras, A. C., et al. (2008) PP4 is a gamma H2AX phosphatase required for recovery from the DNA damage checkpoint. **Embo Rep**, 9: (10): 1019-1026.

Nakamura, J. and Swenberg, J. A. (1999) Endogenous apurinic/apyrimidinic sites in genomic DNA of mammalian tissues. **Cancer Res**, 59: (11): 2522-2526.

Neal, J. A. and Meek, K. (2011) Choosing the right path: Does DNA-PK help make the decision? **Mutat Res**, 711: (1-2): 73-86.

Nevaldine, B., Longo, J. A. and Hahn, P. J. (1997) The scid defect results in much slower repair of DNA double-strand breaks but not high levels of residual breaks. **Radiat Res**, 147: (5): 535-540.

New, J. H., Sugiyama, T., Zaitseva, E., et al. (1998) Rad52 protein stimulates DNA strand exchange by Rad51 and replication protein A. **Nature**, 391: (6665): 407-410.

Nick Mcelhinny, S. A., Havener, J. M., Garcia-Diaz, M., et al. (2005) A gradient of template dependence defines distinct biological roles for family X polymerases in nonhomologous end joining. **Mol Cell**, 19: (3): 357-366.

Nick Mcelhinny, S. A., Snowden, C. M., Mccarville, J., et al. (2000) Ku recruits the XRCC4-ligase IV complex to DNA ends. **Mol Cell Biol**, 20: (9): 2996-3003.

Nightingale, K. P., Wellinger, R. E., Sogo, J. M., et al. (1998) Histone acetylation facilitates RNA polymerase II transcription of the Drosophila hsp26 gene in chromatin. **Embo J**, 17: (10): 2865-2876.

Ochem, A. E., Skopac, D., Costa, M., et al. (1997) Functional properties of the separate subunits of human DNA helicase II/Ku autoantigen. **J Biol Chem**, 272: (47): 29919-29926.

Okano, S., Lan, L., Caldecott, K. W., et al. (2003) Spatial and temporal cellular responses to single-strand breaks in human cells. **Mol Cell Biol**, 23: (11): 3974-3981.

Ouyang, H., Nussenzweig, A., Kurimasa, A., et al. (1997) Ku70 is required for DNA repair but not for T cell antigen receptor gene recombination In vivo. **J Exp Med**, 186: (6): 921-929.

Pace, P., Mosedale, G., Hodskinson, M. R., et al. (2010) Ku70 corrupts DNA repair in the absence of the Fanconi anemia pathway. **Science**, 329: (5988): 219-223.

Pakakasama, S., Sirirat, T., Kanchanachumpol, S., et al. (2007) Genetic polymorphisms and haplotypes of DNA repair genes in childhood acute lymphoblastic leukemia. **Pediatric Blood & Cancer**, 48: (1): 16-20.

Panier, S. and Durocher, D. (2009) Regulatory ubiquitylation in response to DNA double-strand breaks. **DNA Repair (Amst)**, 8: (4): 436-443.

Park, C. J. and Choi, B. S. (2006) The protein shuffle. Sequential interactions among components of the human nucleotide excision repair pathway. **Febs J**, 273: (8): 1600-1608.

Pastinen, T., Sladek, R., Gurd, S., et al. (2004) A survey of genetic and epigenetic variation affecting human gene expression. **Physiol Genomics**, 16: (2): 184-193.

Peddi, P., Loftin, C. W., Dickey, J. S., et al. (2010) DNA-PKcs deficiency leads to persistence of oxidatively induced clustered DNA lesions in human tumor cells. **Free Radic Biol Med**, 48: (10): 1435-1443.

Pegg, A. E. (2000) Repair of O(6)-alkylguanine by alkyltransferases. **Mutat Res**, 462: (2-3): 83-100.

Pfeifer, G. P., You, Y. H. and Besaratinia, A. (2005) Mutations induced by ultraviolet light. **Mutat Res**, 571: (1-2): 19-31.

Pfeiffer, P., Goedecke, W., Kuhfittig-Kulle, S., et al. (2004) Pathways of DNA double-strand break repair and their impact on the prevention and formation of chromosomal aberrations. **Cytogenet Genome Res**, 104: (1-4): 7-13.

Pinato, S., Scandiuzzi, C., Arnaudo, N., et al. (2009) RNF168, a new RING finger, MIU-containing protein that modifies chromatin by ubiquitination of histones H2A and H2AX. **BMC Mol Biol**, 10: 55.

Plosky, B. S. and Woodgate, R. (2004) Switching from high-fidelity replicases to low-fidelity lesion-bypass polymerases. **Curr Opin Genet Dev**, 14: (2): 113-119.

Plumb, M. A., Smith, G. C., Cunniffe, S. M., et al. (1999) DNA-PK activation by ionizing radiation-induced DNA single-strand breaks. **Int J Radiat Biol**, 75: (5): 553-561.

Polanowska, J., Martin, J. S., Garcia-Muse, T., et al. (2006) A conserved pathway to activate BRCA1-dependent ubiquitylation at DNA damage sites. **Embo J**, 25: (10): 2178-2188.

Polesskaya, A. and Harel-Bellan, A. (2001) Acetylation of MyoD by p300 requires more than its histone acetyltransferase domain. **J Biol Chem**, 276: (48): 44502-44503.

Polevoda, B. and Sherman, F. (2000) Nalpha -terminal acetylation of eukaryotic proteins. **J Biol Chem**, 275: (47): 36479-36482.

Pommier, Y., Redon, C., Rao, V. A., et al. (2003) Repair of and checkpoint response to topoisomerase I-mediated DNA damage. **Mutat Res**, 532: (1-2): 173-203.

Postow, L., Ghenoiu, C., Woo, E. M., et al. (2008) Ku80 removal from DNA through double strand break-induced ubiquitylation. **JCB**, 182: (3): 467-479.

Prabhakar, B. S., Allaway, G. P., Srinivasappa, J., et al. (1990) Cell surface expression of the 70-kD component of Ku, a DNA-binding nuclear autoantigen. **J Clin Invest**, 86: (4): 1301-1305.

Rafii, S., O'regan, P., Xinarianos, G., et al. (2002) A potential role for the XRCC2 R188H polymorphic site in DNA-damage repair and breast cancer. **Hum Mol Genet**, 11: (12): 1433-1438.

Rahal, E. A., Henricksen, L. A., Li, Y., et al. (2010) ATM regulates Mre11-dependent DNA end-degradation and microhomology-mediated end joining. **Cell Cycle**, 9: (14): 2866-2877.

Rass, E., Grabarz, A., Plo, I., et al. (2009) Role of Mre11 in chromosomal nonhomologous end joining in mammalian cells. **Nat Struct Mol Biol**, 16: (8): 819-824.

Ratnasinghe, D., Yao, S.-X., Tangrea, J. A., et al. (2001) Polymorphisms of the DNA repair gene XRCC1 and lung cancer risk. **Cancer Epidemiology, Biomarkers and Prevention**, 10: (2): 119-123.

Ravanat, J. L., Douki, T. and Cadet, J. (2001) Direct and indirect effects of UV radiation on DNA and its components. **J Photochem Photobiol B** 63: (1-3): 88-102.

Raynard, S., Bussen, W. and Sung, P. (2006) A double Holliday junction dissolvasome comprising BLM, topoisomerase IIIalpha, and BLAP75. **J Biol Chem**, 281: (20): 13861-13864.

Reddy, Y. V. R., Ding, Q., Lees-Miller, S. P., et al. (2004) Non-homologous end joining requires that the DNA-PK complex undergo an autophosphorylation-dependent rearrangement at DNA ends. **J Biol Chem**, 279: (38): 39408-39413.

Reliene, R., Bishop, A. J., Li, G., et al. (2004) Ku86 deficiency leads to reduced intrachromosomal homologous recombination in vivo in mice. **DNA Repair (Amst)**, 3: (2): 103-111.

Riballo, E., Doherty, A. J., Dai, Y., et al. (2001) Cellular and biochemical impact of a mutation in DNA ligase IV conferring clinical radiosensitivity. **J Biol Chem**, 276: (33): 31124-31132.

Riballo, E., Kuhne, M., Rief, N., et al. (2004) A pathway of double-strand break rejoining dependent upon ATM, Artemis, and proteins locating to gamma-H2AX foci. **Mol Cell**, 16: (5): 715-724.

Riedl, T., Hanaoka, F. and Egly, J. M. (2003) The comings and goings of nucleotide excision repair factors on damaged DNA. **Embo J**, 22: (19): 5293-5303.

Rivera-Calzada, A., Spagnolo, L., Pearl, L. H., et al. (2007) Structural model of full-length human Ku70-Ku80 heterodimer and its recognition of DNA and DNA-PKcs. **EMBO Rep**, 8: (1): 56-62.

Roberts, S. A., Strande, N., Burkhalter, M. D., et al. (2010) Ku is a 5'-dRP/AP lyase that excises nucleotide damage near broken ends. **Nature**, 464: (7292): 1214-1217.

Rodriguez, R., Gagou, M. E. and Meuth, M. (2008) Apoptosis induced by replication inhibitors in Chk1-depleted cells is dependent upon the helicase cofactor Cdc45. **Cell Death Differ**, 15: (5): 889-898.

Rogakou, E. P., Nieves-Neira, W., Boon, C., et al. (2000) Initiation of DNA fragmentation during apoptosis induces phosphorylation of H2AX histone at serine 139. **J Biol Chem**, 275: (13): 9390-9395.

Rogakou, E. P., Pilch, D. R., Orr, A. H., et al. (1998) DNA double-stranded breaks induce histone H2AX phosphorylation on serine 139. **J Biol Chem**, 273: (10): 5858-5868.

Rosidi, B., Wang, M., Wu, W., et al. (2008) Histone H1 functions as a stimulatory factor in backup pathways of NHEJ. **Nucleic Acids Res**, 36: (5): 1610-1623.

Roth, D. B., Porter, T. N. and Wilson, J. H. (1985) Mechanisms of nonhomologous recombination in mammalian cells. **Mol Cell Biol**, 5: (10): 2599-2607.

Ruthenburg, A. J., Li, H., Patel, D. J., et al. (2007) Multivalent engagement of chromatin modifications by linked binding modules. **Nat Rev Mol Cell Biol**, 8: (12): 983-994.

Sampath, S. C., Marazzi, I., Yap, K. L., et al. (2007) Methylation of a histone mimic within the histone methyltransferase G9a regulates protein complex assembly. **Mol Cell**, 27: (4): 596-608.

Samper, E., Goytisolo, F. A., Slijepcevic, P., et al. (2000) Mammalian Ku86 protein prevents telomeric fusions independently of the length of TTAGGG repeats and the G-strand overhang. **Embo Rep**, 1: (3): 244-252.

Sancar, A. (2003) Structure and function of DNA photolyase and cryptochrome blue-light photoreceptors. **Chem Rev**, 103: (6): 2203-2238.

Sawada, M., Hayes, P. and Matsuyama, S. (2003a) Cytoprotective membrane-permeable peptides designed from the Bax-binding domain of Ku70. **Nat Cell Biol**, 5: (4): 352-357.

Sawada, M., Sun, W., Hayes, P., et al. (2003b) Ku70 suppresses the apoptotic translocation of Bax to mitochondria. **Nat Cell Biol**, 5: (4): 320-329.

Schreiber, S. L. and Bernstein, B. E. (2002) Signaling network model of chromatin. **Cell**, 111: (6): 771-778.

Schreiber, V., Dantzer, F., Ame, J. C., et al. (2006) Poly(ADP-ribose): novel functions for an old molecule. **Nat Rev Mol Cell Biol**, 7: (7): 517-528.

Sekiguchi, M., Nakabeppu, Y., Sakumi, K., et al. (1996) DNA-repair methyltransferase as a molecular device for preventing mutation and cancer. **J Cancer Res Clin Oncol**, 122: (4): 199-206.

Serre, D., Gurd, S., Ge, B., et al. (2008) Differential allelic expression in the human genome: a robust approach to identify genetic and epigenetic *cis*-acting mechanisms regulating gene expression. **PLoS Genet**, 4: (2): e1000006.

Shack, S., Miller, A., Liu, L., et al. (1996) Vulnerability of multidrug-resistant tumor cells to the aromatic fatty acids phenylacetate and phenylbutyrate. **Clin Cancer Res**, 2: (5): 865-872.

Shao, G., Lilli, D. R., Patterson-Fortin, J., et al. (2009) The Rap80-BRCC36 de-ubiquitinating enzyme complex antagonizes RNF8-Ubc13-dependent ubiquitination events at DNA double strand breaks. **Proc Natl Acad Sci**, 106: (9): 3166-3171.

Shiloh, Y. (2003) ATM and related protein kinases: safeguarding genome integrity. **Nat Rev Cancer**, 3: (3): 155-168.

Shin, D. S., Chahwan, C., Huffman, J. L., et al. (2004) Structure and function of the double-strand break repair machinery. **DNA Repair (Amst)**, 3: (8-9): 863-873.

Shinohara, A. and Ogawa, T. (1998) Stimulation by Rad52 of yeast Rad51-mediated recombination. **Nature**, 391: (6665): 404-407.

Shreeram, S., Demidov, O. N., Hee, W. K., et al. (2006) Wip1 phosphatase modulates ATM-dependent signaling pathways. **Mol Cell**, 23: (5): 757-764.

Shrivastav, M., De Haro, L. P. and Nickoloff, J. A. (2008) Regulation of DNA double-strand break repair pathway choice. **Cell Res**, 18: (1): 134-147.

Sibanda, B. L., Critchlow, S. E., Begun, J., et al. (2001) Crystal structure of an Xrcc4-DNA ligase IV complex. **Nat Struct Mol Biol**, 8: (12): 1015-1019.

Singleton, B. K., Priestley, A., Steingrimsdottir, H., et al. (1997) Molecular and biochemical characterization of xrs mutants defective in Ku80. **Mol Cell Biol**, 17: (3): 1264-1273.

Smith, G. C. and Jackson, S. P. (1999) The DNA-dependent protein kinase. **Genes Dev**, 13: (8): 916-934.

Smith, S. A., Richards, W. E., Caito, K., et al. (2001) BRCA1 germline mutations and polymorphisms in a clinic-based series of ovarian cancer cases: a gynecologic oncology group study. **Gynecol Oncol**, 83: (3): 586-592.

Solier, S., Sordet, O., Kohn, K. W., et al. (2009) Death receptor-induced activation of the Chk2- and histone H2AX-associated DNA damage response pathways. **Mol Cell Biol**, 29: (1): 68-82.

Sonoda, E., Hochegger, H., Saberi, A., et al. (2006) Differential usage of non-homologous end-joining and homologous recombination in double strand break repair. **DNA Repair (Amst)**, 5: (9-10): 1021-1029.

Soulas-Sprauel, P., Le Guyader, G., Rivera-Munoz, P., et al. (2007) Role for DNA repair factor XRCC4 in immunoglobulin class switch recombination. **J Exp Med**, 204: (7): 1717-1727.

Spange, S., Wagner, T., Heinzel, T., et al. (2009) Acetylation of non-histone proteins modulates cellular signalling at multiple levels. **Int J Biochem Cell Biol**, 41: (1): 185-198.

Stallings, R. L., Yoon, K., Kwek, S., et al. (2007) The origin of chromosome imbalances in neuroblastoma. **Cancer Genet Cytogenet**, 176: (1): 28-34.

Stern, M. C., Lin, J., Figueroa, J. D., et al. (2009) Polymorphisms in DNA repair genes, smoking, and bladder cancer risk: findings from the international consortium of bladder cancer. **Cancer Res**, 69: (17): 6857-6864.

Stern, M. C., Umbach, D. M., Van Gils, C. H., et al. (2001) DNA repair gene XRCC1 polymorphisms, smoking, and bladder cancer risk. **Cancer Epidemiology, Biomarkers and Prevention**, 10: (2): 125-131.

Stewart, G. S., Panier, S., Townsend, K., et al. (2009) The RIDDLE syndrome protein mediates a ubiquitin-dependent signaling cascade at sites of DNA damage. **Cell**, 136: (3): 420-434.

Stewart, G. S., Wang, B., Bignell, C. R., et al. (2003) MDC1 is a mediator of the mammalian DNA damage checkpoint. **Nature**, 421: (6926): 961-966.

Stracker, T. H., Theunissen, J. W., Morales, M., et al. (2004) The Mre11 complex and the metabolism of chromosome breaks: the importance of communicating and holding things together. **DNA Repair (Amst)**, 3: (8-9): 845-854.

Stucki, M., Clapperton, J. A., Mohammad, D., et al. (2005) MDC1 directly binds phosphorylated histone H2AX to regulate cellular responses to DNA double-strand breaks. **Cell**, 123: (7): 1213-1226.

Sturgis, E. M., Castillo, E. J., Li, L., et al. (1999) Polymorphisms of DNA repair gene XRCC1 in squamous cell carcinoma of the head and neck. **Carcinogenesis**, 20: (11): 2125-2129.

Subramanian, C., Opipari, A. W., Jr., Bian, X., et al. (2005) Ku70 acetylation mediates neuroblastoma cell death induced by histone deacetylase inhibitors. **Proc Natl Acad Sci**, 102: (13): 4842-4847.

Sugasawa, K., Okuda, Y., Saijo, M., et al. (2005) UV-induced ubiquitylation of XPC protein mediated by UV-DDB-ubiquitin ligase complex. **Cell**, 121: (3): 387-400.

Sun, Y., Jiang, X., Chen, S., et al. (2005) A role for the Tip60 histone acetyltransferase in the acetylation and activation of ATM. **Proc Natl Acad Sci**, 102: (37): 13182-13187.

Sun, Y., Jiang, X. and Price, B. D. (2010) Tip60: connecting chromatin to DNA damage signaling. **Cell Cycle**, 9: (5): 930-936.

Sun, Y., Jiang, X., Xu, Y., et al. (2009) Histone H3 methylation links DNA damage detection to activation of the tumour suppressor Tip60. **Nat Cell Biol**, 11: (11): 1376-1382.

Sung, J. S. and Demple, B. (2006) Roles of base excision repair subpathways in correcting oxidized abasic sites in DNA. **Febs J**, 273: (8): 1620-1629.

Taccioli, G. E., Gottlieb, T. M., Blunt, T., et al. (1994) Ku80: product of the XRCC5 gene and its role in DNA repair and V(D)J recombination. **Science**, 265: (5177): 1442-1445.

Takata, M., Sasaki, M. S., Sonoda, E., et al. (1998) Homologous recombination and non-homologous end-joining pathways of DNA double-strand break repair have overlapping roles in the maintenance of chromosomal integrity in vertebrate cells. **Embo J**, 17: (18): 5497-5508.

Tamburini, B. A. and Tyler, J. K. (2005) Localized histone acetylation and deacetylation triggered by the homologous recombination pathway of double-strand DNA repair. **Mol Cell Biol**, 25: (12): 4903-4913.

Taniguchi, T., Garcia-Higuera, I., Andreassen, P. R., et al. (2002) S-phase specific interaction of the Fanconi anemia protein, FANCD2, with BRCA1 and RAD51. **Blood**, 100: (7): 2414-2420.

Tauchi, H., Matsuura, S., Kobayashi, J., et al. (2002) Nijmegen breakage syndrome gene, NBS1, and molecular links to factors for genome stability. **Oncogene**, 21: (58): 8967-8980.

Tell, G., Damante, G., Caldwell, D., et al. (2005) The intracellular localization of APE1/Ref-1: more than a passive phenomenon? **Antioxid Redox Signal**, 7: (3-4): 367-384.

Teoh, G., Urashima, M., Greenfield, E. A., et al. (1998) The 86-kD subunit of Ku autoantigen mediates homotypic and heterotypic adhesion of multiple myeloma cells. **J Clin Invest**, 101: (6): 1379-1388.

Tsai, C. J., Kim, S. A. and Chu, G. (2007) Cernunnos/XLF promotes the ligation of mismatched and noncohesive DNA ends. **Proc Natl Acad Sci**, 104: (19): 7851-7856.

Turner, B. M. (2007) Defining an epigenetic code. **Nat Cell Biol**, 9: (1): 2-6.

Tuteja, R. and Tuteja, N. (2000) Ku autoantigen: a multifunctional DNA-binding protein. **Crit Rev Biochem Mol Biol**, 35: (1): 1-33.

Valerie, K. and Povirk, L. F. (2003) Regulation and mechanisms of mammalian double-strand break repair. **Oncogene**, 22: (37): 5792-5812.

Vernole, P., Pepponi, R. and D'atri, S. (2003) Role of mismatch repair in the induction of chromosomal aberrations and sister chromatid exchanges in cells treated with different chemotherapeutic agents. **Cancer Chemother Pharmacol**, 52: (3): 185-192.

Vidali, G., Gershey, E. L. and Allfrey, V. G. (1968) Chemical studies of histone acetylation. The distribution of epsilon-N-acetyllysine in calf thymus histones. **J Biol Chem**, 243: (24): 6361-6366.

Virsik-Kopp, P., Rave-Frank, M., Hofman-Huther, H., et al. (2003) Role of DNA-PK in the process of aberration formation as studied in irradiated human glioblastoma cell lines M059K and M059J. **Int J Radiat Biol**, 79: (1): 61-68.

Vo, A. T., Zhu, F., Wu, X., et al. (2005) hMRE11 deficiency leads to microsatellite instability and defective DNA mismatch repair. **Embo Rep**, 6: (5): 438-444.

Vogel, U., Moller, P., Dragsted, L., et al. (2002) Inter-individual variation, seasonal variation and close correlation of OGG1 and ERCC1 mRNA levels in full blood from healthy volunteers. **Carcinogenesis**, 23: (9): 1505-1509.

Walker, J. R., Corpina, R. A. and Goldberg, J. (2001) Structure of the Ku heterodimer bound to DNA and its implications for double-strand break repair. **Nature**, 412: (6847): 607-614.

Walter, W., Clynes, D., Tang, Y., et al. (2008) 14-3-3 interaction with histone H3 involves a dual modification pattern of phosphoacetylation. **Mol Cell Biol**, 28: (8): 2840-2849.

Wang, B. and Elledge, S. J. (2007) Ubc13/Rnf8 ubiquitin ligases control foci formation of the Rap80/Abraxas/Brca1/Brcc36 complex in response to DNA damage. **Proc Natl Acad Sci**, 104: (52): 20759-20763.

Wang, B., Hurov, K., Hofmann, K., et al. (2009) NBA1, a new player in the Brca1 A complex, is required for DNA damage resistance and checkpoint control. **Genes Dev**, 23: (6): 729-739.

Wang, H., Zeng, Z. C., Bui, T. A., et al. (2001a) Efficient rejoining of radiation-induced DNA double-strand breaks in vertebrate cells deficient in genes of the RAD52 epistasis group. **Oncogene**, 20: (18): 2212-2224.

Wang, H., Zeng, Z. C., Perrault, A. R., et al. (2001b) Genetic evidence for the involvement of DNA ligase IV in the DNA-PK-dependent pathway of non-homologous end joining in mammalian cells. **Nucleic Acids Res**, 29: (8): 1653-1660.

Wang, J., Dong, X., Myung, K., et al. (1998a) Identification of two domains of the p70 Ku protein mediating dimerization with p80 and DNA binding. **J Biol Chem**, 273: (2): 842-848.

Wang, J., Dong, X. and Reeves, W. H. (1998b) A model for Ku heterodimer assembly and interaction with DNA. Implications for the function of Ku antigen. **J Biol Chem**, 273: (47): 31068-31074.

Wang, M., Wu, W., Wu, W., et al. (2007) PARP-1 and Ku compete for repair of DNA double strand breaks by distinct NHEJ pathways. **Nucleic Acids Res**, 34: (21): 6170-6182.

Wang, Y. G., Nnakwe, C., Lane, W. S., et al. (2004) Phosphorylation and regulation of DNA ligase IV stability by DNA-dependent protein kinase. **J Biol Chem**, 279: (36): 37282-37290.

West, R. B., Yaneva, M. and Lieber, M. R. (1998) Productive and nonproductive complexes of Ku and DNA-dependent protein kinase at DNA termini. **Mol Cell Biol**, 18: (10): 5908-5920.

Weterings, E. and Chen, D. J. (2008) The endless tale of non-homologous end-joining. **Cell Res**, 18: (1): 114-124.

Weterings, E., Verkaik, N. S., Bruggenwirth, H. T., et al. (2003) The role of DNA dependent protein kinase in synapsis of DNA ends. **Nucleic Acids Res**, 31: (24): 7238-7246.

Whitby, M. C. (2005) Making crossovers during meiosis. **Biochem Soc Trans**, 33: (Pt 6): 1451-1455.

Wilson, D. M., 3rd (2003) Properties of and substrate determinants for the exonuclease activity of human apurinic endonuclease Ape1. **J Mol Biol**, 330: (5): 1027-1037.

Wilson, D. M., 3rd and Bohr, V. A. (2007) The mechanics of base excision repair, and its relationship to aging and disease. **DNA Repair (Amst)**, 6: (4): 544-559.

Windhofer, F., Wu, W. and Iliakis, G. (2007) Low levels of DNA ligases III and IV sufficient for effective NHEJ. **J Cell Physiol**, 213: (2): 475-483.

Winsey, S. L., Haldar, N. A., Marsh, H. P., et al. (2000) A Variant within the DNA repair gene XRCC3 is associated with the development of melanoma skin cancer. **Cancer Res**, 60: (20): 5612-5616.

Winter, S., Simboeck, E., Fischle, W., et al. (2008) 14-3-3 proteins recognize a histone code at histone H3 and are required for transcriptional activation. **Embo J**, 27: (1): 88-99.

Wood, R. D., Mitchell, M., Sgouros, J., et al. (2001) Human DNA repair genes. **Science**, 291: (5507): 1284-1289.

Woodard, R. L., Lee, K. J., Huang, J., et al. (2001) Distinct roles for Ku protein in transcriptional reinitiation and DNA repair. **J Biol Chem**, 276: (18): 15423-15433.

Wu, C. N., Liang, S. Y., Tsai, C. W., et al. (2008) The role of XRCC4 in carcinogenesis and anticancer drug discovery. **Recent Pat Anticancer Drug Discov**, 3: (3): 209-219.

Wu, J., Huen, M. S., Lu, L. Y., et al. (2009) Histone ubiquitination associates with BRCA1-dependent DNA damage response. **Mol Cell Biol**, 29: (3): 849-860.

Wu, X., Gu, J., Grossman, H. B., et al. (2006) Bladder cancer predisposition: a multigenic approach to DNA-repair and cell-cycle-control genes. **Am J Hum Genet**, 78: (3): 464-479.

Wu, X. and Lieber, M. R. (1996) Protein-protein and protein-DNA interaction regions within the DNA end-binding protein Ku70-Ku86. **Mol Cell Biol**, 16: (9): 5186-5193.

Wyman, C. and Kanaar, R. (2006) DNA double-strand break repair: all's well that ends well. **Annu Rev Genet**, 40: 363-383.

Xiao, A., Li, H., Shechter, D., et al. (2009) WSTF regulates the H2A.X DNA damage response via a novel tyrosine kinase activity. **Nature**, 457: (7225): 57-62.

Xie, A., Kwok, A. and Scully, R. (2009) Role of mammalian Mre11 in classical and alternative nonhomologous end joining. **Nat Struct Mol Biol**, 16: (8): 814-818.

Xu, Y., Wang, X. B., Ding, J., et al. (2010) Lysine acetylation sites prediction using an ensemble of support vector machine classifiers. **J Theoretical Biol**, 264: (1): 130-135.

Yan, C. T., Boboila, C., Souza, E. K., et al. (2007a) IgH class switching and translocations use a robust non-classical end-joining pathway. **Nature**, 449: (7161): 478-482.

Yan, J., Yang, X. P., Kim, Y. S., et al. (2007b) RAP80 interacts with the SUMO-conjugating enzyme UBC9 and is a novel target for sumoylation. **Biochem Biophys Res Commun**, 362: (1): 132-138.

Yaneva, M. and Jhiang, S. (1991) Expression of the Ku protein during cell proliferation. **Biochim Biophys Acta**, 1090: (2): 181-187.

Yang, X. J. and Seto, E. (2008) Lysine acetylation: codified crosstalk with other posttranslational modifications. **Mol Cell**, 31: (4): 449-461.

Yano, K. and Chen, D. J. (2008) Live cell imaging of XLF and XRCC4 reveals a novel view of protein assembly in the non-homologous end-joining pathway. **Cell Cycle**, 7: (10): 1321-1325.

Yano, K., Morotomi-Yano, K., Lee, K. J., et al. (2011) Functional significance of the interaction with Ku in DNA double-strand break recognition of XLF. **Febs Lett**, 585: (6): 841-846.

Yano, K., Morotomi-Yano, K., Wang, S. Y., et al. (2008) Ku recruits XLF to DNA double-strand breaks. **Embo Rep**, 9: (1): 91-96.

Yoo, S. and Dynan, W. S. (1999) Geometry of a complex formed by double strand break repair proteins at a single DNA end: recruitment of DNA-PKcs induces inward translocation of Ku protein. **Nucleic Acids Res**, 27: (24): 4679-4686.

Young, L. C., Hays, J. B., Tron, V. A., et al. (2003) DNA mismatch repair proteins: potential guardians against genomic instability and tumorigenesis induced by ultraviolet photoproducts. **J Invest Dermatol**, 121: (3): 435-440.

Yu, E., Song, K., Moon, H., et al. (1998) Characteristic immunolocalization of Ku protein as nuclear matrix. **Hybridoma**, 17: (5): 413-420.

Yu, X., Fu, S., Lai, M., et al. (2006) BRCA1 ubiquitinates its phosphorylation-dependent binding partner CtIP. **Genes Dev**, 20: (13): 1721-1726.

Yu, Y., Mahaney, B. L., Yano, K., et al. (2008) DNA-PK and ATM phosphorylation sites in XLF/Cernunnos are not required for repair of DNA double strand breaks. **DNA Repair (Amst)**, 7: (10): 1680-1692.

Yu, Y., Wang, W., Ding, Q., et al. (2003) DNA-PK phosphorylation sites in XRCC4 are not required for survival after radiation or for V(D)J recombination. **DNA Repair (Amst)**, 2: (11): 1239-1252.

Yuan, F., Gu, L., Guo, S., et al. (2004) Evidence for involvement of HMGB1 protein in human DNA mismatch repair. **J Biol Chem**, 279: (20): 20935-20940.

Zha, S., Guo, C., Boboila, C., et al. (2011) ATM damage response and XLF repair factor are functionally redundant in joining DNA breaks. **Nature**, 469: (7329): 250-254.

Zhang, Y., Adachi, M., Zou, H., et al. (2006) Histone deacetylase inhibitors enhance phosphorylation of histone H2AX after ionizing radiation. **Int J Radiat Oncol Biol Phys**, 65: (3): 859-866.

Zhang, Y., Yuan, F., Presnell, S. R., et al. (2005) Reconstitution of 5'-directed human mismatch repair in a purified system. **Cell**, 122: (5): 693-705.

Zhivotovsky, B. and Kroemer, G. (2004) Apoptosis and genomic instability. **Nat Rev Mol Cell Biol**, 5: (9): 752-762.

Zhu, C., Mills, K. D., Ferguson, D. O., et al. (2002) Unrepaired DNA breaks in p53-deficient cells lead to oncogenic gene amplification subsequent to translocations. **Cell**, 109: (7): 811-821.